Structural Utilization of Reclaimed Timber in a Reciprocal Frame Canopy

A Sustainable Design Strategy for the Reuse of Timber

Master Thesis

Christoph Haasis

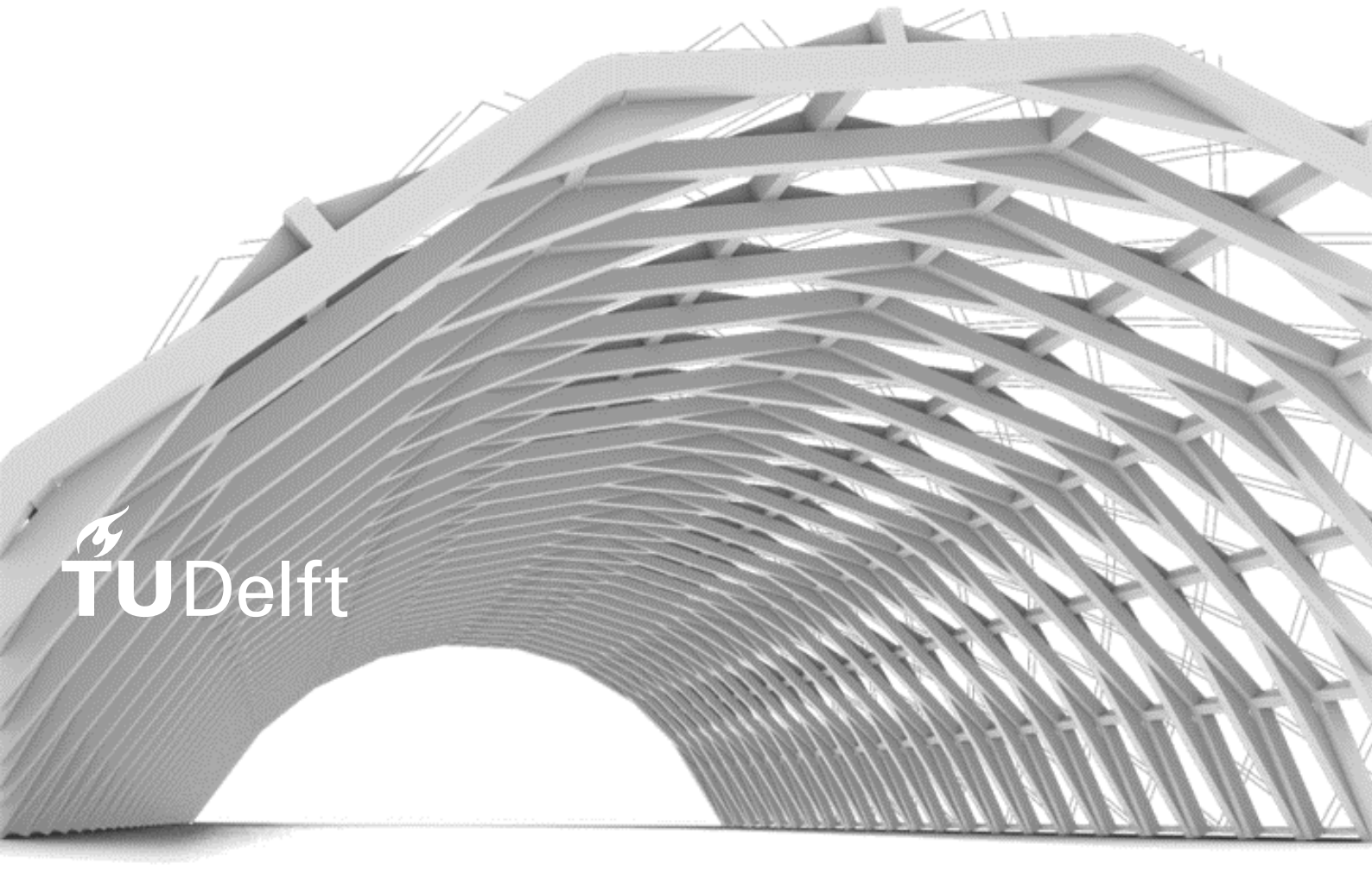

TU Delft

Structural Utilization of Reclaimed Timber in a Reciprocal Frame Canopy

A Sustainable Design Strategy for the Reuse of Timber

Master Thesis

by

Christoph Haasis

to obtain the degree of Master of Science
at the Delft University of Technology,
to be defended publicly on Tuesday July 26, 2022 at 10.00 a.m.

Faculty of Civil Engineering and Geosciences
MSc Civil Engineering - track Building Engineering
Specialization Structural Design
Delft University of Technology
The Netherlands

July 19, 2022

TU Delft

Preface

Shortly before I graduated from high school, I went to have a conversation at a career counseling center. This was the first time that I remember hearing about engineering. I had grown up never really knowing what an engineer is or does. I recall asking the career coach: “What does an engineer do?” His explanation must have gotten me interested because now, eight and a half years later, I am about to graduate from the Delft University of Technology to become an engineer. Looking back at the time of my studies, I must admit that my fascination for Civil Engineering has continued to grow ever since I got interested. Of course, the many impressive construction sites that I have visited and worked on come to my mind when I think about engineering. Yet at some point during my Bachelors, I realized that the daily routine on a construction site was lacking something for me. From this point forward I began to discover the creative potential that lies in structural design.

I am very grateful that I was able to further explore my interest in structural design with this research project. Some months ago, I had just finished some modelling, I went outside to the next playground with a piece of chalk and marked a distance of 14 m on the ground. This helped me to realize the extents of what I was actually doing on my computer. The distance of 14 m is the span of the canopy that is displayed on the cover image. It is this distance that can be spanned with timber that would otherwise be put to waste or be downgraded. And that is proven with the few design decisions, mechanical assumptions, and mathematical calculations that can be found in the following report. Now, is that not cool? I hope that the report will not only convince that a reciprocal frame canopy from reclaimed timber is capable of safely spanning 14 m, but that the writing also passes on some of my fascination for structural design. Ultimately, I would like that the proposed design strategy motivates “reclaimers” and designers to consider the structural utilization of reclaimed timber.

At this point, I would like to thank everyone that helped me throughout this research project. Of course, special thanks goes to my graduation committee: Thank you for taking time for the many meetings that we had, but also the casual conversations that often followed.

The end of this Master thesis does not only mark the end of my studies, but also the end of my time in the Netherlands. At least for now. I am so glad that I studied in the Netherlands, getting to know the language and the culture was a very uplifting experience for me.

Christoph Haasis
July 19, 2022

Personalia

Student

Christoph Haasis
Student Number: 5022967
Master track: Building Engineering - specialization Structural Design
c.haasis@student.tudelft.nl

Graduation Committee

Dr. Roel Schipper - *chair*
TU Delft - Faculty of Civil Engineering and Geosciences
Section: Structural Design & Building Engineering
h.r.schipper@tudelft.nl

Dr. Anjali Mehrotra - *daily supervisor*
TU Delft - Faculty of Civil Engineering and Geosciences
Section: Applied Mechanis
A.A.Mehrotra@tudelft.nl

Prof. Olga Popovic Larsen
Royal Danish Academy - Architecture
Institute: Architecture and Technology
Olga.Larsen@kglakademi.dk

Chris Noteboom, M. Sc.
TU Delft - Faculty of Civil Engineering and Geosciences
Section: Structural Design & Building Engineering
C.Noteboom@tudelft.nl

Dr. Michele Mirra
TU Delft - Faculty of Civil Engineering and Geosciences
Section: Biobased Structures and Materials
M.Mirra@tudelft.nl

Xan Browne, M.A.
Royal Danish Academy - Architecture
Institute: Architecture and Technology
Xbro@kglakademi.dk

Abstract

The buildings construction industry is demanded to reduce its ecological footprint to mitigate its contribution to climate change. In this context, a novel sustainable design strategy for the reuse of timber was developed in this Master thesis. The design strategy focuses on the utilization of the material “reclaimed timber” (RT) in the structural system “reciprocal frame” (RF). RT is timber which is harvested from the load bearing structure of dismantled buildings. Large quantities of RT are currently fixed in the building stock. RFs are a family of structures that boast with a rich variety of forms and diverse functions. The utilization of RT in RFs is favorable because RT items which are relatively short can span distances longer than their length when combined with RFs.

To inform the development of the design strategy a literature review on both RT and RFs was conducted. These theoretical studies were supplemented with more practical methods of investigation: RT was inspected first-hand during a visit of a salvage yard that stores RT. Throughout the project physical modeling was used as tool to explore and illustrate the characteristics of RFs. Moreover, during a three-day workshop in which a RF canopy structure from RT was built, important design aspects of RFs were investigated. This first part of the research concluded with describing the state-of-the art of the structural utilization of RT and providing a comprehensive overview of the structural design with RFs.

Key findings of the theoretical and practical studies on both RT and RFs are that the limited stock of available RT items and the geometric complexity of RFs are the two major problems when designing a RF with RT. To solve the two problems a novel RT database configuration that archives the properties of specific RT items was developed. This RT database was applied in conjunction with a novel bottom-up geometry generation model for Rainbow RFs. The Rainbow RF was identified as advantageous for the combination with RT. It can be used to generate expressive spatial assemblies with a relatively low geometric complexity and a high degree of regularity. From a structural perspective the Rainbow RF has the benefit of efficiently transferring axial forces, which reduces the bending action that is typical for RFs. Moreover, it achieves flexural rigidity without using expensive moment resistant joints.

The key findings were integrated to form a preliminary design strategy. In a case study the preliminary strategy was used to design a RT RF for a railway station canopy that spans an area of 14.0 m x 27.0 m. The RT stock of the case study was defined by a database that is comprised of 30 stacks of RT items. Based on the material stock 118 geometric design proposals were generated using the bottom-up model. Three of the proposals were developed into safe structural designs. The three safe structural designs demonstrate that the RT items compensate their low strength grade with their relatively large cross-sections.

Based on a discussion of the case study’s design process, a complete design strategy for the structural utilization of RT in RF structures is derived. The design phases of the strategy are illustrated in figure 1.

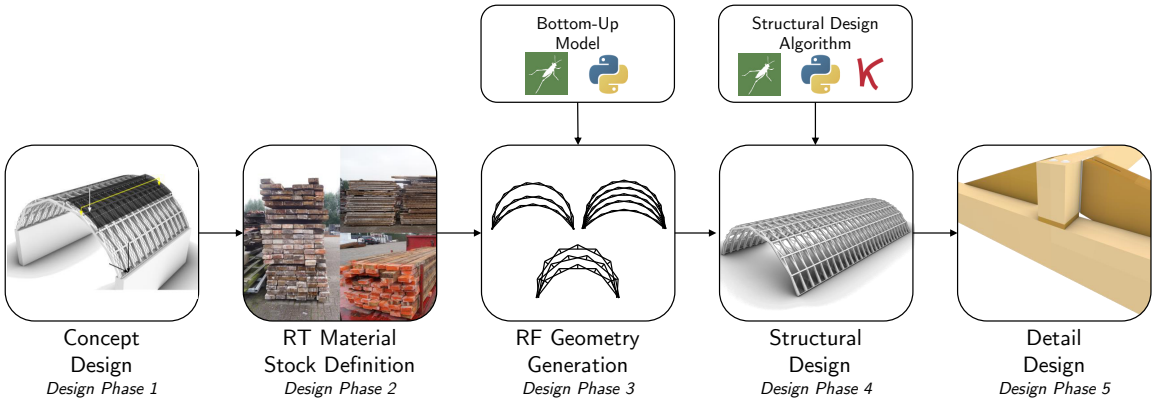

Figure 1: Design Strategy for the Structural Utilization of RT in RF structures

In the first design phase the shape of the building and the flow of forces through the structure are established. The material stock is defined using the novel RT database configuration. For each RT stack multiple geometric design proposals are developed with the bottom-up model in design phase 3. The bottom-up model is set up in “Grasshopper 3D” and “Python”. For the fourth phase, a versatile algorithm is programmed that automates the structural design to a large degree. This enables to assess many geometric design proposals with considerable accuracy in a short time. The structural design concludes with a complete design of the RF structure. The structural design algorithm is also programmed in Grasshopper 3D and Python, the plug-in “Karamba3D” is used for finite-element analyses. The Detail Design rounds the design strategy off by detailing the structure’s joints.

Contents

List of Figures

List of Tables

Part I

Introduction

1

Motivation

In 2021, the Delft University of Technology dedicated itself to a new Climate Action Program. The university determined to “use all [their] capacity to face the challenge through [their] education programs and [their] research” (TU Delft, 2021). To provide a basis to judge the firmness of this statement, the “challenge” is visualized in figure 1.1. This diagram originates from the United Nations sub-organization which is assigned to assess the science related to climate change. The global carbon emissions of the last eighty years are displayed. In addition, two colored graphs illustrate the demanded decline of CO_2 emissions. The target is to limit global warming to the politically appointed value of 1.5 degrees Celsius (Masson-Delmotte et al., 2018).

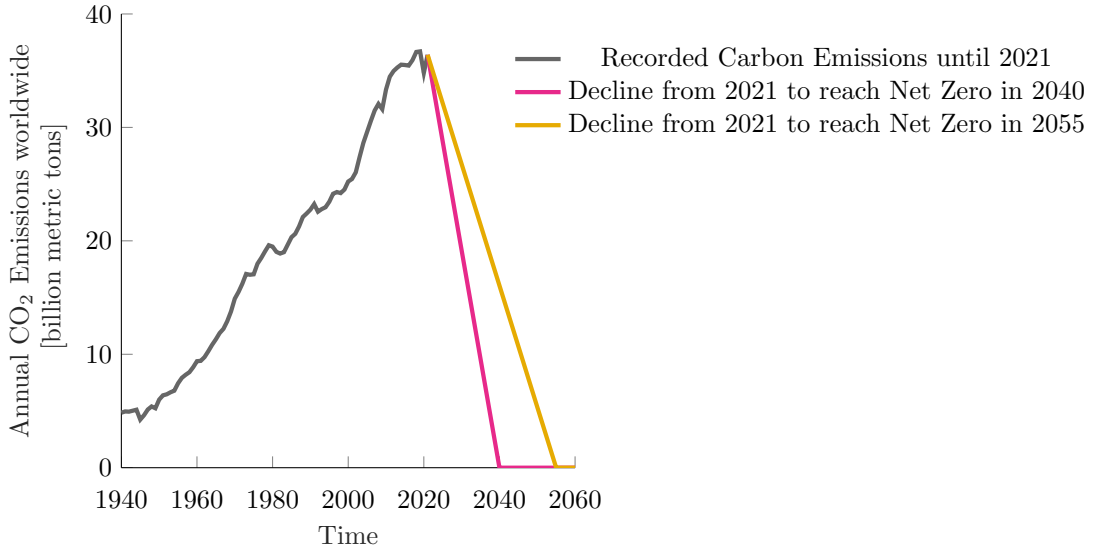

Figure 1.1: Recorded annual Carbon Emissions worldwide (Canadell et al., 2020) and Decline required for Net Zero in 2040 or 2055 (Masson-Delmotte et al., 2018), Data in Billion Metric Tons per Year

If the demanded dramatic decrease of emissions is to be achieved, the industries responsible for emitting CO_2 would need to adapt their business practices. The industries that contribute the carbon emissions are illustrated in figure 1.2. The research project at hand focuses on the demand for reducing carbon emissions in the buildings construction industry. This industry is involved with the production and processing of construction materials such as steel, cement and timber and is responsible for 10% of the global carbon emissions.

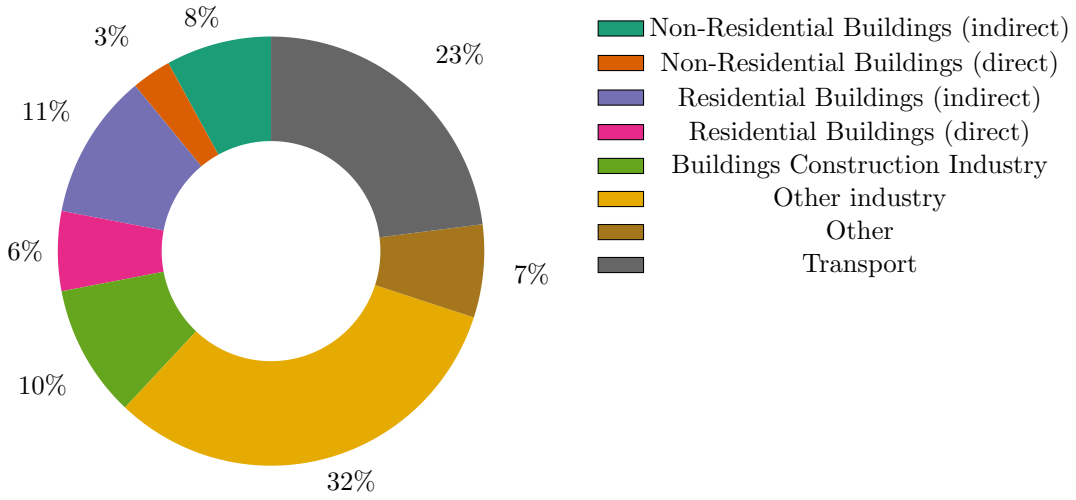

Figure 1.2: Final global Carbon Emissions per Industry Sector in 2019 in Percent (United Nations Environment Programme, 2020)

There are various ways to reduce CO_2 emissions in the buildings construction industry, e.g. the electrification of the steel production, the repurposing of buildings or the reuse of building materials. In figure 1.3 the Villa Welpeloo in Roombeek, designed by Superuse Studio, is displayed (Jongert, 2009). This building is a project that demonstrates the effectiveness of reusing building materials. The carbon emissions for façade and load-bearing structure were reduced by 90% through the application of redundant cable reels as exterior cladding and steel girders of a dismantled elevator as main supporting structure.

Figure 1.3: Villa Welpeloo by Superuse Studio (Jongert, 2009)

According to a survey conducted by Hradil, timber is perceived as the most suitable material for reuse in the building industry (2014). Compared to reinforced concrete and steel, timber already has a significantly lower ecological footprint (Falk et al., 2012; Fraanje, 1999; Hertwich et al., 2019). The structural reuse of timber bears the potential to further reduce the material's environmental impact by postponing carbon emissions, reducing construction waste, decreasing energy needed for processing and increasing resource efficiency. However, the material stock of timber that is harvested from the load-bearing structure of buildings is limited in quantity and is characterized by a dissimilarity of available cross-sections and a shortness of member length. These conditions encumber timber reuse. Alternative design strategies are required for the structural application of reclaimed timber (RT).

Recent research has explored the combination of RT and the structural system "reciprocal frame'' (RF) (Castriotto et al., 2021; Parigi, 2021; Parigi & Damkilde, 2019). RFs can span distances longer than the length of its structural members. This property is advantageous for the structural utilization of relatively short RT members. Castriotto et al. designed a canopy structure with attributing special attention to ease of assembly see figure 1.4a (2021). Parigi and Damkilde (2019) and Parigi (2021) solved the problem of designing from a limited stock of material with a focus on varying member lengths. They suggest to apply an irregular planar RF in combination with RT in a shear wall, see figure 1.4b.

(a) RF Barrel Vault Canopy (Castriotto et al., 2021)

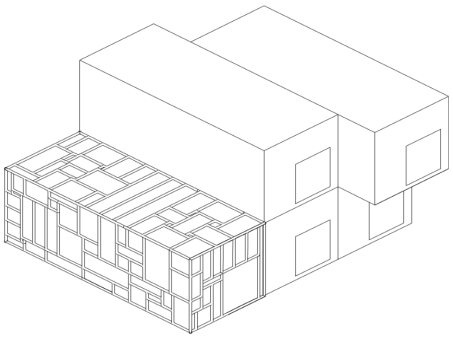

(b) RF Shear Walls in a modular Building (Parigi, 2021)

Figure 1.4: Examples for the Structural Utilization of RT in RFs

Parigi suggests that further work in the research field of combining RT and RFs should reflect on additional material characteristics of RT (2021). Besides the shortness of length, e.g. the utilization of different cross-section sizes should be able to be handled by a design process. A complete design strategy for the utilization of RT in a RF structure must also acknowledge the mechanical properties of RT and include a structural assessment of both members and joints to ensure structural safety.

2

Research Approach

2.1. Research Question

The objective of this research is to develop a holistic design strategy for the structural utilization of RT in a RF structure. The design strategy is required to reflect on important material characteristics of RT and include a structural assessment of the RF's members and joints. By achieving this research objective a sustainable design strategy for the reuse of timber is developed. Hence, it is contributed to the larger goal of reducing the environmental impact of the buildings construction industry. The objective is captured in the main research question:

"How can a reciprocal frame structure of reclaimed timber be designed in a safe, smart and sustainable way?"

The three performance indicators "safe, smart and sustainable" are adopted from TU Delft's research group "Structural Design & Building Engineering" (Louter, 2022). This is the group which the Master Thesis at hand is linked to. In the given context the three terms are interpreted in the following manner:

- Safe: Structures resulting from the application of the design strategy satisfy standard stability, strength and deflection criteria and characteristics of the alternative construction material RT are treated with an appropriate safety margin
- Smart: Computational design strategies such as parametric modelling and plugin programming are employed to deal with design complexity
- Sustainable: The resulting design strategy contributes to the introduction of structural reuse as additional step in the resource cascading of timber

To obtain an answer to the main research question three groups of sub-questions are assessed. The first group is concerned with the state-of-the-art of structural utilization of RT:

1. What is the definition of RT?
2. What are important material properties of RT that is to be used structurally and what are methods to assess these properties?
3. What quantity and quality of RT is available and what steps are part of the reclamation?
4. What are obstacles for and opportunities in the structural design with RT?
5. What RT should be used in the case of structural utilization?

The second group of sub-questions investigates the structural design with RF structures:

6. What is a RF and what are past applications?
7. What are important characteristics of RFs from a structural engineering perspective?
8. What are important aspects for the design of a RF structure?
9. Is the RF a suitable structural system for the utilization of RT from a structural engineering perspective?

The third group of sub-questions provides guidance for a structural design case study that is conducted to develop a holistic design strategy for the structural utilization of RT in a RF structure:

10. What kind of RT items form the material stock of the case study?
11. What RF geometries can be generated with the material stock?
12. Which combinations of RT items and RF geometries lead to a safe design and how much material is needed to construct the complete canopy?
13. What aspects of the RF structure's detail design are important to ensure a safe structural utilization of RT?

2.2. Research Methodology

To find an answer to the main research question, the three groups of sub-questions are assessed consecutively. Figure 2.1 displays the relation between the results found from answering the sub-questions. In the text below, it is specified how the individual groups of sub-questions are approached.

The first group of sub-questions is answered through a literature review. Key topics of the literature analysis are "material properties of RT" (Cavalli, Bevilacqua, et al., 2016; Cavalli, Cibecchini, et al., 2016; Davis, 2012; M. J. Smith, 2012) and "strength grading of RT" (Crews & MacKenzie, 2008; Falk et al., 2008; Jerzy et al., 2013). Additionally, academic case studies that document the dismantling of timber buildings are assessed (de Arana-Fernandez et al., 2020; Diyamandoglu & Fortuna, 2015; Höglmeier et al., 2017; Ogbu, 2011; Sakaguchi et al., 2016). Besides the literature review, a visit to a salvage yard is organized to investigate the material first-hand and to learn about the current practice of reclamation.

The second group of sub-questions is also answered through a literature review. To assess RFs from a structural engineering perspective, the two standard works on RFs are studied (Popovic Larsen, 2008; Thönnissen, 2015) and the large number of research articles that document the design of RF structures is examined (Asefi & Bahremandi-Tolou, 2019; Castriotto et al., 2021; Danz et al., 2015; Godthelp, 2019; Gustafsson, 2016; Kohlhammer, 2013; Koning, 2018; Larena & Ménendez, 2014; Parigi & Kirkegaard, 2014; Popovic Larsen & Lee, 2014; Rizzuto & Popovic Larsen, 2010). Besides the literature review it is planned to participate in a workshop in which a RF mock-up is constructed, the goal is to gain practical insights into the design and construction of RF structures. The outcome of the workshop is the barrel vault canopy that is displayed in figure 1.4a in chapter 1.

The results of the literature reviews are presented in Part II. Findings that directly contribute to the development of the design strategy for the structural utilization of RT in a RF structure are recorded in the final section of the chapters.

The third group of sub-questions is answered by conducting a case study which is set in the context of a realistic architectural and structural concept. The design strategy for the structural design case study is informed by the two previously conducted literature reviews. The case study is reported in Part III. Finally, the main research question is answered by deriving a generalized design strategy from the specific case study. This takes place in Part IV of the report which includes the discussion, conclusions and recommendations.

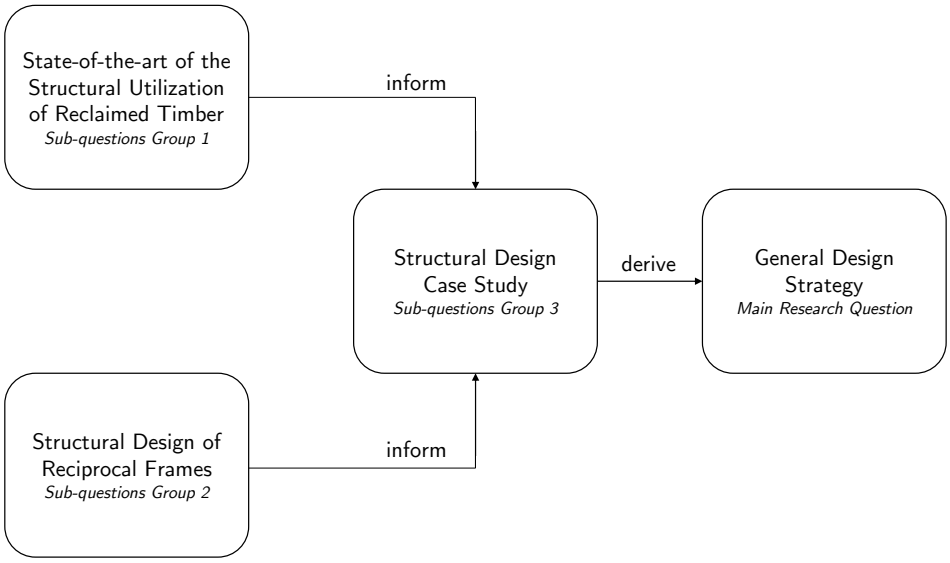

Figure 2.1: Research Methodology

Part II

Literature Review

3

Reclaimed Timber

In the course of the industrialization, the share of timber in the European buildings construction industry was gradually replaced by masonry, steel and concrete. The previously common practice of reusing building materials was consumed by the increasing quantities of material which were available through the development of industries (Diyamandoglu & Fortuna, 2015; Hafner, Ott, et al., 2014).

Due to environmental aspects, timber has begun to gain more attention in the buildings construction industry again. It is a renewable material with a low environmental impact (Falk et al., 2012; Fraanje, 1999; Hertwich et al., 2019). Today, there is also a renewed interest in reusing construction materials. According to a survey conducted by Hradil, timber is perceived as the most suitable material for reuse in the construction sector (2014). This chapter presents the state-of-the-art for the structural reuse of timber, which is also referred to as the structural utilization of RT.

The chapter is structured according to the first group of sub-questions that were defined in section 2.1. Section 3.1 provides a general overview of the material RT. This includes a definition of RT, providing an answer to sub-question 1. Furthermore, this section addresses the context of the material's current applications and research efforts. Section 3.2 corresponds to sub-question 2; the properties of RT relevant to structural utilization are described. Additionally, stress grading is examined as a method for assessing the material properties of RT. The following two sections address sub-question 3. Section 3.3 reviews the steps and actors that are involved in the procedure of reclamation. Section 3.4 examines the amount of RT that is fixed in the building stock and considers the part of it that is available for structural utilization. In section 3.5, sub-question 4 is addressed by listing obstacles for and opportunities in the structural utilization of RT.

On the basis of the reviewed information, section 3.6 formulates recommendations for the structural utilization of timber. This section includes the response to sub-question 5 which specifies the type of RT that is most suitable for structural utilization. The final section highlights the key findings of the literature review with an eye towards the structural design case study.

3.1. Definition and Context

3.1.1. Definition

The concept “reclaimed timber” has no single agreed upon definition. For that reason, the term is approached from different angles. First, the words “to reclaim” and “timber” are assessed separately. The verb “to reclaim” is defined by the Merriam-Webster dictionary as “rescuing from undesirable state” or “to obtain from a waste product or by-product” (2022). The noun “timber” generally refers to wooden construction materials. Lumber is the equivalent term in North America. Comprehensive descriptions of timber are accessible in educational literature and are not explored further in this text (Dinwoodie, 2000; Herzog et al., 2004; Madsen, 1992; Thelandersson & Larsen, 2003).

Academic descriptions of RT and the related material group “waste wood” are considered. According to Fraanje, RT refers to timber which is obtained when a building is deconstructed (1999). Smith adds that RT is reused in a construction without experiencing major processing; adjustments in size and the removal of impurities are permitted. It is key that an element maintains its previous shape (2013). Fraanje emphasizes the origin of the material when characterizing RT while Smith focuses on the processing and the destination of the material.

Besides RT, “waste wood” is a term that is often used in literature (Garcia & Hora, 2017; Hildebrandt et al., 2017; Icibaci, 2019; Irle et al., 2015). The key difference between the two material groups is their origin. The source for waste wood is arbitrary; apart from buildings, sources may be pallets, furniture, municipal house waste etc.

An updated definition of RT is formed by integrating the previous statements and thus differentiating RT from waste wood. The definition reads:

> "Reclaimed timber is timber that originates from the load-bearing structure of a deconstructed building. After harvesting, no major processing occurs. The material is destined to be utilized in a construction again, either for structural or non-structural purposes"

This definition clarifies that RT is a specific subgroup within waste wood. The material group is further specified compared to existing definitions. Not all timber from deconstructed buildings are included, but only material that was previously part of the load-bearing structure. Thus, doors or window frames do not belong to the group according to the updated definition. This is advantageous in the context of structural application. With this definition all types of RT are candidates for structural use. In table 3.1, the definition is exemplified. Applications one through three are not considered as RT because either the material’s destination is not within a building or the timber product is majorly processed. Assuming that there is no major processing, and the application is interior modelling or structural reuse the definition would classify the material as RT.

Lastly, a few remarks are made on the terminology related to RT that will be used throughout the report. The phrases “structural reuse of timber” and the“structural use of RT” are considered equivalent to each other. A “RT item” is an individual RT beam, post, joist or the like. A “RT stack” is an accumulation of RT items that stem from the same building and have similar material properties.

3.1.2. Recent Research

Research on the topic of reusing timber has been conducted for several decades. The results of this research relevant to the structural use of RT will be reviewed in sections 3.2 to 3.5. Recent academic developments have been occurring in three European research initiatives.

The “CaReWood project” stands for cascading recovered wood; the project lasted from 2014 to 2017. The aim of this research was to use recovered waste wood to fabricate laminated timber. The resulting process and product were evaluated to create added value from both a technical and environmental perspective. However, the product was not able to establish a market for itself, due to strong competition of timber products produced from virgin timber (Richter, 2017; Risse & Richter, 2018).

The “Re^4 project”, which lasted from 2016 to 2020, aimed to design energy efficient prefabricated elements from Construction and Demolition Waste. Amongst others the potential of waste wood was investigated. One result was the conceptual design of a completely reversible, multi-storey residential building constructed from prefabricated timber components (Klinge A et al., 2019).

The “InFutURe Wood project” is currently ongoing. It started in 2019 and will last until 2022.“InFutURe Wood” stands for “Innovative Design for the Future - Use and Reuse of Wood (Building) Components”. The focus of this research is solely on RT and its potential for reuse and recycling. The project’s main objective is to identify the potential for structural reuse of timber that is fixed in the building stock (Cristescu et al., 2020; Llana et al., 2020).

One reason for the continued interest in the research on structural utilization of RT may be the remaining environmental potential that lies in an improved resource cascading of timber. To improve resource cascading, the establishment of new material applications is required. Structural reuse is an example for a not yet established application. The following subsection elaborates on the resource cascading of timber.

3.1.3. Current Application

There are five primary applications for timber that originates from deconstructed buildings. Table 3.1 lists the applications, their associated lifetime and material quality decrease. The numeric values are a rough estimation. They are detailed in order to graphically compare different life cycle scenarios.

Table 3.1: Current Applications for Timber after Completing a first Life Cycle in a Building

Application	Estimated Material quality decrease [%]	Estimated lifetime [a]
Energetic Use	remaining quality	-
Disposal in Landfill	remaining quality	-
Timber Product	10	35
Interior Modelling	7	50
Structural Reuse	5	50

The distribution of the material flow varies per country. In most countries, harvested timber is primarily used as a resource for energy. For more specific statistics of various European countries refer to (Brol et al., 2015; Falk et al., 2008; Hafner, Ott, et al., 2014; Höglmeier et al., 2017; Llana et al., 2020; Sakaguchi et al., 2016; M. Smith, 2013).

To evaluate the current application of timber originating from deconstructed buildings, the concept of resource cascading is introduced. A recognized definition of resource cascading is the “sequential exploitation of the full potential of a resource during its use” (Fraanje, 1997). The two main variables of resource cascading are time T and material quality Q. Fraanje defines Q as a function of “embodied energy, chemical composition and its organization” (1997).

According to the concept of cascading it is desirable from the perspective of resource efficiency and postponing carbon emissions to (Fraanje, 1997)

Principle 1: Find an initial application with a high quality Q

Principle 2: Decrease the loss of resource quality ΔQ between cascading steps

Principle 3: Increase the amount of cascading steps, so that the total life time $\sum \Delta T$ is extended

Figure 3.1 illustrates the concept of resource cascading in a diagram. The time of use T in years is displayed on the x-axis. The relative quality of the resource Q is shown on the y-axis. The total lifetime $\sum \Delta T_i$ of a resource is the summation of the lifetimes $\Delta T_{i,j}$ of all life cycles j for the scenario i. At $T = 0$ the resource is new ($Q = 100\%$) and at the end of the total lifetime the resource is non-existent anymore ($Q = 0$). The quality of a material decreases with each life cycle. Each life cycle is marked by an individual arrow.

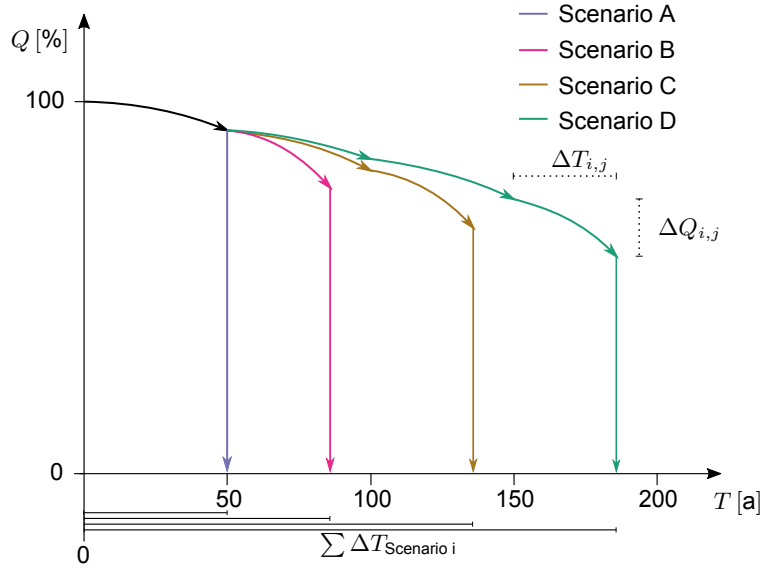

Figure 3.1: Four Resource Cascading Scenarios of Timber, mapping relative Quality of Material Q [-] over Time T [a] (adapted from (Fraanje, 1997))

Four hypothetical scenarios are illustrated in the figure above. Each scenario begins with the structural use of virgin timber. This first life cycle is captured by a black arrow. The following life cycles diverge in number and type of application for the different scenarios. Table 3.2 provides an overview of the scenario’s life cycle applications.

Table 3.2: Overview of the Life Cycles j for the Scenarios i in the Resource Cascading of Timber

Lifecycle j	Scenario A	Scenario B	Scenario C	Scenario D
I	Structural Use	Structural Use	Structural Use	Structural Use
II	Energetic Use/ Landfill	Timber Product	Interior Modelling	Structural Reuse
III	-	Energetic Use/ Landfill	Timber Product	Interior Modelling
IV	-	-	Energetic Use/ Landfill	Timber Product
V	-	-	-	Energetic Use/ Landfill
$\sum \Delta T_i$ [a]	50	85	135	185

Fraanje's principles for resource cascading and the characteristics of reusing timber structurally are set together to evaluate the environmental benefits of adding structural reuse as additional life cycle to the resource cascading of timber. As in the scenarios above it is assumed that in the first life cycle the timber is applied structurally. This agrees with the first principle. If the second life cycle's application is the structural reuse and there is no major loss of resource quality due to processing, then this conforms to the second principle. If the material is handed down to other applications after the structural reuse, as in scenario D, then this conforms to the third principle.

It can be concluded that structural reuse is a valuable addition to the resource cascading of timber, because it adheres to all three principles. Furthermore, scenario D can be identified as the most advantageous scenario in a graphical way. The scenario with the largest area underneath its graph has the most life cycles with the highest utilization of material quality and thus performs best from an environmental perspective (Fraanje, 1997; Höglmeier et al., 2017).

Scenario D involves structural reuse once, generally it would be possible to have more than one life cycle of structural reuse. Such a case would extend the resource's total lifetime even further. The limits of repeated structural use are investigated in the following section by considering RT's material characteristics.

3.2. Material Characteristics and Assessment

The structural utilization of RT requires knowledge of RT's material properties. The geometric and mechanical material properties are an essential part of any structural model. Consequently, relevant geometric and mechanical parameters of RT are investigated in this section. Furthermore, the influence of the material condition that results from the environmental exposure during the previous life cycle is considered. After discussing the named material properties, the state-of-the art of visual strength grading is described. Currently, visual strength grading is the most relevant method for assessing the properties of RT.

3.2.1. Geometry

The geometry of a RT item is detailed by three parameters:

- Cross-sectional height
- Cross-sectional width
- Item length

RT is neither available in standardized cross-sections nor can the length of an item be chosen without restriction. An item's geometry is dependent on the application during its previous life cycle as well as physical damage and processing that occurs between life cycles. Since there is a variety of possible applications and because dismantling can cause uncontrolled damage, there is great dissimilarity in the available geometry of RT.

3.2.2. Material Condition

The characteristic "material condition" specifies the result of the environmental exposure from the previous life cycle. Besides the exposure from the previous life cycle, it is assumed that the material condition of virgin timber, i.e. the condition previous to the assessed life cycle, and essential properties of virgin timber such as the wood species also influence RT's material condition. In the following the chemical, biological and physical material condition are discussed.

Chemical contamination and biological corrosion through living organisms cause a sharp and irreversible reduction of mechanical properties. Fungi and insects are examples for living organisms that cause biological corrosion. Timber may be classified as chemically contaminated, if it was previously impregnated or if it was exposed to harmful chemicals for a long time period. Acids, alkalis, salts and oxidants are examples for harmful chemicals (Davis, 2012; Sakaguchi et al., 2016).

Aging is the biological corrosion due to external factors such as humidity, temperature and weathering. Timber is capable of resisting aging under the condition that the timber is not exposed to moisture and oxygen conditions that lead to quick deterioration by fungi and that no insects such as termites or the like have been in contact with the timber. Under the named conditions, aging does not have an influence on RT's material properties (Blaß, 2017; Brol et al., 2015; Davis, 2012). Cavalli mentions that the impact bending strength is an exception; it decreases due to aging (2016).

The physical condition of RT reflects on an item's damage. More damage leads to a higher reduction of mechanical properties and also increases the likelihood of decreasing an item's geometrical parameters. Different categories of damage have been established. Damage that happens during the service life is called in-service damage. Damage that occurs during dismantling of a structure is called dismounting damage.

Dismounting damage is caused by heavy machinery during demolition. It is irregular and can be avoided by careful deconstruction. An example for dismounting damage is displayed in figure 3.2. The stack numbers that are mentioned in the captions of figure 3.2 and in the captions of following images that were taken during the visit of a salvage yard match the portrayed timber stacks with their material properties that are recorded in a database which is introduced in subsection 3.4.2. For a clarification of what a salvage yard is, refer to section 3.3.2.

Figure 3.2: Physical Damage due to Demolition, Stack not archived

In-service damage has three primary contributors:

- Nail holes along the length of an element which served to fasten attachments, see figure 3.3a
- Cracks, which occur due to loading or other actions on a timber item, see figure 3.3b
- Joints, located at the ends or along the beam, see figures 3.3a and 3.3b

(a) Joint Notches and Nail Holes along the Item, Stack 4

(b) Joint Notches at Item end and longitudinal Crack, Stack 4

Figure 3.3: In-Service-Damage of RT

Nail holes may reduce the strength of an item. Their influence depends on their quantity and spacing and if they created further splitting (M. Smith, 2013). It is advised that a RT item is placed intentionally respecting the edges of an item that have nail holes. Falk et al. state that an edge with a large number of nail holes should be placed in a compression zone and not in a tension zone (2008).

Cracks in a timber item are acceptable to a certain level of severity. Hradil et al. provide an overview of different crack types (2014). The analysis of cracks which includes the recognition of different types of cracks, such as shakes, splits and checks is time intensive and requires expertise (Falk et al., 2008).

Joints can require major processing of RT items which leads to a decrease in geometric parameters and may reduce mechanical properties. Notched joints imply a local reduction of the cross section. Glued and screwed connections or connections with other types of fastenings may not be dismantled without severely damaging an item. Joints at the end of an item may be cut off if necessary, intermediate joints are not easily removed and may lead to a major loss of item length (M. Smith, 2013).

3.2.3. Mechanical Properties

The mechanical properties of RT detail its strength and stiffness behavior. The bending strength, also named modulus of rupture (MOR, $[\mathrm{N}/\mathrm{mm}^2]$), is generally used to represent the strength properties of RT. In the same manner, the modulus of elasticity (MOE, $[\mathrm{N}/\mathrm{mm}^2]$) captures the stiffness behavior (Cavalli, Bevilacqua, et al., 2016; Falk et al., 2008).

The mechanical properties of RT depend on three factors. One, the mechanical properties of the timber before it was used. For instance, if a RT item was assigned a strength grade of C24 in its "virgin timber state", then this strength grade partly determines the mechanical properties of the RT item. Two, the material condition influences the mechanical properties. This was discussed in the previous subsection. Three, load duration effects impact the strength behavior of RT. Load duration effects are considered in more detail below.

A load on a structure causes stresses and deformations. In the case of timber, permanent loading additionally causes two time-dependent effects. One, a strength-reduction; this needs to be considered when assessing stresses. Two, creep deformations; these occur additionally to instantaneous deformations and need to be considered when assessing deflections. The influencing parameters for these two mechanisms are the magnitude and the duration of the permanent load.

The strength loss with time originates from creep rupture. Empirical studies conclude that over time, creep rupture leads to a logarithmic decrease of long-term strength on the one hand. On the other hand, the short-term strength remains the same during the first 90% of the time-interval between load application and failure (Barrett & Foschi, 1978).

Figure 3.4 displays the "Madison curve" which is a model for the discussed strength-loss. The stress-strength ratio r is plotted over the duration of loading to failure t. The function for the graph is based on a testing series from Barrett and Foschi (1978). It can be concluded that in this model the decrease in strength is governed by time. The magnitude of the load does not influence the strength loss before failure. As well, the graph illustrates that the stress-strength ratio r determines the duration until failure. For instance, a low stress-strength ratio of 30% has a much longer duration of loading to failure than a high stress-strength ratio of 80%. According to the Madison curve, the duration of loading to failure t for the latter is approximately two days. For the former percentage it holds that $t = 2.3 \cdot 10^{13}$ years, implying that an item with a stress-strain ratio of 30% will not fail due to load duration effects.

For the structural designer this implies that the longer a permanent load is applied, the lower it may be, because the corresponding material strength decreases. In this context, it is beneficial that timber has a low self-weight. In the Eurocodes this is considered through the factor k_{mod} which reduces the material strength (Barrett & Foschi, 1978; Cavalli, Cibecchini, et al., 2016; European Committee for Standardization, 2020d; M. Smith, 2013). For RT this implies that its strength is a percentage of the strength that it had before its previous life cycle. Furthermore, it can be concluded that due to load duration effects a timber item does not have an infinite service life and could only be reused in a limited number of life cycles.

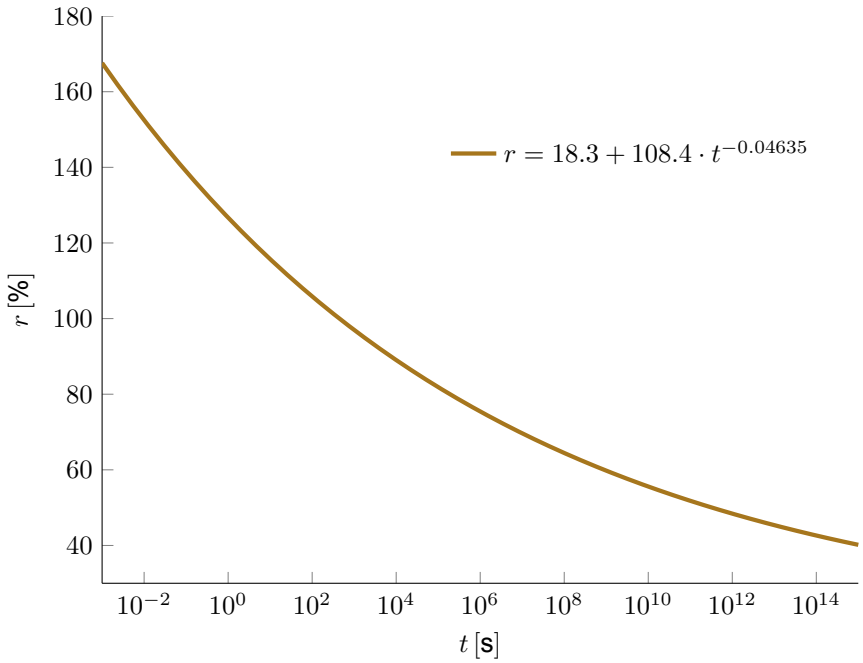

Figure 3.4: Empirical hyperbolic "Madison Curve" illustrating the Strength Loss over Time due to permanent Loading, adapted from Barrett and Foschi (1978)

The second load duration effect is creep. Creep is deformation that occurs under constant loading. Depending on the service class, creep may be up to 200% of the instantaneous deflection. If a timber item which previously experienced creep is unloaded, the reversible part of creep deformation diminishes after a certain time interval. The remaining percentage of plastic creep is small. Thus, the influence of creep deformations on RT is negligible (Blaß, 2017). It is concluded that in contrast to strength, the stiffness of RT only depends on the stiffness of the timber before it was used. Cavalli states that neither aging nor load duration effects have a major influence on the RT's modulus of elasticity (2016).

3.2.4. Strength Grading

The purpose of strength grading is to assign mechanical properties to timber, so that it can be used structurally. The state-of-the-art for strength grading RT is described in three parts. First, it is assessed if the methods existing for virgin timber can be utilized for RT. Second, the development of standards for the visual grading of RT are addressed. Lastly, alternative methods for determining the mechanical properties of RT are considered. For recommendations on the further development of a visual grading standard for RT, refer to subsection 3.6.2.

Applicability of Methods for Virgin Timber

There are two common methods for grading timber. Visual grading was the dominant procedure before machine grading was introduced in the 1960 - 1970s. Now, machine grading is the standard for assigning strength properties to timber. It is fully integrated into the workflow of newly sawn timber (Galligan & McDonald, 2000; Ridley-Ellis et al., 2016).

Visual grading remains an alternative to machine grading. It is a simpler process, as no special equipment is needed and it can take place on-site. Guided by a standard, defects that lead to strength loss are assessed. Examples for defects in virgin timber are knots, slope of grain, fissures, distortion, resin and bark pockets, fungal attack and insect damage. At the end of the assessment a grade stamp is imprinted on the material. The lower accuracy of this procedure limits the strength grades that may be assigned. Visual grading cannot achieve the upper strength grades that can be reached through machine grading (Crews & MacKenzie, 2008; Davis, 2012; M. Smith, 2013).

For several reasons machine grading is not practical for RT. Grading machines are tuned for specific cross-sections with a maximum thickness of four inches. However, RT shows a dissimilarity in available cross-sections and old timbers tend to have oversized cross-sections. Moreover, machine grading cannot be conducted on-site, but on-site grading is favorable for RT as elaborated in section 3.6.2. Another reason to not use machine grading with RT is the risk of steel elements remaining in the items to be graded, an example is displayed in figure 3.5. Residual steel elements, such as nails bear the risk of damaging the expensive testing machines (Davis, 2012; M. Smith, 2013).

Figure 3.5: Nail remaining in RT Item, Stack 3

Visual grading is the better option for determining the mechanical properties of RT. Physical damage, chemical contamination and load duration effects from past life cycles are specific to RT and thus not integrated in standards for visual grading of virgin timber. Consequently, if the standards for grading virgin timber were applied to grading RT, decisions would be inconsistent. Items with proper strength capacity might not be reused structurally and items with insufficient strength might be reused (Falk et al., 2012).

There are instances where virgin timber standards are utilized for RT. One example is the research project Re^4 that was introduced in section 3.1.2. A second example was identified in an American survey. Falk et al. discovered that some of the agencies responsible for grading timber in the United States use their existing standards also to grade RT (2012).

An additional challenge to such a procedure is that existing standards for visual grading of virgin timber are species specific. However, the identification of a RT element's species is not straightforward due to ageing, painting or other circumstances which complicate visual assessment of the species (M. Smith, 2013). This challenge and the differences between virgin timber and RT encourage the development of a visual grading standard specific to RT. It has been suggested that the existing standard for virgin timber could serve as a starting point for this development. The aspects specific to RT would need to be integrated (Hradil et al., 2014).

Standards

The status-quo of visual grading standards for RT is examined for Europe, the United States and Australia. These places have in common that there have been continued efforts in integrating the structural use of RT into the building industry.

There is currently no standard for the visual grading of RT in Europe. The standards for visual grading of virgin timber are the European norm EN1912 in combination with the corresponding national standards as well as the EN338, which specifies the timber strength classes (European Committee for Standardization, 2021, 2022). The corresponding national standard for the Netherlands is the NEN 5499 (Euopean Committee for Standardization, 2022). The Finnish national annex on the related Eurocode is unique in addressing RT, for a reference of the associated national annex refer to Hradil (2014). In general, the Finnish annex recommends to reduce the strength grade by one or two grades relative to the item's virgin timber strength grade. According to the document the reduction of the strength grade should depend on the material condition and especially on the load history. For other European countries, the only way to manoeuvre around the lack of a standard is expensive certified laboratory testing (Davis, 2012; Höglmeier et al., 2017; Hradil et al., 2014).

The currently on-going InFutUReWood research project, that was introduced in section 3.1.2, plans to contribute to the development of a European visual grading standard for RT. Another research initiative adding to this work is Smith's proposal of a flowchart for the visual grading of RT (2012).

In the United States, there is also no visual grading standard for RT. Research efforts including an extensive testing series have been aiming to develop such a standard. Falk et al. reassure RT's potential for structural use. Important conclusions from their work are (2008, 2012):

- The bending strength of RT is 25% lower compared to a reference case of virgin timber with a comparable material
- The modulus of elasticity of RT is about 10% higher compared to a reference case of virgin timber with a comparable material quality
- Shear failures are common when testing RT

The way to manoeuvre around the lack of a standard in the United States is to apply section 104.11 "Alternative materials, design and methods of construction and equipment." of the International Building Code (International Code Council, 2000). It permits building with materials that are not explicitly treated in the code, as long as an engineer approves the structure. In such a case, items are not graded individually, but a number of RT items are integrated into a building design. This design is then approved by a licensed engineer (Falk et al., 2008).

In Australia, an Interim Industry Standard for visual grading of RT was established in 2008. This Standard is specific to hardwood. The purpose of the document is to provide guidance for assessing RT appropriately. It is different to a regular standard in that it was developed faster, so that the industry did not need to wait as long as usual (Crews et al., 2008).

The Australian standard defines two visual grades with respective strength and stiffness properties. The modulus of elasticity is suggested to be of the same magnitude as the material's initial modulus of elasticity. The bending strength is advised to be reduced in dependence of the load history. If an item was subject to short term loading with a low magnitude, the strength should be reduced by 35%. An example for a RT item with such a load is a beam from a roof structure. For an item that was subject to long term loading with a high magnitude, the strength should be reduced by 55 to 60%. An example for an item with such a load is a floor beam in a warehouse. If the load history is unknown, a conservative estimation is recommended, i.e. the strength should be reduced by 55 to 60% which is equivalent to a reduction of two strength grades in the Australian code (Crews & MacKenzie, 2008).

Alternative Methods

Next to grading, there are alternative methods to determine the mechanical properties of RT. These methods are classified into destructive laboratory testing and non-destructive or semi-destructive methods. Destructive laboratory testing is the most accurate way of determining an item's mechanical properties. This method requires extensive resources of money and time.

The group of non-destructive and semi-destructive methods contains a variety of testing procedures. These can be categorized into four subgroups: organoleptic, acoustic, quasi nondestructive, and radiographic methods. The large variety of possible tests that fall into these groups are not discussed at this point. For a list and an evaluation of test methods, refer to (Jerzy et al., 2013).

Semi- and non-destructive tests do not have the capability to accurately determine the strength properties of RT. For example, the density of RT can be determined through X-Ray technology, which is non destructive (Jerzy et al., 2013; M. Smith, 2013). It is well-known that a higher material density implies a larger strength. Such a trend can be identified with this method, yet it is not possible to precisely determine the mechanical properties.

3.3. Reclamation

The reclamation for the structural utilization of RT describes the process that occurs between an initial life cycle of structural use and the following life cycle with the application structural reuse. The reclamation of timber is illustrated in figure 3.6. The steps of reclamation are represented by arrows. The material statuses of timber are named in the yellow boxes. Initially, timber is fixed in the building stock (top of graphic). After the steps "building assessment" and "dismantling", the timber is free for structural reuse. Next, "strength grading" determines if an item is fit for structural reuse. The step that closes the circle is the structural reuse of timber. Different scenarios will be considered for this last step in following subsection. The production of virgin timber, visualized in the top left, feeds new material into the cycle.

The four terms "virgin", "fixed", "free" and "fit" are used to describe the status of the material. They denote the following:

- virgin: newly processed timber which has not been used previously
- fixed: timber is integrated in a building's load-bearing structure. The building has not reached the end of its life time. Data known about the material can be the geometry, number of items per stack and additional information that relates to the current life cycle, e.g. the location in the building
- free: timber was dismantled and subject to initial visual classification. It proved to be a candidate for structural use. Additional data known about the material is its condition
- fit: timber was strength graded and reached at least the lowest attainable strength grade. Data known about the material is the fitness of an item. The fitness is a complete representation of the material characteristics

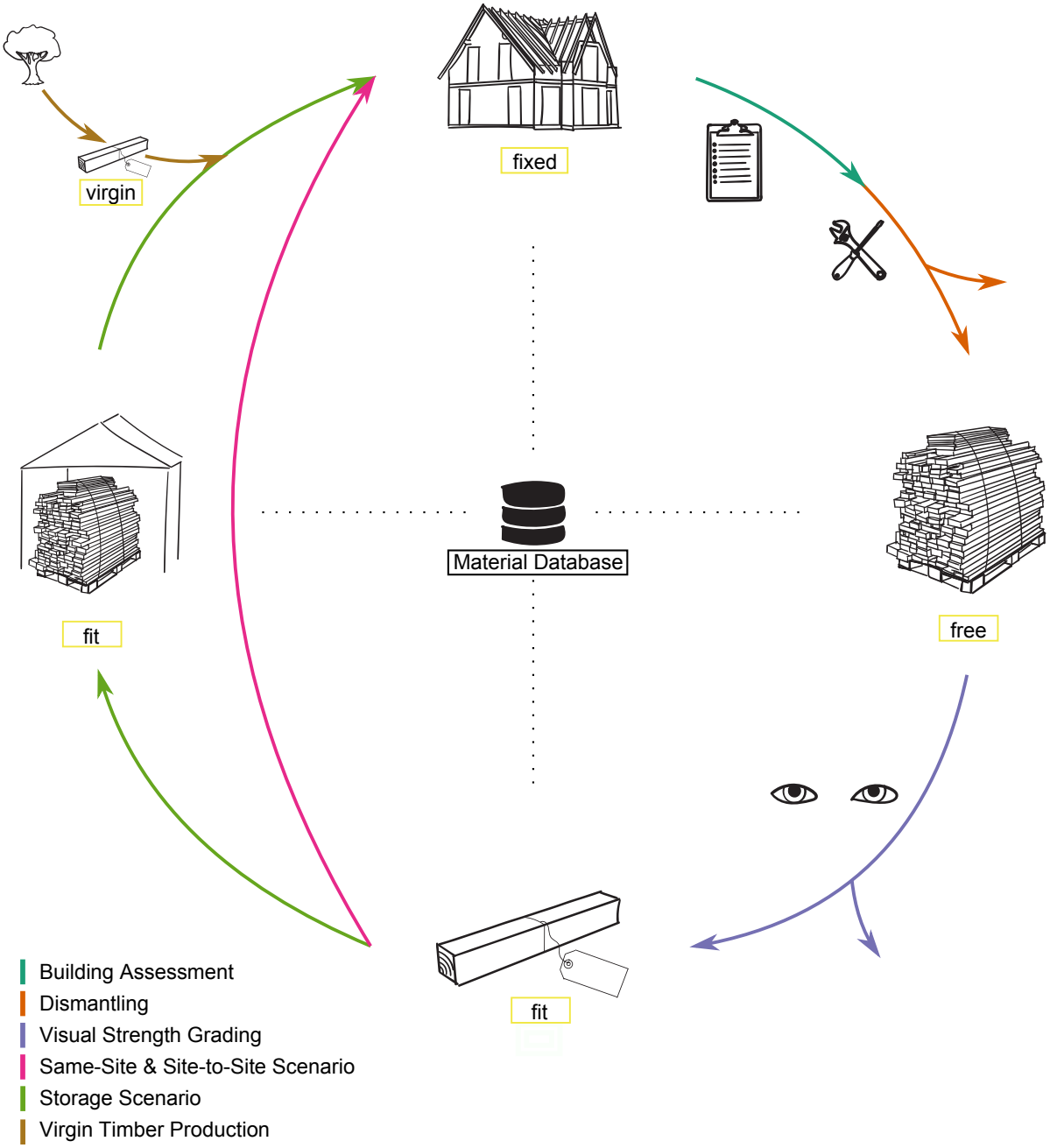

Figure 3.6: Reclamation of Timber for Structural Reuse, illustrating Steps (Arrows) and Material Statuses (yellow Boxes)

There is not only one way for the reclamation to take place in current industry practice. Some of the steps displayed in figure 3.6 may be omitted e.g. the building assessment and other steps may be added, e.g. minimal processing of the material. The reason for dissimilarity in the reclamation is the organizational complexity that stems from the large number of involved actors. The way the process is depicted in figure 3.6 is a recommendation based on the analysis of academic literature. The central element of the suggested approach is a RT database which collects information about the timber at its different stages. The database will be further discussed in subsection 3.4.2.

3.3.1. Steps

Building assessment

The starting point of reclamation is the moment when a building reaches the end of its lifetime. At this point in time, all building components lose their prior purpose and become resources that can be harvested. The purpose of the building assessment is threefold. The material resources that are fixed in the building are identified. It is decided what part is to be harvested and on this basis it is planned how the material can be harvested. Two methodologies for the building assessment are suggested.

The “Reclamation Audit” suggests that all building materials with a high reuse potential are identified. The outcome of the process is a list of selected building items and their characteristics. For a more detailed account of the Reclamation Audit, refer to Deweerdt & Mertens (2020).

The “Scientific Building Assessment” is a more meticulous approach to this step of reclamation (Hafner, Ott, et al., 2014). This method supplements the on-site material resource assessment with two additional actions. Prior to the on-site assessment the building’s documentation is studied to make an estimation of present volumes and masses. Furthermore, a forensic analysis takes place to learn more about the materials’ condition. When deciding what parts are to be harvested, it is encouraged to decide the application of the different material items prior to harvesting. Finally, a method for dismantling is selected that enables reuse and recycling. Two examples for the Scientific Building Assessment are Sakaguchi’s analysis of a kindergarten in Finland (2016) and Hafner’s assessment of an Alpine cottage in Germany (2014). The timber items that were obtained during these studies are included in the database that is documented in table A.1 in appendix A. For an explanation of the database, refer to section 3.4.2.

Dismantling

The dismantling is primarily concerned with the disassembly of a building. It may also include an initial separation of the harvested items according to their material condition. Materials with an unsuitable material condition are taken out of the reclamation cycle and find a different application. Attachments, such nails are removed from items that are to be reused or recycled. Upon completion, a timber item with a satisfactory material condition is free for structural use. Two methods of dismantling are distinguished. Each of these methods can refer to a variety of procedures and to the use of different machinery, for neither is clearly defined.

Demolition is usually associated with the use of heavy machinery, the objective of demolition is to dismantle a building in an economic way in a short time. The drawback of this method is that the material is damaged significantly. The building is taken down and materials are separated afterwards.

Deconstruction is a more careful process. The focus is on reclaiming material. The aim is to avoid damage and to keep the material items in their original shape (Hradil et al., 2014; Irle et al., 2015). Before the industrialization, this method used to be common practice (Falk, 2002). Today it is less common, because it is labor intensive.

Strength Grading

Visual grading of RT takes place to determine if an item is fit for structural reuse. Items to which no strength grade can be attributed are not fit for structural reuse. They are taken out of the reclamation cycle. For more details on the state-of-the-art of RT strength grading, refer to 3.2.4.

Structural Use Scenarios

Three scenarios for structural use of RT are distinguished according to their logistics:

- Same-Site Scenario
- Site-to-Site Scenario
- Storage Scenario

In the Same-Site scenario, RT is used on the same site for a new building. A project that employed the Same-Site Scenario is the Vancouver Asphalt Testing Facility built in 1999. Old warehouses were demolished in order to build a new testing center. The large timber trusses from the previous buildings were dismantled and the timber was reused in the load-bearing structure of the new building on the same site (Fast, 1999; Ogbu, 2011). Figure 3.7 displays the RT truss of the constructed building.

Figure 3.7: RT Truss of the Materials Testing Facility, Vancouver (Fast, 1999)

Another situation in which the Same-Site scenario might be applicable is when buildings are damaged or partly collapsed due a natural catastrophe, such as a hurricane. In this case, the reuse of material on the same site is advantageous because of financial reasons and a possible scarcity of new materials (Guy, 2020).

The Site-to-Site scenario describes the reuse of material in which harvested items are directly transported to another site. This scenario requires detailed planning of logistics, so that materials arrive on time. In the United States, this scenario is employed for industrial buildings built in timber. After dismantling and grading, timber items are transported to building sites of residential timber framing projects (Falk et al., 2008).

The Storage scenario adds an additional step to the reuse process. Timber items are not directly integrated into a structure after grading, but stored at a separate location, such as a salvage yard. Salvage yards will be further elaborated in the following subsection under the group “Timber Reclaimers”.

3.3.2. Actors

Timber Producers

The “Timber Producers” are involved with providing and distributing the virgin material. This group includes businesses that harvest the raw material and manufacture it into construction products and organize their distribution. These actors are only indirectly involved in the reclamation process. They determine the quality of the material which will later be reclaimed.

Engineers

The group “Engineers” includes researchers, designers and builders. The builders are responsible for erecting the construction according to the design. The designer plans the building. Researchers influence the reclamation process indirectly. They define the framework of the reclamation as they establish design codes and develop novel design methods.

Owners and Users

The “Owners and Users” of the building approve the design of the engineers. Thus, they also make the final decision of whether or not reclaimed materials are used in a project.

Timber Reclaimers

The “Reclaimers” include businesses involved in the steps of the reclamation process. Actors belonging to this group are dismantling companies, salvage yards and material graders and dealers. Demolition and deconstruction companies are involved in the dismantling. Deconstruction companies are specialized in reclaiming for reuse. In some cases demolition companies have integrated salvage yards as a side business. Licensed reviewers conduct strength grading of RT. A reviewer works independently or may be employed by a Reclaimer business.

Salvage yards store material. A large quantity of salvage yards exists. Many of them operate on a small scale, not including trade with construction timber. Online platforms such as “Opalis” and “Reusewood” provide an overview of salvage yards in Europe and in the United States respectively (American Wood Council, 2022; Rotor, 2022). It is common that salvage yards catalogue their stock and make this data accessible online.

Material dealers specialize in distributing reclaimed materials, they may also process the material in order to incur a higher value. A variety of material dealers trading with RT operates in the Netherlands. These businesses are not focused on providing RT for structural use, they rather specialize in antique luxury timber for renovation or refurbishments.

3.4. Available Quantity and Quality

3.4.1. Timber in the Building Stock

The quantity of RT is a portion of the timber fixed in the building stock, more specifically of the timber in buildings' load-bearing structures. Thus, when examining the quantity of RT, it is the first step to consider the amount of timber fixed in the building stock.

The accessible data on timber fixed in the building stock is limited. Table 3.3 displays quantities for various countries. The collected data does not have a uniform format. Part of the quantities are volumetric specifications, others are mass values. For some countries, only a rough estimate of buildings that are built in timber are captured.

Table 3.3: Quantity of Timber fixed in the Building Stock by Country, various Units

Country	Quantity of timber fixed in the building stock
Canada	330000 m^3 of dimensional timber in pre-1950s houses of Vancouver (Teshnizi, 2020)
Finland	35% of vertical load-bearing structures of buildings constructed in the last ten years (Cristescu et al., 2020)
Germany	18.7% of new residential buildings (Cristescu et al., 2020)
Ireland	5500 light timber frame units constructed annually (Cristescu et al., 2020)
Netherlands	$\approx$ 3 t per capita in Dutch housing stock (Höglmeier et al., 2017)
Spain	300 family houses and 400 multi storey buildings are built from timber each year (Cristescu et al., 2020)
Sweden	9500 wooden single family houses built per year (Cristescu et al., 2020)
United States	$\approx$ 100 million housing units are wood-framed (Diyamandoglu & Fortuna, 2015)

From this data, a few trends, which are supported by further literature, are pointed out. First, the data indicates that the amount of timber fixed in the building stock varies per country. Two reasons for varying quantities per country are that building traditions differ and that the amount virgin timber resources are not the same. Second, the residential housing sector appears to inhabit the largest quantity of timber in the building stock. This claim is supported by the fact that more than 70% of the developed world's population lives in timber frame housing (Müller, 2005). Third, there is a large amount of timber fixed in the building stock. Müller provides an illustrative example: In the Netherlands there is a larger volume of timber stored in the building stock than in Dutch forests that provide for the wood production sector (2005).

It has also been argued that the total amount of RT is limited and soon will not be available anymore. This specifically addresses old timber (for a definition of old timber, refer to subsubsection 3.5.2.1) and is not related to RT in general (M. Smith, 2013). On the contrary, considering the increasing interest in building with timber (Lyslo et al., 2016), it is expected that the amount of timber in the building stock will increase with time.

3.4.2. RT Database for Designers

A fundamental starting point of structural design is that the engineer can choose from a number of standardized cross-sections which have mechanical properties from a specified range. The values for geometry and material characteristics are catalogued. In these conditions materials are considered abundantly available because of their industrial production. This also holds for virgin timber. Structural design with RT stands in sharp contrast to this approach, simply because the geometry and material characteristics of the material are neither standardized nor is RT abundantly available, but it is limited to what is obtained from deconstruction.

Three studies, cited in the previous subsection, also provide rough estimations of the timber that is free for structural use, see table 3.4. The data indicates that there is a significant amount of RT which could be used structurally. However, this data does not provide a complete starting point for the structural design with RT.

Table 3.4: Timber free for structural Use per Country, various Units

Country	Timber free for structural use
Canada	3000 to 4000 m^3/a in Vancouver (Teshnizi, 2015)
Germany	25% of RT in South East Germany (Höglmeier et al., 2017)
United States	1.8million m^3/a (Falk & McKeever, 2004)

A new RT database configuration is proposed as starting point for the structural design with RT. This database archives RT items that have the same geometry, material condition and mechanical properties in stacks. The number of items within a stack as well as the material status is documented. The material statuses were defined in section 3.3. Additional information about the previous life cycle may be recorded as well. Table 3.5 provides an overview of the information that the database configuration collects. Each listed stack refers to a physical equivalent that is either fixed, free or fit. The proposed database configuration provides a designer a concrete starting point for the structural design with regards to the material that is available.

Table 3.5: Proposed RT Database Configuration illustrating the Information that is collected for a Stack of RT

Material Charac-teristic	Geometry		Material Condition			Mechanical Properties			Additional Information					
Property	Height x Width [cmxcm]	Length [m]	Chemical Contamination	Biological Corrosion	Physical damage	Strength Grade	MOR [N/mm^2]	MOE [N/mm^2]	Number of items [–]	Material status	Virgin timber grade	Location in building	Building year	Building type
Stack i	..x..	..	y/n	y/n	y/n	..	..	..	..	...	...	...	...	...

Currently no comparable database is known of. It was mentioned that salvage yards publish information on RT online, however, the data is limited in quantity and generally does not include all of the information relevant to the designer. On the basis of a visit to a salvage yard and a literature review of case studies that document the dismantling of buildings a hypothetical database is generated, see tables A.1 and A.2 in appendix A. The term hypothetical is used, because it is unknown if the material is still available for structural reuse. A realistic database would be comprised of RT stacks that are stored and can be retrieved. The mentioned appendix also contains notes on the origin of the data and assumptions that were required to format the data according to the proposed configuration, see A.1. Figure 3.8 displays the RT items of the stacks that were documented during the visit of the salvage yard.

(a) RT items, Stack 3

(b) Sideview of RT Items, Stack 1 and 2

(c) Frontview RT Items, Stack 1

Figure 3.8: Stacks of RT on a Salvage Yard

In order to utilize RT for structural design, an item must be fit and its fitness must be known. Less than half of the items recorded in the database meet this criterion. Most of the items are free for structural use, which means they were deconstructed and the material condition was assessed, but strength grading did not take place. The reason for this is that some studies did not consider structural use as an option for the next life cycle. There are also three stacks which are still fixed in the building stock. For them, neither material condition nor strength grade is known. It is important to recognize that if the material status of a stack is fixed or free, it is likely that the number of items fit for structural use is smaller than the number of items in the given material status.

Five trends are observed in the provided data. First, in all cases the number of items per stack is larger than one. Second, during the data collection it was discovered that each research employed a different approach for determining the material condition and only the research by Falk et al. determined the strength grade (2008). This illustrates the lack of a standardized method for assessing RT and supports the call for the development of unified strength grading. Third, the database shows the quantity and properties of RT are different for every building. Because of different building techniques, building projects and their maintenance differs, thus, it is difficult to state a general percentage of a building's fixed timber that is free or fit for structural use.

Fourth, the database identifies common geometries. For example, more than half of the listed stacks in the database have a cross-section width of 38 mm. This measurement is equivalent to the cross-section width of what is referred to as a “2-by” timber beam in North America. This trend is not generalized, but is clear due to the limited amount of data. Lastly, the archived items’ lengths are much larger than the length of the items that were considered in the studies by Castriotto et al. (2021), Parigi (2021) and Parigi and Damkilde (2019). They considered items with lengths shorter or equal to 1.0 m. The range of items’ length in the present database reaches from 1.4 m to 6.3 m.

3.5. Obstacles and Opportunities

For the establishment of a reuse practice, three perspectives need to be considered. Two of the three, the technical and the environmental perspective have already been examined to an extent. The third aspect to consider is how the reuse practice, in this case the structural reuse of timber, fits into the existing market. This is relevant because a reuse practice yields the most benefit, if it is successfully integrated into industry (M. Smith, 2013; TU Delft, 2021). Obstacles and opportunities for the structural use of RT are ordered into the three categories “technical aspects”, “market aspects” and “environmental aspects” and are discussed below.

3.5.1. Obstacles

Technical Aspects

There are four technical aspects that hinder the structural reuse of timber. The greatest technical obstacle to the structural reuse of timber is the previously addressed lack of a grading standard, compare section 3.2.4 (Hradil et al., 2014). If it is not possible to determine the mechanical properties of a RT item according to a certified method, it is generally not permitted to utilize it in a structural design, as specified in section 1.3, sentence (2) of the Eurocode EN1990 that addresses the “Basis of structural design”. (European Committee for Standardization, 2020a). This is true in Europe, exceptions are mentioned in section 3.2.4 (Davis, 2012; Höglmeier et al., 2017; Hradil et al., 2014).

Second, the structural utilization with RT cannot be administered with the conventional approach to structural design. This is because when designing with RT, the fundamental assumption of abundant availability of structural items with standardized geometry and mechanical properties does not hold, compare subsection 3.4.2. Alternative design strategies are required.

Third, it was argued that a database of RT items forms an important starting point for the design with RT. The current lack of data, and the fact that existing data does not have a uniform format, encumbers the structural reuse of timber (Falk et al., 2008; Höglmeier et al., 2017).

Fourth, due to in-service damage, dismounting damage and load duration effects RT is likely to have mechanical properties that are inferior to virgin timber. Low strength properties may therefore render structural use impossible.

Market Aspects

There are four market aspects that hinder the structural reuse of timber. First, there is strong competition over timber that is harvested from the building stock. Current applications have well established markets. For instance, the demand for timber in energy production and the manufacturing of wood products from chips, such as Oriented Strand Board and Medium-Density Fiber Board make strong competitors for the resource (Icibaci, 2019). Furthermore, there is a large demand for old timber in the sector of refurbishing and interior decoration. Due to its aesthetic appearance, old timber (for a definition of old timber, refer to subsubsection 3.5.2.1) is sold at prices higher than virgin timber (Fraanje, 1997; Rohwedder, 2019).

Second, when there is a large amount of virgin timber available on the market, RT may not compete. Labor intensive processes during reclamation such as de-nailing may cause the price of RT to rise beyond that of virgin timber (Falk et al., 2008; Hradil et al., 2014; Teshnizi, 2020). Furthermore, the procurement of RT may be burdened with an organizational complexity, due to the many involved actors. This may cause extended lead-times and additional costs (Hradil et al., 2014; M. Smith, 2013).

Third, if there is no established market for the structural use of RT, demolition companies lack incentive to invest additional effort into its reclamation. As demolition companies continue to be the market leaders in dismantling, in most cases major demounting damage is incurred to RT. Exceptions are the dismantling of buildings where old timber can be reclaimed, because for this material a market exists (Höglmeier et al., 2017; Hradil et al., 2014).

Fourth, neither professionals nor the public recognize RT as a building material with structural potential. Studies suggest that the used character is considered as negative in relation to structural utilization (Hradil et al., 2014; M. Smith, 2013), which hampers the establishment of the reuse practice.

Environmental Aspects

There is one environmental aspect that hinders the structural reuse of RT. Current policies demand an increase of climate neutral energy. The product of the energetic use of RT is considered climate neutral because it stems from a natural resource and replaces possible use of fossil fuels. In 2010, the share of energetically used wood in renewable energy was on average around 50% in the EU27 countries. Large quantities of wood are required to achieve such energy production (Mantau et al., 2010). The EU continues to subsidize the energetic use of RT as a climate neutral energy source (Boytchev, 2022). This provides an environmental incentive for a different application for the timber fixed in the building stock and thus decreases the likelihood of the not well-established application for structural reuse.

3.5.2. Opportunities

Technical Aspects

There are two technical aspects that stimulate the structural reuse of timber. The durability of building materials often exceeds the lifetime of a building, thus construction materials are suited for reuse. In many cases the major factor for demolition is not the state of materials, but how people feel about the building and its components. This notion is called obsolescence and suggests that timber has the capability to be reused structurally (Hradil et al., 2014; Huuhka, 2014).

Another aspect that stimulates the structural use of timber is specific to “old timber”. Old timber is classified as timber that was used before machine grading was introduced. Timber that has been used for construction after the 1960s to 1970s is labelled as “basic modern timber” or “basic modern salvage”, once it is reclaimed (M. Smith, 2013). Old timber has mechanical properties that are superior to timber used today (Fraanje, 1997). This is because a century ago, the knowledge about building with timber was less advanced. Engineering mechanics were at an earlier stage and machine grading did not yet exist. From today’s perspective, this led to over-sizing of members. There was also more timber available. Thus timber was grown and dried more slowly, which led to a higher material quality. The timber had higher density and fewer knots (Davis, 2012). Falk et al. reason that the quality and size, that old timber has, is not being produced in contemporary forestry (2008).

Market Aspects

There are two market aspects which stimulate the structural use of RT. There are financial benefits for reclaimer businesses, they receive a revenue for selling RT, and reduce or omit disposal fees (Diyamandoglu & Fortuna, 2015; Falk et al., 2008). Companies have already made a business case from this. An example is the salvage yard that was visited during the course of this project. Diayamandoglu (2015) and Falk (2002) state approximate prices for RT. A guide from the British Waste Resources and Action Program made a precise suggestion for different types of RT (2008); such values are subject to significant variation which depends on the specific type of RT as well as current market conditions .

Utilizing RT in a building’s load-bearing structure may indirectly increase the market value of a real-e-state. If reused material is used in construction, the positive influence on its ecological footprint is reflected in an environmental certificate. This type of certificate continues to gain importance in industry; it increasingly impacts the real-e-state value of a building. A better certification may lead to higher financial worth (Bratkovich, 2009).

Environmental Aspects

There are four environmental benefits to adding structural reuse as additional life cycle to the resource cascading of timber. First, as previously mentioned in the introduction, carbon emissions are postponed and essentially decreased. Second, energy consumption is reduced because processing that would be required for virgin timber, is omitted (Falk et al., 2012). Third, possible construction waste is reduced if the material is used again instead of ending up in landfill. Especially in countries with large wood consumption, structural reuse can reduce the major waste streams. Fourth, structural reuse increases resource efficiency. This implies savings in primary resource and reduction in rapid deforestation (Davis, 2012; Fraanje, 1997; Risse & Richter, 2018).

The environmental obstacle to the structural use of RT requires consideration. According to the the concept of resource cascading the production of renewable energy from wood is not rejected when structural reuse is added to the life cycle; it is only postponed. Thus, when introducing structural reuse, initially the amount of wood for energetic use would drop, but with time, the drop would be negated again.

3.6. Recommendations for the Structural Reuse of Timber

With the aim to stimulate the structural reuse of timber, recommendations are made for three parts of the reuse practice. It is discussed what type of timber is optimal for structural utilization. The lack of a standard for strength grading is addressed again by providing recommendations for further development. Lastly, suggestions for a favorable reclamation process are made.

3.6.1. Optimal type of timber for reuse

The previous sections have illustrated that RT has a spectrum of possible properties and is available in varying, but limited quantities. This motivates sub-question 5: “What RT should be used in the case of structural utilization?”

Generally, there is no optimal building material, but depending on the structural system, different material characteristics are preferred. This also holds for building with RT. Hence, the optimal type of RT with regards to structural utilization is project specific. However, a key difference between RT and conventional construction materials is its availability, see section 3.4.2. If a designer chooses RT as construction material, his design options become limited to those constructions which can be realized with the available material stock. Consequently, the choice of construction should consider the available RT. Accordingly, the answer is that the type of RT should be used which is available in sufficient quantity and adequate material quality to build the selected type of construction that achieves the design aim.

As such, introducing a parameter that assigns an objective potential for structural use of RT is refrained from. Nevertheless, general tendencies can be drawn for RT to be reused structurally. It holds that the more items a stack contains, and the better the items’ fitness, the higher is the potential for the stack’s structural reuse, due to wider range of possible application. A higher fitness refers to larger geometric parameters, a better material condition, and a higher bending strength and modulus of elasticity.

An example that considers the geometric parameters is considered for illustration. A beam with an industrial cross section of 80 mm x 220 mm and a length of 6.50 m is compared with a small cube which has an edge length of 100 mm. The beam’s dimensions allow for a variety of structural applications. The cube does not have a comparable capability for structural reuse. It is likely to be downgraded through processing or transferred into its final life cycle. The beam is attributed a higher potential for reuse.

3.6.2. Towards Visual Strength Grading of RT

Extending the Virgin Timber Visual Grading Standard

It was argued that a standard for visual strength grading of RT should be similar to that of virgin timber (Hradil et al., 2014). The visual grading of virgin timber focuses on the assessment of physical defects (compare 3.2.4). For RT the assessment of physical defects could be extended to the assessment of physical damage, which is one of the key factors that influences the material’s strength. Hence, the standard for virgin timber can be good starting point for grading RT, yet it would need to be supplemented by characteristic features of in-service and dismounting damage.

Load duration effects cannot be identified through visual assessment, however, this is the second key factor that causes a decrease of RT's strength parameters. This decrease needs to be accounted for by an additional assessment. Two options are recommended below.

An advanced strength grading would combine visual grading with non-destructive or semi destructive testing. Few non-destructive tests may be conducted directly on-site. For instance, the modulus of elasticity can be determined through dynamic testing using a piezoelectric accelerometer. This test requires that the density of the item is determined first. The modulus of rupture can be estimated utilizing the measured modulus of elasticity and an empirical correlation (Cavalli, Bevilacqua, et al., 2016). The additional effort related to this assessment would lead to an increase of the RT price.

The data retrieval method is a more economic option for estimating the reduction of the strength grade due to load duration effects. This method examines data that specifies how a RT item was utilized in the previous life cycle. Similar to semi- and non-destructive testing this approach is not capable of precisely determining the mechanical properties, but important trends can be identified. In combination with visual grading, a strength grade can be determined. This method assumes that ideally both the virgin timber grade and information on the application during the previous life cycle is accessible. Information indicative of the mechanical properties are the material's age, the location of application, the building type and the duration of the previous life cycle. All of this information is included in the proposed RT database configuration. More available information allows a more accurate prediction of the strength grade. With little available information a conservative guess needs to be made.

The age and the virgin timber grade give an indication of initial mechanical properties (compare subsection 3.5.2). Information on the building type and the location suggest the magnitude of the load that was acting on the RT. The aspect of the location allows informed assumptions about both duration of loading effects and physical damage. For instance, structural items from locations with low dead-load and shorter duration of permanent loading, i.e. a lower total lifetime in the previous life cycle, are preferred for structural reuse. Roof and floor beams of residential houses meet this criteria. Indeed, it has been identified that the reclamation of floor and roof beams is most prominent. Icibaci identifies that in the Netherlands items are often harvested from floor and roof structures (2019). Llana states that in Ireland RT generally stems from roofs (2020).

The location may also provide information about the physical damage of an item. Items from integrated units and structural components from independent items are distinguished. Independent items such as roof beams are suited for reuse from the perspective of dismounting, as they can easily be dismantled. Integrated parts, such as exterior wall panels, are less suited for reuse because of the various attached materials. These complicate the reclamation and make the item prone to dismounting damage (Sakaguchi et al., 2016).

Increasing Efficiency of the Grading Process

It is proposed to divide the strength grading process into two stages. In a first step an initial classification of the material takes place directly after deconstruction. The goal is to separate items that are free for structural use from items that are not in a suitable condition. The purpose of this assessment is to avoid in-depth assessments for items which are not likely to be fit for structural use.

Such an initial classification requires a brief visual assessment and can be conducted without expert knowledge. If an item has experienced biological corrosion through living organisms or is chemically contaminated, it should be excluded due to the potential of dramatically reduced mechanical properties (compare section 3.2). It could also be argued that items below a certain threshold for the geometrical parameters would not be considered for structural use.

After the initial classification the mechanical properties are assessed through the discussed advanced strength grading or the combination of visual strength grading and the data retrieval method. It is suggested to randomly select items from a stack and apply the identified strength grade to all items of the stack. Grading in groups should be conducted in a conservative manner and may not be applicable if geometry, material condition or the location in the building differ significantly. This is emphasized as Cavalli et al. found that reclaimed and historic timber items have a large variance in properties (2016).

Recommended Research for Further Developments

Cavalli et al. identify that research on the mechanical properties of RT has been a subject of interest since the 1950's. In his research he compares the results of past investigations and concludes that the outcomes are incoherent. He reasons that this can be explained by the challenges that are inherent to RT, namely missing information about the mechanical properties of the old timber and its load history. Different states of conservation and the use of non-standardized tests further complicate the determination of mechanical properties (2016).

Research into the strength and stiffness characteristics of RT and their assessment is motivated by the incentive that more accurate relations allow a less conservative assignment of mechanical properties. Multiple studies that focus on the physical damage and its influence on RT have been conducted. Less attention is given to the influence of the load duration effect. If physical damage is increasingly reduced through adapting design and dismounting methods, the load duration effect gains further importance as the main contributor to strength loss.

Present research comes to different conclusions of the reduction of RT's strength. The Finnish commentary suggests a reduction of one to two strength grades which is equivalent to a reduction between 10% and 22%, assuming that the initial strength grade is equal to or lower than C30 (Hradil et al., 2014). Falk suggests a reduction by 25% (2008). The Australian Interim Standard for hardwood recommends a reduction by 35% or 55 to 60% depending on the duration and magnitude of loading (2008) (compare also subsection 3.2.4). Based on the Madison curve, which only considers load duration effects and does not account for any physical damage, a reduction of approximately 40% of the strength after a time of 50 years would occur. Table 3.6 displays what strength grades the cited references would conclude with if the grade of the virgin timber was C24.

Table 3.6: Strength Grades for a RT Item with initial Virgin Timber Grade of C24 according to different Studies

Reference number	Reference for reduction	Resulting strength grade(s)
R1	Finnish Commentary (Hradil et al., 2014)	(a) C22 or (b) C20
R2	Falk (2008)	C18
R3	Crew & MacKenzie (2008)	(a) C16 or (b) < C14
R4	Madison Curve (1978)	C14

The results do not coincide. This is partially because the research is not aimed at this specific application. Crew and MacKenzie address hardwood, but the example's strength grade considers softwood (2008). Further, the Madison curve is not aiming to determine the strength of RT, but the long-term strength of regular timber. Falk's research was conducted on a softwood species and comes closest to the present example (2008). The basis for the assumption that the Finnish commentary makes is not documented (Hradil et al., 2014).

Considering the above, specific aspects for further research are recommended:

- The assessment of the influence of the information of an item's location in a building for the prediction of the strength grade.
- The investigation that analyzes after what time the strength grade needs to be reduced.
- The inquiry of the effect on short-term loading. If the strength grade of a RT item is reduced, then the short-term strength is reduced as well. It would be interesting to investigate if the short term strength decreases to the same degree as the long term strength.
- The investigation of how to grade RT "species independent", a starting point can be the work by Ravenshorst on "Species independent strength grading of structural timber" (2015).

3.6.3. Favorable Reclamation process

It is recommended to utilize a procedure for dismounting that inflicts the least physical damage. However, a more careful dismantling is equivalent to increased cost for the dismounting company. These costs can be reduced through a proper building assessment that identifies the items to be carefully deconstructed. Yet, such a building assessment incurs additional costs in itself, thus the goal of reducing the physical damage may only be achieved if the dismounting company has an economic incentive for it. The existing practice of reclaiming old timber and selling it as a luxury good demonstrates that a market is capable of providing such an economic incentive. Environmental certification that highly regards the structural utilization of RT in new buildings has the potential to promote the establishment of a market that provides the required economic incentive for a careful deconstruction of RT.

Among the three proposed structural use scenarios, the storage scenario is recommended. There are three disadvantages to this process, nevertheless it adds reasonable benefit to the reclamation overall. The drawbacks are an additional logistical effort and the need for sufficient storage space. Moreover, potential information about the previous life cycle of a RT item may be lost if proper documentation is omitted. The benefits of the storage scenario are that the organizational complexity of the reuse practice is reduced because the dismantling and the reuse of the material in the next life cycle are independent in their timing. Thus, lead times for materials and other planning dependencies are reduced. Moreover, this scenario accommodates the development of a RT database; all stacks that reach a salvage yard can be archived.

Throughout the previous sections the central RT database that collects information about timber at different stages during the reclamation has been discussed. Currently there is little data for timber within the reclamation cycle for structural reuse of timber. Implementing the proposed database in industry can benefit the establishment of a market for the structural use of RT. More specifically such a database would aim to achieve:

- The link between the many actors involved in the reclamation and thus reduce organizational complexity.
- The foundation for the structural design of RT with regards to available material.
- The projection of RT available for structural use at a certain time point in the future based on data that specifies the timber that is fixed in the building stock.
- The improvement of strength grading for RT through collecting data for the data retrieval method.
- The furthering of research in the field. Through proper documentation, more may be learned about the effects that reduce mechanical properties.

3.7. Key Findings

The objective of this research is to develop a holistic design strategy for the structural utilization of RT in a RF structure. During the literature review on the state-of-the-art of structural utilization of RT, it was discovered that a database, which defines material characteristics of specific RT items, forms an appropriate starting point for the sought design strategy.

A novel configuration for a RT database was developed. The geometric and mechanical properties of the material are the database' primary concern. Additionally, selected information about the material's previous life cycle is archived. This information is useful for determining the mechanical properties of RT. Furthermore, it has been pointed out that the introduction of a centralized database has additional benefits, e.g. it can reduce organizational complexity in the reclamation process and it can project the quantity of RT that will be available in the future based on the amount of timber that is fixed in the stock.

Visual strength grading was identified as the preferred method for assigning mechanical properties to a RT item. Currently, no standard for visual strength grading exists in Europe. However, based on the analysis of the current state of research on RT strength grading, the formulation of informed assumptions for the strength grade of RT items in the case study is possible. From four different standards and research projects a rule for determining the RT strength grade in relation to the virgin timber strength grade was extracted.

4

Reciprocal Frames

A RF has the ability to span distances longer than the length of its structural members. This primarily geometric consideration suggests that the RF is a structural system that increases the potential for the structural utilization of RT. Besides the obvious geometric match between structural system and material, it must be evaluated if the mechanical properties of RT can be handled by a RF. Before evaluating the combination of RT and RFs both from a geometric and a structural perspective, this chapter introduces RFs and evaluates their structural behavior.

The chapter is structured according to the second group of sub-questions that were defined in section 2.1. Section 4.1 provides an overview of RF structures. This includes a definition and a number of descriptive RF applications. Section 4.2 presents a classification for RFs. These first two sections form the response to research sub-question 6. Section 4.3 corresponds to sub-question 7; it examines characteristics that influence the structural behavior of RFs. In section 4.4, sub-question 8 is addressed; three aspects that need to be considered during the design of a RF structure are assessed.

Where the previous sections all consider RFs as a diverse family of structural systems, section 4.5 assesses the geometric properties and the structural behavior of one specific RF in more depth. The final section highlights key findings of the literature review with an eye towards the structural design case study. This includes a discussion of the suitability of combining RFs and RT, which forms the response to sub-questions 9.

4.1. Definition and Context

4.1.1. Definition

“Reciprocal frame” is the most accepted name for referring to a family of structural systems, which is defined by a combination of the following four criteria:

1. Members mutually support each other,
2. along the span
3. and are arranged in a closed circuit
4. with only two members meeting in a joint.

In figure 4.1, three cups and three knives are arranged to demonstrate the defining criteria:

1. Mutual support: Each knife both supports a knife and is being supported by a knife.
2. Along the span: The knives do not meet in their end points, but at points along the length.
3. Closed Circuit: The knives are arranged in a closed circuit, i.e. the knife from cup one rests on the knife from cup. two, the knife from cup two rests on the knife from cup three, and the knife from cup three rests on the knife from cup one.
4. Number of members per joint: In every point where knives meet, only two knives are present.

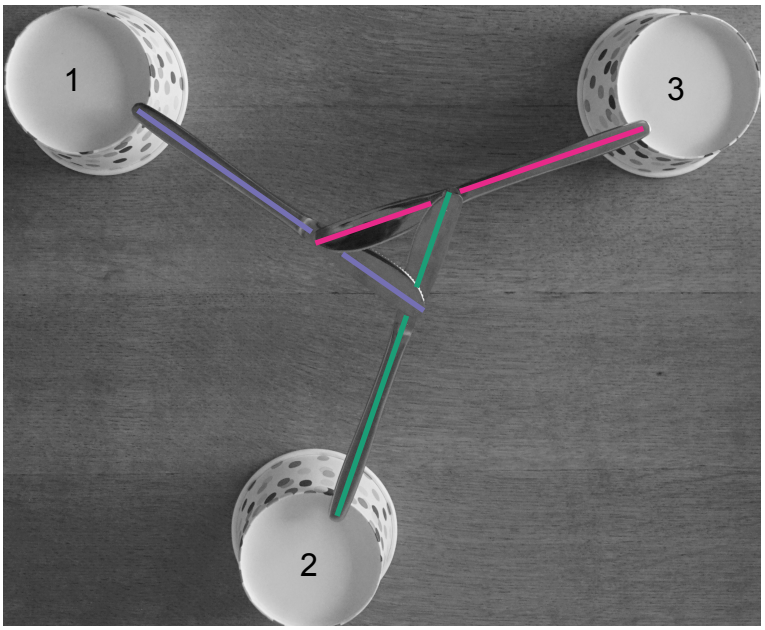

Figure 4.1: RF Criteria Demonstration

The demonstrating example fulfills all four criteria. Yet, not all structures labelled as RFs comply with the four criteria. Different standards are held for what a RF is. The common denominator is that RFs are structures that conform to criteria one and two. Few authors also require that a RF approves criterion three (Popovic Larsen, 2014; Pugnale, 2014).

Another group of authors demands that a RF must satisfy criterion four (Kohlhammer, 2013; Mesnil et al., 2018; Pugnale et al., 2014). The result of this ambiguous definition is that today the term RF refers to a family of structural systems, rather than to one specific type. Consequently, if the term RF is used in this report, it is referred to a family of structural systems whose constituents comply with criteria one and two and possibly with criteria three and or four.

The meaning of the term RF suits such a general definition, for it only relates to one of the four criteria. The word reciprocal originates from the latin word reciprocus which is a combination of the two words recus and procus. The translation of these words is backwards and forwards respectively and thus relates to the mutual support criterion (Pugnale et al., 2014). A frame is a structural system which consists of a skeleton of members that achieves stability without incorporating planar elements such as plates or slabs, i.e. bracing is achieved through rigid joints or one dimensional elements (Collins, 2021).

Only in the last few decades, the term RF gained importance. Before the term was coined, many different names were used to refer to structural systems belonging to the family of RFs (Bertin, 2001; Popovic Larsen, 2008; Pugnale et al., 2011; Pugnale et al., 2014). These include:

- Interlocking frame
- Lamella flock
- Leonardo's lattice
- Lever beam structures
- Leverworks
- Mandala roof
- Multi-reciprocal element
- Multi-reciprocal grid
- Mutually supported elements
- Nexorades
- Reciprocal structures
- Self-supporting framework
- Serlio floor

Today, the term reciprocal frame is most accepted. Other terms continue to be used synonymous.

4.1.2. Context

The timeline in figure 4.2 displays examples of RFs that point to important aspects of the structural system's historical development. For a detailed chronological account, refer to Larsen (2008) or Thönnissen (2015).

RFs do not have one clear origin. There appear to be independent accounts of RFs in Eastern and Western culture. Well-known early examples are the Chinese Rainbow Bridge and Honnecourt's planar grillage (Popovic Larsen & Lee, 2014; Pugnale, 2014).

Throughout the following centuries, several individuals designed and investigated structural systems which in retrospect are classified as RFs. Among the designers are renowned thinkers such as Renaissance polymath Leonardo Da Vinci and English clergyman and mathematician John Wallis.

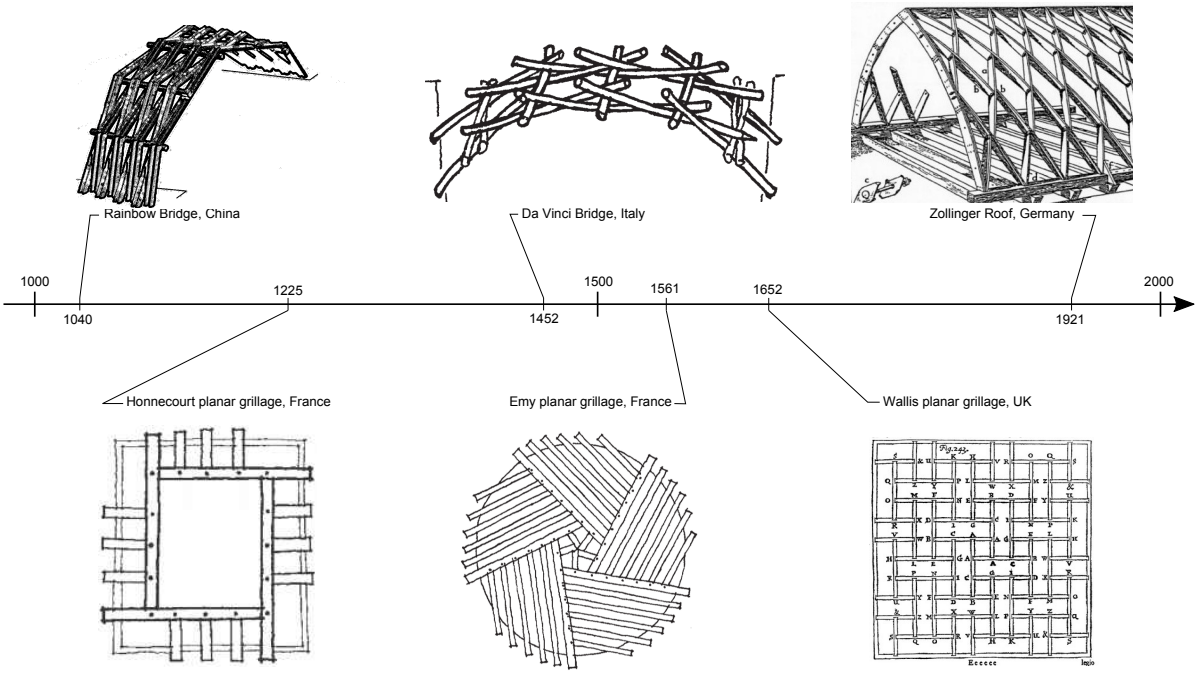

Figure 4.2: RF Historical Timeline; Image Credits from top left: Rainbow Bridge (Viscardi et al., 2011), Da Vinci Bridge (Popovic Larsen, 2008), Zollinger Roof (Nan, 2016), Honnecourt Grillage (Popovic Larsen, 2008), Emy Grillage (Popovic Larsen, 2008), Wallis Grillage (Houlsby, 2014)

Da Vinci designed a self supporting bridge reminiscent of the Rainbow Bridge (Popovic Larsen, 2008). Wallis analyzed the internal forces of the planar grillage displayed in the bottom right of figure 4.2 (Houlsby, 2014). Where Da Vinci and Wallis focussed on the theory, other individuals considered RFs more practically. For instance, the engineers Amand Rose Emy and Friedrich Zollinger. Both utilized the RF to solve the problem of material scarcity at their time. Emy considered reclaimed timber beams for his planar grillages (Thönnissen, 2015). Zollinger's roof was an effective response to high material costs and low labor wage, as it reduced the amount of material to 60% of a conventional timber roof structure of the time (Kohlhammer, 2013).

The british engineer Tredgold reasoned that the RF is "more curious than useful" (Popovic Larsen, 2008). With this statement he draws attention to the issue that on the one hand thinkers and builders have been fascinated with RFs, on the other hand the structures find little application. This fact might also be a reason for why RFs did not experience an unequivocal effort for further development until scientific research gained interest in them about 30 years ago.

Pugnale and Sassone categorized the main publications on RFs up to 2014 into 14 subtopics (2014). Both architectural and engineering aspects are considered. A large part of the relevant research was published in the *Nexus Network Journal*. Two important standard works on RFs are Larsen's *Reciprocal Frame Architecture* (2008) and Thönnissen's *Reciprocal Frameworks - Tradition and Innovation* (2015).

Outside of a relatively small group of curious architects and engineers, RFs remain largely unknown. Many of the built historical examples decayed and the RF remains to be an uncommon structural solution. Consequently, the percentage of RF buildings is negligible. The application of RFs appears to often require a special boundary condition that justifies the considerable design efforts for the structural system.

The following four buildings provide examples for boundary conditions in which RFs were considered as a viable solution. The associated photographs also highlight the variety of structural systems which belong to the family of RFs.

The Bunraku Puppet Theatre exhibition hall in Seiwa, Kumamoto Prefecture of Japan is a prominent example of a spatial roof structure composed of a single unit RF. In this case the place itself forms a special boundary condition. Japan is home to a relatively large number of RFs. Larsen reasons that this family of structural systems has the capacity to integrate qualities which are important in Japanese architecture (2008). Other RF examples in Japan are the Stonemason Museum by Yasufumi Kijima and the the Life Science Laboratory by Yoichi Kan.

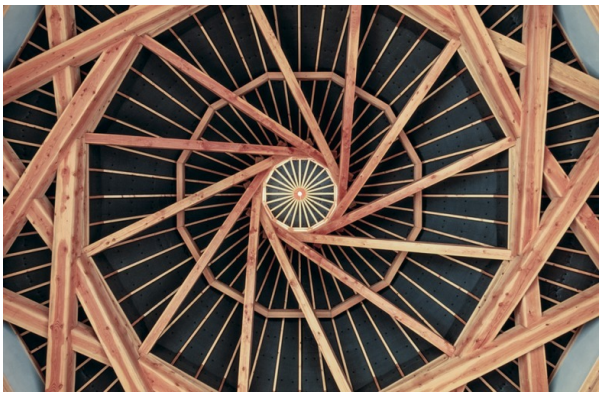

Figure 4.3: Roof Structure of the Bunraku Puppet Theatre Exhibition Hall in Seiwa, Japan (Apers, 2020)

A second boundary condition which makes RFs a candidate for a project are free-form shapes. The Mount Rokko-Shidare Observatory by Hiroshi Sambuichi, also placed in Japan, has an irregular RF pattern (Popovic Larsen, 2014). Another example for the close tie between RFs and free-form shapes are educational workshops that utilize RFs for exploratory form studies, for the documentation of a number of workshops, refer to Gelez (2011), Knau (2018), Parigi and Pugnale (2014), Popovic Larsen (2014), Thönnissen and Werenfels (2011) as well as Vrontissi and Thönnissen (2015).

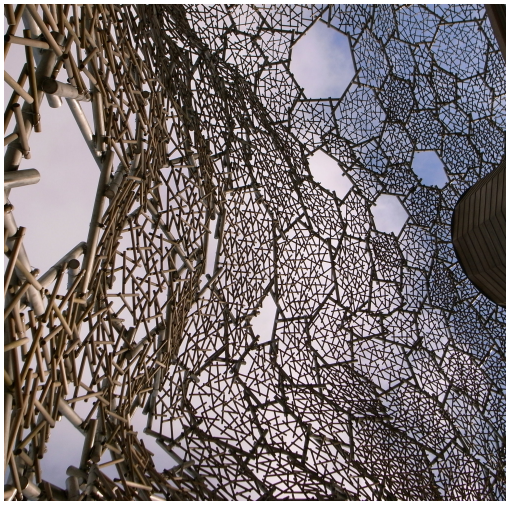

Figure 4.4: Free-Form Shape of the Mount Rokko-Shidare Observatory (Trout, 2010)

Temporary structures have been a third field of application for RFs. One example is the Archaeological shelter at Bibracte, France. The canopy is built from steel profiles that are connected in a reciprocal manner. The RF units consist of identical lightweight elements which are assembled in a regular pattern without the need of heavy lifting equipment. The resulting structure is able to withstand high loads and extreme weather conditions (Danz et al., 2015). Another example for a temporary structure is the Kreod Pavilion designed by Chun Qing Li (Popovic Larsen, 2014).

Figure 4.5: Members of the Archaeological Shelter at Bibracte, France (Vaudeville, 2009)

An example that contradicts the notion that the application of RFs must be justified by a special boundary condition is the Community Center of the Mill Creek Public Housing Project II in Philadelphia by Louis Khan. In this building, a single unit planar RF with four members spanning 15 m is utilized in a building project without any of the above conditions, in a place where alternative structural systems would have sufficed (Lauf, 2017; Popovic Larsen, 2008).

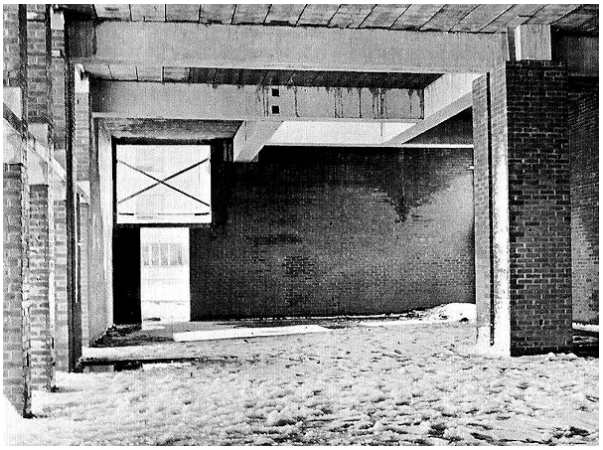

Figure 4.6: Community Center of the Public Housing Project II, Philadelphia; under Construction (Lauf, 2017)

4.2. Classification of Reciprocal Frames

In the previous section it was disclosed that RFs are a family of structural systems, the referenced examples demonstrate the diversity of this structural family. In this section the variety of RFs are sorted into a framework that is illustrated in figure 4.7.

The four boxes of the figure's second row refer to attributes that describe how individual RF units relate to each other. For each of these attributes two or three classes are defined. A specific RF structure can be described by matching it with one class of each attribute. For instance, the RF of the Mount Rokko-Shidare Observatory is an irregular, single-layer surface RF with multiple units.

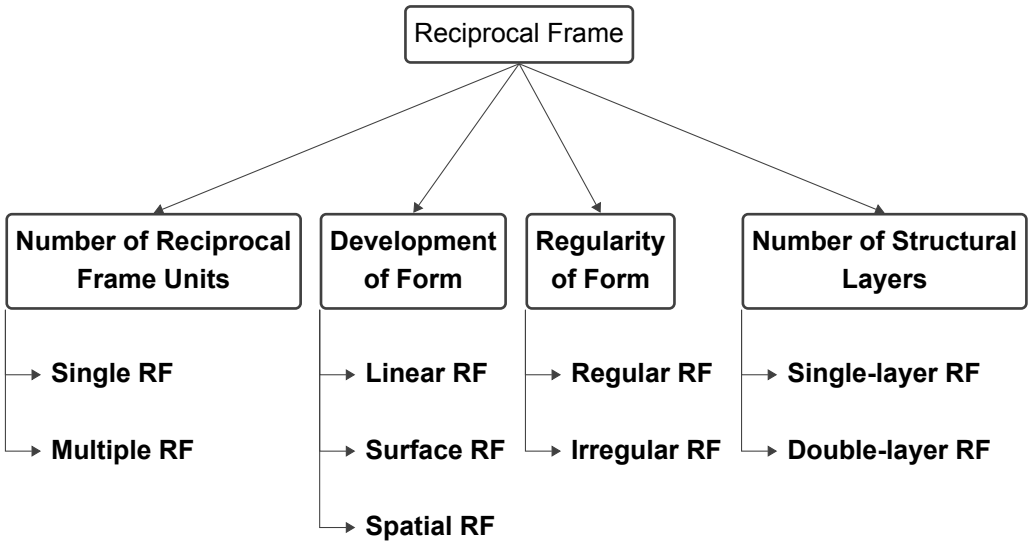

Figure 4.7: Classification of RFs by four Attributes that describe the Relation between RF Units

The proposed classification takes the most important aspects into account. Yet, it is not exclusive. The classification could also be done in a slightly different manner. For instance, this classification focuses on the relation between units, a different classification might focus on the geometric parameters of an individual unit. In this study the unit parameters are discussed separately in subsection 4.3.3.

The four attributes and the associated classes are described in more detail below. For illustration of the classes it is referred back to the examples in the previous section.

4.2.1. Number of reciprocal frame units

There are two classes of RFs that can be distinguished according to the number of RF units. Single RFs consist of only one RF unit, see figure 4.8a. Multiple RFs consist of more than one RF unit, see figure 4.8b (Popovic Larsen, 2008). Built examples are the Bunraku Puppet Theatre exhibition hall and the Mount Rokko-Shidare Observatory respectively.

(a) Single RF **(b)** Multiple RF

Figure 4.8: RF Classes for Attribute Number of RF Units

4.2.2. Development of Form

To develop a RF in x-number of directions means that RF units are added on to a starting unit in x-number of directions. With regards to the development of form Thönnissen distinguishes three classes of RFs (2015):

Linear RFs are developed in one direction. Examples are the Rainbow Bridge and the Da Vinci Bridge, which were both displayed on the historical timeline. This class of RFs will be discussed in more detail in section 4.5 . Surface RFs are developed in two directions. Resulting surfaces can have a single or a double curvature. A special type of the surface RF is the planar RF. An example for a surface RF is the Mount Rokko-Shidare Observatory; the archaeological shelter at Bibracte is a planar RF. Spatial RFs are developed in three directions. This class has primarily been subject to architectural form exploration, refer to Parigi for an example (2014).

The name of the classes is to be understood with regards to the development of the form and not as indicative of the number of dimensions in which the final structure expands. From the mentioned examples, it is clear that not only the spatial RF has a three-dimensional form. Also the linear and the surface RF are spatial arrangements, planar formations are the exception.

4.2.3. Regularity of Form

With regards to the regularity of the form, two classes of RFs can be distinguished. Regular RFs have identical members, i.e. members with the same geometric and mechanical properties, as well as identical joints. Consequently, the structure is a repetition of one and the same RF unit. Irregular RFs have either members with varying properties or diverse joint details (Parigi et al., 2014).

The efforts related to structural design, fabrication and assembly are lower for a regular RF than for an irregular RF. Zollinger's roof and the archaeological shelter at Bibracate are examples for regular RFs. The Mount Rokko-Shidare Observatory is an example for an irregular RF, because the joint details differ.

4.2.4. Number of structural layers

Single-layer RFs and double-layer RFs differ by the number of geometric layers that participate in the force transfer. Most RFs have one structural layer. A benefit of a double-layer RF is an increased structural robustness. Furthermore, the added structural height increases the structural capacity. The major disadvantage of double-layer RFs is an increase in geometrical complexity. All examples in section 4.1 are single-layer RFs, for an academic investigation of double-layer RFs, refer to Douthe and Baverel (2014).

4.3. Characteristics

This section examines characteristics that influence the structural design and behavior of RFs. The two defining criteria that apply to all RFs are revisited and their implications for the structure are discussed. Consecutively, the parameters that control the geometry of the smallest repeating unit of members in a RF, a RF unit, are described. Lastly, the joint design of RFs is addressed.

4.3.1. Geometrical and structural interdependence

The criterion of mutual support implies a “structural interdependence” and a “geometric interdependence” between the members of a RF (Parigi & Kirkegaard, 2014; Thönnissen, 2014, 2015). The two introduced terms are defined:

- Structural Interdependence: If one member is stressed, all other members are stressed
- Geometric Interdependence: The position of a member is not only determined by its neighboring members, but by all members of the structure

These relations are made more concrete by formulating their consequences for the structural behavior and the design process.

First, the structural consequences are considered. The structural interdependence implies that the RF is a redundant structure, i.e. loads are taken down via multiple load paths. However, the RF is not a robust structure because in case of local failure the geometric interdependence implies a progressive collapse. This can simply be illustrated with the demonstrating example from subsection 4.1.1. If one of the knives experiences a load, all knives participate in the load take down (redundancy). Further, if one of the knives is removed, the remaining knives will fall to the ground (lack of robustness). There are a number of approaches to prevent progressive collapse in a RF, these are applicable primarily in structures that belong to the multiple RF class. For instance, joints can be detailed to transfer bending and torsional moments (Godthelp, 2019). An alternative is to utilize an attached cladding as a secondary structural system which is activated in case of local failure (Thönnissen, 2015).

Two more structural issues must be addressed in relation to the geometric interdependence. RFs tend to have large deformations because the global deformation is the sum of the deformations of all members. Moreover, the assembly of a RF requires extra care because small changes in geometry have a large influence on the global form. Deviations in the assembled structure relative to the original design may evoke stresses which were not accounted for (Larena & Ménendez, 2014).

Lastly, the consequences of the structural and geometric interdependence for the design process are reviewed. In contrast to the simplicity of developing the geometry of an individual RF unit, which was demonstrated in subsection 4.1.1, stands the complexity of determining the geometry of a multiple RF for a predetermined shape. This complexity stems from the geometric interdependence which requires that geometrical constraints are respected for each individual unit, but also in between units. In most cases, finding the geometry for a RF consisting of multiple units requires an elaborate “geometry generation” (Mesnil et al., 2018). The term geometry generation and the associated process are described in subsection 4.4.1.

4.3.2. Load-bearing Mechanism and Detailing

The second defining criterion distinguishes the RF from structural bar assemblies such as trusses, grid-shells, and space frames. While the named bar assemblies also have the capability to span distances longer than their structural member’s length, members meet at their endpoints. In a RF the members meet along the span with an eccentricity between the members’ axes. This property has two major implications for the structural behavior of RFs.

The first consequence is that bending is the main load-bearing mechanism of RFs (Douthe & Baverel, 2014; Thönnissen, 2015). Each member acts as a single span beam. The second consequence is that a RF can resist out of plane forces with hinged joints. Through a comparison with a pinned and a rigid grid-shell, which are introduced in the following two paragraphs, the named properties of RFs are evaluated.

In a pinned grid-shell, members are connected through hinged joints. This structural system is a form-active structure according to the definition of Engel (1967). That implies that the form of the structure is found for one dominate load combination, so that a single stress state is present in the structural members. Ideally, only compression forces are acting. A pinned grid-shell may react unstable to load cases that differ to the one that was considered in the form-finding procedure (Kohlhammer, 2013).

The joints of a rigid grid-shell are moment resistant. The structural system is a semi-form-active structure according to the definition of MacDonald (2019), i.e. form and force are independent of each other. Besides axial thrust, bending and torsion can be transferred. The bending moments in the structural members are smaller than in a post-and-beam structure with equivalent span. The moments' magnitude depends on the extent to which the shape is different from the form-active shape for the acting loads (Kohlhammer, 2013). Grid-shells transfer forces primarily through axial thrust, in contrast RFs transfer forces mainly through bending. The RF is inferior to the grid-shells from a perspective of structural efficiency because bending action is a less efficient mechanism than axial action.

Hinged joints are less elaborate in detailing than moment resistant joints, thus less expensive in their execution. Pinned grid-shells have both the more efficient force transfer and the more effective joint detail. This sets this structural system apart from the other two. However, the pinned grid-shell is not an effective solution for structures with multiple load distributions that have very different results in form-finding. The rigid grid-shell is capable to resist multiple load distributions, but it demands the more elaborate moment resistant joints. The RF is capable to transfer bending moments with pinned joints, i.e. it is capable to resist a variety of load distributions with joint details that do not need to transfer moments. This property can give the RF an edge over grid-shells in spatial bar assemblies with a large number of joints and more than one governing load distribution with varying corresponding forms (Kohlhammer, 2013).

It is concluded that the property of spanning distances longer than the structural member's length is not unique to RF structures. Thus, the utilization of RT is not predetermined to be combined with RFs. However, the RF is a favorable structural system for the utilization of RT because spatial bar assemblies can be detailed with hinged joints.

4.3.3. Geometric Parameters

A set of geometric parameters determines the form of a RF. The geometry of a regular RF can be described by the parameters that define an individual unit. Different sets of parameters can be used to describe the geometry of RFs. Figure 4.9 visualizes the parameters that were introduced by Thönnissen (2015): Engagement length a, excess length o, eccentricity e, member dimensions h, w and L, number of members per unit n and the rotational direction. The unit in figure 4.9 is regular, i.e. the parameters of member two and three are identical to those of member one. The influence of the parameters on form and structural behavior of a RF are described below.

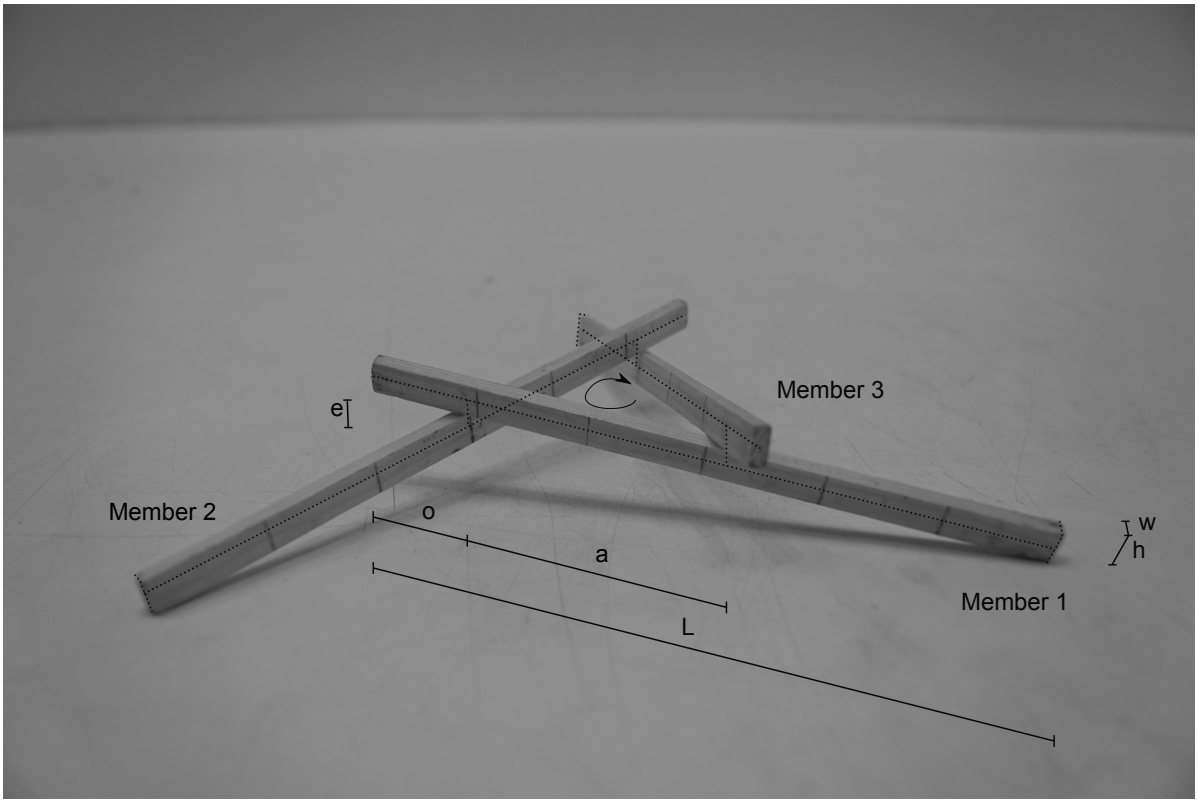

Figure 4.9: Geometric Parameters of a RF visualized on a Three-Member Unit

Number of members per reciprocal frame unit

RF units are the smallest repeating unit of members in a RF. The number of members per RF unit depends on the RF's development of form. Linear RFs always have two number of members per unit, compare section 4.5. A surface RF has at least three members per unit. The three-member unit is advantageous for a surface RF. The stable triangular arrangement has benefits for assembly and load takedown. The four-member unit is unstable when connected with hinges for both planar and non-planar situations.(Godthelp, 2019; Kohlhammer, 2013; Parigi & Kirkegaard, 2014; Thönnissen, 2015).

Eccentricity

The eccentricity is the distance between the center axes of the members that are connected in a joint. The exact positions on the center axes that mark the endpoints of the eccentricity line depend on the joint detail. On the one hand, the eccentricity influences how forces are transferred in the joint. On the other hand, by determining the form of the RF, it also alters the flow of forces in the structure. For instance, a zero eccentricity results in a planar RF. Planar RFs transfer forces only through bending. If the eccentricity is non-zero, the RF develops a non-planar form, this causes normal forces to run through the structure.

Engagement length

The engagement length is the distance between the support point and the supporting point of a member. An increase in engagement length causes the RF unit to decrease the angle with which the members are sloped. Besides its influence on the form, the engagement length also has a significant influence on the bending resistance of a RF unit. With an increase of engagement length, the leverarm between the members increases and the bending moments in the structural members decrease. This is illustrated for a single RF unit and a RF with multiple units in the following paragraphs.

Figure 4.10 displays a four-member unit of a surface RF with three different values for the engagement lengths in the x- and y-direction. On the first image the engagement length a is identical in both directions. It is approximately one third of the member length.

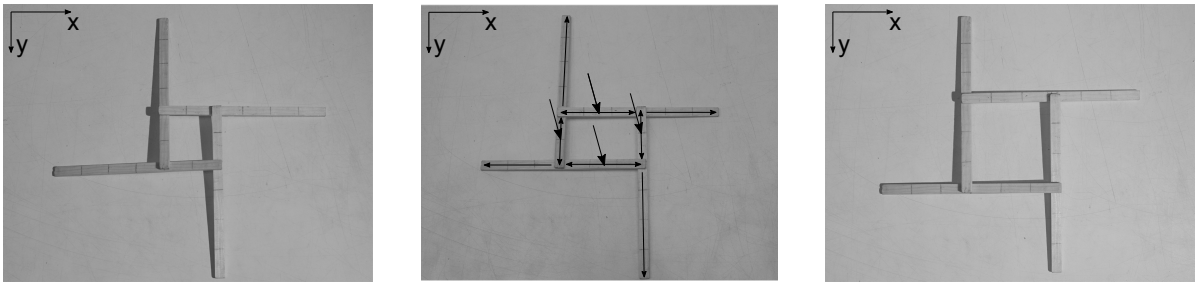

(a) Engagement Length is a third of the Member Length

(b) Engagement Length differs in X- and Y-Direction

(c) Engagement Length is half of the Member Length

Figure 4.10: Engagement Length Observation Single RF Unit

In the second image the engagement length in the x-direction is set to half of the member length, while the engagement length in the y-direction does not change. It is observed that when lifting the individual members while a force is applied as displayed, most of the load is taken down in the x-direction, the direction with the larger engagement length. It is concluded that the bending stiffness in this direction is larger. In the third image the engagement length of both directions is set to half the member length. From the intermediate step it is concluded that the bending stiffness in this arrangement is larger than in the initial arrangement. In other words the resulting bending moments are smaller. The reasoning for the named relation between engagement length and bending stiffness is confirmed by an analytical model in appendix B.1.

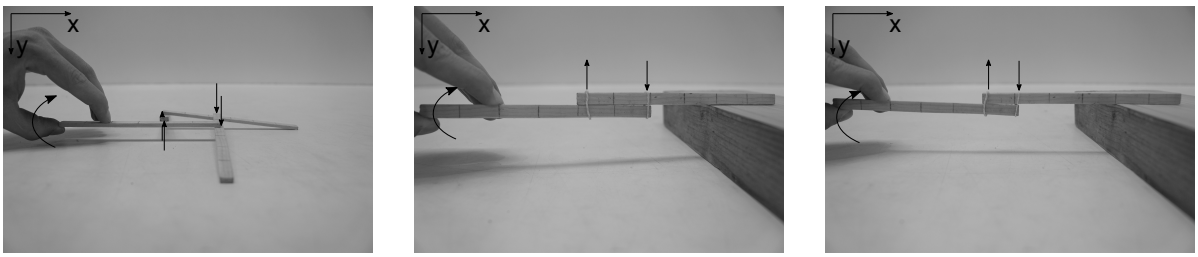

(a) RF Unit loaded with a Moment

(b) Simplified 2D Model with $a = 1/3L$

(c) Simplified 2D Model with $a = 1/6L$

Figure 4.11: Engagement Length Observation Multiple RF Unit

With the help of the physical models displayed in figure 4.11, it is reasoned that the trend for the bending stiffness in relation to the engagement length is valid also for RFs with multiple units.

The first image shows a RF unit loaded with a moment; this moment represents the forcing that is applied from a unit which would be attached here. Arrows indicate the loads that are transferred in the joints. To make the relation more obvious, the second and third image illustrate a simplified two-dimensional model of the first image. Again the engagement length is varied. The models demonstrate that a larger engagement length is equivalent to a larger lever arm of the RF unit. Thus, it also holds for a multiple RF that a larger engagement length reduces the internal forces that act in the structural members.

Member dimensions

The member dimensions, illustrated in figure 4.9 , also contribute to the final form of the RF. The length of a unit's members determines the density of the RF grid and thus influences the global structural resistance. If cross-sectional height and eccentricity are coupled, the height influences form and structural behavior as does the eccentricity. Moreover, the cross-sectional height is a key contributor to the bending resistance and the cross-sectional width is an influential parameter for member stability.

Rotational direction

For a surface RF, the rotational direction is an additional geometric parameter. It determines how two members meet in a joint. The rotational direction is defined by the direction of the supported member in relation to the supporting member. The two possible directions are clockwise (CW) and counterclockwise (CCW). The three-member unit in figure 4.9 is arranged CW, the four-member units in figure 4.10 are arranged CCW.

Excess length of the member

This parameter describes the length of the supported member that extends over the supporting member. The excess length of the member is often set to zero unless the joint geometry benefits from an overhang. This part of a member does not participate in the load take-down except that an external force is introduced along the excess length.

4.3.4. Joint

The comparison between RFs and grid-shells in subsection 4.3.2 highlighted that joints have a major influence on both form and structural behavior of bar assemblies. In this subsection the relation between detailing the joint geometry and the form of RFs is elaborated. Moreover, three categories of RF joints as suggested by Thönnissen are reviewed to inform the choice of a joint in the structural design case study (2015).

Interaction between joint design and form

The most important link between the joint design and the form of a RF is the geometric parameter eccentricity. The final geometry of the joint determines the eccentricity of the structure. At the same time, the eccentricity is a key parameter in the geometry generation, see subsection 4.4.1.

Consequently, there are two ways to approach the design of a RF. One, the design of the joint detail is based on the results of the geometry generation. Two, the detail of the joint is designed and the resulting eccentricity of the joint is used as constraint in the geometry generation. Subsection 4.4.1 provides examples for the two ways of approaching the detailing of joints.

Contact-bearing Joint

The detail of the contact bearing joint suggests to stack two connecting members on top of each other. Vertical forces are transferred via contact and horizontal forces through friction. The eccentricity parameter equals to the member height and cannot be varied independently. As members are positioned above each another, only forms with a positive Gaussian curvature are possible with this joint type (Parigi & Kirkegaard, 2014). Examples for the contact-bearing joint are the physical models that were used to illustrate the geometrical parameters, see figures 4.9, 4.10 and 4.11.

The joint's fabrication requires minimal effort; no additional components need to be produced. However, the simplicity of the joint detail induces a global complexity. For this joint to work, positioning needs to be exact, this also requires small tolerances in fabrication and assembly of structural members. During the assembly of a RF with this joint type the structure is not stiff, thus temporary supports are required (Gustafsson, 2016).

Lastly, although connection elements are not required for the force transfer, for reasons of safety against uplift and to ensure that members stay in their position, fasteners do need to be applied (Gustafsson, 2016).

Addition Joint

An addition joint contains one or more supplementary connection elements. Two groups of details are contained within this category, the coupler joints and the dowel and plate joints. The eccentricity of these joints can vary and in some cases be decoupled from the member height.

The coupler joint has a connection element that presses structural members against each other. Forces are transferred via the additional device, which depending on the exact detailing constrains translations and or rotations. An example for a coupler joint is the contractible clamp as discussed by Larsen and Rizzuto (2010), Castriotto et al. prototyped a clamp visualized in figure 4.15a, that constrains translation and rotation (2021). Another coupler prototype that only constrains translation is the bilateral joint as introduced by Parigi et al. (2014), see figure 4.12a.

The dowel and plate joints are characterized by additional connection components that pierce through both members. The force transfer is dependent on the exact detailing. Generally the translation is constrained and the rotational stiffness is partially constrained. Slip may be an issue with this type of joint (Gustafsson, 2016). An example for a dowel and plate joint is the conventional timber joint detail "joist hangar".

The fabrication of addition joints requires the production of one or more additional connection elements. Often, the structural members also need to be manipulated at their ends. For some joint details, RF units are already form-stable during assembly (Gustafsson, 2016).

Subtraction Joint

The subtraction joint integrates the joint and the members by locally notching the cross-section of one or both members. For an example of a structural member with notches, refer to figure 4.13a. Larsen states that this joint is the most common among RFs (2008). In most cases the eccentricity of this joint is smaller than the member height.

The character of a notched joint generally induces a torsional moment in the members. Furthermore, the local reduction of the cross section reduces the load bearing capacity of the members. If the notch is close to the center of a member, the bending resistance is reduced significantly. If the notch is close to the end of a member, the shear capacity is reduced (Gustafsson, 2016; Rizzuto & Popovic Larsen, 2010).

The production of a notched joint requires the manipulation of the members. This may potentially be executed in a cost effective and time saving manner through digital fabrication. However, this infers a dependency on available machinery; the degree of notch design complexity may not exceed the capability of the machines (Gustafsson, 2016).

The process of assembly depends on the type of notch. Deep notches are complicated to assemble, other notch formations can be quick to assemble and disassemble. For the assembly process a certain amount of leeway is required in the notches. Once assembled, this leeway will contribute to the global deformation of the structure. Examples for notched joints are the half lap joint, the mortise and tenon joint and the dovetail (Gustafsson, 2016).

4.4. Design Aspects of a RF Canopy

In this section three aspects that are important to the design of a RF structure are discussed. It is explained how a RF geometry can be generated, so that it complies with all geometric constraints. In a second part, design aspects that benefit the assembly of RFs are addressed. Lastly, different options for cladding a RF structure are elaborated.

4.4.1. Geometry Generation

RFs are capable of utilizing members with varying geometries to generate standard forms, a project that employs this concept is the research by Parigi, that was illustrated in figure 1.4b in chapter 1 (2021). The more prominent way to apply RFs is to generate non-standard forms from short and straight members (Parigi et al., 2014; Popovic Larsen, 2014; Thönnissen, 2015; Vrontissi & Thönnissen, 2015). An expressive example is the Mount Rokko-Shidare Observatory, see figure 4.4. How such a geometry can be developed will be elaborated in this subsection.

A RF consists of RF units. Once a RF type is specified, the geometrical parameters of the units need to be determined so that the RF form satisfies the design brief of a given project. Besides achieving a desired global form, the core problem of specifying the geometric parameters is to satisfy the geometrical constraints involved in connecting the individual RF units (Popovic Larsen, 2008).

In this project, the process of solving for the geometric parameters is called “geometry generation”. This term is used instead of the name “form-finding”, which is commonly used in literature. From a structural perspective the term form-finding is associated with a different process. In structural engineering form-finding refers to the process of identifying the structurally most efficient geometry for a given load case. A grid-shell is an example for a structural system that utilizes form-finding during the design process. Different to the form-finding of grid-shells, the geometry generation of RFs does not involve a structural analysis, but is a purely geometric exercise.

The geometry generation can be approached in three ways. When choosing an analytical approach, the geometric parameters are the input of the geometry generation, the RF geometry can be controlled by altering the geometric parameters. Because existing analytical methods are restricted to Platonic solids in their application, the analytical approach is not further discussed here (Godthelp, 2019). When employing a top-down approach, a RF geometry is fitted to an initial base geometry. Lastly, the bottom-up approach assumes a set of geometric parameters for one RF unit, then the RF is developed by adding units on to the sides of the first unit. The top-down and the bottom-up approach will be described in more detail below.

Top-Down Approach

There are a variety of methods that apply the top-down approach. Most methods, begin by defining a base surface and continue by utilizing an algorithm for generating a RF geometry onto the surface. The principle of optimization in combination with genetic algorithms is the core of most methods.

With the top-down approach free-form surfaces can be achieved. This comes at the cost of irregularity in the RF because at least one of the geometric parameters engagement length, eccentricity or member length is needed as variable for the optimization. As a result, either joint geometry, member geometry or both vary across the RF. A number of top-down methods are presented below.

The “Reciprocalizer” fixes the eccentricity parameter, so that the resulting RF has only one type of joint detail. Engagement and member length are determined through an optimization so that the resulting RF geometry approximates the base surface. Figure 4.12a illustrates the joint detail of an one application of the Reciprocalizer. Figure 4.12b shows the RF geometry that was fitted onto a predefined free-form surface for the same application (Parigi & Kirkegaard, 2014).

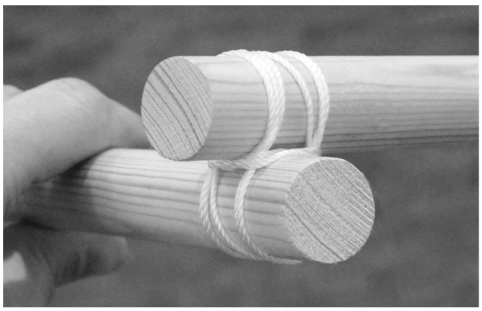

(a) Bilateral Joint

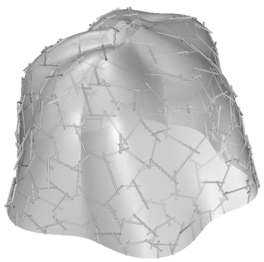

(b) RF Geometry fitted onto a Base Surface

Figure 4.12: Application of the “Reciprocalizer” (Parigi & Kirkegaard, 2014)

In contrast to the Reciprocalizer, the “Timber Reciprocal Frame Designer” uses the eccentricity as parameter for fitting the RF geometry onto a predefined base surface. The varying eccentricity is coped with by customized digital fabrication of notched joints, i.e. the notch depth of the members differ (Godthelp, 2019). Figure 4.13 shows a member of a RF that was designed with the Timber Reciprocal Frame Designer and the scale model of a cupola that also comes forth from the application of this method.

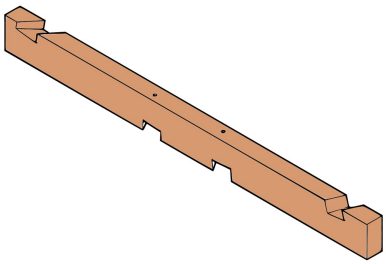

(a) Member with varying Notch Depth

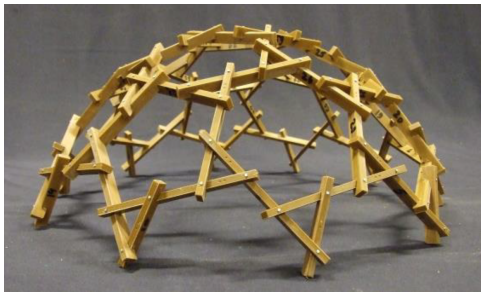

(b) Scale Model of a RF Cupola

Figure 4.13: Application of the “Timber Reciprocal Frame Designer” (Godthelp, 2019)

Another set of top-down methods does not use a base surface but an abstract planar representation as starting point. The resulting RF geometry is also generated through an optimization. An example for this method is the “form-finding tool” that was developed by Thönnissen (2014). In this case, the planar represenation is comprised of cells and cell relations. An example for the application of the form-finding tool is displayed in figure 4.14.

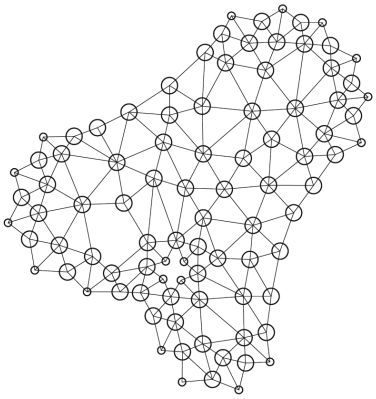

(a) Abstract Representation of a RF

(b) Resulting RF Structure

Figure 4.14: Application of Thönnissen’s “Form-Finding Tool” (Thönnissen, 2014)

A top-down method that achieves to reduce irregularity to a minimum is introduced by Castriotto et al. (2021). Two type of members that differ only in the cuts that are conducted at member ends suffice to construct the structure. Due to a minimal engagement length, the joints of a RF unit are integrated into one central clamp, see figure 4.15a. The joint detail is the same throughout the resulting structure which is displayed in 4.15b. From a perspective of fabrication and ease of assembly and disassembly, this structure is favorable.

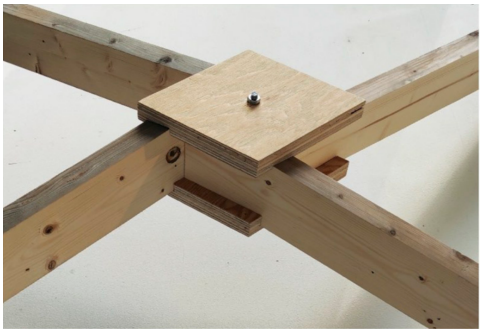

(a) Joint Design of the Clamp Link (Castriotto et al., 2021)

(b) Resulting RF Structure (Castriotto et al., 2021)

Figure 4.15: "Clamp Links" Project by Castriotto et al. (2021)

During a workshop that was participated in as part of this Master Thesis, the canopy structure displayed in figure 4.15b was assembled anew for an exhibition. It was concluded that while the short engagement length allows for a beneficial assembly, from a structural perspective the short engagement length and the detailing of the joints as moment-resistant clamps makes the structure reminiscent of a rigid grid-shell. However, because the joint is detailed according to the second defining criterion of RFs, namely the members do not meet in one point, the transfer of normal forces is inefficient.

The input parameters for the top-down approach differ per method. Either shape and size of the base surface as well as division of the mesh or the abstract representation of the RF geometry are to be defined by the user. Each of the methods also has at least one additional parameter which can be used to manipulate the resulting RF geometry. But neither the direct manipulation of the geometrical parameters of individual units, nor the prescription that the resulting RF geometry is regular are possible with the top-down approach.

Bottom-Up Approach

Different to the top-down approach, the bottom-up approach does not assume a base surface at the start, instead the RF form is a result of consecutively adding units onto each other. Figure 4.16 illustrates the bottom-up approach, the form is developed in two directions, a surface RF is the result.

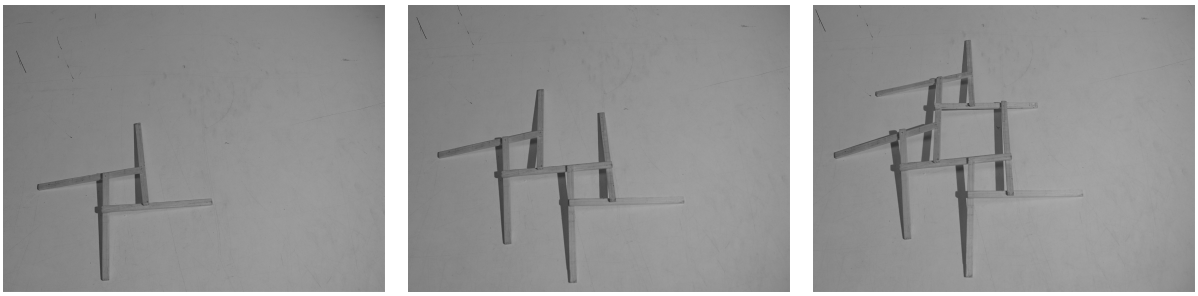

Figure 4.16: Bottom-Up Approach

Where the top-down approach is generally bound to the application of software, the bottom-up approach is primarily employed in the context of physical modelling. In this way, RFs' potential geometries and the related freedom of form can be explored intuitively. According to Pugnale et al. the bottom-up approach cannot be implemented computationally (2014).

Moreover, Godthelp argues that it is difficult to reconcile geometric requirements of a building design with this approach because input parameters are related to the RF units and not to the global form (2019). However, in the context of designing with RT, a bottom-up approach could be advantageous. If a bottom-up method would be programmed to use a material stock of RT members as input, then this method could solve the problem inherent to RT, that is designing from a limited stock of material, see section 3.4.2.

4.4.2. Assembly

It is common for spatial structures such as space frames and grid-shells that numerous detail drawings and a long on-site erection are required. The two primary reasons for that are convoluted joinery and geometric complexity of the global form (Koning, 2018). The design of a RF can mitigate issues related to assembly by considering the following points.

The time for on-site erection and related labor costs are majorly influenced by the joint design. The detailing of the joint determines the necessary time and effort for it to be put in place. If the fourth defining criterion is complied with and only two members meet in a joint, the detail and and also the assembly are simplified. An example for a joint in a RF that facilitates a quick assembly is the design of the umbrella-like structures of the Melilla Visitors Centre for Nature Interpretation in North Africa. The joint is displayed in figure 4.17, it permits rotation and translation of attached members until surrounding units are placed in their final position. Only after this has occurred, the joint is fixed (Apolinarska, 2018).

Figure 4.17: Joint of the Melilla Visitors Centre for Nature Interpretation, North Africa (Apolinarska, 2018)

A joint that can easily be put in place also reduces labor costs, for no expert work is required. Moreover, if the weight of the structural members allows, the assembly can be conducted without the use of heavy-duty lifting equipment and if members are short in length transport is possible without any costly extra-ordinary solutions.

The assembly can be prepared through developing a construction sequence that addresses each member individually. If members are marked with a corresponding index off-site, the duration of on-site assembly can be reduced further (Rizzuto & Popovic Larsen, 2010; Thönnissen, 2015). If the RF is not regular, the joints should be indexed as well. It is important to ensure accurate positioning, so that stress states that were not accounted for during the structural design are avoided. A RF might require temporary supports for this (Larena & Ménendez, 2014).

4.4.3. Cladding

Cladding covers the area below a RF and protects the structural members from external factors. The choice for cladding depends on the structure's function and should consider the ventilation and natural lighting that is required in the interior space (Danz et al., 2015). An additional function of cladding can be the bracing of the RF (Mesnil et al., 2018; Popovic Larsen, 2008). Materials that have been used for the cladding of RFs are timber lamellas, polycarbonate sheets and tensile fabrics (Apolinarska, 2018; Asefi & Bahremandi-Tolou, 2019; Danz et al., 2015; Thönnissen, 2015)

Thönnissen distinguishes three types of cladding (2015). The first type is a RF whose members have a plate form. The members of the RF serve as cladding themselves, this means that the members fully cover the surface of the structure. Asefi provides an example for a RF with this type of cladding, see figure 4.18a (2019). This example shows that not all RFs are designed as bar assemblies. Bar assemblies consist of structural members whose length is much larger than their cross sectional dimensions. Besides elongated and plate members, RFs have also been built by vertical panels, blocks and rings, for illustrations refer to Gustafsson (2016).

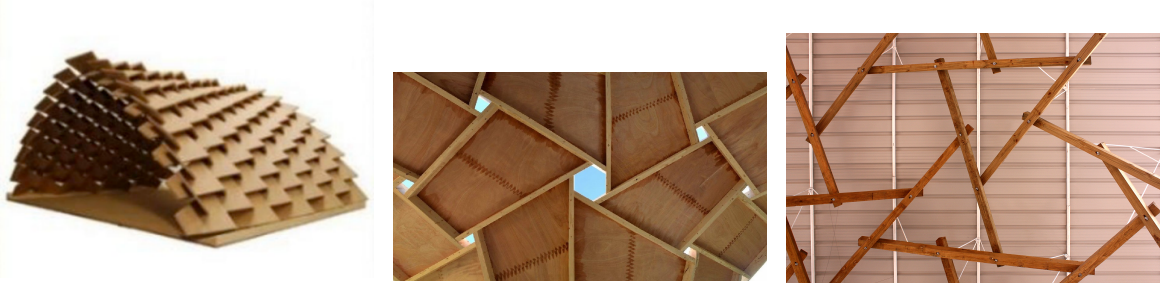

(a) Members act as Cladding (Asefi & Bahremandi-Tolou, 2019)

(b) Cladding on top of Members (Oval et al., 2019)

(c) Cladding with separate Connectors (Thönnissen, 2018)

Figure 4.18: Cladding Types

The second type attaches the cladding directly onto the RF structure. This requires that either the upper or lower edge of the RF members lay in one plane, so that panels or a layer of lamellas can be connected to the structure. An example for a structure that utilizes this type of cladding was designed by Mesnil, see figure 4.18b (2018). The third cladding type uses an additional element to connect cladding and RF. That means the cladding is not applied directly onto the load-bearing structure. This may be necessary when the members do not form a continuous surface. An example for this type of cladding is the Mkombozi Promenade Roof in Dar es Salaam, Tanzania, see figure 4.18c (Thönnissen, 2015).

4.5. Linear Reciprocal Frames

In preparation for the Structural Design Case Study, this section characterizes the geometrically less complex RF type "Linear RF''. It is favorable to choose a RF type with relatively low geometric complexity in a RT design because RT designs have in themselves a geometric complexity. This complexity stems from the fact that RT structures are built from a limited stock of material. Following this line of thought, Parigi (2021) and Damkilde and Parigi (2019) chose the geometrically less complicated RF class "Planar RF'' for their projects. In this study the Linear RF is selected instead of the planar RF because Linear RFs have the benefit of creating spatial assemblies.

The unit of a Linear RF is displayed in figure 4.19. It consists of two identical parts that are connected through transverse beams. The two parts are each comprised of two longitudinal beams, whose endpoints form a polygonal arch. The two identical parts are named “polygonal reciprocal frame arches” (PRFAs). The term PRFA refers to the longitudinal beams. In contrast, when the term polygonal arch is used, it is referred to the shape that is associated with the PRFA.

The members of a PRFA lay in separate planes. If the geometric parameter “number of members per unit” considers the members per PRFA, then this parameters is fixed to two because the PRFAs in the unit expand only in one direction. According to the description of RFs in the previous sections, adding a member in this direction would not mean to increase the number of members per unit, but to increase the number of units. The rotational direction is another geometric parameter that does not have meaning to this RF class because the members of a PRFA are developed in parallel planes and not in 3D space. For the same reason the third defining criterion for RFs is not satisfied; a unit as it is defined in this context that only expands in one direction cannot have members that are arranged in a closed circuit. The defining criteria one and two are complied with. The members mutually support each other and also meet along the span. Also criterion four is fulfilled, as only two members meet in one joint.

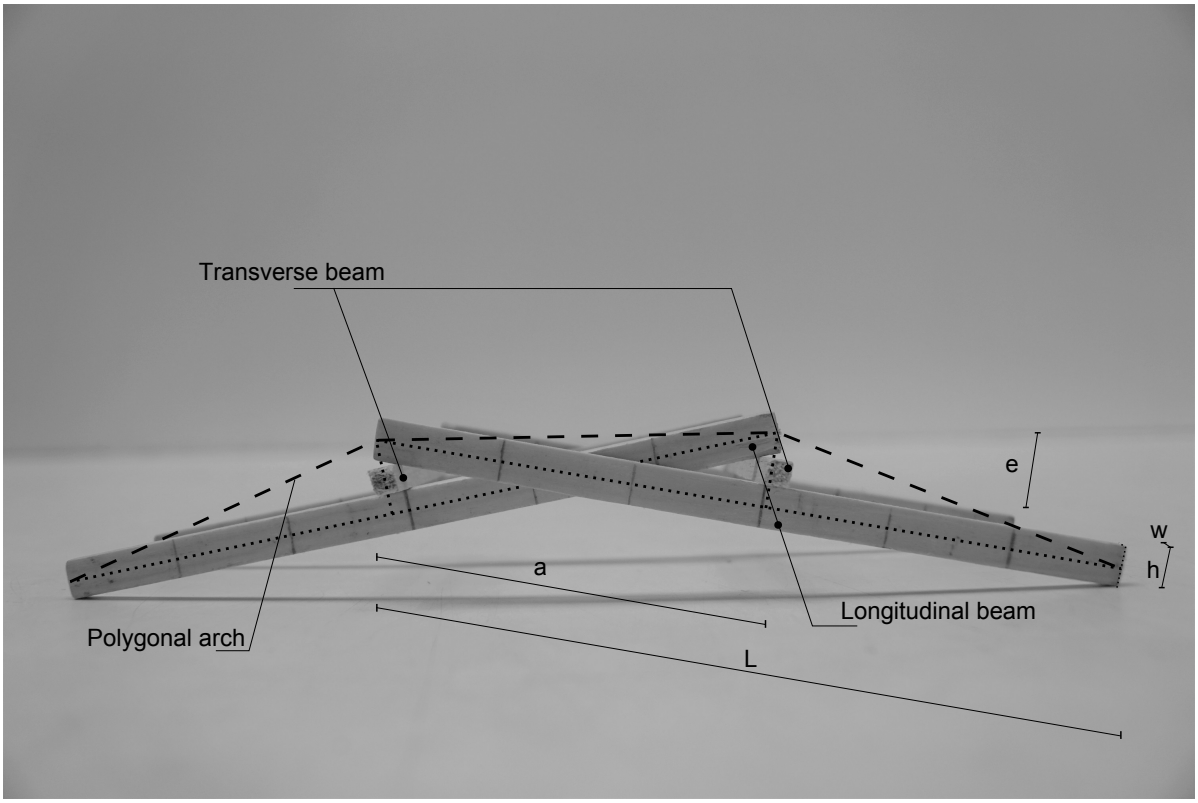

Figure 4.19: Linear RF Unit

The Da Vinci Bridge and the Rainbow Bridge are two historic examples of Linear RFs, compare section 4.1.2. Past applications have demonstrated that the RF arrangements of the two structures can also be applied to canopy constructions. An example is the Nishiiyayama Village Monorail Station in Tokusima, Japan, see figure 4.20. Instead of the names of the initial applications, in the following the terms “Da Vinci Reciprocal Frame” and “Rainbow Reciprocal Frame” are used to refer to the way the members of the respective RFs are assembled.

Figure 4.20: Nishiiyayama Village Monorail Station in Tokusima, Japan (Thönnissen, 2015)

4.5.1. Da Vinci RF

The Da Vinci RF does not fix any of the geometric parameters and thus is the more general of the two RFs. A none-zero excess length can be required depending on the joint detail, an example is the Da Vinci Bridge in which lashing requires excess length, see figure 4.2. An increase of excess length with constant member length decreases the span. The longitudinal and transverse members' height determine the eccentricity. An increase in eccentricity increases the curvature of the arc that runs through the vertices of the polygonal arch of a regular Linear RF. This is illustrated in figure 4.21. Due to the change of eccentricity the curvature in the right image is about 36% larger compared to the left image. This is visualized by drawing the associated arcs. The arcs do not perfectly coincide with the vertices of the polygonal arches due to inaccuracies in physical modelling.

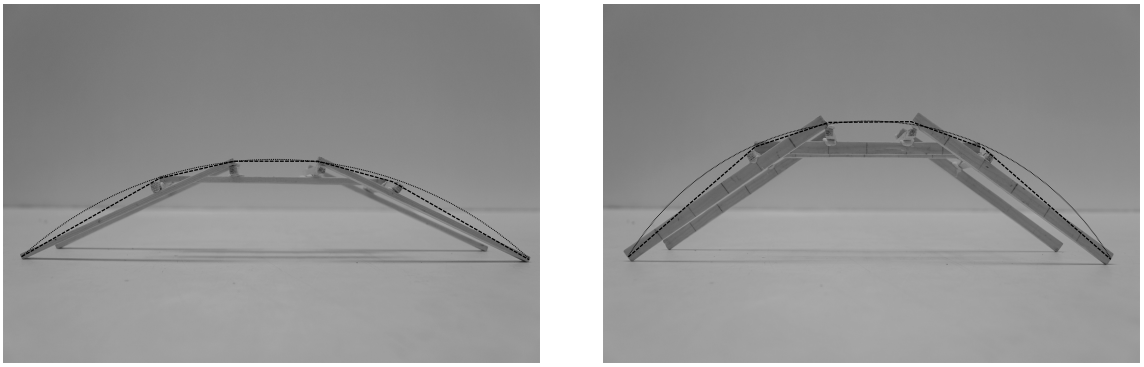

Figure 4.21: Da Vinci RF with two different Eccentricity Values

Figure 4.22 shows two Da Vinci RFs with different engagement lengths. The engagement length is approximately a third of the member length on the left and half of the member length on the right image respectively. A smaller engagement length leads to a larger curvature and also increases the span of a unit, if other parameters remain constant. From a structural perspective, it is desirable to set the engagement length to the maximum value of half the member length, see section 4.3.3. This specific Da Vinci RF also has the advantage that the number of required transverse beams decreases to almost 50% compared to the number of transverse beams in Da Vinci RFs with other engagement lengths. As a result the longitudinal members of one PRFA lay in three different planes and not in two, compare figure 4.25a.

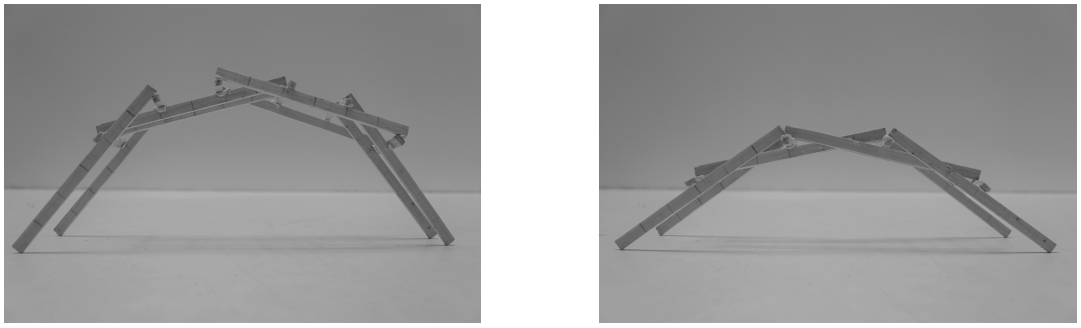

Figure 4.22: Da Vinci RF with two different Engagement Length Values

The images in this section show Da Vinci RFs with non-zero eccentricity and non-planar forms. In a non-planar RF, loads are not only transferred to the supports via bending moments, but also through axial action. From a perspective of structural efficiency this is beneficial. Nevertheless, for a structure according to the Da Vinci RF to transfer a normal force, at least one of the two longitudinal beams that are connected to a transversal beam at a vertex of the polygonal arch must be detailed as a moment resistant joint, else the structure will respond kinematic.

4.5.2. Rainbow RF

In the Rainbow RF, the engagement length is fixed to half of the longitudinal member length. Hence, transverse beams are located at the center of the longitudinal beams. The parameters that remain to manipulate the form of a Rainbow RF with a set number of longitudinal members are the eccentricity and the member length. These parameters influence the form as was described for the Da Vinci RF.

The excess length is fixed to zero because different to the Da Vinci RF the longitudinal members, which are supported by the same transverse beam, are placed in one plane. Thus the PRFA of the Rainbow RF can be considered as a composition of two interwoven arches, a main and an auxiliary arch. At the longitudinal ends of the Rainbow RF a member with approximately half the length of the other longitudinal members is placed, so that both of the interwoven arches connect to the foundation. The count of main arch members $n_{member,MA}$ and auxiliary arch members $n_{member,AA}$ is dependent on the number of polygonal arch vertices $n_{vertices,PA}$. The shorter longitudinal end members are included in the count.

$$n_{member,MA} = \lceil \left(\frac{n_{vertices,PA} - 1}{2} \right) \rceil$$

$$n_{member,AA} = n_{member,PA} - n_{member,MA}$$

If $n_{vertices,PA}$ is an even number, the main and the auxiliary arch are identical and mirrored. If $n_{vertices,PA}$ is an uneven number, then the number of members in the main arch is one less than the number of members in the auxiliary arch. Figure 4.23 shows a Rainbow RF with an even and and uneven number of members.

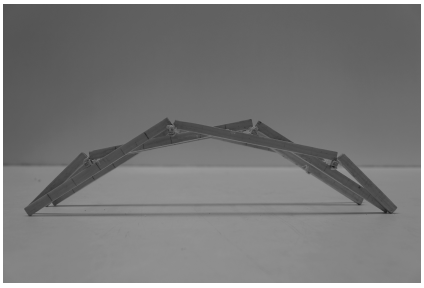

(a) Even Member Count, six Members per PRFA

(b) Uneven Member Count, seven Members per PRFA

Figure 4.23: Rainbow RFs with different Member Count

From a structural perspective the Rainbow RF is preferable to the Da Vinci RF for three reasons. Fixing the engagement length at its maximum value is structurally optimal and legitimizes the reduction of form freedom. Placing the members of an interwoven arch in one plane and adding the end members enables the PRFAs to transfer forces not only via bending but also via axial action. Refer to figure 4.24 for a visual comparison of the planes in which the structural members of the Da Vinci and the Rainbow RF lay.

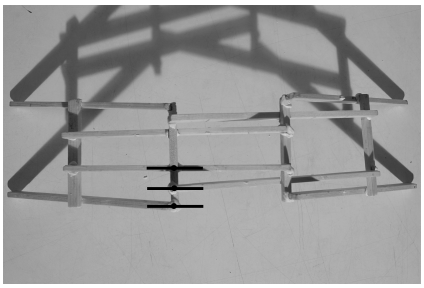

(a) Da Vinci, longitudinal Members of a PRFA in three Planes

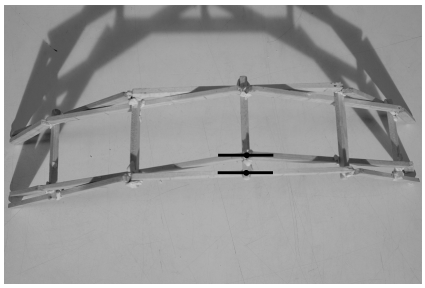

(b) Rainbow, longitudinal Members of a PRFA in two Planes

Figure 4.24: Top View of Rainbow RFs

Because the longitudinal members that are supported by the same transverse beam are in one plane, no moment resistant joints are required to achieve rigidity. This is demonstrated with a physical model which is loaded symmetrically and asymmetrically, see figure 4.25

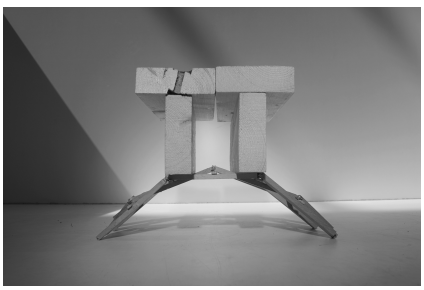

(a) Symmetric Loadcase

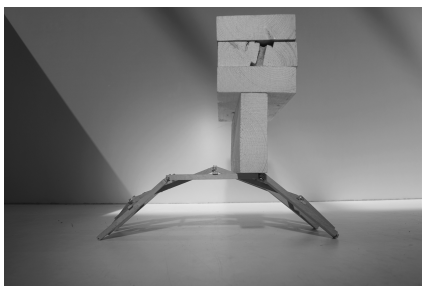

(b) Asymmetric Loadcase

Figure 4.25: Demonstrating Rigidity of the Rainbow RF

Considering that both the transfer of forces and the detailing of joints is more effective in the Rainbow RF, it is decided that only this type is studied further in the Structural Design Case Study.

4.6. Key Findings

RFs are a family of structures that boast with a rich variety of forms and diverse functions. A recently rediscovered application for RFs is the structural utilization of RT. The conducted literature review confirmed that also from a structural perspective the RF is favorable for the combination with RT. RFs achieve their flexural rigidity through their characteristic geometry and can thus be constructed with hinged joints. This circumvents the elaborate detailing of moment resistant joinery which would not only be expensive, but could also be limiting the design with RT considering the material's restricted geometric and mechanical properties.

The major challenge in the design of a RF structure is geometric complexity. Satisfying geometrical constraints is not a trivial task but requires a sophisticated geometry generation process. Different to form-finding processes known from spatial structures such as grid-shells, the geometry generation of RFs is a purely geometric exercise, the structural assessment occurs separately.

From the family of RFs, the geometrically less complex "Linear RF'' is selected for the case study. It is favorable to choose a RF type with relatively low geometric complexity in a RT design so that also the geometric complexity that RT designs have in themselves can be accommodated. The complexity of RT designs stems from the fact that RT structures are built from a limited stock of material. An advantage of the Linear RF is that it can generate spatial assemblies despite its manageable geometric complexity.

All of the reviewed case studies have in common that the computationally generated RF geometries use the top-down approach to geometry generation. The bottom-up approach was judged as not compatible for computation and not suitable for design applications. However, the context of designing with RT raises interest for reassessing if the programming of a bottom-up approach is possible for specifc RF types. If a bottom-up method was programmed to use a material stock of RT members as input, then this method could solve the problem inherent to RT, that is designing from a limited stock of material. The following case study is used as testing ground for this novel approach.

Lastly, joints play an important role in the design of RF structures. Detailing of joints influences both the geometry generation and the flow of forces between members. Hence, to confirm that a structural utilization of RT in a RF structure is safe and geometrically possible, not only member verifications are required but also a joint design needs to be carried out.

Part III

Structural Design Case Study

5

Introduction

The goal of the case study is to design a RF structure from RT. This goal is achieved by integrating the acquired knowledge on RT and RFs (compare Part II) to a preliminary design strategy. Through the case study this design strategy is tested and developed into further detail for a specific building application. The design strategy is comprised of the five design phases that are illustrated in figure 5.1. Each design phase is considered in a separate chapter.

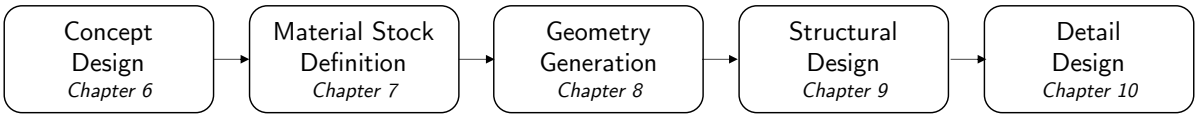

Figure 5.1: Preliminary Design Strategy

The building of the case study is defined through an architectural and a structural concept. Next, the case study's stock of RT is defined. For this material stock RF geometries are generated with a novel bottom-up model. The structural assessment follows the geometry generation, it includes the proposal of three safe RT RF designs. Finally, the structure's most important joint is detailed for one of the proposed RT RF designs.

6

Concept Design

6.1. Architectural Concept

One obstacle to the structural utilization of RT is that neither public nor professionals recognize RT as a structural building material, compare section 3.5.1.2. A successful RT design of a public building could positively influence public and professional opinion on building with RT. The roofs of European railway station sheds are often designed in the form of a barrel vault. This shape can be achieved with the Linear RF type that was selected for the case study and introduced in detail in section 4.5. Hence, it is decided that the architectural aim of the case study is to design a railway station roof.

Instead of drawing up a hypothetical railway station design for the case study, an existing transit hub is chosen as starting point for defining an architectural concept. It is assumed that building regulations are complied with by using the dimensions of an existing station. For instance, instead of reviewing building regulations that specify track widths and minimum distances between tracks and platform, the span of the structure of an existing station is used as input for the design.

The roof of the Norrebro Railway Station in Copenhagen, Denmark is selected as reference for the case study's architecture. The station and its barrel vault shaped roof are displayed in figure 6.1.

(a) Station Building from the Outside (Bloch, 2022)

(b) Station Building from the Inside (Rost, 2012)

Figure 6.1: Norrebro Railway Station in Copenhagen, Denmark

This specific station is selected because it is constructed from a RF in timber. Due to the similarity in material and structural system, this building is a useful testing ground to identify if a span that is reached with timber can also be achieved with RT.

The Norrebro Railway Station was built around the time when the Zollinger roof, which was introduced in the RF historic timeline in figure 4.2, was popular. The station began operating in May of 1930 (Pedersen, 2009). It is located in Copenhagen's Norrebro district. The tracks above ground which are covered by the considered canopy construction are part of the S-line transit network. The global dimensions of the roof structure were estimated during a site visit and are illustrated in figure 6.2.

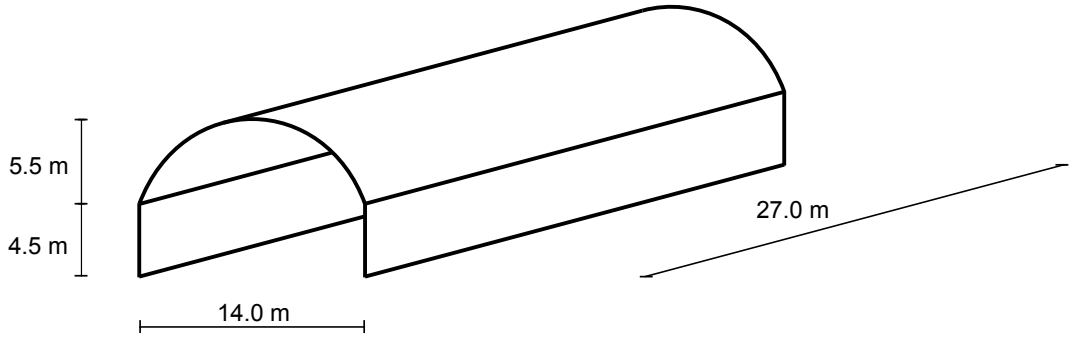

Figure 6.2: Estimated Geometry of the Norrebro Station Canopy Roof

Besides the dimensions, it is specified that for the redesign with RT, a design working life of 50 years is expected. Moreover, the building is categorized as a "Consequence Class 3" object because large numbers of people have access to the area that is covered by the canopy.

6.2. Structural Concept

The load-bearing structure for the vertical load take down consists of four components:

- Cladding
- Transverse Beams
- PRFAs
- Supporting Walls

In figure 6.3, a conceptual design of the structure is displayed in which the four components are labelled and in part the loads acting on the components are illustrated. The rendered image is based on assumptions for geometric parameters. While the span is set to 14.0 m as suggested above, the bay span, the geometry of the PRFA beams and other parameters are estimated. It is the purpose of the design phases "Geometry Generation" and "Structural Assessment" to determine the exact geometric parameters and to assess the resulting geometries structurally. At this point in the design process, an estimated geometry suffices to introduce the load-bearing components and to demonstrate the load take down.

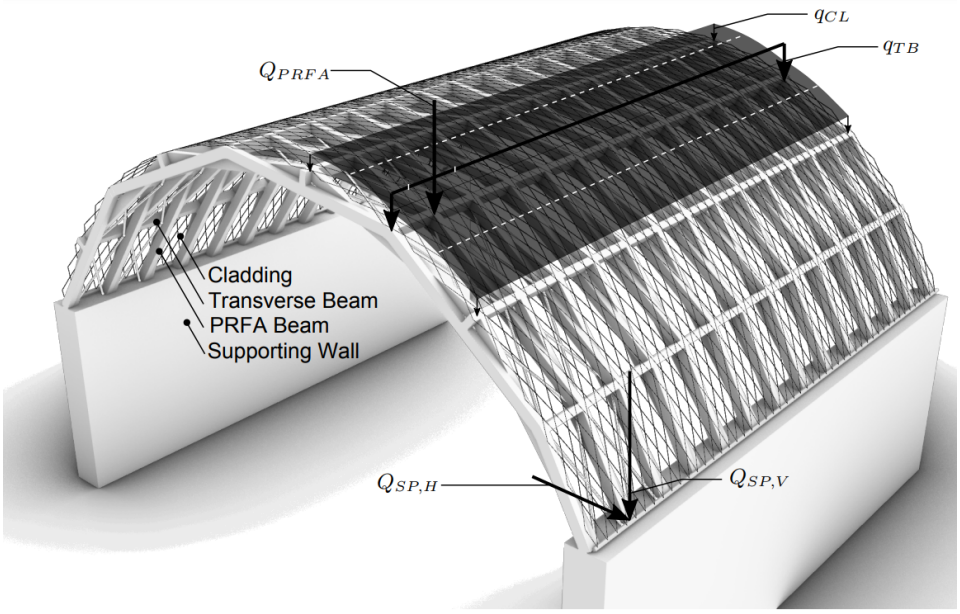

Figure 6.3: Structural Concept illustrating load-bearing Components and their Loads

The first component of the vertical load take down is the cladding. It carries an area load q_{CL} that is induced by self-weight, wind and/or snow. The load take down is illustrated in figure 6.3 by demonstrating how a vertical area load travels from the cladding through remaining structural components. The cladding is a composition of a thin timber lath grid and a poly-carbonate sheet, and thus similar to the reference case of the Nishiiyayama Village Monorail Station in Tokusima, Japan, which was illustrated in figure 4.20. The poly-carbonate sheet forms a transparent layer that protects the inside of the canopy as well as the structural members from external factors. Hence, the canopy can be considered as a ventilated roof structure, protected against precipitation and thus be classified as “Service Class 2” structure (Danish Standards Foundation, 2013b). The timber lath diagrid adds stiffness to the cladding and is fastened on the transverse beams.

The second component in the load take down are the transverse beams. These solid timber beams run across the entire length of the canopy. It is assumed that the beams are composed of shorter beams that are joined through half-lap joints at regular intervals. The transverse beams are considered to have the same cross-section and strength grade as the PRFA beams. Thus, the transverse beams are much stiffer than the cladding. It is therefore assumed that the load on a transverse beam q_{TB} attracts half of the load that is acting on the cladding in the area between two transverse beams, this is illustrated by the two white dashed lines on the black surfaces representing the load on the cladding.

The third component in the load take down is the PRFA which consists of multiple “longitudinal beams”. It is assumed that the forces that act on the transverse beams are equally distributed onto the PRFAs, i.e. the point loads Q_{PRFA} that act on the PRFA attract the load from a transverse beam that acts on the length equal to the bay span. The bay span is defined as the distance between the PRFAs. This is illustrated in figure 6.3 through two white dashes on the line load q_{TB}.

It is assumed that all PRFAs have the same geometry. With this assumption and the assumption of how the load travels through the previous two components, the structural conceptualization of the barrel vault can be reduced to a single PRFA. Thus the following design phases will focus on designing one PRFA instead of the complete canopy structure.

The PRFA transfers the loads via its longitudinal beams to the fourth component in the load take down, the supporting walls. The structural behavior of the PRFA will be discussed in more detail in section 9.3.1. The resulting horizontal thrust $Q_{SW,H}$ that acts on the supporting walls is resisted by the stair case enclosures that are to the left and to the right of the supporting wall. The stair case enclosures are not illustrated in figure 6.3; in figure 6.1, the enclosure on one side of the canopy can be seen. The vertical load $Q_{SW,V}$ is passed on to the substructure below.

The canopy structure is braced by a truss that is comprised of hollow steel tubes. The steel tubes are added in between one or two of the PRFAs, depending on the final bay span. The steel tubes act as tension bars which transfer loads that act in the transverse direction of the structure. A conceptualization of the bracing is illustrated in figure 6.4.

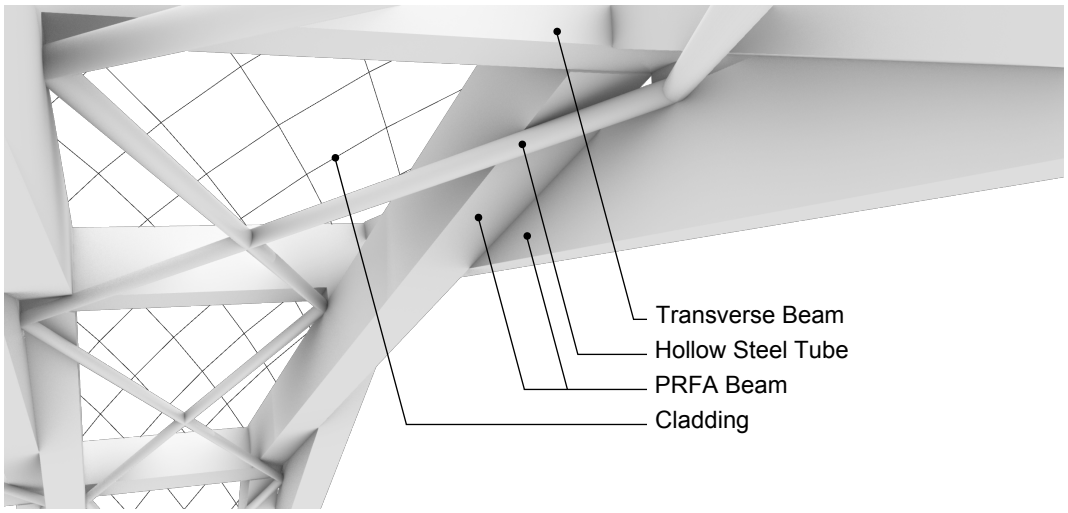

Figure 6.4: Conceptualization of a Steel Tube Truss Bracing

Besides addressing the transfer of loads through the members, the structural concept also considers the joint detail of the PRFA, more specifically its force transfer, detailing and influence on the global geometry. By selecting the Rainbow RF as geometry, it is determined that both shear and normal forces are transferred in the hinged joints (compare section 4.5).

With regards to detailing, the addition joint is favored amongst the three categories of details that were introduced in section 4.3.4. This detail decouples the height of the longitudinal beams from the eccentricity parameter without reducing the cross-section of the structural members. With this joint detail the eccentricity parameter must be equal or larger than the height of the longitudinal beams, but it is not fixed to one value. Hence, the eccentricity can be used as variable in the geometry generation. Figure 6.5 shows a canopy in the Zhongshan Road Museum in Hangzhou, China. This is an existing structure which works as a Linear RF and has a detail as the described addition joint.

Figure 6.5: Joints of the Canopy in the Zhongshan Road Museum in Hangzhou, China, (Thönnissen, 2015)

7

Material Stock Definition

The RT material stock is defined at this point in the design process so that it can influence both the geometry generation and the structural design of the RT RF structure. The RT database that was defined in chapter 3 is used as the material stock for the case study. It contains 30 different RT stacks that add up to 3735 individual timber items with a total volume of 243 m^3. The smallest and largest timber items by volume are a beam with a cross-section of 19x89 mm^2 with a length of 3.0 m and a column with a cross-section of 210x280 mm^2 with a length of 4.2 m respectively. Hence, although the item's lengths are larger than those used by Castriotto et al. (2021) and Parigi (Parigi, 2021), it still applies that the RT items are short relative to the structure's span of 14.0 m.

The material data was collected on a salvage yard and from research articles that document the dismantling of buildings in Finland, Germany, the Netherlands, Spain and the United States. When the data was recorded, 64% of the material was fixed in the building stock, 25% was dismantled but not yet structurally graded and 11% had assigned mechanical properties. Figure 7.1 illustrates a part of the RT material stock. Figure 7.1a shows a photograph of a Spanish Corrala; stacks 8 through 10 which have the material status "fixed" are still part of this building, that means they were not yet dismantled. Figure 7.1b shows a portion of stack 1 and 2, this RT was dismantled and transported to a salvage yard, but was not yet graded. Figure 7.1c displays how items from stack 22 through 25 are being graded.

(a) RT Stack 8 - 10 fixed in a Spanish Corrala (Berne, 2019)

(b) Part of Stack 1 and 2 on a Salvage Yard

(c) Grading of Stack 22 - 25 (Falk et al., 2008)

Figure 7.1: Illustrations of Part of the Material Stock

For approximately half of the database's stacks the mechanical properties are unknown. To include them in the material stock for the case study, strength grades are assigned to these items based on two assumptions. Before assigning a strength grade to the RT stacks, their virgin timber strength grade is assumed. This assumption is based on the construction year of the building in which the material was previously used. Two categories are distinguished: Old timber and basic modern timber. For a description of the two groups, refer to section 3.5.2.1. From the stacks with unknown mechanical properties, stack five through seven belong to the group of basic modern timber. To these items a virgin timber strength grade of C24 is assigned. This is a standard grade in today's engineering practice. The remaining items with unknown strength grade belong to the group of old timber. It is assumed that they have a virgin timber strength grade of C30. This high strength grade is assigned based on the argument that old timber has mechanical properties superior to basic modern timber, compare section 3.5.2.1.

In the second place, a strength grade is assigned to the RT stacks by reducing the assumed virgin timber grade. In place of basing the reduction on a standard, which at present does not exist in Europe, references from research that were presented in table 3.6 are used to determine the extent of the strength grade reduction. That means, multiple strength grades are assigned to the stacks with unknown mechanical properties. In the design phase "structural assessment'' all strength grade reductions will be considered in order to identify the sensitivity of the design's safety to the strength grade of the material. Table 7.1 displays the various strength grades that are assigned to the RT items depending on their virgin timber strength grade.

Table 7.1: Assumed Strength Grade Reduction

Virgin Timber SG	Reduced Strength Grade according to reference					
	R1 (a)	R1 (b)	R2	R3 (a)	R3 (b)	R4
C24	C22	C20	C18	C16	C14	C14
C30	C27	C24	C22	C18	C14	C18

The case study's material stock is displayed in tables 7.2 and 7.3, the assignment of multiple strength grade reductions is indicated by the the word "various'' (var.). The modulus of elasticity is not effected by the previous life cycle, compare section 3.6.2. Nevertheless, instead of assigning the stiffness properties of the virgin timber grade, a more conservative approach is taken in which the properties of the strength grade which is two classes above the RT strength grade is assigned. An exception is reduction R1 (a), here the stiffness properties of the virgin timber strength grade are used.

In order for the material stock to conform to a single standard, the stacks with originally American strength grades are matched with a European equivalent grade. For the species "Douglas fir – larch'' the strength grades "SS'' and "No.2'' have a bending strength of $28.1 \frac{\mathrm{N}}{\mathrm{mm}^2}$ and $17.0 \frac{\mathrm{N}}{\mathrm{mm}^2}$ respectively (Walford, 2003). The European grades with the closest bending strength are assigned as equivalent values, C27 and C16 respectively.

Table 7.2: RT Material Stock, Stacks 1 - 15, for Data References see Appendix A.1

Material Charac-teristic	Geometry		Material Condition			Mechanical Properties			Additional Information					
Property	Width x Height $[mm x mm]$	Length $[m]$	Chemical Contamination	Biological Corrosion	Physical damage	Strength Grade	MOR [N/mm^2]	$E_{m,0,mean}$ [N/mm^2]	Number of items [-]	Material status	Virgin timber grade (assumed)	Location in building	Building year	Building type
Stack 1	70x175	2.3	no	no	yes	var.	var.	12000	126	free	C30	-	1950s	-
Stack 2	70x175	3.6	no	no	yes	var.	var.	12000	120	free	C30	-	1950s	-
Stack 3	60x160	6.3	no	no	yes	var.	var.	12000	84	free	C30	-	1950s	-
Stack 4	60x160	3.3	no	no	yes	var.	var.	12000	63	free	C30	-	1950s	-
Stack 5	95x95	3.6	no	no	yes	var.	var.	11000	90	free	C24	roof beam	1977	Kindergarten
Stack 6	45x95	1.4	no	no	yes	var.	var.	11000	157	free	C24	roof pillar	1977	Kindergarten
Stack 7	45x120	4.2	no	no	yes	var.	var.	11000	119	free	C24	roof rafter	1977	Kindergarten
Stack 8	210x280	4.2	-	-	-	var.	var.	12000	153	fixed	C30	column	19th cent.	Corrala
Stack 9	140x200	3.7	-	-	-	var.	var.	12000	984	fixed	C30	floor beam	19th cent.	Corrala
Stack 10	140x210	4.0	-	-	-	var.	var.	12000	132	fixed	C30	roof beam	19th cent.	Corrala
Stack 11	80x240	4.0	no	no	-	var.	var.	12000	420	free	C30	-	19th cent.	Alpine Cottage
Stack 12	38x140	3.0	no	no	yes	C16	16.0	9500	98	fit	-	rafter (roof)	1940s	Army barack
Stack 13	38x140	3.0	no	no	yes	C27	27.0	13000	12	fit	-	rafter (roof)	1940s	Army barack
Stack 14	38x184	3.7	no	no	yes	C16	16.0	9500	220	fit	-	floor joist/ stringer	1940s	Army barack
Stack 15	38x184	3.7	no	no	yes	C27	27.0	13000	40	fit	-	floor joist/ stringer	1940s	Army barack

Table 7.3: RT Material Stock, Stacks 16 - 30, for Data References see Appendix A.1

Material Charac-teristic	Geometry		Material Condition			Mechanical Properties			Additional Information					
Property	Width x Height $[mm x mm]$	Length $[m]$	Chemical Contamination	Biological Corrosion	Physical damage	Strength Grade	MOR [N/mm^2]	E$_{m,0,mean}$ [N/mm^2]	Number of items [-]	Material status	Virgin timber grade (assumed)	Location in building	Building year	Building type
Stack 16	38x140	3.0	no	no	yes	C16	16.0	9500	16	fit	-	Wall stud	1940s	Naval Supply Center
Stack 17	38x140	3.0	no	no	yes	C27	27.0	13000	47	fit	-	Wall stud	1940s	Naval Supply Center
Stack 18	38x235	4.3	no	no	yes	C16	16.0	9500	53	fit	-	roof joist	1940s	Naval Supply Center
Stack 19	38x235	4.3	no	no	yes	C27	27.0	13000	197	fit	-	roof joist	1940s	Naval Supply Center
Stack 20	38x235	4.3	no	no	yes	C16	16.0	9500	53	fit	-	roof joist	1940s	Army Munition Plant
Stack 21	38x235	4.3	no	no	yes	C27	27.0	13000	117	fit	-	roof joist	1940s	Army Munition Plant
Stack 22	38x140	3.0	no	no	yes	C16	16.0	9500	20	fit	-	rafter (roof)	1940s	University housing
Stack 23	38x140	3.0	no	no	yes	C27	27.0	13000	36	fit	-	rafter (roof)	1940s	University housing
Stack 24	38x184	3.7	no	no	yes	C16	16.0	9500	43	fit	-	roof joist	1940s	University housing
Stack 25	38x184	3.7	no	no	yes	C27	27.0	13000	2	fit	-	roof joist	1940s	University housing
Stack 26	38x89	3.0	no	no	yes	var.	var.	12000	190	free	C30	-	-	Wood framed house
Stack 27	38x140	3.0	no	no	yes	var.	var.	12000	2	free	C30	-	-	Wood framed house
Stack 28	38x184	3.0	no	no	yes	var.	var.	12000	111	free	C30	-	-	Wood framed house
Stack 29	19x89	3.0	no	no	yes	var.	var.	12000	8	free	C30	-	-	Wood framed house
Stack 30	19x140	3.0	no	no	yes	var.	var.	12000	13	free	C30	-	-	Wood framed house

8

Geometry Generation

In this chapter, it is explored what RF geometries, more specifically what Rainbow RF geometries, can be generated for the defined material stock. Of interest are those geometries that have the architecturally required span of 14.0 m. The geometry generation is a purely geometric exercise, thus not all properties of the material stock need to be considered. In fact, only the RT item's length influences the process. The number of items per stack is not relevant in this design phase since the geometry generation focuses only on one PRFA and not on the complete canopy. The number of items per stack as well as the cross-section size and the mechanical properties are integrated into the design in the next phase.

To generate the geometries for the material stock a parametric bottom-up model is developed in the visual programming language "Grasshopper 3D". This model is used to investigate the geometric behavior of the Rainbow RF and to generate geometries for the material stock. Instead of constructing geometries for each RT stack individually, geometries are generated for the material stock's distinct lengths. This covers the material's stock complete design space with regards to geometry because the length is the only material stock parameter that influences the geometry generation. The geometric parameters "eccentricity" and "number of members per PRFA" are varied to generate multiple geometric variants per distinct length. This broadens the design space and increases the potential of identifying a structurally safe solution in the next design phase. In a last step the geometric variants of the distinct lengths are assigned to the RT stacks with the corresponding item's length. This leads to a total of 118 geometric design proposals.

8.1. Bottom-Up Model

Since the RT item's length is the only parameter that is implemented into the bottom-up model of the PRFA, the structural members can be modelled with lines instead of three-dimensional objects. The longitudinal beams are represented by their center axes and are referred to as longitudinal elements. The transverse members are modelled by their vertical axes and referred to as eccentricity elements. This name is chosen because the length of the eccentricity element corresponds to the value of the eccentricity. All longitudinal and eccentricity elements are modelled in one plane.

Figure 8.1 illustrates the geometric parameters that are relevant to developing and evaluating the bottom-up model. The input parameters eccentricity e, member length L and number of members per PRFA n_m were introduced in chapter 4. The RF is regular, i.e. except for the shorter side elements, the element length L and the engagement length a are identical for all elements. Five parameters are used to describe the output geometries of the bottom-up model: the span L_{span}, the rise h_r, the arc length s, the relative central angle θ_r and the curvature κ, which is the reciprocal of the associated arc's radius R. The relative central angle is the value of the central angle θ divided by 2π. Thus, a value of $\theta_r = 1$ means that the PRFA is a complete circle, indicating that the span is 0. To give another example, the PRFA displayed in figure 8.1 has a central angle of less than 180 degrees, that means the relative central angle will be less than one half.

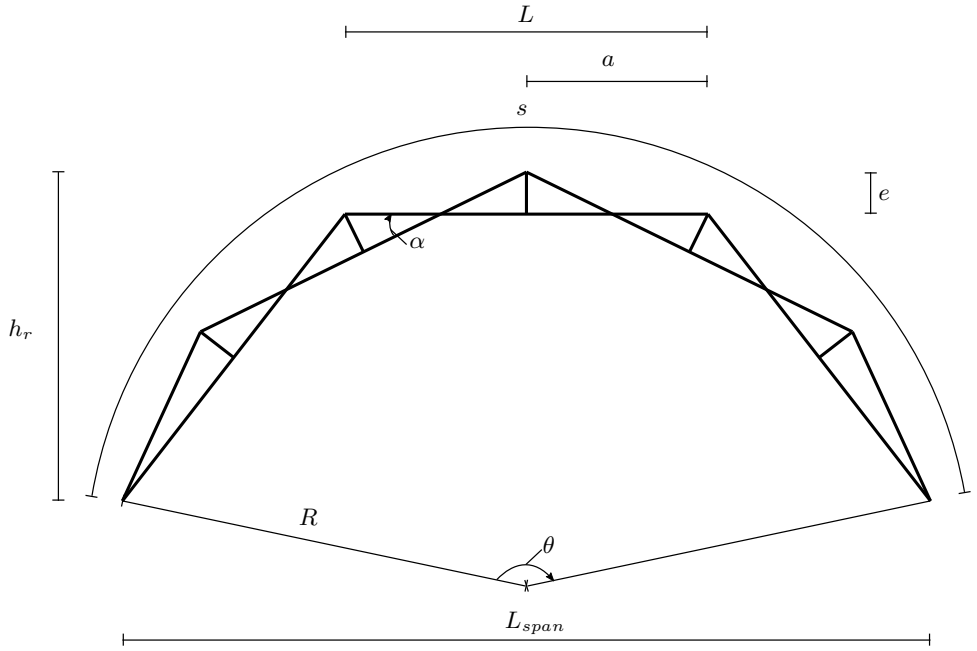

Figure 8.1: Geometric Parameters of the Bottom-Up Model

The bottom-up model is comprised of the four program steps, that are illustrated in the flowchart in figure 8.2.

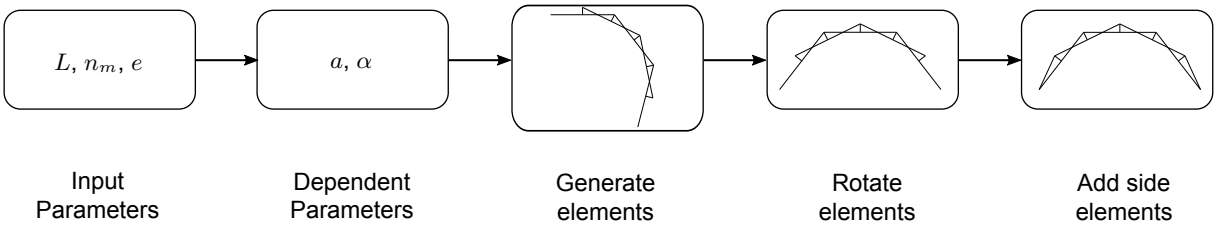

Figure 8.2: Flowchart of the Bottom-Up Model

In a first step, the geometric variables that are dependent on the input parameters are computed. The relations are as follows:

$$a = \frac{L}{2}$$

$$\alpha = arctan\left(\frac{e}{\frac{1}{2}\left(a - \frac{e^2}{a}\right)}\right)$$

In a second step, the longitudinal and eccentricity elements are generated with a for-loop. Then, the position and orientation of the elements are adjusted so that the support points lay on the x-axis. Finally, the side elements are added in.

The bottom-up model can be linked to the material stock by feeding it the distinct lengths as input. An infinite number of Rainbow RFs can be generated by varying the remaining two input parameters.

8.2. Parameter Study

With the help of the bottom-up model the geometric behavior of the Rainbow RF is investigated through a parameter study for the smallest and largest distinct length (DL) of the material stock, these are DL1 $= 1.40$ m and DL10 $= 6.30$ m. Two DLs are investigated to ensure that observed trends are not specific to one item length. While disregarding the constraint of achieving a specific value for the span, the input parameters n_m and e are varied. The domains for the input parameters are $e = (0.00\,\text{m}, 1.00\,\text{m}]$ and $n_m = [4, 20]$. The lower limits are chosen according to what is geometrically possible, the upper limits have more practical reasons. An eccentricity of $e > 1.00$ m is not expected to be relevant for a practical application. In the same way, it is not expected that more than 20 members will be integrated in a PRFA.

Only valid geometries are evaluated, i.e. a combination of input parameters that leads to a geometry with a span $L_{span} > 0$. This is equivalent to the left supporting point and the right supporting point staying on their respective sides. In figure 8.3 data points display the combination of input parameters that lead to valid geometries. Since the interval between the data points regarding the eccentricity is only 1 cm, the data points appear as columns.

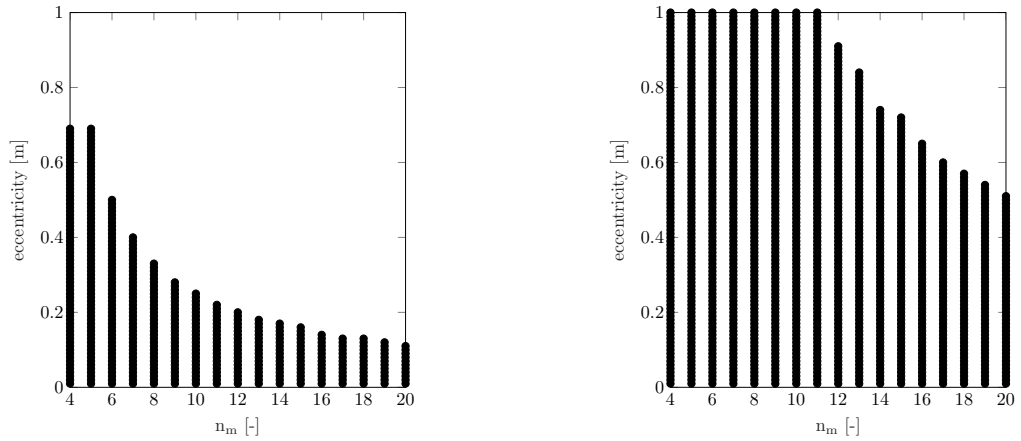

(a) DL1 **(b)** DL10

Figure 8.3: Valid Combinations of Input Parameters for a PRFA

In the considered domain of input parameters, DL1 has a lower number of valid combinations than DL10. The reason for this is illustrated in figure 8.4, which displays the relative central angle of the data points. Surface plots are employed to display the behavior of the relative central angle and the other parameters which describe the form. This serves a better illustration of the originally discrete data. The nodes of the triangles represent the data points.

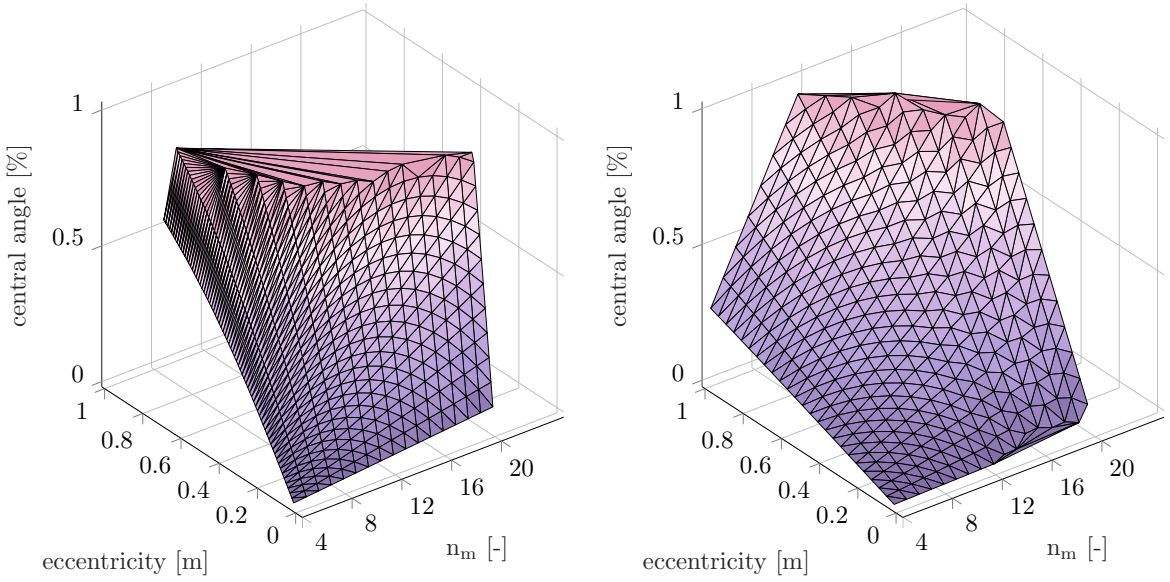

(a) DL1 **(b)** DL10

Figure 8.4: Relative Central Angle of the PRFA for the Valid Combination of Input Parameters

From a closer investigation of the plots in figure 8.4 it is discovered that the data points that have a $\theta_r \approx 1$, are also the data points that mark the line between the valid and invalid combination of input parameters. This corresponds to the definition of valid combinations above. It is obvious from the plots that a smaller member length L reaches a $\theta_r = 1$ for lower eccentricities than a larger member length.

The arc length s and the curvature κ are only sensitive to a change of one of the two input parameters that are varied. Figure 8.5 illustrates the linear relation between n_m and s. The eccentricity has a minor influence on the arc length, which diminishes with an increase of n_m. The relation between e and s is non-linear. The difference in the slope of the arc length plots for the two DLs is equal to the ratio of the two DLs' L. That implies, a larger member length leads not only to a larger absolute arc length, but also to a larger slope in the relation between n_m and s.

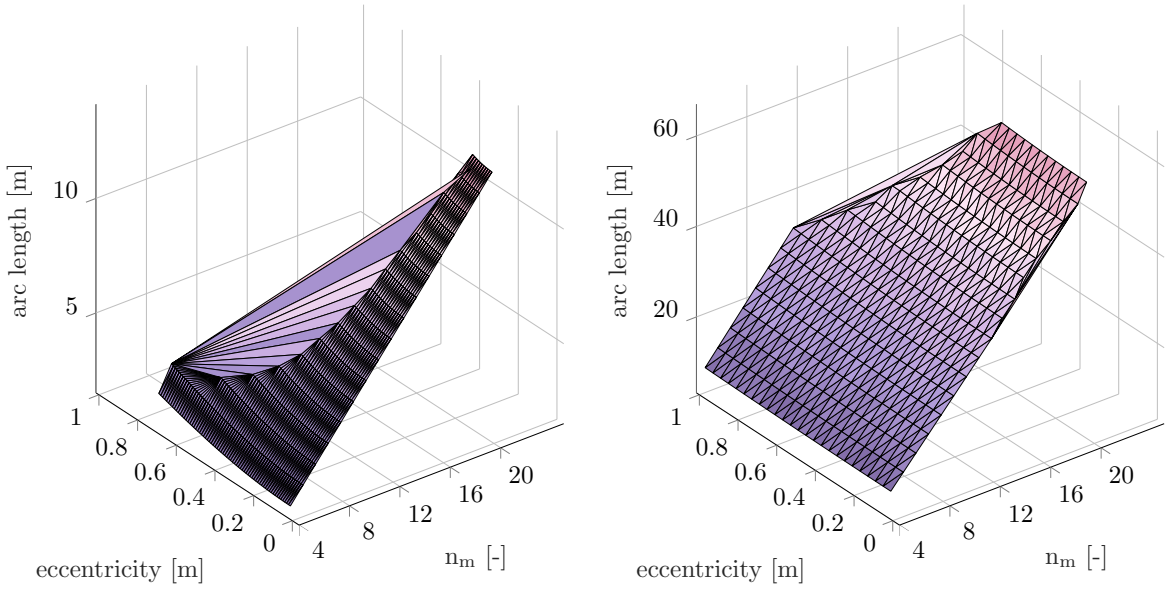

(a) DL1 **(b)** DL10

Figure 8.5: Arc Length of the PRFA for the Valid Combination of Input Parameters

Figure 8.6 illustrates that the curvature increases asymptotically with e and is independent of n_m.

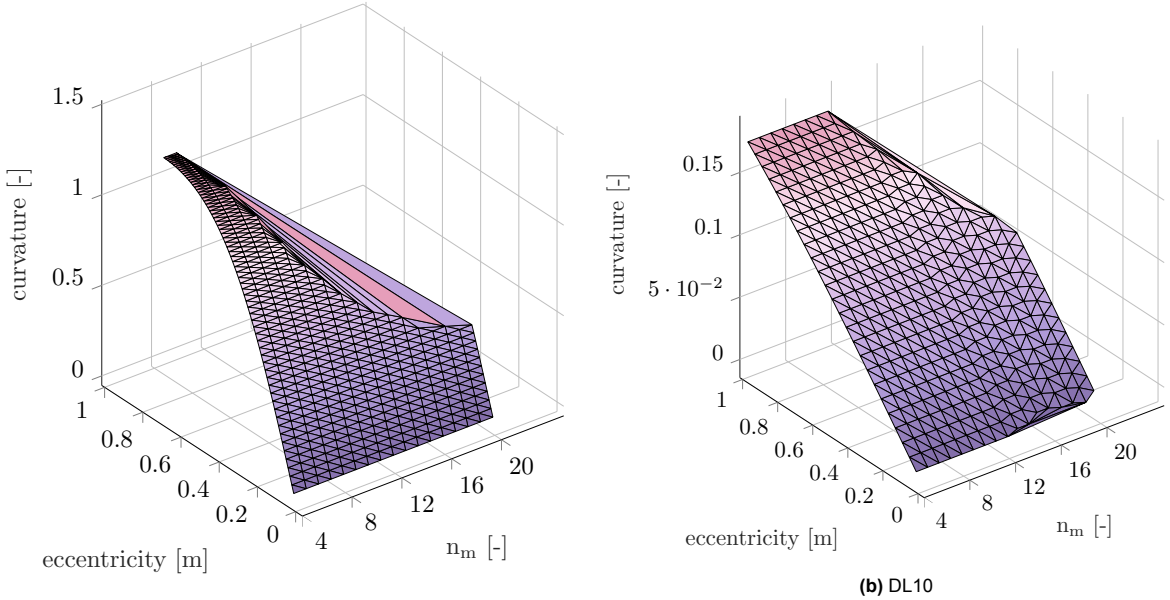

(a) DL1 **(b)** DL10

Figure 8.6: Curvature of the PRFA for the Valid Combination of Input Parameters

This holds for both DLs, yet DL1 shows a more obvious asymptotic increase, while DL10 does not yet converge in the selected eccentricity domain.

The span and the rise of the PRFA are sensitive to both input parameters. The surface plots of these two descriptive parameters have the shape of a double-curved saddle with a ridge that marks the maximum values for L_{span} and h. It is apparent that both parameters are very sensitive to a change in eccentricity for a large number of members.

Figure 8.7 shows that for small eccentricities the relation between n_m and L_{span} is approximately linear and thus similar to the trend of the arc length. Upon an increase of eccentricity the relation between n_m and L_{span} becomes non-linear and the maximum of the span for a set eccentricity value shifts increasingly to a lower number of members. Conversely, starting from a certain value for e, an increase of n_m does not always lead to a larger span, but from a certain point decreases the span, for DL1 this value is $e = 0.06\,\text{m}$ and for DL10 $e = 0.27\,\text{m}$. The relation between e and L_{span} is more straightforward. An increase of eccentricity always leads to a decrease of the span. It can be concluded that the maximum L_{span} is achieved through minimum eccentricity and maximum number of members.

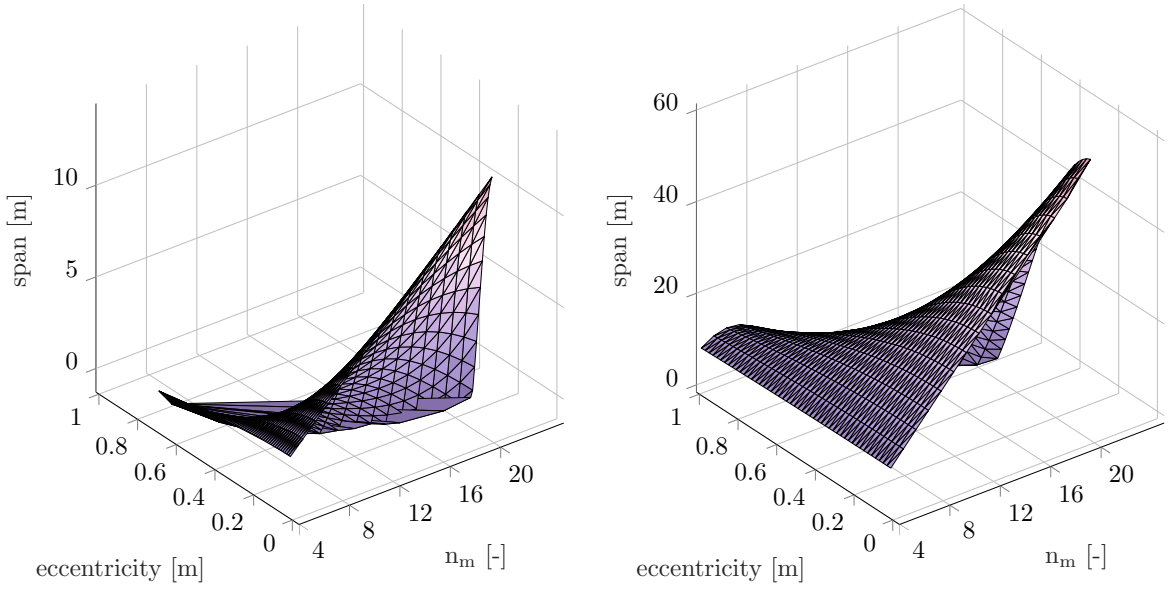

(a) DL1 **(b)** DL10

Figure 8.7: Span of the PRFA for the Valid Combination of Input Parameters

A key difference between the two DLs regarding the span is the position of the ridge. For a lower member length the ridge is defined through a combination of lower input values. For a larger member length, the ridge is shifted in the direction of the border between valid and invalid geometries. Further, it is obvious that the maximum of the span for DL10 is larger than for DL1, again it holds that the difference is defined by the ratio of the two member lengths.

Figure 8.8 shows that the maximum rise is achieved with the largest number of members. However not with the lowest eccentricity value. For DL1 the maximum rise is achieved with an eccentricity of $e = 0.09\,\text{m}$ for DL10 with $e = 0.39\,\text{m}$. For a set value of n_m and an increase of eccentricity past the ridge leads to a decrease in rise.

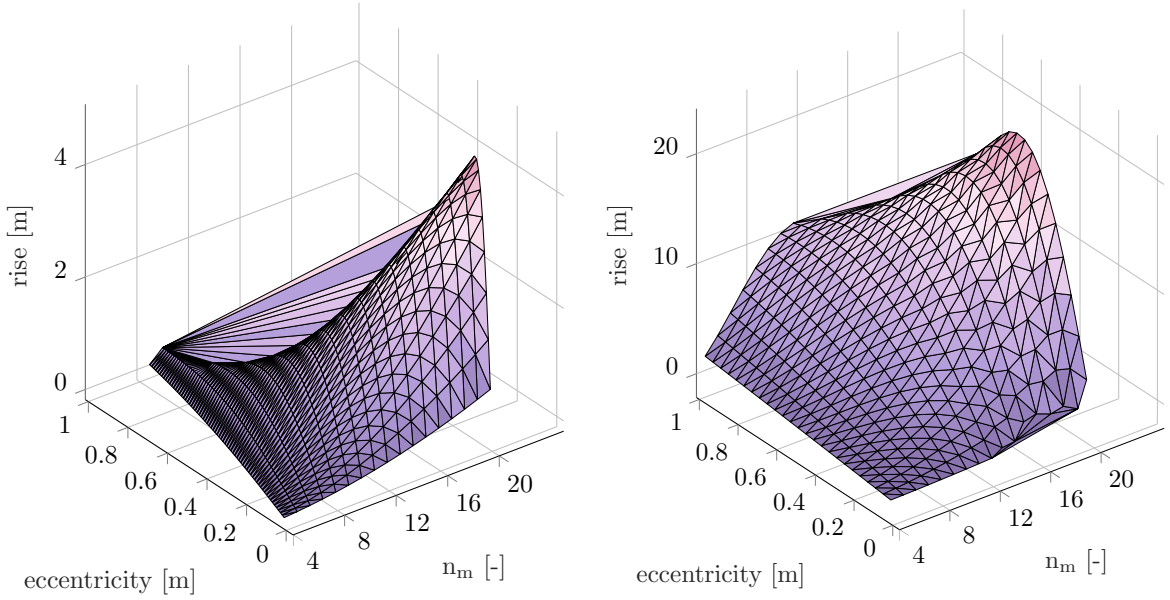

(a) DL1

(b) DL10

Figure 8.8: Rise of the PRFA for the Valid Combination of Input Parameters

8.3. Directed Method

With the knowledge of the Rainbow RF's geometric behavior, the "directed method" is developed. Its purpose is to efficiently identify for a given item length L the combinations of input parameters e and n_m that lead to a PRFA with a good approximation of a predetermined span. Efficient in this context means to identify the combinations of interest, also called geometric variants (GVs), without computing all possible input parameter combinations as was done in the parameter study.

Two additional criteria are programmed into the directed method. The specification from the conceptual joint design that the eccentricity is equal or larger than the cross-sectional height (compare section 6.2) motivates to program the method so that the eccentricity values are as large as possible. On the contrary, the number of members is aimed to be kept small, because this leads to a lower use of material.

The first step of the directed method is to generate a GV0 by setting the eccentricity parameter to a value of $e = 0.000001$ m. To achieve GV0, the number of members is increased until a span of $L_{span} \geq$ 14.0 m is reached. GV0 is a planar RF, thus, not a Rainbow RF and the considerations of this study do not apply. No structural analysis will be conducted for this GV. Nevertheless, GV0 is relevant for it sets the input parameter n_m to a starting value for the generation of the following variants. The following GVs are generated with the following procedure: n_m is increased by one and the eccentricity is increased until the span of 14.0 m is reached from the upper side. GVs are defined for every additional member with which the eccentricity can be increased. For the case that n_m is increased by one and an increase of the eccentricity directly results in a span smaller than 14.0 m, the member count is increased further before the next GV is defined.

8.4. Resulting Geometries

To obtain the Rainbow RF geometries that can be generated for the material stock defined in chapter 7, the directed method is applied to the bottom-up model for the material stock's distinct lengths. The material stock's distinct lengths are listed in table 8.1.

Table 8.1: Distinct Lengths of RT in the Database

Distinct Length ID [-]	DL1	DL2	DL3	DL4	DL5	DL6	DL7	DL8	DL9	DL10
Corresponding Length [m]	1.4	2.3	3.0	3.3	3.6	3.7	4.0	4.2	4.3	6.3

Figure 8.9 shows the PRFA geometries that result from applying the directed method to DL5. Next to the visualization of the GVs, the corresponding input parameters as well as the resulting rise and span are displayed.

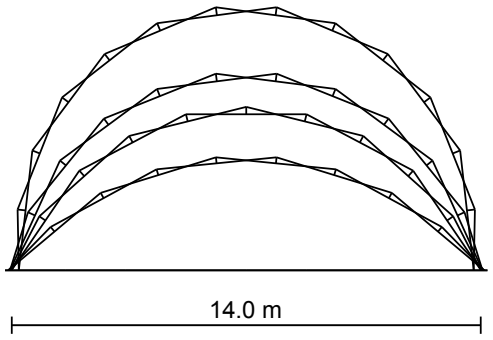

GV	n_m [-]	e [m]	L_{span} [m]	h_r [m]
4	14	0.24	13.58	7.91
3	12	0.23	14.10	5.93
2	11	0.22	14.02	4.88
1	10	0.18	14.21	3.42
0	9	0.00	14.40	0.00

Figure 8.9: Geometric Variants of DL5 ($L = 3.60m$)

With the directed method, five GVs are identified for DL5. GV0 marks the reference case and is not further discussed. GV1, GV2 and GV3 are potential geometries for the PRFA of the RF canopy. GV4 is not a potential geometry. Although its number of members is increased, it has a span lower than the required 14.0 m. That means the eccentricity value is past the ridge that was identified in section 8.2. Hence, for DL5 beyond GV3 no further GVs can be generated when following the directed method. GV3 is called the upper limit case for possible GVs of DL5. For the illustration of the GVs for DL1 - DL4 and DL6 - DL10, refer to appendix C.1.

Figure 8.10 shows RT stack 2. The item's length of this stack corresponds to DL5, i.e. with the displayed RT stack a span of approximately 14.0 m can be achieved in the three ways that are illustrated in figure 8.9. In other words, RT stack 2 has three geometric design proposals. In the following design phase, the "structural design", these and all other geometric design proposals are evaluated by integrating the remaining material properties from the RT material stock into the design process.

This phase also serves to evaluate which of the geometries is optimal, not only from a perspective of geometry, but also from a structural perspective. The deviation of the actual span from the required span will be addressed in the design phase “detail design”.

Figure 8.10: Sideview of RT Stack 2

9

Structural Design

Based on the geometric design proposals, it is identified in this chapter with which of the RT stacks a structurally safe canopy can be constructed. For the identified stacks the proposals are further developed by optimizing the bay span and integrating the number of items per stack into the design. Figure 9.1 displays the four steps that are used to approach the structural design (displayed as arrows). During the structural modelling the geometric design proposals are combined with the RT strength grade and the cross-sectional parameters in a finite element model. Then, a linear elastic analysis is conducted. Because the structural geometry is none conventional, special effort is dedicated to a validation of the analysis' results. The structural verification compares the actions in the structure with limit criteria regarding strength, stability and deflections. Consecutively, the safe design proposals are further developed as mentioned above.

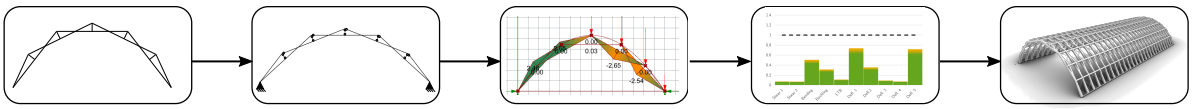

Geometric Design Proposal | Structural Model | Structural Analysis Response | Structurally verified design proposals | Structural Canopy Design

Figure 9.1: Flowchart for the Structural Design

Considering that there are more than a hundred geometric design proposals, an algorithm is developed that automates the structural design to a large degree. The results of the geometry generation serve as input for the algorithm, the algorithm's output is a visualization that indicates which of the geometric design proposals are structurally safe and which design proposals fail to comply with engineering standards.

9.1. Structural Model

The parametric structural model is described in sub sections that correspond to the set-up of a conventional structural analysis model, i.e. geometry, material and section properties, supports and joints, loads and the type of analysis are addressed respectively.

9.1.1. Geometry

The geometric design proposals are the starting point for the structural model with regards to geometry. In the geometry generation the longitudinal members were reduced to their central axes and the transverse beams to the eccentricity elements. All elements were modelled in a plane. For the structural analysis of the PRFA, the geometry is not expanded into 3D, the model remains 2D. Consequently, no major additional geometry operations are required. The only change that is conducted is splitting the longitudinal center axes at the positions where an eccentricity element is attached. This adjustment ensures connectivity of the model's elements at this position.

Figure 9.2 illustrates the geometry of the geometric design proposal S9V2. The abbreviation S9V2 indicates that the geometric design proposal is generated with timber from stack 9; V2 implies that the second GV is considered. In this specific case, the geometry was slightly altered, to reduce the deviation in span. Specifically, the eccentricity was adjusted to $e = 0.238$ m. The new span is $L = 14.00$ m and the rise is $r = 5.21$ m.

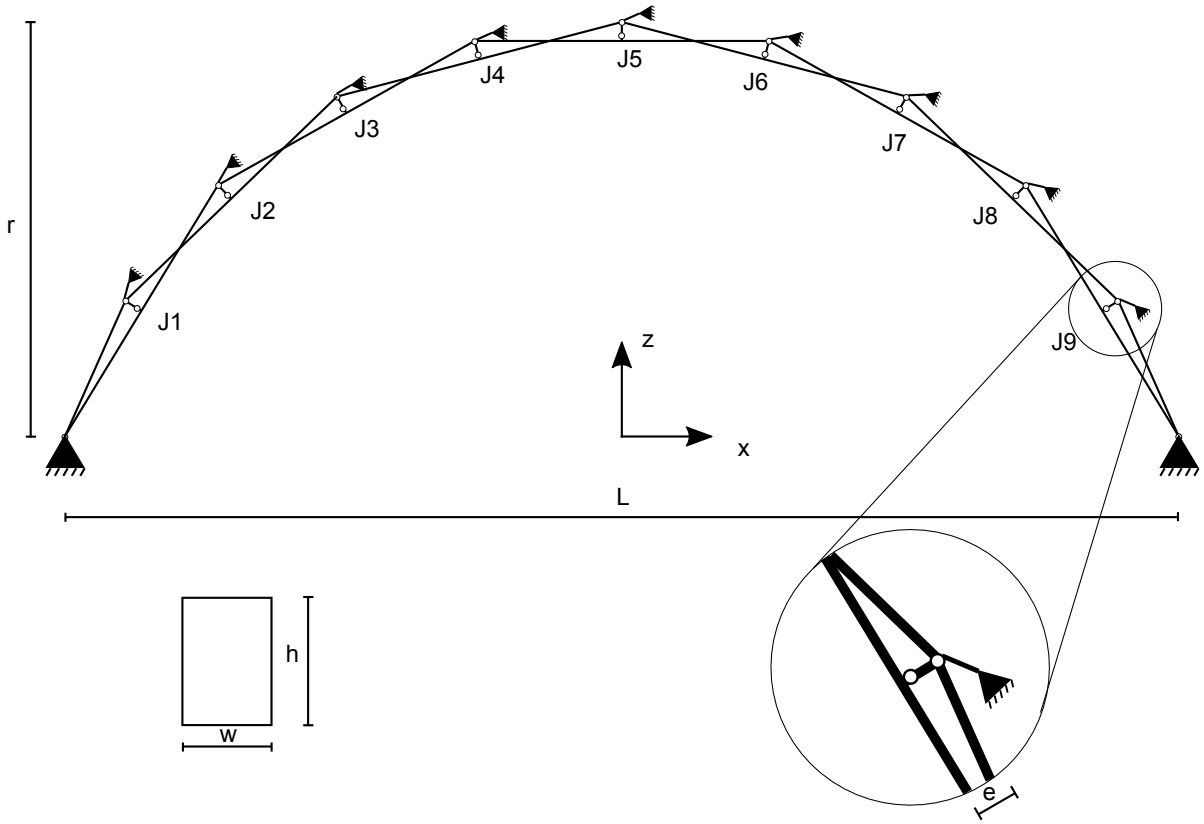

Figure 9.2: Mechanical Scheme of the Geometric Design Proposal S9V2

The geometric design proposal S9V2 is used throughout this chapter for exemplifying calculations that serve to clarify steps during the structural design. All illustrative calculations for S9V2 consider a bay span of $L_{bay} = 1.0\,\text{m}$, a cross-section of $w\text{x}h = 140\,\text{x}\,200\,\text{mm}^2$ and a strength grade of C18.

9.1.2. Material and Section Properties

The geometric and mechanical properties for the longitudinal elements of a PRFA are determined by the design proposal's RT stack. The eccentricity elements have a squared cross-section with the side-lengths being equal to the width of the longitudinal beams. This specification originates from the assumption that the transverse beams have the same cross-section as the longitudinal beams, compare section 6.2. The strength grade of the transverse beam was also assumed to be identical with the strength grade of the longitudinal beam. The eccentricity element is assigned the strength and stiffness properties of the longitudinal beam's strength grade, more specifically those that apply to the direction perpendicular to the grain because the eccentricity line is orthogonal to the transverse beam's center axis.

9.1.3. Supports and Joints

Figure 9.2 illustrates the mechanical scheme of the structural PRFA model and introduces the global coordinate system. The PRFA lies in the x-z plane, the y-direction is the out-of-plane direction.

At its endpoints the PRFA is supported by pinned supports that resist the vertical load and the horizontal thrust. As described in section 4.5.2, the joints of the Rainbow RF do not need to transfer bending moments to achieve global rigidity. Thus, the connections are modelled as hinges.

In the employed modelling software, that is "Karamba3D" , the degrees of freedom at the interface of elements are not released per node, but per structural element (Preisinger, 2011). Consequently, the joint hinges are implemented in the following way: At the ends of the eccentricity elements the rotation around the y- and the z-axis are released. In addition, the rotation around the y- and z-axis of one of the two longitudinal elements that are joined at the outer end of the eccentricity element are released. This is required to avoid a moment transfer between the two longitudinal elements. For the same reason, it is required to release the rotation around the y- and the z-axis for one of the two longitudinal elements that are joined to the supports.

9.1.4. Loads

In section 6.1 the Norrebro Station in Copenhagen, Denmark was determined as the main reference for the architectural design of the RF canopy. Also the location of this station is assumed as a starting point for the design. The location of the building site determines the applicable National Annex which influences amongst others the modelling of the loads. In the following the Eurocode and the Danish National Annex are used for modelling the loads.

In this structural analysis, self-weight, wind load and snow load are considered. In table 9.1 the actions are classified and a load duration class as well as the corresponding k_{mod} factor are assigned.

Table 9.1: Classification of Loads

	Variation in Time	Nature of the Load/ structural Response	Load Duration Class	k_{mod}
Self-Weight	permanent	static/static	permanent action	0.60
Snow	variable	(quasi-)static	short-term action	0.90
Wind	variable	(quasi-)static	instantaneous action	1.10

Figure 9.3 shows one of the two self-weight loads that are applied to the PRFA. The distributed line loads that are applied to the longitudinal elements which represent the dead load of the longitudinal members act additionally to the illustrated point forces. The point forces applied to the outer end of the eccentricity elements represent the self-weight of the roofing and the transverse members.

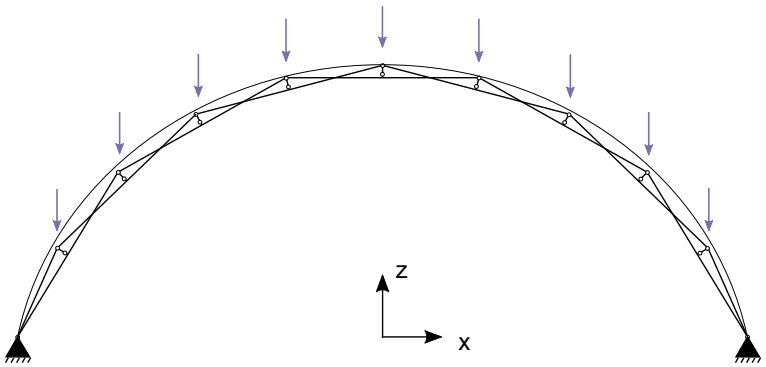

Figure 9.3: Self-Weight Point Forces acting on the PRFA

The wind and snow load act on the roof cladding and are transferred to the PRFA via the transverse beams as described in section 6.2. Consequently, wind and snow load are applied to the structural model at the same position as the self-weight point loads. The magnitude and distribution of the wind and snow load is different for every GV of the PRFA. Appendix C.2 describes assumptions, provides numerical examples that demonstrate the computations and elaborates the programming implementation of the loads to the structural model.

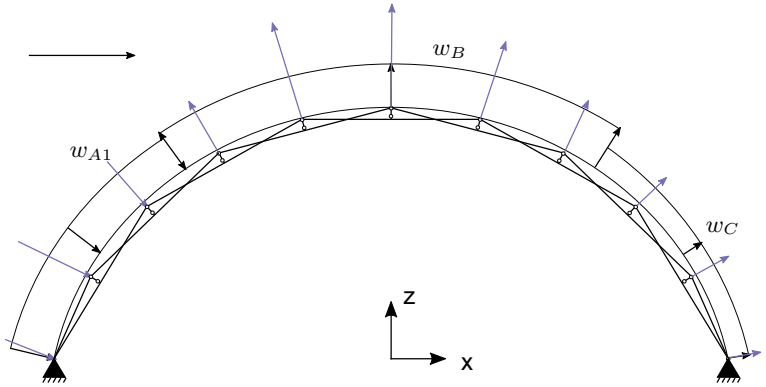

Figure 9.4: Wind Load acting on the Cladding and resulting Forces on the PRFA

Figure 9.4 and 9.5 illustrate an example for the implementation of wind and snow load to the model by showing the loads that are applied to the cladding (black) as well as the corresponding resulting point forces (purple). For the definition of the two load cases $w1$ and $s3$, refer to the mentioned appendix.

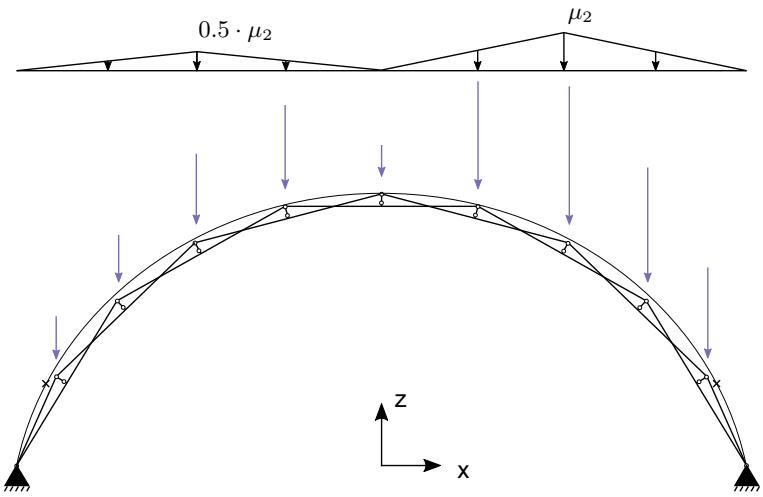

Figure 9.5: Snow Load acting on the Cladding and resulting Forces on the PRFA

9.2. Structural Analysis

The structural model is analyzed with the finite element program Karamba3D. The line geometry is converted to Timoshenko beam elements. No mesh refinement analysis is conducted, because the power series method is used for the integration of the elements. According to the software developer, this integration method allows to compute beams with an exact solution for the displacements independent of the number of finite elements.

Deflections and internal forces are computed with the first order linear-elastic analysis. A second order analysis is conducted to compute the buckling factor.

9.2.1. Model Validation

To validate resulting deflections and internal forces the numerical model is compared with an analytical equivalent. The continuous arch is a structural system that is related to the PRFA regarding the shape. The arch associated with the PRFA has a constant curvature. Because the arch theory does not provide an analytical solution for this arch shape, the comparison is conducted for an alternative arch form.

A parabolic PRFA is modelled and compared with an analytical model. A symmetric and an asymmetric load case are considered. Appendix C.3 contains a description of the models that are used for the comparison. Besides the two model descriptions, the named appendix also contains a comparison of an analytical and a numerical model of the continuous parabolic arch. This comparison is conducted to ensure that boundary conditions and input parameters are identical for the different software environments and to identify differences that occur due to the modelling technique.

Table 9.2 and 9.3 list characteristic values of the analytical arch model and two variants of the parabolic PRFA that differ in number of members for the symmetric and asymmetric load case respectively. The vertical support reactions are identical for all models. The horizontal support reactions are lower in the PRFA. The parabolic PRFA with 23 members has the lowest horizontal thrust at the supports for both load cases.

Table 9.2: Symmetric Load Case (A.M. is short for Analytical Model)

	A. M.	PRFA $n_m = 7$	Deviation [%]	PRFA $n_m = 23$	Deviation [%]
$w(x \approx L/2)$ [mm]	0.00	0.02	100.00	0.20	100.00
$w(x \approx L/4)$ [mm]	0.00	-0.19	100.00	0.13	100.00
w (x=3L/4) [mm]	0.00	-0.19	100.00	0.13	100.00
A_v [N]	7000.00	7000.00	0.00	7000.00	0.00
B_v [N]	7000.00	7000.00	0.00	7000.00	0.00
A_h[N]	6125.00	5043.00	0.02	4652.00	31.66
B_h [N]	-6125.00	-5043.00	0.02	-4652.00	31.66
N(x=L/2) [N]	-6125.00	-2982.00	0.03	-2360.00	159.53
N(x=0) [N]	-9301.00	-4371.00	0.33	-4200.00	121.45
M(x=L/2) [Nmm]	0.00	0.00	100.00	24000.00	100.00

Table 9.3: Unsymmetric Load Case (A.M. is short for Analytical Model)

	A. M.	PRFA $n_m = 7$	Deviation [%]	PRFA $n_m = 23$	Deviation [%]
w(x=L/2) [mm]	0.00	0.01	100.00	0.10	100.00
$w(x \approx L/4)$ [mm]	-20.00	-16.34	16.67	-22.85	12.47
$w(x \approx 3L/4)$ [mm]	20.00	16.16	16.67	22.71	11.93
A_v [N]	-1750.00	-1750.00	0.00	-1750.00	0.00
B_v [N]	5250.00	5250.00	0.00	5250.00	0.00
A_h [N]	3063.00	2522.00	0.03	2326.00	31.69
B_h [N]	3063.00	2522.00	0.03	2326.00	31.69
N(x=L/2) [N]	0.00	-1990.00	100.00	-1450.00	100.00
N(x=0) [N]	-3333.00	-1640.00	0.21	-1390.00	139.78
N(x=L) [N]	-5968.00	-2730.00	0.13	-2820.00	111.63
M(x=L/2) [Nmm]	0.00	0.00	0.00	0.00	0.00
M(x ≈ L/4) [Nmm]	$3.06 \cdot 10^6$	$2.65 \cdot 10^6$	0.10	$3.04 \cdot 10^6$	0.76

The displacement values of the numeric models that are listed in tables 9.2 and 9.3 are taken from the nodes closest to the named x-coordinates. Similar to the numerically modelled continuous arch, the PRFA does not achieve to model the ideal zero displacements for the symmetric load case. Nevertheless, the magnitude of the displacements is negligible compared to the span. The displacement shapes of the analytic and numeric model have a similar form. The displacements are also of the same magnitude. For $n_m = 7$ the displacements are 17% lower, for $n_m = 23$ the displacements are slightly larger. This is not considered an inaccuracy in modelling, but an indicator that a parabolic PRFA with less members responds stiffer than the continuous arch and the PRFA with more members.

The axial forces in the longitudinal elements of the PRFA have a similar distribution to those in the analytical arch. However, the magnitude is not the same. The axial forces in the PRFA arch are smaller than 50% of those in the continuous arch. This can be explained by the fact that the the normal force is divided into the two interwoven arches. The moment distributions of the two models are also comparable. For the symmetric load case, the parabolic PRFA shows negligible moments as expected. For the unsymmetrical load case, the moment distribution of the continuous arch is imitated by the PRFA through a “continuous chain of single span beams”, see figure 9.6. The magnitude of the moments for the PRFA with $n_m = 27$ is almost identical with a relative difference with less than 1%. The PRFA with $n_m = 7$ appears to respond with a moment of a lower magnitude. The magnitude of the axial forces in the pendulums corresponds to the magnitude of the moments in the adjacent longitudinal elements. A large moment in neighboring elements implies a high axial force in the pendulum.

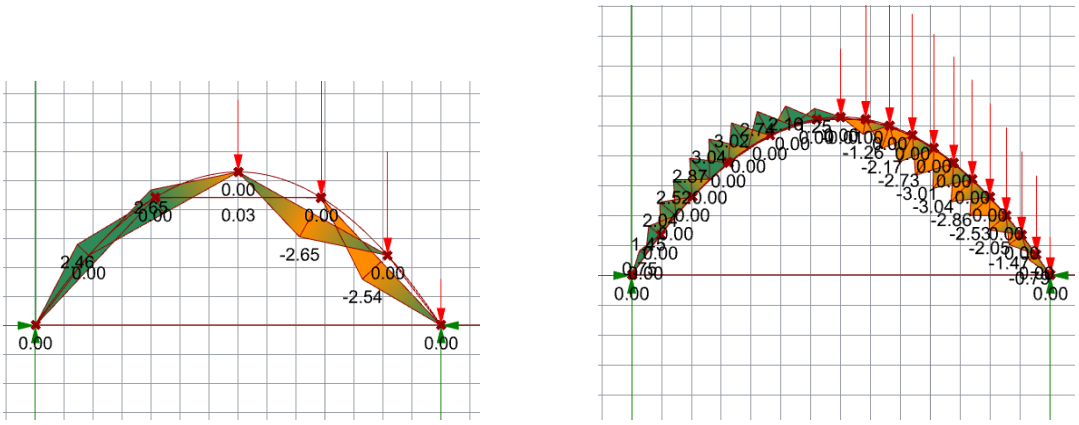

(a) $n_m = 7$ **(b)** $n_m = 23$

Figure 9.6: Moment Distribution PRFA, unsymmetrical Load Case

It is concluded that the structural behavior of the PRFA is similar to a continuous arch. Support reactions, deflections and internal forces show comparable behavior quantitatively and qualitatively. Different to the continuous arch, the PRFA has a lower horizontal thrust at the support points and the magnitude of the axial forces is only 50% of the axial forces in the continuous arch. Furthermore, the moments in the PRFA are of the same magnitude as in the continuous arch. Distributions are different locally, as the individual longitudinal elements of the PRFA act as single span beams. No major differences are observed in the deformation behavior. The comparative study validates the numerical model of the PRFA.

9.3. Structural Verification

9.3.1. Structural Behavior

Before evaluating the geometric design proposals, the structural behavior of the PRFA is assessed to identify the locations in which stresses are the largest. The structural evaluation of the geometric design proposals can then limit itself to the found locations.

In the previous subsection, it was identified that the structural behavior is comparable to that of a continuous arch, but not identical, because the individual members act as single span beams. All beams of the structure, with exception of the side members, have the same boundary conditions and the same type of forcing. Hence, the load bearing principles are identical and it is sufficient to consider one beam to further investigate the PRFA's load bearing behavior.

Figure 9.7a displays a longitudinal element with its boundary conditions and connected members. At both ends an eccentricity element and a longitudinal element are connected via a hinged joint. At the center an eccentricity element is connected to the longitudinal element under a right angle. The eccentricity element is pinned at both ends; it acts as a strut.

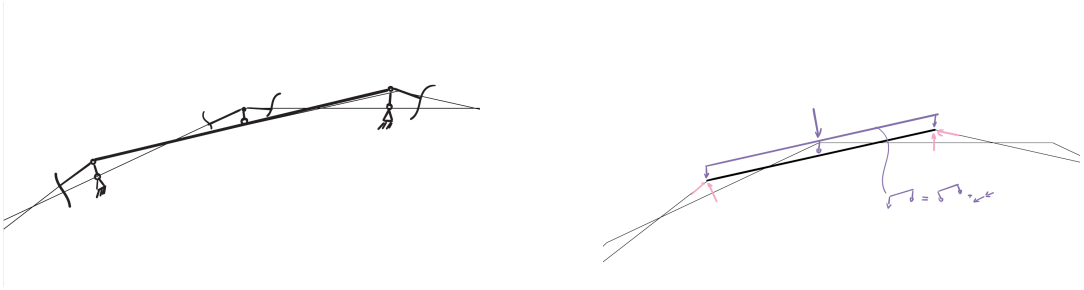

(a) Partial System

(b) Forces on Partial System

Figure 9.7: PRFA Geometry

Figure 9.7b illustrates the forces that act on the longitudinal member. The only external load that is directly applied to the beam is a distributed gravity load. This load has a parallel and perpendicular component with respect to the coordinate system of the beam. At mid span, the pendulum introduces a perpendicular point load. Decisive for the structure's load bearing behavior is what happens at the nodes where the point load is introduced. In this node the forces of connected members and the point load that is introduced from the transverse beam are in equilibrium. The part of the point load that is taken by the eccentricity element will lead to bending; the part of the point load that is taken by the longitudinal beams does not lead to bending. The members' stiffness and their orientation in space decide how the point load is split up.

In the previous subsection it was observed that if a PRFA is of the form that is the single stress state shape of the associated continuous arch, then the eccentricity elements attract minimal load and the structure acts as a truss, compare appendix C.3. The further the PRFA moves from this perfect shape, the more load enters the eccentricity element and bending occurs. The resulting moment distribution is typical for a RF. Globally it corresponds to the moment distribution that would be present on the equivalent continuous structural form, in this case a continuous arch, but per element, it has the moment distribution of a single span beam.

Figure 9.8 displays the distributions of the internal forces. A member acts as a combination of a single span beam due to the forces introduced along the span and a strut due to the forces introduced at the end nodes. The distributions are always the same. The signs and the magnitude of the internal forces however depend on the relation between load and form and stiffness of the members as described above.

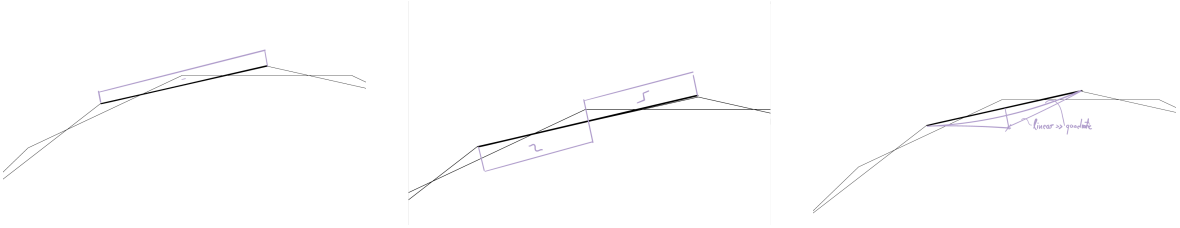

(a) Normal Force **(b)** Shear Force **(c)** Moment

Figure 9.8: Internal Forces

The normal force is linear, the slight slope originates from the parallel component of the distributed gravity load, the main contribution of the normal force is constant. A similar behavior is observed for the shear force. The perpendicular component of the gravity load introduces a slight slope, but the main contribution stems from the point load at mid span, which causes a sudden shift. The bending moment is a combination of a linear and a quadratic distribution. The linear distribution due to the point load is governing.

9.3.2. Structural Verification of Geometric Design Proposals

To determine whether a geometrical design proposal is safe, the output of the validated structural model is assessed in the ultimate limit state (ULS) and the serviceability limit state (SLS). A design proposal is labelled as safe, if stability and strength unity checks are verified and deflections stay within prescribed limits.

A number of prerequisite steps are taken to conduct the structural verification. The modelled load cases are integrated to load combinations according to the NEN-EN 1990. The values of the design strength R_d are computed for the relevant strength and stability verifications. For the strength verification of the longitudinal elements, shear stresses and stresses resulting from combined bending and axial force are assessed. With regards to stability, lateral buckling and lateral torsional buckling are investigated per longitudinal element. For the SLS, the limit criteria for the deflections are established and the corresponding instantaneous and final deflections are computed at characteristic positions. Vibrations and other phenomena that may be addressed in the context of the SLS are not considered in this study. In total there are ten criteria that are checked for every geometric design proposal in order to determine whether it is structurally safe. For each criterion a unity check is computed, an example is illustrated in figure 9.9.

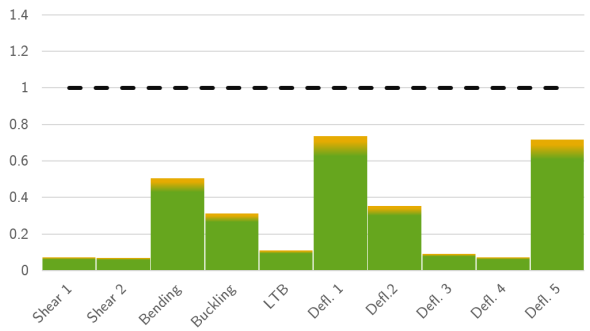

Figure 9.9: Unity Checks for Limit Criteria for Geometric Design Proposal S9V2

It is illustrated that all ten unity checks are below 1.0, that means the geometric design proposal is labelled as safe.Appendix C.4 elaborates the steps that prepare the unity checks of the ten criteria.

Figure 9.10 and 9.11 display the results of the case assessment for the RT stack 1 - 11 and 26 - 30. The results were generated with assuming strength grade reduction R3(a) (compare chapter 7) and a bay span of $L_{bay} = 1.0\,\text{m}$. The displayed results reflect on all of the ULS unity checks and SLS verifications for all structural elements and all load combinations.

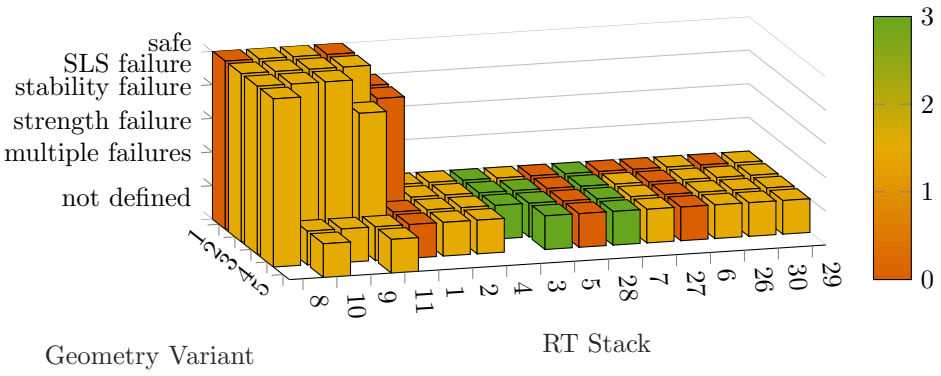

Figure 9.10: Assessment of Geometric Design Proposals (Strength Grade Reduction R3a), Color-Code indicating e/h-ratio

The x- and y-axis of the bar plot specify the indices of the GV and the RT stack respectively. The GVs are ordered according to the generation sequence, i.e. for a higher GV index n_m and e increase. The RT stacks are ordered according to their cross-sectional area, the largest cross sectional area is closest to the diagrams origin. On the z-axes it can be read if a geometric design proposal is safe or if it is not safe, what type of unity check failed. If for example one of the characteristic deflections exceeds its limit criterion, the bar will indicate “SLS failure” or if one or more stability and strength unity checks fail, then the bar will indicate “multiple failures”. The bar indicates that a design proposal is safe only when all unity checks are ≤ 1.0. In the case that no bar is displayed for a PRFA case, then the corresponding GV does not exist for that RT stack.

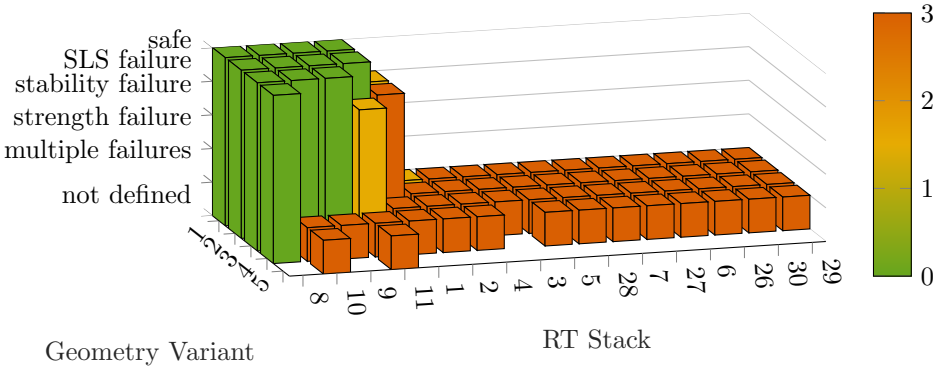

Figure 9.11: Assessment of Geometric Design Proposals (Strength Grade Reduction R3a), Color-Code indicating critical Unity Check

The only difference between figure 9.10 and 9.11 is the color-code of the bar plot.

Figure 9.11's color shows the ratio of the eccentricity over the member height. An orange bar implies a ratio smaller than one and a yellow or green bar mean that the ratio is larger than one. This ratio is displayed in order to assess if a design proposal accommodates the conceptualized joint detail. Figure 9.10's color shows the value of the unity check with the highest magnitude. A green bar implies that the value of the critical unity check is below 1.0, a yellow bar indicates that the critical unity check fails with a value between 100% and 200%. An orange bar implies that the failing unity check has a value of at least 200%. Displaying the value of the critical unity check allows to identify geometric design proposals that fail, but are not too far from being safe.

The primary purpose of the plots is to function as a tool for identifying geometric design proposals that span a distance of 14.0 m in a safe manner. To utilize the plots for this purpose, the focus is directed to those cases that have a bar which reaches the label "safe" on the z-axes. From these bars, the ones with an eccentricity to cross-sectional height ratio of below 1 are disregarded, these are the orange colored bars in figure 9.11. For the remaining PRFA cases essential information about the RT item such as member length L, material status, number of pieces, and the building year and function of the previous life cycle are looked up in the updated database in tables 7.2 and 7.3. With the member length and the index of the GV, the proposal's graphical representation that was developed as part of the geometry generation is pinpointed and it is ensured that the GV has a span $L_{span} \geq 14.0\,\text{m}$ (compare appendix C.1). Lastly, the actual strength grade of the design proposal's RT members are identified through the previous life cycle's building year and the strength grade reduction table 7.1.

Figure 9.10 and 9.11 visualize the results for a strength grade reduction of R3(a). For the results of the remaining strength grade reductions and the output data of the RT items 12 - 25 for which the strength grades are known, refer to appendix C.5. To identify the safe design proposals for the RF canopy, strength grade reduction R3(a) is used, i.e. for RT with a virgin timber strength grade of C24 and C30, the RT strength grade is reduced to C16 and C18 respectively.

It is observed that twelve design proposals are capable of safely spanning $14.0\,\text{m}$. Two of the safe proposals, S8V1 and S11V1 do not comply with the conceptual joint design requirement of the eccentricity being larger than the cross-sectional height. The safe proposal S8V4 is also not further considered because its span is smaller than 14.0 m. Table 9.4 gathers relevant data of the nine safe design proposals that are selected for a further investigation which is conducted in the following subsection. For the graphical representation of the safe proposals, refer to appendix C.1.

Table 9.4: Properties of the safe Design Proposals

PRFA case	L [m]	w x h [mm x mm]	RT SG [-]	L_{span} [m]	h_r [m]	Pieces per PRFA [-]	Number of pieces [-]	Material status
S8V2	4.2	210 x 280	C18	14.08	5.46	10	153	fixed
S8V3	4.2	210 x 280	C18	14.08	6.64	11	153	fixed
S9V1	3.7	140 x 200	C18	14.04	3.91	10	984	fixed
S9V2	3.7	140 x 200	C18	14.28	5.08	11	984	fixed
S10V1	4.0	140 x 210	C18	14.14	3.31	9	132	fixed
S10V2	4.0	140 x 210	C18	14.10	4.86	10	132	fixed
S10V3	4.0	140 x 210	C18	14.33	5.98	11	132	fixed
S11V1	4.0	80 x 240	C18	14.14	3.31	9	420	free
S11V2	4.0	80 x 240	C18	14.10	4.86	10	420	free

Besides the safe cases, many of the geometric design proposals fail. The large part has multiple failures with a critical unity check of beyond 200%. Failure in the SLS is the only failure type that occurs by itself, it is inferred that SLS checks are critical for the PRFA. To illustrate the purpose of color plotting the value of the critical unit check, three proposals that have a yellow bar, i.e. its highest unity check is below 200%, are considered in more detail.

Proposal S1V1 does not comply with an SLS unity check, strength and stability are verified. Yet, this proposal is not further considered, because its e/h-ratio is smaller than one. S11V3 also only fails to comply with the SLS criteria. Upon a closer assessment of the unity checks, it is identified that only the instantaneous deflection w_{inst} exceeds the corresponding limit criterion by 23%. All other unity checks are fulfilled. The deflection limit criteria are agreed upon per project, if this proposal was preferable to e.g. the architect, it could be considered to either adjust the limit or look to a way to stiffen the construction, so that this option could be used for the detail design.

S19V1, displayed in figure C.36 in the appendix C.5 has multiple failure types with the critical unit check of smaller or equal to 200%. Upon a closer look, it is identified that both local buckling types fail for at least one member with the critical unity check of 195% and 177%. The second failure type is related to deflections, a unity check is exceeded by 26%. One possible option to adjust the design of the PRFA so that the stability unity checks are lowered is to assume that the longitudinal beam is laterally supported at mid span through the connection with the transverse beam. This would reduce the buckling and critical factor. For the considered proposal, this would lead to values of $\leq 100\%$ for both stability unity checks. As a result the design proposal would only fail to comply with deflection limits.

9.3.3. Structural Design

For determining the safe geometric design proposals a bay span of $L_{bay} = 1.0\,\text{m}$ was assumed. With the aim to determine the maximal possible bay span, an optimization of the bay span is conducted. This restricts itself to the safe PRFA cases. The results are plotted again in two graphs that only differ in their colorcode. On the x-axes the bay span is displayed in meters. The y-axes specifies the geometric design proposal. The z-axes is is used in the same manner as in the previous sub section to determine if a case is safe or if it fails, what failure type occurs. The color-code in graph 9.12 displays the PRFA's buckling factor.

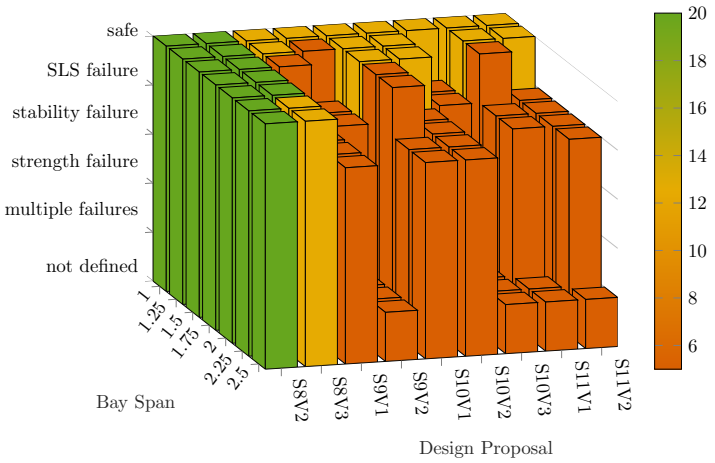

Figure 9.12: Selected Geometric Design Proposals varying d_A and Buckling Factor Color-Coded

If a bar is green or yellow, the buckling factor is above 10 and it is assumed that the structure is not sensitive to second order effects which means that the forces and displacements that were computed with the first order linear-elastic analysis are sufficiently accurate, compare also appendix C.4. The color in figure 9.13 indicates the maximum length that the structure can achieve in transverse direction for a specific bay span. This maximum length is computed as follows

$$L_{canopy,t} = \left(\frac{\text{number of pieces for RT item}}{\text{number of members per PRFA}} - 1 \right) \cdot L_{bay} + 2 \cdot w$$

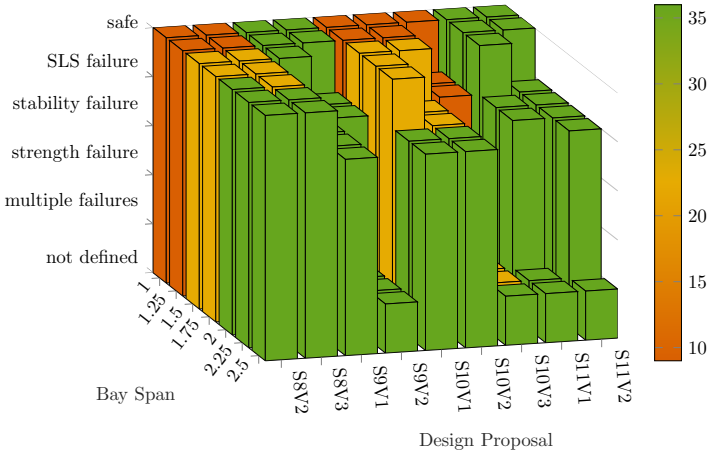

Figure 9.13: Selected Geometric Design Proposals varying d_A and transverse Span Color-Coded

Because there are multiple safe options, additional criteria are considered to decide which design proposal is further developed in the detail design. From the RT stacks, stack 11 is disregarded because relative to the other safe RT items its cross-sectional width is much smaller. This could turn out to be a disadvantage in the joint detailing. For each of the remaining three RT stacks the GV that has a rise closest to the rise $h_r = 5.5m$ of the reference structure is selected. These are proposals S8V2, S9V2 and S10V3 with a rise of $h_r = 5.46m$, $h_r = 5.08m$ and $h_r = 5.98m$ respectively.

Before specifying the final bay span, the properties of the RT stacks are evaluated once more. All three stacks originate from the same building, a Spanish Corrala. The material status is fixed, that means the donor building was not yet deconstructed. As recommended in section 3.4.2, the number of items will be reduced because it is likely that a part of the RT stack's items will be damaged during dismantling and another part will not have the anticipated geometrical and mechanical properties. It is estimated that only 50% of the fixed items will be fit for structural reuse.

Moreover, based on the location in the previous stress grade the strength grade of RT stack 8 is reduced from C18 to C14. Items from RT stack 8 served as columns, items from stack 9 and 10 as floor and roof beams respectively. The strength grade of RT stack 8 is reduced because it is expected that columns experience a larger dead load leading to a larger strength reduction, compare section 3.6.2. This additional strength grade reduction is already accounted for in figure 9.12 and 9.13.

For the three named design proposals, the maximum possible bay span with a buckling factor of above 10 and the corresponding maximum transverse beam are read from the graphs. S8V2 is capable to span 2.5 m. The graph indicates that the bay span can be even larger for this proposal while maintaining a buckling factor larger than 10. It is decided to choose a bay span of $L_{bay} = 3.0\,\text{m}$. The maximum canopy length in transverse direction that corresponds to this bay span for the reduced number of pieces is $L_{canopy,t} = 36.4\,\text{m}$. S9V2 and S10V3 have already reached their maximum bay span with $L_{bay} = 1.0\,\text{m}$ for the presented criterion of the buckling factor. The corresponding maximum canopy length in transverse direction is larger for case S9V2 because the number of items is much larger. The two lengths are $L_{canopy,t} = 88.3\,\text{m}$ and $L_{canopy,t} = 11.3\,\text{m}$.

According to these results at least three RF structural canopy designs can be proposed. Two design options are to construct the canopy only from S8V2 or S9V2. A third option is to combine the different geometric design proposals. Figure 9.14 - figure 9.16 contain renders of the three design options. The third render combines five PRFAs of case S8V2, six PRFAs of case S10V3, and eleven PRFAs of case S9V2.

Figure 9.14: Design Proposal S9V2

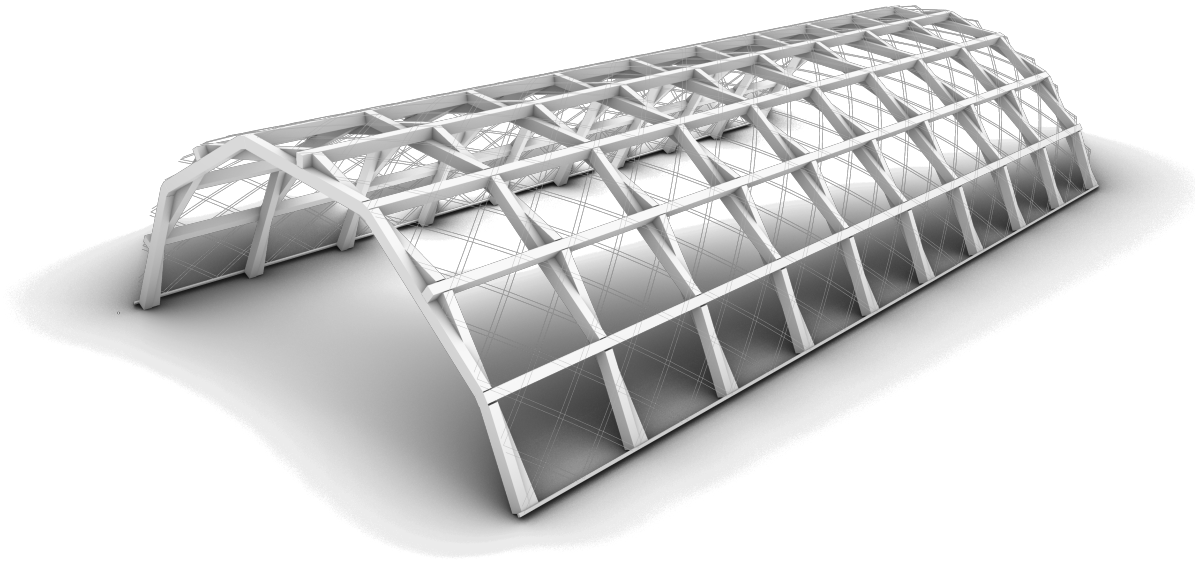

Figure 9.15: Design Proposal S10V3

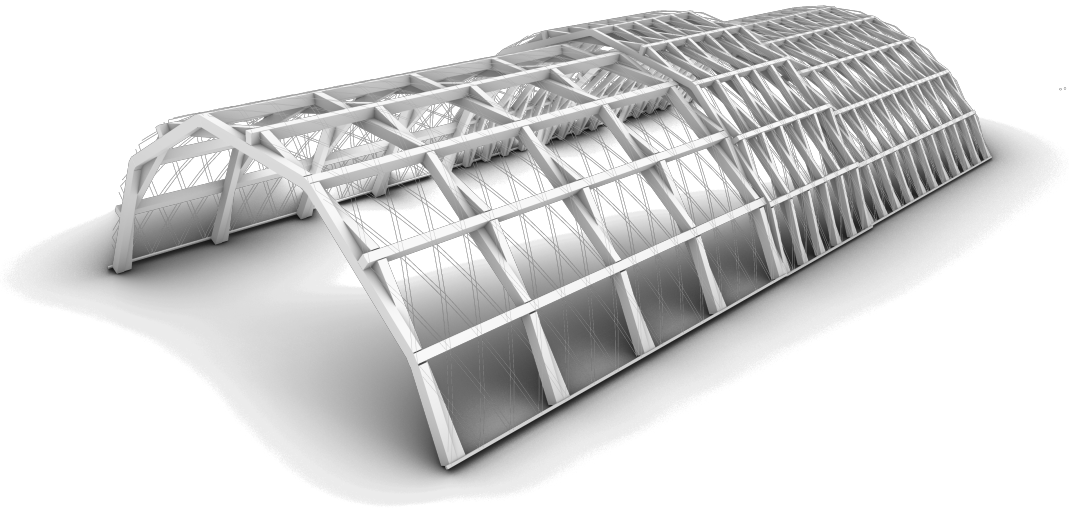

Figure 9.16: Design Proposal Combination of PRFAs

10

Detail Design

In this chapter the joint details of the canopy are considered. The focus is on the joints of the PRFA because its detail design is required to verify that the structural utilization of RT is viable in the design proposals. The remaining joint details are listed, due to time constraints they are not further developed.

10.1. PRFA Joint Design

The joint of geometric design proposal S9V2 is detailed. The generated geometry is slightly altered to decrease the span deviation, compare section 9.1.1. Through increasing the eccentricity by $8\,\text{mm}$ to $e = 238\,\text{mm}$, the span decreases from $L_{span} = 14.27\,\text{m}$ to $L_{span} = 14.00\,\text{m}$. As a side effect, the rise increases and the internal forces grow slightly, yet it can be verified that all SLS and ULS verifications are still satisfied.

Joint geometry

In figure 10.1a a front view illustrates the relation between the two-dimensional structural model and the three-dimensional joint geometry.

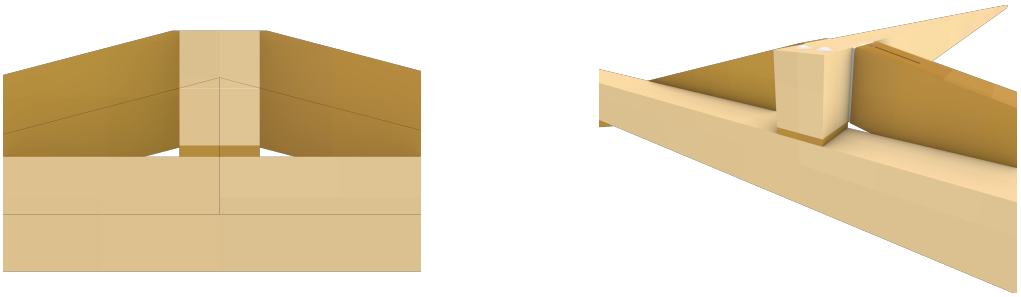

(a) Front View **(b)** Perspective View

Figure 10.1: Geometry of the PRFA Joint

The longitudinal beams are placed so that their center axes coincides with the longitudinal elements of the two-dimensional model, then the beams of the interwoven arches are separated in two planes, so that their side faces are aligned as visualized in figure 10.1b. The ends of the longitudinal beams are cut off, so that their end-face is aligned with the side of the transverse beam.

The transverse beam is placed on the axes of the eccentricity element. The position of the transverse beam is shifted, so that its center axes lies on the level, marked with a white line in figure 10.1a, at which the longitudinal beams' center axes are at the location of the cut. This placement avoids eccentricities in the force transfer. The gap that results from a e/h-ratio > 1 is filled with a "timber block". This timber block also enables to compensate irregularities of geometry from the connected members on-site. Against this background, it is also expected that the proposed accuracy of the eccentricity, namely 1 mm can be achieved. To ensure that the top face of the transverse beam is the outermost face of the joint, an additional cut at the end of the longitudinal beams is conducted to take off a small edge that juts out at the top.

The joint is divided into two connections. Connection I, modelled by the inner endpoint of the eccentricity element, joins transverse beam, timber block and the longitudinal beam at mid span. Connection II, modelled by the outer endpoint of the eccentricity line, joins the ends of the longitudinal beam with the transverse beam. Both connections are modelled as hinges, hence the detailing is executed so that no moments are transferred.

Connection I

Connection I transfers compression and tension between the longitudinal beam at mid span and the transverse beam. It is assumed that no shear forces are transferred. Compression forces travel through contact. Figure 10.2 shows a side and front view of the connection detail.

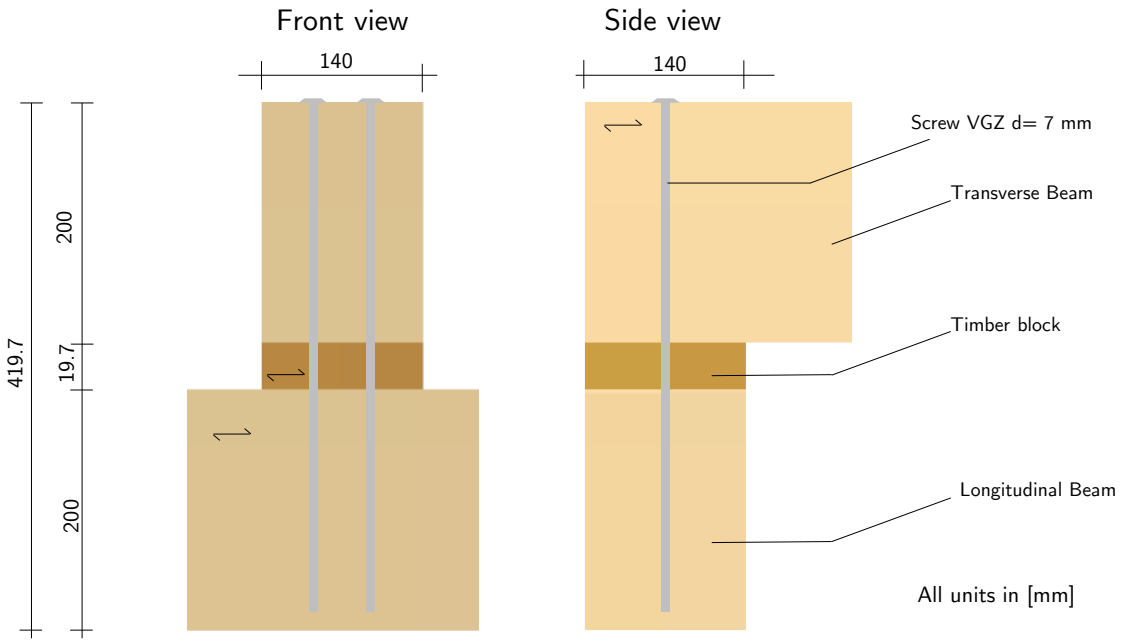

Figure 10.2: Connection I - Front View and Side View

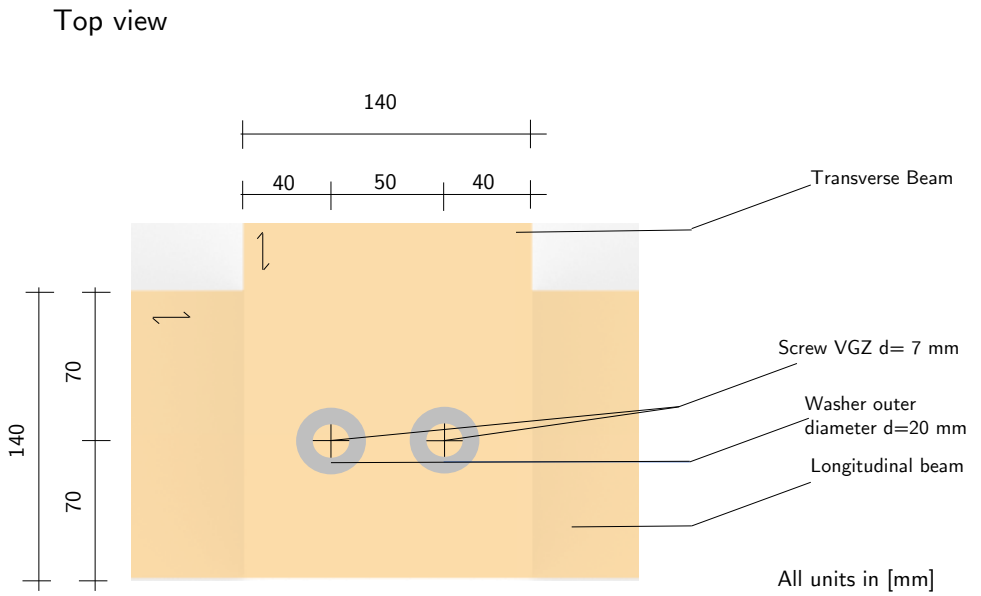

Figure 10.3: Connection I - Top View

Figure 10.3 displays a top view. Tension forces are contained through two screws that are inserted at the top face of the transverse beam and reach through the timber block almost to the bottom face of the longitudinal beam. Washers ensure a force distribution at the top end of the screw.

To verify the connection, the compression stress that acts perpendicular to the grain is evaluated at the contact surface between transverse beam and timber block, and the surface between timber block and longitudinal beam. For the axially loaded screws, withdrawal capacity of the screws' threaded part, pull through strength of the screw heads and tension strength of the screws are assessed. For fastener specifications, verifications, and detail drawings of all connections, refer to appendix C.6.

The governing unity check is the pull through strength of the screw head with a utilization of 70%. The connection is not further optimized through a reduction of fastener because at least two connection components are required for robust design. Moreover, the diameter of the screws is not lowered because more slender screws are not available in conventional catalogues.

Connection II

It is sufficient to consider one side of Connection II, because its geometry is symmetrical and the connection is detailed identical on both sides. The connection is executed with a joist hanger steel plate which acts as an intermediator between the two timber beams. The connection is characterized in two parts. Part A joins the side of the transverse beam with the steel plate and part B joins the end of the longitudinal beam with the steel plate. Figure 10.4 and 10.5a show front view, side view and top view respectively of Connection II.

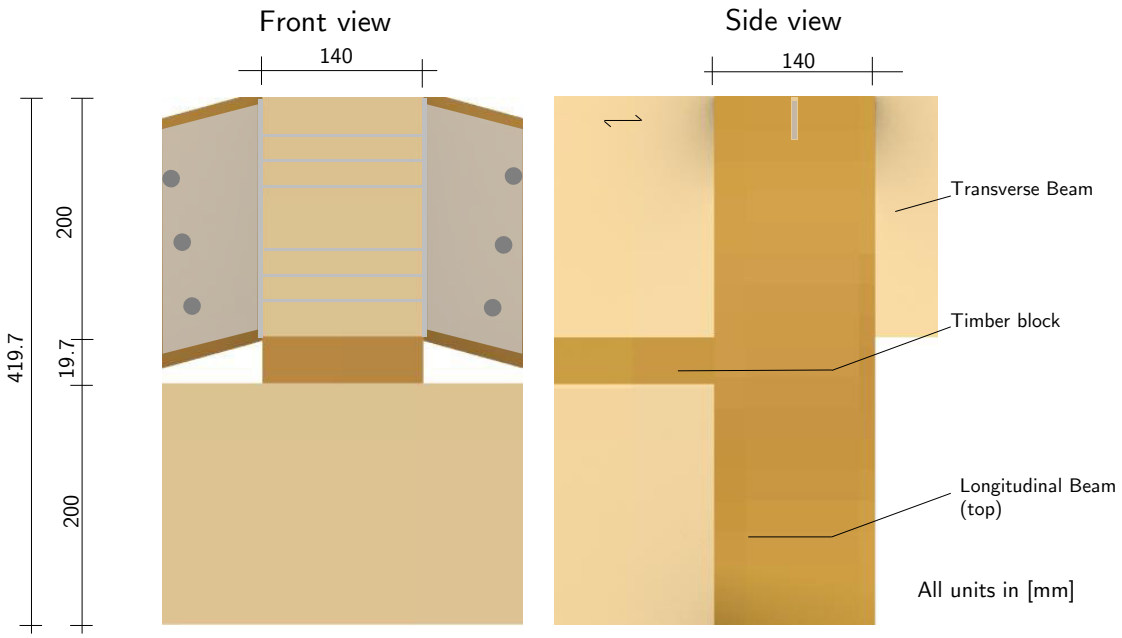

Figure 10.4: Connection II - Front View and Side View

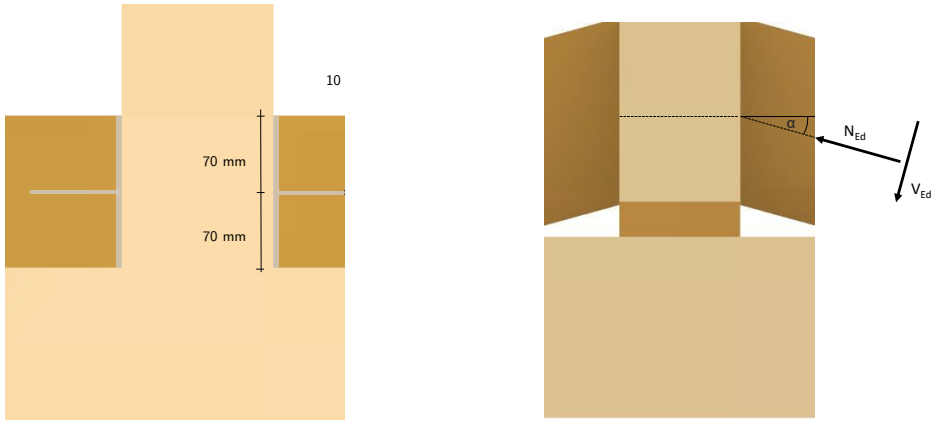

(a) Connection II - Top View

(b) Connection II - Acting Forces

Figure 10.5: Geometry of the PRFA Joint

Connection II-A transfers compression, tension and shear between steel plate and transverse beam, compare figure 10.5b.

Compression forces travel through contact. The tension force is transferred through axial action of 12 screws from steel plate to timber and through rolling shear to the opposite site. The shear force is transferred through lateral action of the screws.

For the verification, the compression stresses that act perpendicular to the grain on the side of the transverse beam are evaluated. For the axial action of the screws, withdrawal capacity of the screws' threaded part and tension strength of the screws are assessed. Additionally, the rolling shear in timber is examined. The lateral action of the screws is verified with the Johansen model. The three failure mechanisms for a thick steel plate in single shear are considered.

The governing unity check is the rolling shear verification in the transverse beam with a utilization of 64%. The number of screws is not reduced, because the next symmetric pattern with a lower number of screws would already not be safe. Moreover, the chosen type of screw is not available with a smaller diameter.

Connection II-B transfers compression, tension and shear between longitudinal beam and slotted in steel plate. Compression travels via contact of the end-face and the steel plate. Tension and shear force are transferred through lateral action of two dowels and a bolt that have two shear planes between timber and steel. In the designed symmetrical fastener arrangement, the dowels are used to reduce the slip, the bolt holds the connection in place. The fastener arrangement as well as the acting forces are illustrated in figure 10.6

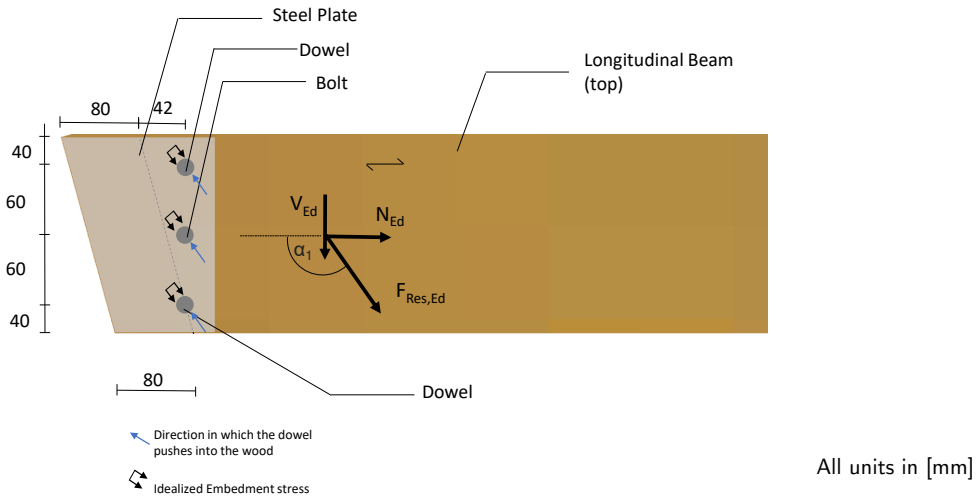

Figure 10.6: Connection II-B Joist Hanger with Fasteners

To verify this part of the connection, the compression stresses that act under an angle to the grain on the end-face of the longitudinal beam as illustrated in figure 10.7 are evaluated.

Figure 10.7: Connection II-B Compression under an Angle to the Grain

The lateral action of the dowels and bolts is verified with the Johansen model. The three failure mechanisms for a steel plate as central member of a double shear connection are assessed.

The governing unity check is the ductile failure mode of the steel-to-timber connection in which two plastic hinges develop per fastener per shear plane. With 27%, the utilization of the connection is low. The diameter of the dowels is already at its minimum. To maintain symmetry and low slippage the low utilization is accepted.

10.2. Remaining Canopy Joint Details

For the cladding three connection types must be detailed. The connection between the poly carbonate sheet and the timber lath grid must ensure water tightness because the poly carbonate sheet is the roof's skin. The connection that joins the timber laths to a grid and the connection of the grid to the transverse beams must be detailed, so that the loads acting on the roof are transferred to the transverse beams.

The transverse beams were assumed to be composed of shorter beams that are connected through half lap-joints. The size of the transverse beams were determined to have the same size as the longitudinal members. A detail design could revise this choice depending on the utilization of the transverse beams which is influenced by the bay span. Furthermore, it is to be investigated if it is possible to utilize RT also for the transverse beams.

Because the geometry of the PRFA is regular, its joints are identical with the exception of the two joints to which the side members connect. In this position the joint geometry is slightly different. The joints are yet to be detailed.

The PRFA is supported by a concrete wall. One type of joint is required to transfer the vertical and horizontal force. The horizontal force should be transferred in a way that activates the rest of the building for this loads take down.

The steel tube truss, which braces the canopy structure, is integrated into a number of PRFAs through an additional connection at the PRFA joints.

Part IV

Reflections

11

Discussion

In this chapter the case study is discussed with the goal to derive a design strategy for the structural utilization of reclaimed timber in RF structures. The design phases are addressed individually. The first design phase is omitted because it focuses on the specific building concept and does not add to the subject of the design strategy. In the final section, the relation between the phases of the design strategy are discussed and their relation to the structural utilization of RT is emphasized.

11.1. Material Stock Definition

Little data on timber fixed in the building stock and timber that can potentially be reused structurally is accessible, compare section 3.4. Existing research on the interface between RT and RFs has taken different approaches in compensating the lack of material data. Castriotto et al. based their research on one specific stock of material that was reclaimed from waste (2021). Besides the obvious geometric properties, the stock's prior application and its initial strength grade were identified in the named study. Parigi and Damkilde (2019) and Parigi (2021) have based their research on randomly assumed geometric properties, mechanical properties are not addressed explicitly.

The present study chose the novel approach of defining a database for RT. The database aims to present the stock of fixed, free and fit RT to designers as specific as possible to form an appropriate starting point for a structural design as elaborated in section 3.4.2. The utilization of such a RT database shifts the issue of sustainability which is often considered as an evaluation criteria at the end of a design process, to the very beginning of a building's conceptualization. This prioritization of sustainability changes the design process in its essence and leads to a novel design strategy with which the environmental benefits of the structural utilization of reclaimed timber are reaped. The benefits were mentioned in section 3.5.2.

The example for a database that was developed as part of the literature review is incomplete. Two assumptions were required, so that the database can function as starting point for a structural design. These assumptions relate to two problems in the reuse practice of timber.

First, an initial strength grade for the RT items was assumed. This assumption is a rough estimate. The choice for an initial strength grade is solely based on the year when the material was utilized in a structure. It is problematic to assign a timber grade in this manner. Certainly, not all timber, which was used in construction before and after machine grading existed, had the same strength grade as this assumption implies. Furthermore, the assumption erroneously infers that only softwood was used and that the quality of timber was the same in all places. Second, the reduction of the strength grade due to prior structural use was assumed. This assumption is ambiguous as well. Even if the initial strength grade was known, the RT strength grade could not be determined in a certified way, because no related European standard exists.

The fact that the database is hypothetical and that mechanical properties are based on coarse, potentially inaccurate assumptions forbid a realistic application of the database and the related structural utilization of RT. However, this does not deny the relevance of the present academic study. Considering that the problems that require the assumptions are currently being tackled, the assumptions are viewed as a temporary necessity. The present investigation of the structural utilization of RT has the potential to spur on the efforts of developing a visual grading standard and a realistic database for RT by demonstrating the capability of RT to be utilized in a building structure. Specific suggestions for further research and practical steps leading to a strength grading standard have been discussed in section 3.6.2 and applications of a RT database beyond structural utilization have been listed in section 3.6.3. Furthermore, an influence of the assumptions that could lead to erronerous results is prevented by investigating a range of mechanical properties for each item and eventually choosing for an arguably conservative estimate, compare section 9.3.3.

Considering that a large part of the infrastructure for this reuse practice already exists, compare section 3.3, and that there is an increasing interest in sustainable building practice, an application of the design method developed in this case study in a realistic context could soon be possible. Investigating the implementation of a RT database in practice is beyond the scope of this research. It is recommended to consider two questions in this context.

One, how to manage contracts related to a RT database. An answer to this question should specify who owns and maintains data, who has access to the data and how material can be claimed during different stages of a design process? Two, what is an effective procedure to add data to the database? A possible direction for answering this second question could be to investigate the feasibility of a “material donor card” which contains information about material geometry, initial mechanical properties and further potentially relevant details for structural reuse, compare subsection 3.4.2. Information from material donor cards of newly build constructions could be fed into a central material database that designers have access to.

If the two issues related to the implementation of a RT database in practice were to be explored, the goal should be to answer the research questions in a way that the resulting database is as large as possible, because the design options for a construction project that utilizes RT is limited to what can be build from the available stock of material. A larger stock is equivalent to an increased design freedom which in turn renders structural design with reclaimed timber more attractive.

11.2. Geometry Generation

11.2.1. Comparison of Directed Method and Parameter Study

To evaluate the directed method the resulting GVs are compared with the results of the parameter study. The GVs are valid geometries, thus they are also expected to appear in the parameter study.

In figure 11.1 the span of the PRFA with DL10 is plotted again for all valid combinations of input parameters. Additionally, a plane at $z = 14.0\,\text{m}$ is displayed in the graph. The plane is plotted with a transparency of 50%; the lighter part of the surface plot illustrates combinations of input parameters that have a span larger than 14.0 m; the shaded part of the surface which lies below the plane illustrates geometries with a span smaller than 14.0 m. The data points that lie in the proximity of the intersection of the two objects and belong to the upper part of the surface plot are candidates for geometric variants. Table 11.1 compares these candidates with the GVs that were identified through the directed method.

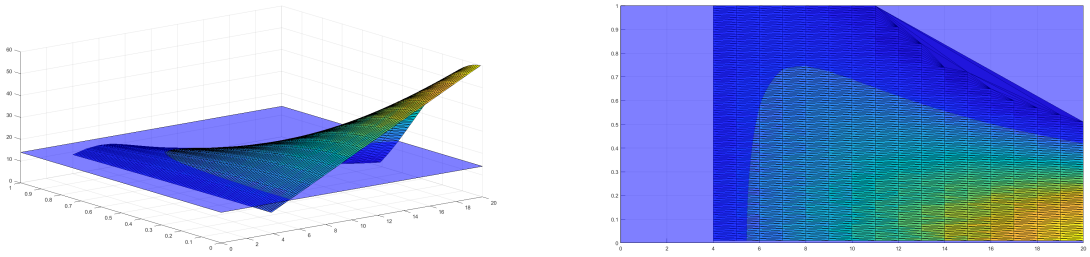

(a) Perspective View **(b)** Top View

Figure 11.1: Span of PRFA for valid Combination of Input Parameters with DL10 and Plane at $z = 14.0\,\text{m}$

Table 11.1: Comparison of Geometric Variants identified with the Directed Method vs. Parameter Study

	Directed Method			Parameter Study		
	n_m [-]	ec [m]	sp [m]	n_m [-]	ec [m]	sp [m]
GV0	6	0.0	15.75	6	0.57	14.02
GV1	7	0.73	14.02	7	0.73	14.02
GV2	8	0.74	14.13	8	0.74	14.13
GV3	9	0.75	13.36	9	0.72	14.13
GV4	-	-	-	10	0.69	14.05
GV5	-	-	-	11	0.65	14.23
GV6	-	-	-	12	0.62	14.02
GV7	-	-	-	13	0.58	14.45
GV8	-	-	-	14	0.55	14.29
GV9	-	-	-	15	0.52	14.74
GV10	-	-	-	16	0.50	14.31
GV11	-	-	-	17	0.47	15.05
GV12	-	-	-	18	0.45	14.99
GV13	-	-	-	19	0.43	15.13
GV15	-	-	-	20	0.42	14.03

The table shows that the input parameter study identifies a larger number of GVs than the directed method. For DL10 the directed method concludes with two suitable GVs and the input parameter study with 15. It is concluded that the directed method is efficient in drawing up GVs that comply with the criteria that were previously defined, namely aiming for an increase in eccentricity and a decrease in number of members. At the same time the method is blind for possible additional GVs that were only identified through the parameter study. However, these GVs are not further considered, because they are characterized by an increasingly larger number of members and a smaller value for the eccentricity.

If in an initial iteration none of the GVs which were found with the directed method turn out to be structurally safe, then the conceptual structural design and the directed method would be revised. For example, a joint detail that is capable to accommodate small eccentricities could be investigated, for many of the short DLs require small eccentricities to span the distance of $L_{span} = 14.0$ m. Considering the results of DL10, the additional GVs could also be interesting for items with large member lengths with the current joint detail, because the eccentricity values for a span of 14.0 m are high for the full spectrum of number of members relative to shorter RT items.

It is concluded, that the parameter study helps to understand the geometry of the parametric model. The knowledge from conducting a parameter study for a DL can be used to quickly estimate what input parameters are required to achieve a certain span with a DL. For instance, when considering figure 8.7a, it is obvious that to reach a span of 14.0 m with DL1 more than 20 members and a very low eccentricity are required, because none of the displayed input parameter combinations reaches this span. With an increase in member length the span will be reached with an increasingly larger value of the eccentricity. The numerical estimation of a required eccentricity for a span is a helpful tool during the conceptual design when deciding for the relation between cross-sectional height and eccentricity.

11.2.2. Evaluation of the Bottom-Up Model

The utilization of a computational bottom-up model is a novel approach for the geometry generation of a RF. Similar to physical models, it enables to intuitively explore the geometry of Linear RFs by consecutively adding units onto each other. In section 4.4.1, it was referenced that the computational modelling of RFs is restricted to the top-down approach. The present model demonstrates that at least for Linear RFs a bottom-up approach can be implemented computationally as well. The development of a bottom-up model for Surface RF structures is expected to be more complex due to additional geometrical constraints. Both from a structural and an architectural perspective, it is interesting to investigate a bottom-up model for a Surface RF. It is expected that a Surface RF is structurally more efficient than a Linear RF. Furthermore, resulting Surface RF structures have the appealing aesthetic of double curved geometries and they might be more capable in utilizing short members compared to linear RFs.

The developed bottom-up model cannot precisely comply with the architectural requirement of the span. In section 4.4.1, it was already mentioned that Godthelp points this out as a disadvantage of bottom-up models. Yet, the directed method allows to filter the geometric design proposals from the computational bottom-up model that comply with the architectural requirement with a good approximation. Moreover, it is possible to reduce the deviation from the span through adjusting the eccentricity parameter as was done in the detail design phase. The remaining deviation is less than 1%. This approach however requires a joint detail that can deal with the required degree of geometric accuracy.

11.3. Structural Design

11.3.1. Planar representation of a 3D-structure

A major simplification of the structural PRFA model is that the two interwoven arches are modelled in the same plane. The benefit of modelling in 2D is that the complexity of modelling is reduced which allows to investigate the utilization of RT in depth within a limited time frame.

The intersection points that do not exist in the 3D configuration, but result from working in a plane can be modelled without structural connectivity. This avoids building additional stiffness into the model that does not exist. A drawback of modelling the PRFA in a plane is that the out of plane dimension of the transverse beam's part that connects the two interwoven arches is not modelled. As a result, possible effects that are introduced by this dimension are neglected in the model. Informed by working with the physical models that were introduced in section 4.5, it is not expected that important structural effects that influence the behavior of the PRFA are neglected by the planar model. It is recommended to confirm this assumption through a three-dimensional global model in a more elaborate detail design which is out of the scope of this project.

11.3.2. Relation Geometry and Structural Behavior

The goal of the structural design is to identify the safe geometrical design proposals. The proposals vary in form and material properties, this implies that both internal forces and the strength parameters are proposal specific. Hence, comparing unity checks of different proposals does not allow an unambiguous conclusion about the structural performance of a PRFA geometry. It would be a separate study to evaluate the influence of the parameters e, L and n_m on the PRFA's structural behavior. The outcomes of such a study could serve as additional guide for the conceptual design of the PRFA. Due to time constraints, it was refrained from doing such an investigation.

Nevertheless, when observing the selected safe design proposals, a few conclusions about the required member geometry are possible. The members of the safe cases have the largest cross-sectional geometries, they provide a relatively large height and a significant width. Furthermore, it appears that the RT item's length of the safe proposals is of the same magnitude, it lays in between 3.70 m and 4.20 m. This can be explained with the relation of member length and eccentricity and the requirement of the e/h-ratio. In the section 8.2, it was argued that when the member length increases, a larger eccentricity value is required to achieve the same span with the same number of members. For the given span, members that are rather short do not comply with the e/h-ratio requirement, members that are rather long comply with the e/h-ratio requirement but have an insufficient cross-section for achieving a safe result. Of the present RT items, the members with a length of 4.0 m and a cross section of approximately 140 x 200 mm^2 are favorable for spanning a distance of 14.0 m.

If the RT items with a safe performance for $L_{span} = 14.0$ m were to be used for a larger span, a reduction of eccentricity and or an increase of member number would be required. Furthermore, an increase of internal forces and deflections would be expected. Depending on the assumed stress grade the items have additional capacity for an increase in stress, however the items' e/h-ratio is already very close to one for the span of 14.0 m, hence it is not expected that for the conceptualized joint detail and the RT items from the database a much larger span could be achieved.

11.3.3. Interpretation of Failed PRFA Cases

The large number of failed PRFA cases does not mean that the assessed RT items cannot be reused structurally. It signifies that the conceptual design and the generated geometries do not match the material. There are several options to cope with the situation that no or few safe cases exist for a given database and conceptualized design. First the geometry generation, then the detailing assumptions and if that does not lead to success also the choice of the structural principle should be revised. The revision should be directed at a better reflection of the database RT items' properties. If the revision process fails it could be sought to expand the RT database or as a last resort, structural members could be replaced with virgin timber.

A suggestion for altering the geometry generation was concluded from the parameter study in section 11.2.1. An example for revising the detailing was presented in section 9.3.2 for the PRFA case S19V1. The local stability failures were prevented through modelling an additional lateral support at mid span, which would need to be reflected in the joint design. An example for revising the detailing of the members would be appropriate in the context of the items from stack 12 through 25 which are characterized by a small width. It could be investigated if doubling the longitudinal members and intertwining them between the interwoven arches allows to construct a safe PRFA.

11.3.4. Evaluation of the Design Proposals

Going into the case study, it was expected that the structural reuse of RT is primarily dependent on the RT's strength grade and that the assignment of a low strength grade would render an RT item useless for structural purposes. This expectation was falsified. On the one hand, the diagrams of the PRFA case assessment in appendix C.5 obviously show that a decrease in strength grade is accompanied by a decrease of safe geometric design proposals, on the other hand it is also illustrated that RT items can lead to a safe structure with a low strength grade if they have a sufficient cross-section. Demonstrative examples are RT items from stacks 8, 9 and 10.

The strength grades that were assigned to the RT items cannot be verified without a visual assessment of the deconstructed material, hence the proposed design options remain hypothetical. Nevertheless, through a comparison with the research from Falk which concludes with assigning strength grades between the American equivalents of C16 and C27 to RT beams, it can be concluded that the strength grades that were assigned to RT with the reduction R3(a) are theoretically possible.

With the aim to avoid a more elaborate structural analysis, a buckling factor of 10 was determined as one of the limiting criteria for specifying the bay span. If internal forces and displacements were computed with a second order analysis this conservative criterion would become superfluous. As a result, larger bay spans and more safe design proposals might be achieved. This study restricted itself to computing internal forces and displacements with a first order linear-elastic analysis due to time constraints.

All of the three RT items that are considered for the design proposals have the material status "fixed". That implies that the donor building is not yet demolished. If this scenario was to occur in practice, i.e. that reclaimed material is already integrated into a design before it is reclaimed.

The value of the material would increase and the party responsible of dismantling would have a strong incentive for a careful deconstruction, which is supporting the concept of a sustainable material use. One approach to tackling resulting problems for construction management and planning would be to make conservative assumptions about the amount of available material, as was done in section 9.3.3.

The three design proposals achieve the goal of the case study: The utilization of RT in a RF building structure. There are two main differences between the design proposals 1 and 2 and design proposal 3. The required effort in the detail design stage is lower for the structures that only apply one PRFA case. The richer architectural expression with regards to RT in design proposal 3 is bound to additional detailing and design work.

Design proposal 3 has three instead of one type of joints and the interfaces between the different PRFA cases require additional thought, e.g. with regards to wind turbulence. The benefit of the more complex proposal is that the utilization of RT is not only expressed in the longitudinal section through the Rainbow RF, but also in the transverse section through the varying PRFA cases. The composition of the three different parts that are constructed from different structural components reclaimed from the same building lend a unique character to the canopy. Compartmentalizing the station roof transforms the uniform space of a railway station platform into a space which allows individuals to locate themselves in reference to the structure.

11.4. Detail Design

11.4.1. Evaluation of the Detail Design

Design proposal 1 which is composed of PRFAs from stack 9 was selected for the detail design mainly due to time constraints. From the three RT stacks which were selected in section 9.3.3, RT stack 9 has the items with the smallest cross-section. It is therefore likely, that the designed PRFA joint detail can also be applied in a similar manner to the other two cross sections. This claim would need to be verified as the PRFA's geometry, internal forces and material differ partially.

It is beyond the scope of this study to execute the complete detail design. The joints of the structural components other than the PRFA that were named in section 10.2 remain to be worked out. Furthermore, the influence of wind in the transverse direction and at the ends of the canopy should be investigated. Moreover, the assessment of fire safety is yet to take place.

11.4.2. Evaluation of the Joint Design

The designed PRFA joint approves the design proposal 1. It verifies that the used RT items are not only capable to resist member forces, but that they can also resist stresses at member intersections for the design at hand. A part of resisting the stresses is also to respect minimum edge distances and spacings. It was observed that this might be critical for the joint design with RT. For instance, the cross sectional width of items from stack 11 would not accommodate for the minimum space needed to fit two screws into Connection I.

Benefits of the chosen joint design are that the steel components are hidden, this increases fire safety and it allows for a timber aesthetic that is not obstructed by a large number of steel components. Another benefit of the joint is that mostly standard components are used. Only the joist hanger with its unconventional geometry requires a custom fabrication, all other fasteners are available in producer catalogues. Standard components are less costly than customized solutions and do not require expert workers for assembly which reduces labor costs. This is an important aspect especially for structures with small members because they have a large number of joints. For instance, the assessed canopy proposal consists of 28 PRFAs that each have nine joints. A joint consists of three connections. If only the PRFA joints are counted, the structure has 756 connections.

A drawback of the Connection II-B is the eccentricity which adds a considerable additional force to be transferred by Connection II-A. Another drawback of the joint design is the low utility. In the light of the large number of joints in the canopy, it would have a large impact from a material perspective if the utility is increased. It was reasoned that for the present joint design the options for increasing utility are limited, hence design alternatives should be considered.

Threaded bars could be used in both connection I and in connection II in combination with the joist hanger. The benefit would be a cleaner disassembly and a possible reuse of the timber item. A disadvantage of threaded bars is initial slip. In the PRFA SLS deflection criteria are critical, initial slip would increase deflection, hence the threaded bar is not a favorable alternative.

A second alternative is to use bolts in combination with a hollow steel tube that is placed inside a pre-drilled hole. This connection has the benefits of the threaded bars with regards to disassembly, but avoids initial slip. This detail is expected to be stiffer than the two screws in Connection I and could lead to the assumption of a lateral support at the longitudinal beam's mid span. Related benefits were discussed in section 9.3.2. This connection detail could also improve the transfer of the tension force in Connection II-A by avoiding that the tension must be transferred through the timber. A disadvantage of the connection is that it is not a standard detail for timber connections. This might lead to increased cost in fabrication and assembly.

11.5. Final Design Strategy

The first design phase of the strategy relates to the structural utilization of RT in combination with RFs in two ways. The form of the building and the type of the RF need to match. Moreover, it is characteristic for this strategy that in the structural concept design, it is selected which part of the structure is to be constructed with RT. The motivation for designing only a part of the structure in RT is to manage complexity. For the RF canopy, the PRFA was selected because it is the key component of the RF and also the most present in the structure. Thus, by choosing the PRFA to be designed by RT the largest part of the canopy will be constructed from RT. In the second design phase, the material stock is defined. This definition takes place at this point because this enables influencing both the geometry generation and the structural design.

The following two design phases solely focus on the utilization of RT in the selected structural component. First, it is sought to combine the structural system of the selected component with architectural requirements and the available material. To solve this problem in a systematic way, a bottom-up model is developed that is capable of generating multiple geometrical variants for the same RT stack through varying geometric parameters that are inherent to the structural system.

Second, the geometries are assessed with a structural model which integrates the remaining parts of the conceptual design through boundary conditions. One of these boundary conditions, the bay span, is used as a variable parameter to optimize the structural utilization of the PRFA.

The process of identifying a safe solution is more complex and requires more effort when designing from a limited stock compared to designing with conventional structural materials. The design strategy at hand encounters increased complexity with the application of “smart methods”. In this context, smart methods are considered parametric programs or methods that are capable of managing large amounts of data. An example for applying a smart approach in the structural assessment of the PRFA is the modelling of the loads. A program was developed that automatically models the load cases self-weight, wind load and snow load depending on the specific geometry of the PRFA. The initial effort of programming allowed to evaluate a large number of variants with considerable accuracy and in significantly less time.

In the last step of the design strategy a structurally safe PRFA geometry is taken as the starting point for the detail design of the complete canopy. In this detail design a focus is set on the joints of the component which is designed of RT, because cross-sections and material grade cannot be altered. Other structural components and joints are designed consecutively. It might also be investigated if remaining structural parts can be designed from RT.

The developed design strategy is one option for designing with RT. The associated geometry generation model and structural assessment algorithm are specific to Rainbow RF and the joint that was conceptualized in section 6.2. That means if the design strategy was applied to a different structural system, for example a Surface RF, the existing tools could not be used, but a new model and algorithm would need to be developed. Hence, the application of the design strategy requires computational skills from the structural engineer. According to this design strategy, the structural engineer also takes a different role in the design process as it is suggested that he influences the choice of the structural system and generates possible forms for the part of the structure that is designed by RT. These tasks usually lie in the domain of the architect. Hence a close collaboration between the engineer and architect is required for the application of this method.

12

Conclusions and Recommendations

The conclusions of this Master thesis respond to the main research question, which reads:

> "How can a reciprocal frame structure of reclaimed timber be designed in a safe, smart, and sustainable way?"

By first answering the sub-questions that were formulated to approach the research question, the state-of-the-art of the structural utilization of RT is described and important aspects for the structural design of RFs are highlighted. Answering the third group of sub-questions, allows to conclude what is achieved by applying the developed design strategy to a building structure. The final conclusion to the main research question is formulated by providing a concise description of the design strategy for the structural utilization of RT in a RF structure. The chapter closes with recommendations for further research activity on RT and RFs.

12.1. Structural Utilization of Reclaimed Timber – State-of-the-art

Sub-question 1: What is the definition of reclaimed timber?

This study proposes to integrate descriptions of reclaimed timber by Smith (2013) and Fraanje (1997) to a single definition: "Reclaimed timber is timber that originates from the load-bearing structure of a deconstructed building. After harvesting, no major processing occurs. The material is destined to be utilized in a construction again, either for structural or non-structural purposes."

Sub-question 2: What are important material properties of reclaimed timber that is supposed to be used structurally and what are methods to assess these properties?

The length, cross-section and the strength grade of a RT item as well as the number of items that have the same properties and can thus be merged to a stack are decisive for structural reuse. The preferred method for the assessment of RT properties is visual strength grading.

Sub-question 3: What quantity and quality of reclaimed timber is available and what steps are part of the reclamation?

A large amount of timber is fixed in the building stock. For example in the late 90's, it was estimated that 1.8 million m^3 of timber could potentially be reclaimed from single family homes in the United States per year (Falk & McKeever, 2004). The quality of RT depends on its in-service damage and dismantling damage.

It is favorable to execute the reclamation with the following five steps:

1. Building Assessment: Identify the timber in a building and decide how to dismantle it
2. Dismantling: Disassemble and remove attachments, e.g. nails
3. Visual Strength Grading: Assign mechanical properties through a visual grading assessment which is possibly supplemented by non-destructive testing
4. Storage: Store material and publish material properties that are important for structural reuse
5. Structural Reuse: Design and utilize RT in new a building

Sub-question 4: What are obstacles for and opportunities in the structural design with reclaimed timber?

Obstacles:

- Lack of a visual strength grading standard for RT
- Lack of data on material quantity and quality
- RT has mediocre mechanical properties
- Standard structural design strategies are not applicable to RT

} Technical

- Strong competition over the timber from the building stock
- Reused material is perceived as negative
- Lack of an incentive for a careful dismantling
- Careful dismantling and storage incur additional cost

} Market

Opportunities:

- RT material properties allow for structural reuse

} Technical

- Financial benefits: Profit for selling RT, omission of disposal fees
- Better environmental certification for buildings that utilize RT

} Market

- Postponement of carbon emissions
- Reduction of energy consumption
- Reduction of construction waste
- Increase of resource efficiency

} Environmental

Sub-question 5: What reclaimed timber should be used in the case of structural application?

The type of RT to be used in a structural application depends on the specific requirements of a project. The developed design strategy is able to analyze a stock of RT and select the RT items that are capable of satisfying requirements for a structural application.

12.2. Structural Design of Reciprocal Frames

Sub-question 6: What is a reciprocal frame and what are past applications?

RFs are a family of structural systems that can be defined by two binding and two optional criteria. Every RF consists of members that mutually support each other and meet along the span. Some RFs are arranged in a closed circuit and have only two members meeting in a joint.

RFs have been applied in roof and bridge structures. An early example of a built RF structure is the Rainbow Bridge, it dates back to the year 1040. Over the centuries a number of great thinkers studied RF structures, among them is polymath Leonardo da Vinci. A recent example of a RF structure is the roof of the Bunraku Puppet Theatre Exhibition Hall in Seiwa, Japan.

Sub-question 7: What are important characteristics of the reciprocal frame from the structural engineering perspective?

- Bending is the main load bearing mechanism of RFs
- RFs tend to have large deflections, thus the serviceability limit state is likely to be governing
- Measures to prevent progressive collapse are required
- RFs are capable of resisting out of plane forces without moment resistant joints

Sub-question 8: What are important aspects for the design of a RF structure?

- Geometry Generation: The complex process of generating flawless geometries is the core design activity of RFs
- Joint Detailing: Detailing joints is another important design aspect because it is inherent to RFs to have a large number of joints
- Cladding Design: For canopies, the cladding design determines how the roof loads are introduced to the RF, this is decisive for the flow of forces in the RF
- Assembly: Regularity in the design can reduce costs related to assembly

Sub-question 9: Is the reciprocal frame a suitable structural system for the utilization of reclaimed timber from a structural engineering perspective?

Yes, the RF's capability of spanning distances longer than the structural members' length favors the combination of RT and RFs. Specifically the Rainbow RF is effective with regards to a safe structural utilization of RT. A key advantage of this RF is that it can be used to generate expressive spatial assemblies with a relatively low geometric complexity and a high degree of regularity. From a structural perspective the Rainbow RF has the benefit of efficiently transferring axial forces, which reduces the bending action that is typical for RFs. Moreover, it achieves flexural rigidity without using expensive moment resistant joints.

12.3. Application of the Design Strategy

Sub-question 10: What kind of reclaimed timber items form the material stock of the case study?

The material stock contains 30 different RT stacks that contain 3735 individual timber items which have a total volume of 243 m^3. The smallest and largest timber items by volume are a beam with a cross-section of 19 x 89 mm^2 and a length of 3.0 m and a column with a cross-section of 210 x 280 mm^2 and a length of 4.2 m. The material was sourced from buildings built in in Finland, Germany, the Netherlands, Spain and the United States. The material data was collected on a salvage yard and from research articles that document the dismantling of buildings. When the data was recorded, 64% of the material was fixed in the building stock, 25% was dismantled but not yet structurally graded and 11% had assigned mechanical properties. For the RT items for which the mechanical properties are unknown, a strength grade was assumed. As a result the stock's strength grades range from C14 to C27.

Sub-question 11: What RF geometries can be generated from the material stock?

A novel computational bottom-up model was developed to explore the geometries that can be generated from the material stock. The length of the items in the material stock is the key input parameter for the geometry generation. For each of the material stock's ten distinct lengths up to four geometries are generated by varying two characteristic parameters of the RF. In total 29 Rainbow RF geometries were generated. The barrel vault geometries have a span of approximately 14.0 m and a rise that ranges between 1.1 m and 7.4 m. Only Rainbow RFs were investigated because this RF type had previously been selected for the case study due to its advantageous geometrical and structural properties, see answer to sub-question 9. By assigning the 29 geometries to the 30 RT stacks, 118 geometric design proposals were established.

Sub-question 12: Which geometric design proposals lead to a safe design and how much material is needed to construct the complete canopy?

Three of the 118 geometric design proposals were developed into structurally safe designs. The RT items from which the three design proposals were constructed can compensate their low strength grade (C18, C18, C14) through a relatively large cross-section (140 x 210, 140 x 210, 210 x 280 [mm x mm]). The three barrel vault geometries' low member count (10, 11, 11) satisfies material efficiency and the high rise-to-span ratio (0.36, 0.38, 0.42) ensures that besides bending also axial action is activated to take down loads. The RT needed for the canopy proposals (36, 37, 43 [m^3]) can be reclaimed from a single building. The donor is a "Spanish Corrala" built in the 19th century.

Sub-question 13: What aspects of the RF structure's detail design are important to ensure the structural utilization of RT?

The focus of the detail design is to verify that joints which connect RT items can transfer the forces while the material resists the related stresses. The relevant joint detail was solved by connecting the RT items with a combination of two joist hangers. Screws are added to ensure the safe transfer of tension forces in the case of wind uplift.

12.4. Final Conclusion on the Main Research Question

The structural utilization of RT in a RF structure can be achieved with the design strategy illustrated in figure 12.1.

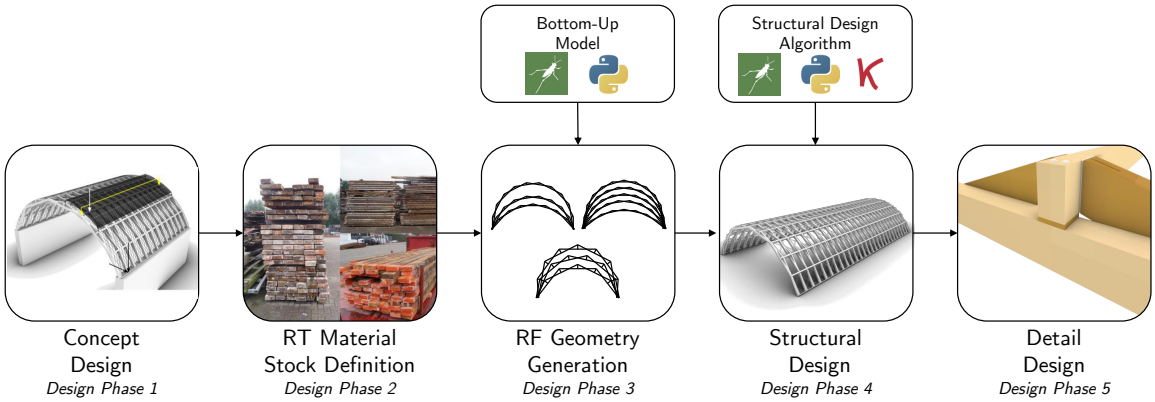

Figure 12.1: Design Strategy for the Structural Utilization of RT in RF Structures

The individual design phases are described in brief:

1. Concept Design: Determine the architectural requirements for the structure, select a RF type and specify the flow of forces through the structural components.
2. Material Stock Definition: Define the material stock through a RT database that archives the material properties of specific RT items that are available for reuse. RT items with the same properties are merged to stacks.
3. Geometry Generation: Generate geometric design proposals for each RT stack using the bottom-up approach. Identify design proposals that comply with the architectural requirements by using the developed directed method.
4. Structural Design: Model, analyze, and verify the geometric design proposals structurally and identify the structurally safe variants using a smart algorithm that can process many proposals with considerable accuracy in a short time.
5. Detail Design: Design the joint details, first focus on those joints that connect RT items to verify that possible local stress peaks can be handled by the RT.

The structural reuse of timber that is facilitated by this design strategy leads to reductions in carbon emissions, decreases construction waste and increases resource efficiency.

12.5. Recommendations

With the aim to stimulate further research on the structural utilization of RT and RF structures four recommendations for further research are elaborated.

The buildings construction industry already provides a large part of the infrastructure for the structural utilization of RT. Hence, it is recommended to test the proposed design strategy in the industry in cooperation with a reclaimer business, e.g. a salvage yard. In this cooperation a database with actually available material could be used as starting point for the design. By building a mock-up structure, the influence of further characteristics of RT that were not yet recognized in this study could be investigated. An example for such a RT property is the irregularity in cross section along the length of a RT item.

The cooperation with a partner from industry also permits to investigate the implementation of a RT database in practice. In this context, it is recommended to investigate two specific questions: “How can contracts related to a RT database be managed?’’ An answer to this question should specify who owns and maintains data, who has access to the data and how material can be claimed during different stages of a design process. The second question reads: “What is an effective procedure to acquire data on RT stacks for the database?’’ A possible direction for answering this second question could be to investigate the feasibility of material donor cards for newly built buildings, as suggested in this research. The goal should be to answer the two research questions in a way that the resulting database is as large as possible, because the design options for a construction project that utilizes RT are limited to what can be built from the available stock of material. A larger stock is equivalent to an increased design freedom which in turn renders structural design with RT more attractive.

Surface RF are the most applied RF type. Currently, the geometries of Surface RFs are generated exclusively with the top-down approach. In this study, it was verified that a computational bottom-up approach can be used for the geometry generation of the geometrically less complex Linear RFs. Moreover, it was also possible to generate RF geometries with this approach that comply with geometric requirements of a building design. The benefit of the bottom-up approach over the top-down approach is that regular geometries can be generated. Regularity enables to reduce efforts in structural design, fabrication and assembly. Against this background, it is recommended to develop a geometric model that can generate Surface RFs with the bottom-up approach. This would allow to reap the benefits of regularity also for Surface RFs. Moreover, in conjunction with the proposed design strategy, a bottom-up approach for Surface RFs would also permit to utilize RT in this RF type.

The existing research on strength grading standards for RT was extensively discussed in this study’s literature review. Further research in this field is recommended to investigate the potential of the proposed “data retrieval method’’ to contribute to visual strength grading, i.e. to test to what extent information about the previous life cycle of RT can support visual strength grading. Another aspect for research that can contribute to developing a strength grading standard is the investigation of reducing short-term strength and long-term strength with different percentages. The Madison curve suggests that short term strength is reduced less than long-term strength. Considering that many structural timber members have a low permanent load and that short-term loading is generally governing, this investigation could increase the potential for the structural utilization of RT.

Part V

References and Appendices

References

American Wood Council. (2022). Reusewood.org. https://reusewood.org/

Apers, J. (2020). JEROEN APERS ARCHITECT BLOG. https://blog.jeroenapers.nl/post/613731261009281025/de-zelfdragende-houten-dakconstructie-van-het

Apolinarska, A. A. (2018). *Complex Timber Structures From Simple Elements* (Doctoral dissertation). ETH Zürich. https://doi.org/https://doi.org/10.3929/ethz-b-000266723

Asefi, M., & Bahremandi-Tolou, M. (2019). Design challenges of reciprocal frame structures in architecture. *Journal of Building Engineering*, *26*(July), 100867. https://doi.org/10.1016/j.jobe.2019.100867

Barrett, J., & Foschi, R. (1978). Duration of load and probability of failure in wood. Part I. Modelling creep rupture. *Canadian Journal of Civil Engineering*. https://doi.org/https://doi.org/10.1139/l78-057

Baylor, C. (2020). Understanding Actual vs. Nominal Lumber Sizes. https://www.thesprucecrafts.com/understanding-wood-sizes-in-softwood-lumber-3536905

Berne, J. (2019). Lavapies. http://madridbyheart.es/lavapies

Bertin, V. (2001). Variations of lever beam structures. *Proceedings of Conference on Growth and Form: The Engineering of Nature*.

BioRegional. (2008). *Reclaimed building products guide* (tech. rep.). Waste Resources and Action Programme. https://www.bioregional.com/resources/reclaimed-building-products-guide

Blaß, H. (2017). *Timber Engineering Principles for Design* (Vol. 21). https://doi.org/10.1016/s1474-6670(17)54538-3

Bloch, M. (2022). Tag-arkiv: Nørrebro Station. https://ronnowarkitekter.dk/tag/noerrebro-station/

Bouma, A. L. (1993). *Mechanik schlanker Tragwerke: Ausgewählte Beispiele der Praxis*. Springer.

Boytchev, H. (2022). Klimaneutral Energie? Von wegen. https://www.zeit.de/green/2022-04/heizen-holz-gas-waelder-europa-subvention

Bratkovich, S. (2009). *Reclaiming Lumber Products From Waste Wood* (tech. rep.). Dovetail Partners, INC. www.dovetailinc.org

Brol, J., Dawczy, S., & Adamczyk, K. (2015). Possibilities of timber structural members reuse. *3rd International Conference on Structural Health Assessment of Timber Structures*, (September), 1–7.

Canadell, J. G., Jackson, R. B., Andrew, R. M., Friedlingstein, P., Jones, M., Le Quere, C., Peters, G., Poulter, B., Saunois, M., & Stavert, A. R. (2020). Global Fossil CO2 Emissions: Global Carbon Project. *United in science 2020: A multi-organization high-level compilation of the latest climate science information* (pp. 6–7). World Meteorological Organization.

Castriotto, C., Tavares, F., Celani, G., Popovic Larsen, O., & Browne, X. (2021). Clamp links : A novel type of reciprocal frame connection. *0*(0), 1–22. https://doi.org/10.1177/14780771211054169

Cavalli, A., Bevilacqua, L., Capecchi, G., Cibecchini, D., Fioravanti, M., Goli, G., Togni, M., & Uzielli, L. (2016). MOE and MOR assessment of in service and dismantled old structural timber. *Engineering Structures*, *125*, 294–299. https://doi.org/10.1016/j.engstruct.2016.06.054

Cavalli, A., Cibecchini, D., Togni, M., & Sousa, H. S. (2016). A review on the mechanical properties of aged wood and salvaged timber. *Construction and Building Materials*, *114*, 681–687. https://doi.org/10.1016/j.conbuildmat.2016.04.001

Collins, P. (2021). Architecture. https://www.britannica.com/topic/architecture

Crews, K., Hayward, D., & MacKenzie, C. (2008). *Interim Industry Standard Recycled Timber – Visually Stress Graded Recycled Timber for Structural Purposes*. Forest&Wood Products Australia.

Crews, K., & MacKenzie, C. (2008). Development of grading rules for re-cycled timber used in structural applications. *10th World Conference on Timber Engineering 2008*, *1*, 231–238.

Cristescu, C., Honfi, D., Sandberg, K., Sandin, Y., Shotton, E., Walsh, S. J., Cramer, M., Ridley-, D., Arana-fernández, M. D., Llana, D. F., Barbero, M. G., Nasiri, B., & Krofl, Ž. (2020). *Design for deconstruction and reuse of timber structures – state of the art review*. https://doi.org/10.23699/bh1w-zn97

Danish Standards Foundation. (2007). EN 1991-1-6 DK NA : 2007 National Annex to Eurocode 1 : Actions on structures - Part 1-6 : General actions – Actions during execution, 2–9.

Danish Standards Foundation. (2013a). DS / EN 1990 DK NA : 2013 National Annex to Eurocode : Basis of structural design, 1–16.

Danish Standards Foundation. (2013b). DS/EN 1995-1-1 DK NA:2014 National, 1–10.

Danish Standards Foundation. (2015). DS/EN 1991-1-3 DK NA:2015 2nd edition - National Annex to Eurocode 1: Actions on structures - Part 1-3: General actions - Snow loads, 1–7.

Danz, C., Corser, R. J., Johnson, B. R., & Griggs, K. (2015). *Re-Frame : form-finding within the constraints of mutually supporting assemblies* (Doctoral dissertation). University of Washington.

Davis, J. B. (2012). Suitability of salvaged timber in structural design. https://dspace.mit.edu/handle/1721.1/73782

de Arana-Fernandez, M., Llana, D. F., & Nasiri, B. (2020). Cascading Potential for Recovered Wood from Heavy Timber Frame Typologies in Pre-Modern Dwelling Buildings in Madrid. *Proceedings of the 2020 Society of Wood Science and Technology International Convention Cascading*, 16–27.

Deweerdt, M., & Mertens Marilyn. (2020). A guide for identifying the reuse potential of construction products. (March). http://www.nweurope.eu/fcrbe

Dinwoodie, J. M. (2000). *Timber: its nature and behaviour*. CRC Press.

Diyamandoglu, V., & Fortuna, L. M. (2015). Deconstruction of wood-framed houses: Material recovery and environmental impact. *Resources, Conservation and Recycling*, *100*, 21–30. https://doi.org/10.1016/j.resconrec.2015.04.006

Douthe, C., & Baverel, O. (2014). Morphological and Mechanical Investigation of Double-Layer Reciprocal Structures, 191–206. https://doi.org/10.1007/s00004-014-0185-9

Engel, H. (1967). *Tragsysteme: structure systems*. Deutsche Verlags-Anstalt.

Euopean Committee for Standardization. (2022). NEN-EN 5499.

European Committee for Standardization. (2020a). NEN-EN 1990.

European Committee for Standardization. (2020b). Nen-en 1991-1-3. *3*.

European Committee for Standardization. (2020c). NEN-EN 1991-1-4. *4*(april 2005).

European Committee for Standardization. (2020d). NEN-EN 1995-1-1. *1*.

European Committee for Standardization. (2021). NEN-EN 1912.

European Committee for Standardization. (2022). NEN-EN 338.

Falk, R. (2002). Wood-Framed Building Deconstruction A Source of Lumber? *Forest products journal*, *52*(March), 8–15.

Falk, R., Maul, D., Cramer, S., Evans, J., & Herian, V. (2008). Engineering Properties of Douglas-fir Lumber Reclaimed from Deconstructed Buildings. *Forest Products Laboratory*, 1–47. https://www.fpl.fs.fed.us/documnts/fplrp/fpl_rp650.pdf

Falk, R., Cramer, S., & Evans, J. (2012). Framing lumber from building removal: How do we best utilize this untapped structural resource? *Forest Products Journal*, *62*(7-8), 492–499. https://doi.org/10.13073/0015-7473-62.7.492

Falk, R., & McKeever, D. (2004). Recovering Wood For Reuse and Recycling, A United States Perspective. In C. Gallis (Ed.), *Management of recovered wood recycling, bioenergy and other options* (pp. 29–40).

Fast, P. (1999). Material Testing Facility A structural Phoenix. https://www.fastepp.com/portfolio/asphalt-testing-facility/

Fraanje, P. J. (1999). Use of wood in new Dutch one family dwellings since 1969. *Holz als Roh- und Werkstoff*, *57*. https://link.springer.com/article/10.1007/s001070050065

Fraanje, P. J. (1997). Cascading of pine wood. *Resources, Conversation and Recycling*, *19*, 21–28. https://doi.org/ps://doi.org/10.1016/S0921-3449(96)01159-7

Galligan, W. L., & McDonald, K. A. (2000). Machine Grading of Lumber Practical Concerns for Lumber Producers. *Gen. Tech. Rep. FPL–GTR–7 (Revised). Madison, WI: U.S. Department of Agriculture, Forest Service, Forest Products Laboratory.*, 34.

Garcia, C. A., & Hora, G. (2017). State-of-the-art of waste wood supply chain in Germany and selected European countries. *Waste Management*, *70*(September), 189–197. https://doi.org/10.1016/j.wasman.2017.09.025

Gelez, S., Aubry, S., & Vaudeville, B. (2011). Behavior of a simple nexorade or reciprocal frame system. *International Journal of Space Structures*, *26*(4), 331–342. https://doi.org/10.1260/0266-3511.26.4.331

Godthelp, T. (2019). *Timber reciprocal frame structures* (Doctoral dissertation). Eindhoven University of Technology. https://pure.tue.nl/ws/files/131842016/Godthelp_0946277.pdf%20https://www.youtube.com/watch?v=Oh8_AX_hzoo

Gustafsson, J. (2016). *Connections in Timber Reciprocal Frames* (tech. rep.). Chalmers Univeristy of Technology. https://odr.chalmers.se/handle/20.500.12380/243237

Guy, B. (2020). After Disaster: Deconstruction, Rebuilding and Resilience Lessons from Hurricanes Katrina and Irma. https://www.epa.gov/smm/sustainable-materials-management-web-academy

Hafner, A., Ott, S., & Winter, S. (2014). Recycling and End-of-Life Scenarios for Timber Structures. In S. Aicher, H.-W. Reinhardt, & H. Garrecht (Eds.), *Rilem bookseries* (pp. 89–98). Springer International Publishing. https://doi.org/10.1007/978-94-007-7811-5{_}3

Hafner, A., Ott, S. J., Bodemer, E., & Winter, S. (2014). A Case Study for End of Life Reuse and Recycling Survey Methodologies: The Höllentalanger Cottage. (July 2016). https://doi.org/10.17265/1934-7359/2014.10.001

Hertwich, E. G., Ali, S., Ciacci, L., Fishman, T., Heeren, N., Masanet, E., Asghari, F. N., Olivetti, E., Pauliuk, S., Tu, Q., & Wolfram, P. (2019). Material efficiency strategies to reducing greenhouse gas emissions associated with buildings, vehicles, and electronics - A review. *Environmental Research Letters*, *14*(4). https://doi.org/10.1088/1748-9326/ab0fe3

Herzog, T., Natterer, J., Schweitzer, R., Volz, M., & Winter, W. (2004). *Timber Construction Manual*. https://doi.org/10.11129/detail.9783034614634

Hildebrandt, J., Hagemann, N., & Thrän, D. (2017). The contribution of wood-based construction materials for leveraging a low carbon building sector in europe. *Sustainable Cities and Society*, *34*(June), 405–418. https://doi.org/10.1016/j.scs.2017.06.013

Höglmeier, K., Weber-Blaschke, G., & Richter, K. (2017). Potentials for cascading of recovered wood from building deconstruction — A case study for south-east Germany. *"Resources, Conservation & Recycling"*, *117*, 304–314. https://doi.org/10.1016/j.resconrec.2015.10.030

Houlsby, G. T. (2014). John Wallis and the Numerical Analysis of Structures. *Nexus Network Journal*, *16*, 207–217. https://doi.org/10.1007/s00004-014-0179-7

Hradil, P., Talja, A., Wahlstr, M., Huuhka, S., Lahdensivu, J., & Pikkuvirta, J. (2014). *Re-use of structural elements, Environmentally efficient recovery of building components*. VTT. http://www.vtt.fi/publications/index.jsp

Huuhka, S. (2014). Future-oriented building stock studies and the significance of values: addressing demolition behaviour with the Delphi method. In K. van Breugel (Ed.), *Ageing of materials & structures* (pp. 56–62).

Icibaci, L. (2019). Re-use of Building Products in the Netherlands - The development of a metabolism based assessment approach. *A+BE | Architecture and the Built Environment*, 424. https://journals.open.tudelft.nl/index.php/abe/article/view/3248

International Code Council. (2000). Alternative materials, design and methods of construction and equipment. https://codes.iccsafe.org/content/IBC2018/chapter-1-scope-and-administration

Irle, M., Privat, F., Deroubaix, G., & Belloncle, C. (2015). Intelligent recycling of solid wood. *Pro Ligno*, *11*, 14–20.

Jerzy, J., Tomasz, N., & Katarzyna, H. (2013). Selected methods of diagnosis of historic timber structures – principles and possibilities of assessment. *Advanced Materials Research*, *778*, 225–232. https://doi.org/10.4028/www.scientific.net/AMR.778.225

Jongert, J. (2009). Villa Welpeloo. https://www.superuse-studios.com/projectplus/villa-welpeloo/

Klinge A, Roswag-Klinge E, Paganoni S, & Lehmann, R. L. (2019). IOP Conference Series: Earth and Environmental Science Design concept for prefabricated elements from CDW timber for a circurlar building Design concept for prefabricated elements from CDW timber for a circurlar building. https://doi.org/10.1088/1755-1315/323/1/012022

Knau, M., Hemmerling, M., Lemberski, D., Brand, G., Allahdin, K., Benke, E., Fa, L., Frenz, L., Friedman, T., Hilbert, J., Heidemann, J. C. K., Kirsten, L., Lianarachchi, J., Nolte, V., Steffen, H., Stiboy, F., Tish, G., Trittin, M., & Varadharajan, M. (2018). Reciprocal Structure, 169–176. https://doi.org/10.1007/978-3-319-53135-9

Kohlhammer, T. (2013). *Strukturoptimierung von stabförmigen Flächentragwerken mittels reziproker Analyse* (Doctoral dissertation No. 21565). ETH Zürich.

Koning, L. F. M. (2018). *Digital Fabrication of a Timber Bridge* (tech. rep.). TU Delft. https://repository.tudelft.nl/islandora/object/uuid%3A0298448c-5bad-4760-9382-06d58ed07edc

Larena, A. B., & Ménendez, D. G. (2014). Extension of euskalduna conference centre and concert hall: A contemporary application of irregular reciprocal frames. *Structural Engineering International: Journal of the International Association for Bridge and Structural Engineering (IABSE)*, *24*(1), 63–67. https://doi.org/10.2749/101686614X13830788506233

Lauf, S. (2017). Mill Creek Housing II. https://www.quondam.com/40/4003o.htm

Llana, D. F., Íñiguez-González, G., de Arana-Fernández, M., Uí Chúlian, C., & Harte, A. M. (2020). Recovered Wood as Raw Material for Structural Timber Products. Characteristics, Situation and Study Cases: Ireland and Spain. *2020 Society of Wood Science and Technology International Convention Recovered Wood as Raw Material for Structural Timber Products. Characteristics, Situation and Study Cases: Ireland and Spain Daniel*, (July), 117–123.

Louter, C. (2022). Structural Design & Building Engineering. https://www.tudelft.nl/chairs/structural-design-building-engineering

Lyslo, J., André, R., & Lohne, J. (2016). High-Rise Timber Buildings as a Climate Change Mitigation Measure - A Comparative LCA of Structural System Alternatives. *Energy Procedia*, *96*(1876), 112–123. https://doi.org/10.1016/j.egypro.2016.09.112

MacDonald, A. (2019). *Structure and Architecture*. https://doi.org/https://doi.org/10.4324/9781315210513-11

Madsen, B. (1992). *Structural behavior of timber*. Timber Engineering Ltd.

Mantau, U., Saal, U., Prins, K., Steierer, F., Lindner, M., Verkerk, H., Eggers, J., Leek, N., Oldenburger, J., Asikainen, A., & Anttila, P. (2010). EUwood - Real potential for changes in growth and use of EU forests. Final report. *EUwood*, (June), 106p.

Masson-Delmotte, V., Zhai, P., & Pörtner, H.-O. (2018). Summary for Policy Makers. *Global warming of 1.5°c. an ipcc special report on the impacts of global warming of 1.5°c above pre-industrial levels and related global greenhouse gas emission pathways, in the context of strengthening the global response to the threat of climate change,*

Merriam-Webster. (2022). Reclaim. https://www.merriam-webster.com/dictionary/reclaim

Mesnil, R., Douthe, C., Baverel, O., & Gobin, T. (2018). Form finding of nexorades using the translations method. *Automation in Construction*, *95*, 142–154. https://doi.org/10.1016/j.autcon.2018.08.010

Müller, D. B. (2005). Stock dynamics for forecasting material flows — Case study for housing in The Netherlands. *Ecological Economics*, *59*, 142–156. https://doi.org/https://doi.org/10.1016/j.ecolecon.2005.09.025

Nan, C. (2016). *Digitally Fabricated Lamella Structure* (tech. rep.). Univeristy of Edinburgh. Edinburgh. https://issuu.com/adieste/docs/mp3ad/5

Natalini, M. B., Morel, C., & Natalini, B. (2013). Mean loads on vaulted canopy roofs. *Journal of Wind Engineering and Industrial Aerodynamics*, *119*, 102–113. https://doi.org/10.1016/j.jweia.2013.05.001

Ogbu, L. (A. (2011). Vancouver Materials Testing Facility. *Design for Reuse Primer*. https://issuu.com/publicarchitecture/docs/design_for_reuse_primer_issuu

Oval, R., Rippmann, M., Mesnil, R., Van Mele, T., Baverel, O., & Block, P. (2019). Feature-based topology finding of patterns for shell structures. *Automation in Construction*, *103*(March), 185–201. https://doi.org/10.1016/j.autcon.2019.02.008

Parigi, D. (2021). Minimal-waste design of timber layouts from non-standard reclaimed elements: A combinatorial approach based on structural reciprocity. *International Journal of Space Structures*, *36*(4), 270–280. https://doi.org/10.1177/09560599211064091

Parigi, D., & Damkilde, L. (2019). Multi-objective optimization of reciprocal timber layouts from reclaimed stock elements. *IASS Symposium 2019 - 60th Anniversary Symposium of the International Association for Shell and Spatial Structures; Structural Membranes 2019 - 9th International Conference on Textile Composites and Inflatable Structures, FORM and FORCE*.

Parigi, D., & Kirkegaard, P. H. (2014). Design and Fabrication of Free-Form Reciprocal Structures. *Nexus Network Journal*, *16*, 69–87. https://doi.org/10.1007/s00004-014-0177-9

Parigi, D., & Pugnale, A. (2014). Three-Dimensionality in Reciprocal Structures: Concepts and Generative Rules. *Nexus Network Journal*, *16*, 151–177. https://doi.org/10.1007/s00004-014-0183-y

Parigi, D., Sassone, M., Kirkegaard, P. H., & Napoli, P. (2014). Static and Kinematic Formulation of Planar Reciprocal Assemblies. *Nexus Netw J*, *16*, 37–59. https://doi.org/10.1007/s00004-014-0175-y

Pedersen, E. V. (2009). Nørrebro station through the ages. https://web.archive.org/web/20090205150758/http://www.sitecenter.dk/erik-vpedersen/nrrebrostationgennemtiderne/

Popovic Larsen, O. (2008). *Reciprocal Frame Architecture*. Elsevier.

Popovic Larsen, O. (2014). Reciprocal Frame (RF) Structures: Real and Exploratory. *Nexus Network Journal*, *16*(1), 119–134. https://doi.org/10.1007/s00004-014-0181-0

Popovic Larsen, O., & Lee, D. S. H. (2014). Reciprocal Frame (RF) optimized timber truss structure : a design and build case study. In N. De Temmerman & C. A. Brebbia (Eds.), *Mobile and rapidly assembled structures iv* (pp. 257–265). WITPress. https://doi.org/10.2495/MAR140211

Preisinger, C. (2011). Linking Structure and Parametric Geometry, 110–113.

Pugnale, A. (2014). Letter from the Guest Editor: Reciprocal Structures, An Overview. *Nexus Network Journal*, *16*(1), 1–4. https://doi.org/10.1007/s00004-014-0171-2

Pugnale, A., Parigi, D., Kirkegaard, P. H., & Sassone, M. (2011). The principle of structural reciprocity: history, properties and design issues. *The 35th Annual Symposium of the IABSE 2011, the 52nd Annual Symposium of the IASS 2011, incorporating the 6th International Conference on Space Structures*, 414. http://forskningsbasen.deff.dk/Share.external?sp=S7edc081d-d377-44ef-9de3-45733e66b98d&sp=Saau

Pugnale, A., Sassone, M., Pugnale, A., & Sassone, M. (2014). Structural Reciprocity: Critical Overview and Promising Research/Design Issues. *Nexus Network JournalJ*, *16*, 9–35. https://doi.org/10.1007/s00004-014-0174-z

Ravenshorst, G. (2015). *Species independent strength grading of structural timber* (Doctoral dissertation). TU Delft University. https://doi.org/10.4233/uuid

Richter, K. (2017). *Cascading Recovered Wood (CaReWood) - Final Report* (tech. rep.). http://www.carewood.eu

Ridley-Ellis, D., Stapel, P., & Baño, V. (2016). Strength grading of sawn timber in Europe: an explanation for engineers and researchers. *European Journal of Wood and Wood Products*, *74*(3), 291–306. https://doi.org/10.1007/s00107-016-1034-1

Risse, M., & Richter, K. (2018). *Schlussbericht CaReWood – Cascading Recovered Wood Holznutzung* (tech. rep.). https://www.fisaonline.de/projekte-finden/details/?tx_fisaresearch_projects%5Bp_id%5D=8139&tx_fisaresearch_projects%5Baction%5D=projectDetails&tx_fisaresearch_projects%5Bcontroller%5D=Projects&cHash=7abad6ffe0742e698d1bcd4df60fd890#more

Rizzuto, J. P., & Popovic Larsen, O. (2010). Connection Systems in Reciprocal Frames and Mutually Supported Elements Space Structure Networks. *International Journal of Space Structures*, *25*(4), 243–256. https://link.springer.com/journal/4/volumes-and-issues/16-1%20https://link-springer-com.tudelft.idm.oclc.org/journal/4/volumes-and-issues/16-1

Rohwedder, C. (2019). Old Wood Can Cost More Than New Lumber. People Want It Anyway. https://www.wsj.com/articles/old-wood-can-cost-more-than-new-lumber-people-want-it-anyway-11554907971

Rost, J. (2012). Norrebro S-Train Station. https://www.flickr.com/photos/56380734@N05/8750030739/

Rotor. (2022). Opalis. https://opalis.eu/en

Sakaguchi, D., Takano, A., & Hughes, M. (2016). The potential for cascading wood from demolished buildings: the condition of recovered wood through a case study in Finland. *International Wood Products Journal*, *7*(3), 137–143. https://doi.org/10.1080/20426445.2016.1180495

Smith, M. (2013). Use of recycled and reclaimed timbers. In A. Richardson (Ed.), *Reuse of materials and byproducts in construction* (pp. 111–149). Springer International Publishing. https://doi.org/10.1007/978-1-4471-5376-4{_}5

Smith, M. J. (2012). *An investigation into the strength properties of reclaimed timber joists* (Doctoral dissertation). Northumbria University. http://nrl.northumbria.ac.uk/21436/

Teshnizi, Z. (2015). *Opportunities and Regulatory Barriers for the Reuse of Salvaged Dimensional Lumber from Pre-1940s Houses* (tech. rep.). The University of British Columbia. Vancouver. https://sustain.ubc.ca/about/resources/opportunities-and-regulatory-barrier-reuse-salvaged-dimensional-lumber-pre-1940s

Teshnizi, Z. (2020). Vancouver pre-1940 houses : a cache for old-growth forest wood. *Journal of Cultural Heritage Management and Sustainable Development*, 41–51. https://doi.org/10.1108/JCHMSD-06-2019-0077

Thelandersson, S., & Larsen, H. J. (Eds.). (2003). *Timber Engineering*. John Wiley & Sons.

Thönnissen, U. (2014). A Form-Finding Instrument for Reciprocal Structures. *Nexus Network Journal*, *16*(1), 89–107. https://doi.org/10.1007/s00004-014-0172-1

Thönnissen, U. (2015). *Reciprocal Frameworks - Tradition and Innovation*. gta Publishers Zurich.

Thönnissen, U. (2018). Mkombozi Promenade Roof Dar es Salaam Tanzania. https://thoennissen.ch/MKO

Thönnissen, U., & Werenfels, N. (2011). Reciprocal frames-teaching experiences. *International Journal of Space Structures*, *26*(4), 369–371. https://doi.org/10.1260/0266-3511.26.4.369

Trout, M. (2010). Membrane. https://www.flickr.com/photos/troutfactory/5390181032

TU Delft. (2021). Climate Action Programme 2021-2030. (April). https://d2k0ddhflgrk1i.cloudfront.net/News/2021/04_April/TU%20Delft/Climate%20Action_april%202021_ENG_DEF.pdf

United Nations Environment Programme. (2020). 2020 GLOBAL STATUS REPORT.

Vaudeville, B. (a. d. (2009). Excavation shelter. https://www.tess.fr/en/projet/excavation-shelter#

Viscardi, T., Brandt, M., Girardot, N., & Dongning, W. (2011). *Chinese Bridge Project* (tech. rep.). Lehigh University. http://english.hanban.org/node_8080.htm

Vrontissi, M., & Thönnissen, U. (2015). Full-scale design explorations in architecture education: small-scale reciprocal structures for outdoor use. *Proceedings of the International Association for Shell and Spatial Structures Symposium (IASS 2015): Future Visions, Amsterdam, The Netherlands, August 17-20, 2015*, (September).

Walford, G. B. (2003). COMPARISON OF VARIOUS STANDARDS FOR THE CHARACTERISTIC STRENGTH AND STIFFNESS OF STRUCTURAL TIMBER. *NZ Timber Design Journal*, *11*(2), 13–18.

A

Reclaimed Timber

A.1. Explanatory Comments on the Reclaimed Timber Database

The following explanatory notes provide additional information on the data displayed in tables A.1 and A.2. A cell with a dash indicates that the data item is missing. The virgin timber grade is not displayed in the tables because it is unknown for the listed stacks. The following paragraphs address the group of stacks that stem from the same source consecutively. The origin of the data is mentioned as well as assumptions that were made in order to display the data in the format which it has in the table.

Stack 1 through 4

The data for stacks one through four stems from a visit at a Dutch Salvage Yard. Additional remarks on the stacks' item geometry and physical damage are stated on the base of a visual assessment.

The provided size of cross section and length is an average estimate, i.e. the geometry of the items in a stack are not identical. The length can alter significantly (>10%), the cross section size does not alter much (<10%). Physical damage is observed on the beam ends, cut outs from notched joinery are common. Moreover, on the top side of the beam nail holes are present at roughly regular intervals. Several cracks are observed along the span of the items. The item ends are colored, this originates from their contact with masonry walls.

Stack 5 through 7

The data for stacks five through seven stems from a Finnish two-storey high kindergarten which was deconstructed. Subsequently the harvested material was analyzed (Sakaguchi et al., 2016). The following operations were conducted to apply the chosen format to the source data: The average length was rounded. Only timber which was classified to be class A (minimal damage) was considered.

Stack 8 through 10

The data for stacks eight through ten stems from a traditional Spanish timber building type, called Corrala. The building from which the data stems is five-storeys high (de Arana-Fernandez et al., 2020). The data for these stacks was generated during a building assessment, that means at this stage the building was not yet deconstructed and information was extracted from plans and other construction documents. The species of this timber is either Scots pine or European black pine.

The following operations were conducted to apply the chosen format to the source data. The item length for stacks nine and ten was assumed. This assumption is based on a range that was specified in the source. For stack nine a range of 5.00 m to 2.78 m was provided and for stack ten 6.50 m to 3.34 m respectively. For stack eight a length of 4.2 m was assumed, no data on the item length of this stack was provided. The number of items was computed from a volume specification. For stack eight, this was $38\,\mathrm{m}^3$, for stack nine $102\,\mathrm{m}^3$ and for stack ten $15.4\,\mathrm{m}^3$ respectively.

Stack 11

The data for stack eleven stems from a German Alpine Cottage, which was two-storeys high (Hafner, Ott, et al., 2014).The following operations were conducted to apply the chosen format to the source data. It was assumed that the terms solid wood and construction wood were used synonymous. The uncontaminated part of the construction wood then is $54.66\,\mathrm{m}^3$. For the given cross section this amounts to about 1708 running meters. Further, an average length of 4 m is assumed, this results in 420 items.

Stack 12 through 25

The data for stacks 12 through 25 stems from an extensive test series which was conducted in the United States (Falk et al., 2008). The timber was visually graded. Subsequently, the mechanical properties were obtained through destructive laboratory testing. Only a selection of timber items were tested. Thus the number of items does not represent the total number of items fit for structural use from the respective buildings. Timber was taken from four different buildings that were built around the same time period with the same type of wood. The species of the timber is Douglas-fir-larch.

The following operations were conducted to apply the chosen format to the source data. The geometric parameters were transferred from the imperial to the metric system (Baylor, 2020). The mechanical properties that belong to the assigned strength grades are characteristic values and were taken from (Walford, 2003). The bending strength is the 5th percentile value.

Stack 26 through 30

The data for stack 26 through 30 stems from an American wood framed house, which was two-storeys high (Diyamandoglu & Fortuna, 2015). The following operations were conducted to apply the chosen format to the source data. A length of 3.0 m was assumed for all elements, since no data on the length was provided. No information on the building year was provided, the building year was assumed to be 1950.

A.2. Reclaimed Timber Database

Table A.1: Database for Reclaimed Timber Stacks from various Sources (Part 1), for Source see A.1

Material Characteristic	Geometry		Material Condition			Mechanical Properties			Additional Information				
Property	Width x Height $[mmxmm]$	Length $[m]$	Chemical Contamination	Biological Corrosion	Physical damage	Strength Grade	MOR $[N/mm^2]$	$E_{m,0,mean}$ $[N/mm^2]$	Number of items [-]	Material status	Location in building	Building year	Building type
Stack 1	70x175	2.3	no	no	yes	-	-	-	126	free	-	1950s	-
Stack 2	70x175	3.6	no	no	yes	-	-	-	120	free	-	1950s	-
Stack 3	60x160	6.3	no	no	yes	-	-	-	84	free	-	1950s	-
Stack 4	60x160	3.3	no	no	yes	-	-	-	63	free	-	1950s	-
Stack 5	95x95	3.6	no	no	yes	-	-	-	90	free	roof beam	1977	Kindergarten
Stack 6	45x95	1.4	no	no	yes	-	-	-	157	free	roof pillar	1977	Kindergarten
Stack 7	45x120	4.2	no	no	yes	-	-	-	119	free	roof rafter	1977	Kindergarten
Stack 8	210x280	4.2	-	-	-	-	-	-	153	fixed	column	19th century	Corrala
Stack 9	140x200	3.7	-	-	-	-	-	-	984	fixed	floor beam	19th century	Corrala
Stack 10	140x210	4.0	-	-	-	-	-	-	132	fixed	roof beam	19th century	Corrala
Stack 11	80x240	4.0	no	no	-	-	-	-	420	free	-	19th century	Alpine Cottage
Stack 12	38x140	3.0	no	no	yes	No. 2	17.0	11030	98	fit	rafter (roof)	1940s	Army barack
Stack 13	38x140	3.0	no	no	yes	SS	28.1	13100	12	fit	rafter (roof)	1940s	Army barack
Stack 14	38x184	3.7	no	no	yes	No. 2	17.0	11030	220	fit	floor joists/ stringers	1940s	Army barack
Stack 15	38x184	3.7	no	no	yes	SS	28.1	13100	40	fit	floor joists/ stringers	1940s	Army barack

Table A.2: Database for Reclaimed Timber Stacks from various Sources (Part 2), for Source see A.1

Material Characteristic	Geometry		Material Condition			Mechanical Properties			Additional Information				
Property	Width x Height $[mm x mm]$	Length $[m]$	Chemical Contamination	Biological Corrosion	Physical damage	Strength Grade	MOR $[N/mm^2]$	$E_{m,0,mean}$ $[N/mm^2]$	Number of items [-]	Material status	Location in building	Building year	Building type
Stack 16	38x140	3.0	no	no	yes	No. 2	17.0	11030	16	fit	Wall stud	1940s	Naval Supply Center
Stack 17	38x140	3.0	no	no	yes	SS	28.1	13100	47	fit	Wall stud	1940s	Naval Supply Center
Stack 18	38x235	4.3	no	no	yes	No. 2	17.0	11030	53	fit	roof joist	1940s	Naval Supply Center
Stack 19	38x235	4.3	no	no	yes	SS	28.1	13100	197	fit	roof joist	1940s	Naval Supply Center
Stack 20	38x235	4.3	no	no	yes	No. 2	17.0	11030	53	fit	roof joist	1940s	Army Munition Plant
Stack 21	38x235	4.3	no	no	yes	SS	28.1	13100	117	fit	roof joist	1940s	Army Munition Plant
Stack 22	38x140	3.0	no	no	yes	No. 2	17.0	11030	20	fit	rafter (roof)	1940s	University housing
Stack 23	38x140	3.0	no	no	yes	SS	28.1	13100	36	fit	rafter (roof)	1940s	University housing
Stack 24	38x184	3.7	no	no	yes	No. 2	17.0	11030	43	fit	roof joist	1940s	University housing
Stack 25	38x184	3.7	no	no	yes	SS	28.1	13100	2	fit	roof joist	1940s	University housing
Stack 26	38x89	3.0	no	no	yes	-	-	-	190	free	-	-	Wood framed house
Stack 27	38x140	3.0	no	no	yes	-	-	-	2	free	-	-	Wood framed house
Stack 28	38x184	3.0	no	no	yes	-	-	-	111	free	-	-	Wood framed house
Stack 29	19x89	3.0	no	no	yes	-	-	-	8	free	-	-	Wood framed house
Stack 30	19x140	3.0	no	no	yes	-	-	-	13	free	-	-	Wood framed house

B

Reciprocal Frames

B.1. Analytical Investigation of the Parameter Engagement Length

The aim of this section is to illustrate with an analytical model that an increase in engagement length increases the bending stiffness.

At first a planar reciprocal frame unit with four members will be analyzed from a structural mechanics stand point. The members are assumed to be connected with hinges and simply supported on the exterior points.

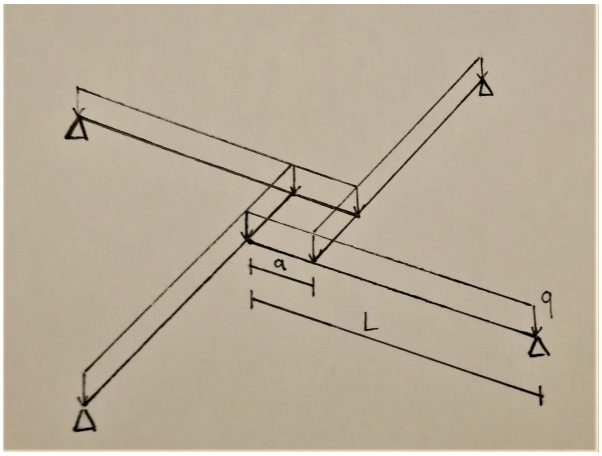

Figure B.1: Planar RF Unit with four Members

Due to symmetry the internal forces and also the reactions at the exterior supports will be identical in all four members. Thus a simplified mechanical model of one member is sufficient for the analytical structural analysis.

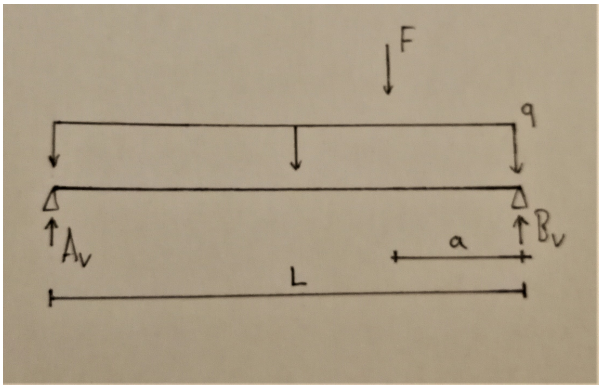

Figure B.2: Single Member of the RF Unit

Further from the symmetry in the system the value of the exterior supports can be identified as

$$A_v = q * L$$

Now the individual member can be further analyzed, i.e. the two unknowns F and B_v are determined. From the global system another condition can be derived. The interior support B_v must have the same magnitude as the point force F.

$$B_v = F$$

Now, it is straightforward to solve for the value of the interior support and the force respectively through a moment equilibrium in point B.

$$F = \frac{1}{a}(A_v * L - \frac{q * L^2}{2}) = \frac{q * L^2}{2 * a}$$

The vertical equilibrium condition is considered to verify the result:

$$\sum V = A_v + B_v - F - q * L = q * L + \frac{q * L^2}{2a} - \frac{q * L^2}{2a} - q * L = 0$$

Lastly, the bending moment in the RF unit is considered. The maximum bending moment occurs at the position of the force F.The moment is determined in dependence of the engagement length.

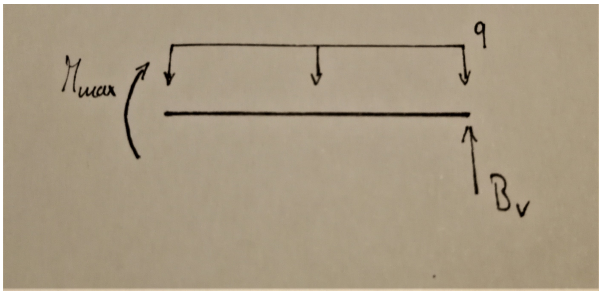

Figure B.3: Free Body Diagram

$$M_{max} = B_v * a - \frac{q * a^2}{2} = \frac{q * L^2}{2} * \frac{a}{a} - \frac{q * a^2}{2} = \frac{q}{2}(L^2 - a^2)$$

The equation infers that for an increase in engagement length, the term inside the parenthesis decreases, that means the maximum bending moment decreases. Finally, when member dimensions and load are kept constant, but the engagement length increases, the maximum bending moment decreases.

C

Structural Design Case Study

C.1. Visualization of PRFA geometries

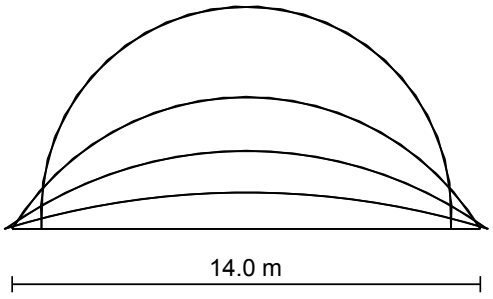

GV	n_m [-]	e [m]	L_{span} [m]	h_r [m]
4	30	0.04	12.25	6.66
3	25	0.03	14.01	3.96
2	23	0.02	14.41	2.34
1	22	0.01	14.48	1.09
0	21	0.00	14.00	0.00

Figure C.1: Geometric Variants of DL1 ($L = 1.40m$)

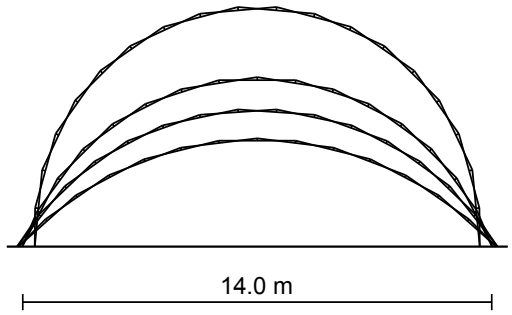

GV	n_m [-]	e [m]	L_{span} [m]	h_r [m]
4	20	0.10	13.29	7.18
3	17	0.09	14.03	5.06
2	16	0.08	14.34	4.11
1	15	0.07	14.26	3.23
0	14	0.00	14.95	0.00

Figure C.2: Geometric Variants of DL2 ($L = 2.30m$)

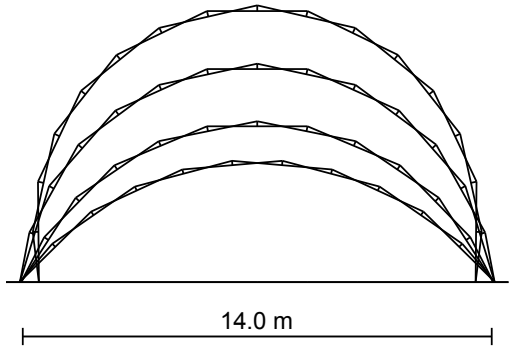

GV	n_m [-]	e [m]	L_{span} [m]	h_r [m]
4	17	0.17	13.04	8.26
3	15	0.16	14.17	6.52
2	13	0.15	14.10	4.80
1	12	0.13	14.19	3.65
0	11	0.00	15.00	0.00

Figure C.3: Geometric Variants of DL3 ($L = 3.00m$)

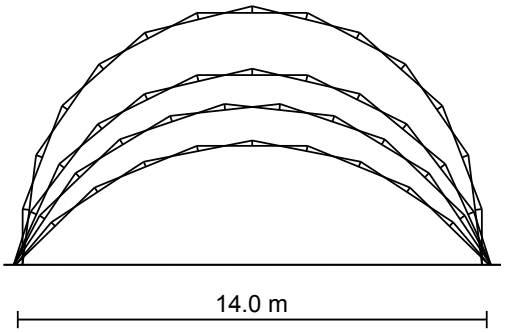

GV	n_m [-]	e [m]	L_{span} [m]	h_r [m]
4	15	0.20	13.72	7.72
3	13	0.19	14.24	5.85
2	12	0.18	14.24	4.85
1	11	0.16	14.14	3.71
0	10	0.00	14.85	0.00

Figure C.4: Geometric Variants of DL4 ($L = 3.30m$)

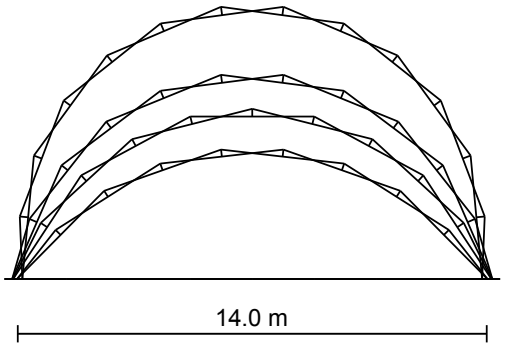

GV	n_m [-]	e [m]	L_{span} [m]	h_r [m]
4	14	0.25	13.73	8.19
3	12	0.24	14.33	6.15
2	11	0.23	14.28	5.08
1	10	0.21	14.04	3.91
0	9	0.00	14.80	0.00

Figure C.5: Geometric Variants of DL6 ($L = 3.70m$)

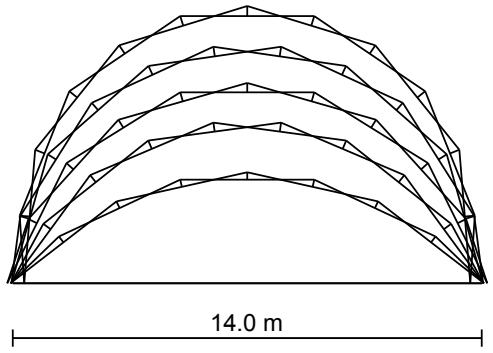

GV	n_m [-]	e [m]	L_{span} [m]	h_r [m]
5	13	0.30	13.32	8.28
4	12	0.29	14.08	7.13
3	11	0.28	14.33	5.98
2	10	0.27	14.10	4.86
1	9	0.22	14.14	3.31
0	8	0.00	14.00	0.00

Figure C.6: Geometric Variants of DL7 ($L = 4.00m$)

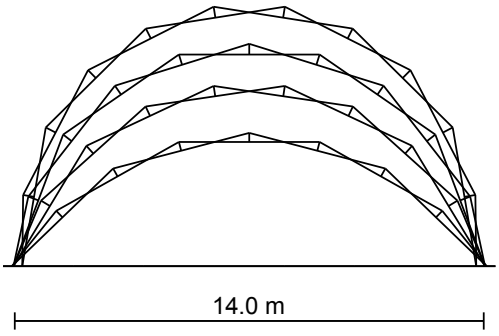

GV	n_m [-]	e [m]	L_{span} [m]	h_r [m]
4	12	0.33	13.55	7.83
3	11	0.32	14.08	6.64
2	10	0.31	14.08	5.46
1	9	0.27	14.17	3.98
0	8	0.00	14.70	0.00

Figure C.7: Geometric Variants of DL8 ($L = 4.20m$)

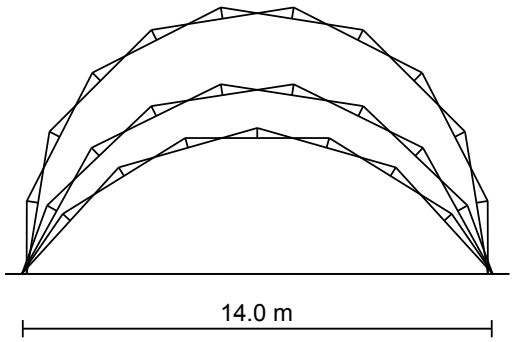

GV	n_m [-]	e [m]	L_{span} [m]	h_r [m]
3	12	0.34	13.77	8.04
2	10	0.33	14.05	5.74
1	9	0.30	14.06	4.36
0	8	0.00	15.05	0.00

Figure C.8: Geometric Variants of DL9 ($L = 4.30m$)

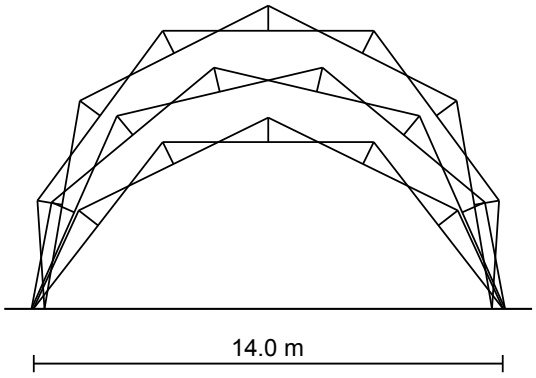

GV	n_m [-]	e [m]	L_{span} [m]	h_r [m]
3	9	0.75	13.36	9.05
2	8	0.74	14.13	7.39
1	7	0.73	14.02	5.71
0	6	0.00	15.75	0.00

Figure C.9: Geometric Variants of DL10 ($L = 6.30m$)

C.2. Modelling of Loads

C.2.1. Self-Weight

The distributed line load for the longitudinal elements of the PRFA is computed in the following manner. The example assumes the cross-section of RT stack 9 with a strength grade of C18.

$$\text{Longitudinal beams: } 3.8\,\frac{\text{kN}}{\text{m}^3} \cdot 0.14\,\text{m} \cdot 0.20\,\text{m} = 0.11\,\frac{\text{kN}}{\text{m}}$$

The point loads at the vertices of the polygonal arch are a summation of the self-weight of the cladding, which is composed of a timber diagrid and a poly-carbonate sheet, as well as the dead load of the transverse beams. The supporting diagrid is assumed to have two layers with a total thickness of 10 cm. The layers are composed of C24 laths. Moreover, it is estimated that half of the surface area is covered by the laths.

$$\text{Polycarbonate Sheet: } q_{sheet} = 3.1\,\frac{\text{kg}}{\text{m}^2} \cdot 10\,\frac{\text{m}}{\text{s}^2} = 0.03\,\frac{\text{kN}}{\text{m}^2}$$

$$\text{Diagrid: } q_{grid} = 4.2\,\frac{\text{kN}}{\text{m}^3} \cdot 0.1\,\text{m} \cdot \frac{1}{2} = 0.02\,\frac{\text{kN}}{\text{m}^2}$$

$$\text{`Transverse beams: } q_{trans} = 3.8\,\frac{\text{kN}}{\text{m}^3} \cdot 0.14\,\text{m} \cdot 0.20\,\text{m} = 0.11\,\frac{\text{kN}}{\text{m}}$$

To generate the point loads that act on the vertices of the polygonal arch, the area loads originating from the cladding are multiplied with the length of two cladding segments, that each have a length of L_{arc}. A cladding segment (CS) includes half of the cladding that lies in between two transverse beams. For the x-z-plane that means, the arc is divided at the vertices of the polygonal arch and at the mid distance between these vertices as illustrated in figure C.10.

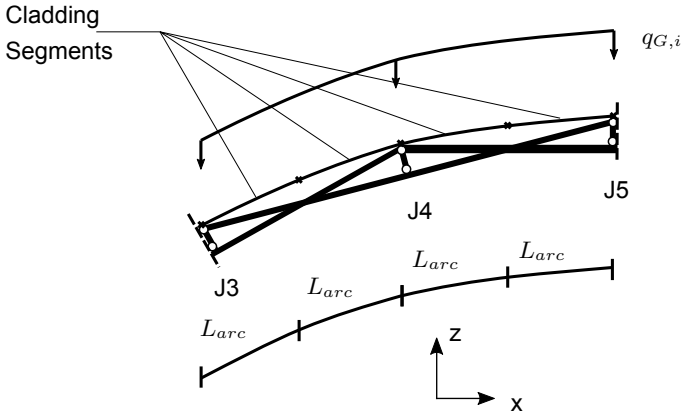

Figure C.10: Geometry of Part of the PRFA with Cladding

After adding the line load of the transverse beams, the sum is multiplied with the bay span. For example, geometric design proposal S9V2, has an arc length of $L_{arc} = 0.94\,\text{m}$. This leads to the following point load on position J4:

$$(L_{arc} + L_{arc}) \cdot (q_{sheet} + q_{grid}) = 0.09\,\frac{\text{kN}}{\text{m}}$$

$$F_{p,J4} = (0.09 + 0.11)\,\frac{\text{kN}}{\text{m}} \cdot 1.0\,\text{m} = 0.20\,\text{kN}$$

C.2.2. Wind load

The modelling of the wind load is described in three steps. First the assumptions that form the basis of the model are explained. Second, the wind pressure is computed for the location of the Norrebro station and the calculation of the wind pressure coefficients is demonstrated with the example of S9V2. Third, the implementation of the wind load to the parameteric PRFA model is described.

Basic assumptions

The Eurocode provides models which enable to compute a wind load as a product of wind pressure and pressure coefficients for common structural systems. A vaulted canopy with two open sides is not part of these systems. In the case that the Eurocode does not provide a guideline for the computation of a structure's wind load, it suggests to conduct wind tunnel tests (EN1991-1-4 1.5) (European Committee for Standardization, 2020c). For the present design process, in which the shape is a parameter of the structural design, it is not considered reasonable to conduct a wind tunnel test at the point of designing the PRFA, neither does the project scope allow such an elaborate testing procedure. Besides the Eurocode, also research activities have not yet concluded with recommendations for a wind load model that could be used for the structure at hand (Natalini et al., 2013).

The Eurocode's wind load model for closed vaulted roofs has the same geometry as the RF barrel vault. However, the RF barrel vault is open at its transverse ends. If the RF barrel vault was infinitely long, the difference between the closed and open sides would have a negligible influence on a PRFA. The wind load is modelled under this assumption. Turbulences that occur at the sides of a RF barrel vault with a finite transverse length are required to be investigated in the detail design of a RF barrel vault, which is out of the scope of this project.

The Eurocode specifies only the wind load for wind in the direction perpendicular to the transverse sides. The load resulting from wind in the transverse direction is relevant when designing the bracing of the structure, this is out of the scope of this project. For the structural analysis of the PRFA only the wind direction which is addressed by the Eurocode is considered.

Besides the external wind pressure, also an internal wind component is considered. Again the Eurocode does not provide a guideline for a canopy with a curved roof and two open sides. The norm DIN 1055-4 which is still part of German design practice is used to provide a starting point for computing the internal wind component. The norm specifies for a duo pitched roof with two open sides on opposite ends and a wind in transverse direction that a negative pressure of half of the peak velocity pressure acts on the entire inside of the roof. The internal wind component is added to the external wind component, if this leads to an increase of the total load value.

Wind load computation

The external wind load is computed in two consecutive steps. First, the wind pressure for the location of the Norrebro station is computed. Second, the wind pressure coefficients for the RF barrel vault are determined.

The fundamental value of the basic wind velocity is determined according to the Danish NA (Danish Standards Foundation, 2007) as

$$v_{b,0} = 24 \,\frac{\mathsf{m}}{\mathsf{s}}$$

The following computations are based on EN 1991-1-4 Section 4 "Wind velocity and velocity pressure" (European Committee for Standardization, 2020c). The basic wind velocity is computed with the directional factor c_{dir} and the seasonal factor c_{season}. Both factors are chosen as 1.0 for no specific direction nor a definite season are investigated.

$$v_b = c_{dir} \cdot c_{season} \cdot v_{b,0} = 1.0 \cdot 1.0 \cdot 24 \,\frac{\mathsf{m}}{\mathsf{s}} = 24 \,\frac{\mathsf{m}}{\mathsf{s}}$$

The mean wind velocity is influenced by a roughness factor c_r and an orography factor c_o.

$$v_m(z) = c_r(z) \cdot c_o(z) \cdot v_b$$

Both factors are a function of the building height z. The roughness factor is dependent on the terrain factor k_r and is computed as follows.

$$\begin{aligned} c_r(z) &= k_r \cdot \ln(\frac{z}{z_0}) = 0.234 \cdot \ln(\frac{z}{1.0}) \\ k_r &= 0.19 \cdot (\frac{z_0}{z_{0,II}})^{(0.07)} = 0.234 \\ z_{0,II} &= 0.05\,\text{m} \\ z_0 &= 1.0 \end{aligned}$$

The terrain category is determined as category IV as the building is located in a central area of a large European city. The values associated with this category are $z_0 = 1.0$ and $z_{min} = 10\,\text{m}$.

The orography factor is chosen according to the code as 1.0.

$$c_0 = 1.0$$

For a roof the dependence on the building height z is usually simplified to considering only the height of the roof's topmost point. The height of the RF barrel vault is a summation of the height of the structure above ground, the height of the supporting walls and the rise of the geometrical design proposal. For instance, for S10V3, the following height z_max and the corresponding mean velocity v_m are determined

$$\begin{aligned} z_{max} &= h_{aboveground} + h_{wall} + h_{PRFA} = 6.5\,\text{m} + 4.5\,\text{m} + 6.0\,\text{m} = 17.0\,\text{m} \\ v_m(17.0\,\text{m}) &= c_r(17.0\,\text{m}) \cdot c_o(17.0\,\text{m}) \cdot v_b = 15.8\,\frac{\text{m}}{\text{s}} \end{aligned}$$

To compute the peak velocity pressure, the wind turbulence is considered first. Standard deviation σ_v and turbulence intensity $I_v(z)$ are computed as follows with a turbulence factor $k_I = 1.0$.

$$\begin{aligned} \sigma_v &= k_r \cdot v_b \cdot k_I = 5.6 \\ I_v(17.0\,\text{m}) &= \frac{\Sigma_v}{v_m(17.0\,\text{m})} = 0.35 \end{aligned}$$

The resulting peak velocity pressure is computed with the air density $\rho = 1.25\,\frac{\text{kg}}{\text{m}^3}$.

$$q_p(17.0\,\text{m}) = (1 + 7 \cdot I_v(17.0\,\text{m})) \cdot \frac{1}{2} \cdot \rho \cdot v_m^2(z) = 0.55\,\frac{\text{kN}}{\text{m}^2}$$

Finally, the peak velocity pressure is compared with a simplified way of determining the peak velocity pressure. This value validates the computation.

$$\begin{aligned} q_p(17.0\,\text{m}) &= c_e(17.0\,\text{m}) \cdot q_b = 0.55\,\frac{\text{kN}}{\text{m}^2} \\ q_b &= \frac{1}{2} \cdot \rho \cdot v_b^2 = 0.36\,\text{m}\frac{\text{kN}}{\text{m}^2} \\ c_e(17.0\,\text{m}) &= 1.52 \end{aligned}$$

In the second step the wind load pressure coefficients are determined for the vaulted roof according to section 7.2.8 of EN 1991-1-4 (European Committee for Standardization, 2020c). Figure C.11a illustrates that there are three areas on the roof to which different pressure coefficients are assigned. The coefficients are determined depending on the geometry using the diagram displayed in figure C.11b.

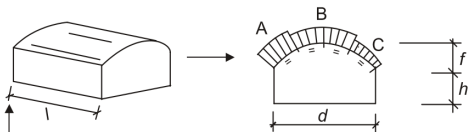

(a) Geometry

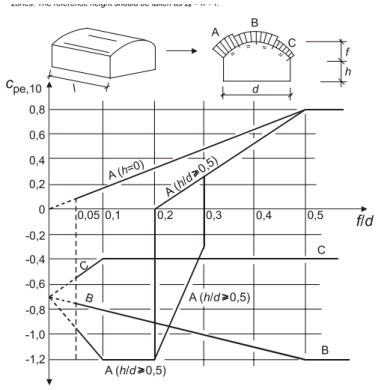

(b) Diagram

Figure C.11: Pressure Coefficients for Vaulted Roof EN 1991-1-4 (European Committee for Standardization, 2020c)

The geometric values for the span and rise are dependent on the geometric design proposal, for S9V2 the following holds.

$$f = 5.21\,\text{m}$$
$$d = 14.00\,\text{m}$$

The height of the walls and the transverse length of the building are fixed and determined in reference to the Norrebro Station.

$$h = 4.5\,\text{m}$$
$$l = 27.0\,\text{m}$$

To obtain the pressure coefficients $c_{pe,10}$ for the three wind areas A,B and C, the two input ratios for the diagram are computed.

$$\frac{f}{d} = 0.37$$
$$\frac{h}{d} = 0.32$$

The pressure coefficients and the resulting wind pressure are listed in table C.1. The wind pressure is computed according to the following formula.

$$w = c_{p,net,10} \cdot q_p$$

considering that

$$c_{p,net,10} = c_{pe,10} + c_{pi,10} \text{if} c_{pe,10} > 0$$

Table C.1: Pressure Coefficients and resulting Wind Pressure

	$c_{pe,10}$ [-]	$c_{p,net,10}$ [-]	$w[\frac{kN}{m^2}]$
A_1	0.51	1.01	0.56
A_2	n.a.	n.a	n.a.
B	-1.07	-1.07	-0.59
C	-0.4	-0.4	-0.22

As a result of the diagram a certain range of geometry has two possible values for the wind load area A. For the given geometric design proposal only one value applies.

Application to the RF Barrel Vault

The wind load is applied to the PRFA in three steps. First, the wind load for the vaulted roof is computed. Second, the geometry of the PRFA's cladding is generated. Third, the wind load is assigned to the vertices of the polygonal arch.

The first step is programmed according to the above computation of the wind load. To enable the computation of the wind load for all of the geometric design proposals, the rise and span of the vaulted roof change according to the input geometry. Moreover, the diagram in figure C.11b is programmed to automate the computation of the $c_{pe,10}$ values for varying geometries. Figure C.12 illustrates the assignment of the wind load to the wind load areas.

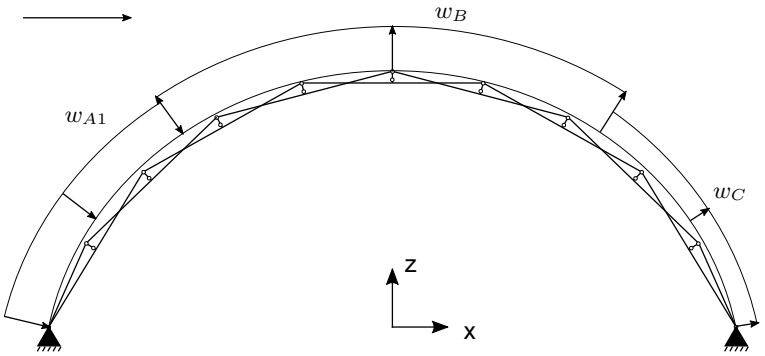

Figure C.12: Wind Load assigned to Wind Load Areas (PRFA S9V2)

In the second step, the wind load associated with the wind load areas is assigned to the cladding segments, see figure C.13.

This prepares the assignment of the wind load to the transverse beams, which attracts half of the load that is acting on the area in between two transverse beams, see section 6.2. To assign the computed wind load values to the CS, it is evaluated per segment which wind load area is applicable. If the positions at which the wind loads change, do not coincide with an end of a CS, the distribution of the wind load is slightly altered through the assignment.

In the third step, the point load is computed by assigning the wind load from the CSs to the vertices at the positions of the transverse beams. Figure C.14 illustrates the computation for the wind point load at position J4. The true length of the CSs is $L_{arc} = 0.94\,\text{m}$. The distance between the endpoints of the CSs is $L_{lin} = 0.93\,\text{m}$.

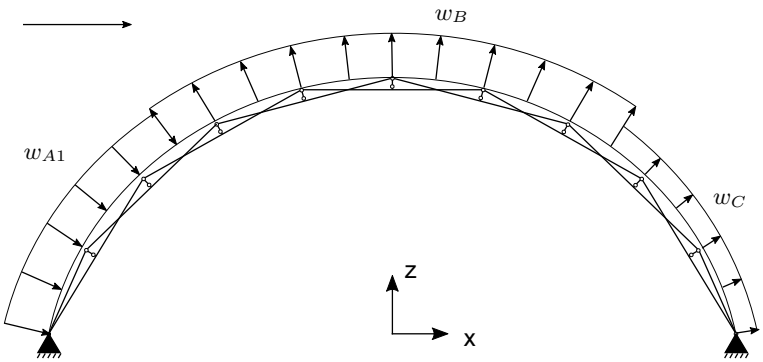

Figure C.13: Wind Load assigned to Cladding Segments (PRFA S9V2)

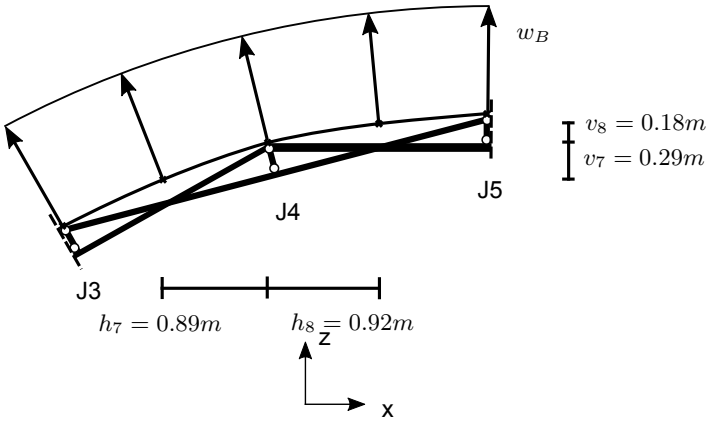

Figure C.14: Wind Point Load Calculation for Position J4 (PRFA S9V2)

From the wind area loads on the CSs the horizontal and vertical component of the line load that results from multiplication with the segment's length is computed. Consecutively, per quadrant the signs of the wind line loads are adjusted from suction and pressure to the global coordinate system.

CS left of J4

$$\text{Horizontal component: } w_B \cdot L_{arc} \cdot \frac{v_7}{L_{lin}} = -0.17 \, \frac{\text{kN}}{\text{m}}$$

$$\text{Vertical component: } w_B \cdot L_{arc} \cdot \frac{h_7}{L_{lin}} = -0.52 \, \frac{\text{kN}}{\text{m}}$$

CS right of J4

$$\text{Horizontal component: } w_B \cdot L_{arc} \cdot \frac{v_8}{L_{lin}} = -0.11 \, \frac{\text{kN}}{\text{m}}$$

$$\text{Vertical component: } w_B \cdot L_{arc} \cdot \frac{h_8}{L_{lin}} = -0.54 \, \frac{\text{kN}}{\text{m}}$$

Finally, the horizontal and vertical line loads of neighboring CS are added and matched to the vertices of the polygonal arch. The multiplication with the bay span transforms the line load into the point load.

Horizontal component:

$$(-0.17\,\text{kN} + (-0.11\,\text{kN})) \cdot 1.0 = -0.28\,\text{kN}$$

Vertical component:

$$(-1) \cdot (-0.52\,\text{kN} + (-0.54\,\text{kN})) \cdot 1.0 = 1.06\,\text{kN}$$

In the process of combining the load form neighboring CS an inaccuracy can occur at the position where the load areas change. In the case that the sign of the wind loads between two areas changes the resulting point load on the PRFA is lower than in reality.

C.2.3. Snow load

The modelling of the snow load is described in two steps. First, the snow load is computed according to the model that the Eurocode provides for a barrel vault. Second, the implementation of the snow load to the parameteric PRFA model is described.

Computation of the Snow load

The Danish National Annex (Danish Standards Foundation, 2015) determines that the snow load on the ground as

$$s_k = 1.0\,\frac{\text{kN}}{\text{m}^2}$$

The calculation of the snow load on the roof is conducted as follows.

$$s_i = \mu_i \cdot C_e \cdot C_t \cdot s_k$$

The factor μ_i reflects the distribution of the snow load for relevant load cases i that are specific for a roof shape. The factor C_e and C_t depend on the surrounding topography and thermal influence. Both are specified as 1.0, because no special circumstances apply to the case at hand. Hence the snow load on the roof simplifies to the following.

$$s_i = \mu_i \cdot s_k$$

The Eurocode EN1991-1-3 (2020b) and the corresponding Danish National Annex (Danish Standards Foundation, 2015) prescribe three different snow load cases for a vaulted roof shape, one case with an undrifted snow load on the roof, named s_1, and two cases with a drifted snow load, named s_2 and s_3. The distribution of the load cases is visualized in figure C.15. In all three load cases the snow load is only applied between the points where the angle between the tangent of the arch and the x-axis is smaller than 60 degrees. Outside of this domain the snow is assumed to fall off. Thus the load is zero in this region.

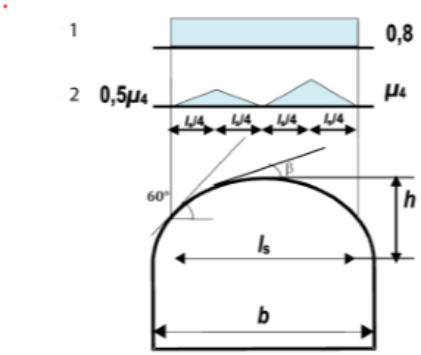

(a) Case s_1 and s_2 according to EN 1991-1-3 (European Committee for Standardization, 2020b)

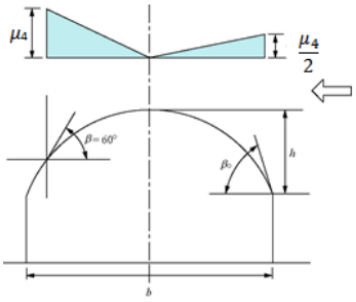

(b) Case s_3 according to 1991-1-3 NA:DK (Danish Standards Foundation, 2015)

Figure C.15: Schematic Visualization of the relevant Snow Load Cases for a Vaulted Roof

For case s_1 the form factor $\mu_1 = 0.8$ is constant over the roof. For cases s_2 and s_3 the form factor μ_2 and μ_3 are dependent on the span of the roof, here denoted as b and the rise of the roof, here denoted as h. In figure C.15 μ_2 and μ_3 are named μ_4.

$$\mu_2 = \mu_3 = 0.2 + 10\frac{h}{b} \leq 2.0$$

For instance, for geometric design proposal S9V2, as introduced in section 9.1.1 the form factor is computed as follows

$$\mu_2 = 0.2 + 10 \cdot \frac{5.21}{14.00} = 3.92 \leq \underline{2.0}$$
$$\mu_2 = 2.0$$

Application to the PRFA

Similar to the wind load, the snow load is modelled in three steps. First, the basic parameters s_k and μ_i are determined. Second, the geometry to which the snow load is applied is generated. Third, the snow load distributions are generated and applied to the generated structural geometry.

First, the form factors for load case s_2 and s_3 are computed specific for every geometric design proposal, the snow load on the ground s_k is computed only once, because it is independent of the geometry.

Second, the snow load is applied to the CSs that were defined for the wind load. However, only to those which lie between the two points on the arc, that have an angle between tangent of the arc and x-axis of 60 degrees. For the case that these points do not coincide with a polygonal arch vertex, the vertices outside of the domain to which the snow load is applied, would also directly participate in the load take down. As it is simpler to program, the endpoints of the load domain are moved to the vertices that are just outside the range to which the load would be applied according to the criterion above. Figure C.16 shows, that for the geometric design proposal S9V2, the snow load is applied to the entire span, because the points at which the 60 degree angle is reached lie in between support point and J1 and support point and J9.

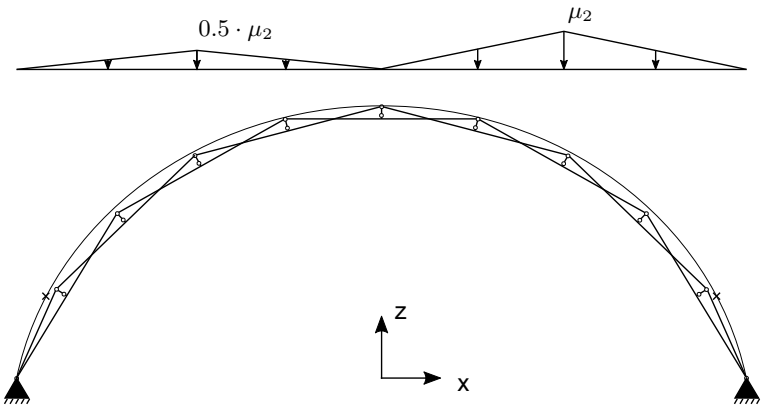

Figure C.16: Snow load s_2 and Points that mark the outer End of the Snow Load Distribution (PRFA S9V2)

The snow load is not applied to the CSs themselves, but to their projections. Hence, the relevant vertices are selected and projected. As illustrated in figure C.17 at mid distance between the projected vertices are defined, these mark the ends of the area of load that is attracted by the vertices.

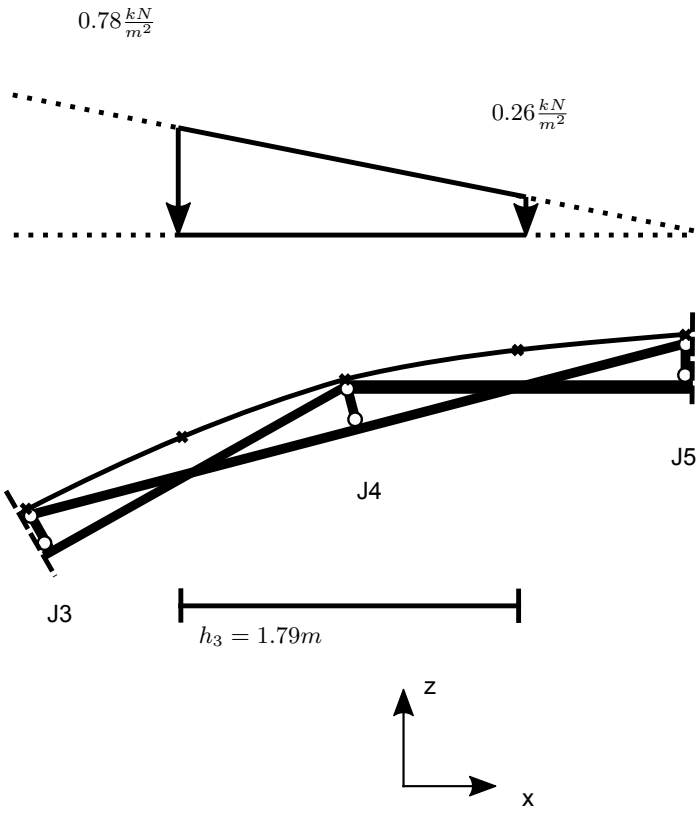

Figure C.17: Snow Load s_2 on Cladding Segments (PRFA S9V2)

Third, the load distributions of the three snow load cases are modelled geometrically. The points that mark the end of a vertex load area are projected onto the load distributions. The values of the resultant line load on a vertex is computed as the average of the snow area load on the points that mark the end of the areas that attract load multiplied with the distance between these points. Thus the load distribution is approximated. To construct the point load, the line load is multiplied with the bay span.

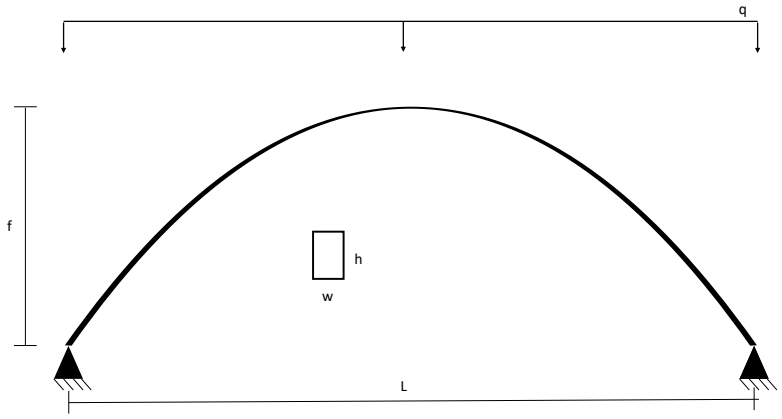

Figure C.18: Mechanical Scheme of the Parabolic Arch

$$\frac{0.78 + 0.26}{2} \cdot 1.79 \cdot 1.0 = 0.93kN$$

C.3. Model Validation

A parabolic arch is considered. The shape of the arch is described through the following function with $z(x)$ being the height of the arch in dependence of the position x. The span L and the rise f determine the form of the arch

$$z(x) = -4 \cdot f \cdot x \cdot \frac{(L - x)}{L^2}$$

The arch is assumed to have a rectangular timber cross-section w x h with an elastic modulus E. It is to be loaded with a distributed line load q The numeric parameter are listed below.

$$\begin{aligned} w &= 80mm \\ h &= 220mm \\ E &= 11000\frac{N}{mm^2} \\ q &= 1\frac{N}{mm} \\ f &= 4000mm \\ L &= 14000mm \end{aligned}$$

It is assumed that the arch is supported by pinned supports on both ends. Figure C.18 shows a mechanical scheme of the arch with the symmetric load case.

C.3.1. Analytical Model of the Parabolic Arch

The mechanical problem of the arch is modelled using the classical displacement method. Substituting kinematic relation and constitutive relation into the equilibrium the following ordinary differential equation with the displacement $w(x)$ as primary variable is obtained.

The bending stiffness is the multiplication of the second moment of inertia I and the elastic modulus E. The normal force H is assumed to be constant in the arch. For a derivation, refer to (Bouma, 1993).

$$E \cdot I \cdot \frac{d^4 w(x)}{dx^4} + H \cdot \frac{d^2}{dx^2} z(x) = q(x)$$

Figure C.19 displays the resulting moment $M(x)$ and displacement function for the unsymmetric load case. For a symmetric load, the moment and displacement are zero in case of a parabolic arch. For the unsymmetric load case, moment and displacement are zero at mid span and have maxima at $x = \frac{L}{4}, \frac{3L}{4}$.

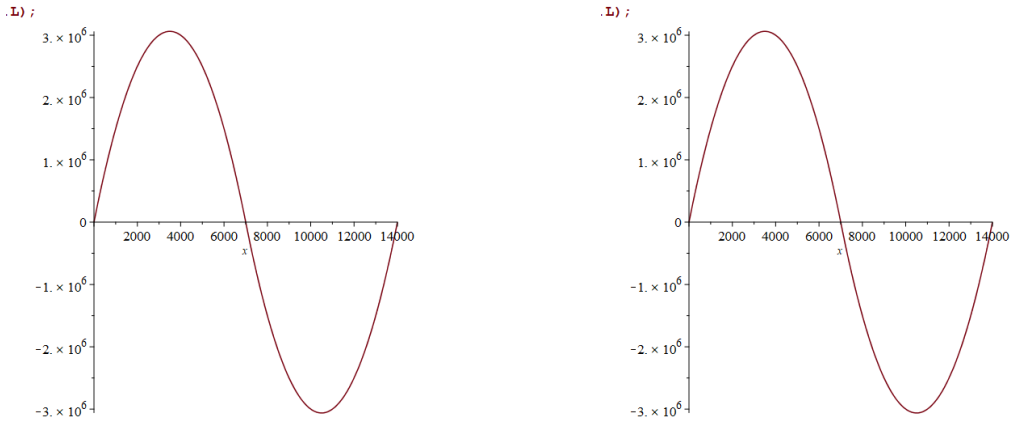

(a) Analytical Moment **(b)** Analytical Displacement

Figure C.19: Analytical Model Results, asymmetric Load Case

C.3.2. Numerical Model of the Parabolic Arch and Comparison

For the numerical model the arch shape is decomposed into 50 straight Timoshenko beam elements. Figure C.20 shows the resulting moment $M(x)$ and displacement function for the asymmetric load case.

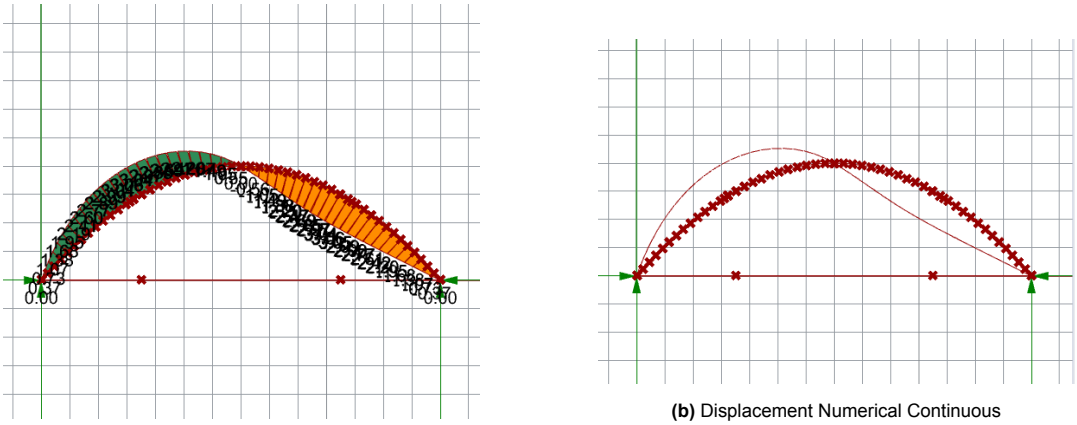

(a) Moment Numerical Continuous **(b)** Displacement Numerical Continuous

Figure C.20: Numerical Model Results

As expected the displacement and moment curve of the the numerical and analytical model of the continuous arch are of identical shape. Tables C.2 and C.3 compares the two solutions numerically.

Table C.2: Symmetric Load Case

	Analytical Model	Numerical Model	Deviation [%]
w(x=L/2) [mm]	0.00	0.51	100.00
w(x=L/4) [mm]	0.00	-0.39	100.00
w (x=3L/4) [mm]	0.00	-0.39	100.00
A_v [N]	7000.00	7000.00	0.00
B_v [N]	7000.00	7000.00	0.00
A_h [N]	6125.00	6124.00	0.02
B_h [N]	-6125.00	-6124.00	0.02
N(x=L/2) [N]	-6125.00	-6127.00	0.03
N(x=0) [N]	-9301.00	-9332.00	0.33
M(x=L/2) [Nmm]	0.00	3040.00	100.00

Table C.3: Asymmetric Load Case

	Analytical Model	Numerical Model	Deviation [%]
w(x=L/2) [mm]	0.00	0.26	100.00
w(x=L/4) [mm]	-20.00	-24.00	16.67
w (x=3L/4) [mm]	20.00	24.00	16.67
A_v [N]	-1750.00	-1750.00	0.00
B_v [N]	5250.00	5250.00	0.00
A_h [N]	3063.00	3062.00	0.03
B_h [N]	3063.00	3062.00	0.03
N(x=L/2) [N]	0.00	-3014.00	100.00
N(x=0) [N]	-3333.00	-3340.00	0.21
N(x=L) [N]	-5968.00	-5960.00	0.13
M(x=L/2) [Nmm]	0.00	0.00	0.00
M(x=L/4) [Nmm]	3.06 \cdot 10^6	3.06 \cdot 10^6	0.10

For both load cases, the numerical model approximates the support reactions accurately. The deformations in the analytic model are zero for the symmetric load case, which is an ideal value that the numeric solution does not approximate. The absolute value of the numerically computed deformations remain negligible compared to the span. For the unsymmetric load case the ideal zero value at midspan is again failed to be approximated. The deformation at the quarter points are of the same magnitude. The internal forces are approximated well for both load cases. Only the moment and the normal force at midspan for the symmetric and for the unsymmetric load case respectively experience a deviation for the same reason as for the deformations. At midspan the ideal zero value of the analytical solution is not approximated numerically. Nevertheless, it is concluded that the numerical model is a good approximation of the analytical solution.

C.3.3. Parabolic Polygonal Reciprocal Frame Arch

The parabolic PRFA is modelled in the same manner as described in the section 9.1.1. However, the geometry is not modelled as described in chapter 8, instead a top-down approach is applied. The parabolic arch with the span of 14.0 m and a rise of 4.0 m is the base form into which the RF is fitted in. The result is an irregular RF with varying member lengths and different eccentricities. Because the PRFA is a composition of two interwoven arches, the implementation of the above material and section properties implies that the total cross-section in the PRFA is double of that in the continuous arch. For an illustration of the arch, see figure 9.2 in section 9.1.1.

The load cases are applied as point loads on the vertices of the associated polygonal arch. The value of the point loads are chosen so that the load case is equivalent to that of the continuous arch.

C.4. Prerequisite Steps for the Structural Verification

C.4.1. Ultimate Limit State

EC1990 (3.3) specifies three different types of Ultimate Limit States. In this context, the limit state that addresses “failure by excessive deformation, transformation of the structure or any part of it into a mechanism, rupture, loss of stability of the structure or any part of it, including supports and foundations” is relevant. This limit state is abbreviated with *STR* (European Committee for Standardization, 2020a).

Actions

To determine the design values of the actions the selfweight, wind and snow load cases must be combined in a systematic way. According to the Eurocode the following nine load combinations are relevant for the geometric design proposals.

A Self-weight only

$$\sum_{j\geq 1} 1.2 \cdot 1.1 G_{k,j}$$

B Wind load w_1 leading

$$\sum_{j\geq 1} 1.0 \cdot 1.1 G_{k,j} + 1.5 \cdot 1.1 \cdot Q_{k,w1}$$

C Wind load w_2 leading

$$\sum_{j\geq 1} 1.0 \cdot 1.1 G_{k,j} + 1.5 \cdot 1.1 \cdot Q_{k,w2}$$

D Snow load s_1 leading

$$\sum_{j\geq 1} 1.0 \cdot 1.1 G_{k,j} + 1.5 \cdot 1.1 \cdot Q_{k,s1} + 1.5 \cdot 0.3 \cdot 1.1 \cdot Q_{k,w1}$$

E Snow load s_1 leading

$$\sum_{j\geq 1} 1.0 \cdot 1.1 G_{k,j} + 1.5 \cdot 1.1 \cdot Q_{k,s1} + 1.5 \cdot 0.3 \cdot 1.1 \cdot Q_{k,w2}$$

F Snow load s_2 leading

$$\sum_{j\geq 1} 1.0 \cdot 1.1 G_{k,j} + 1.5 \cdot 1.1 \cdot Q_{k,s2} + 1.5 \cdot 0.3 \cdot 1.1 \cdot Q_{k,w1}$$

G Snow load s_2 leading

$$\sum_{j\geq 1} 1.0 \cdot 1.1 G_{k,j} + 1.5 \cdot 1.1 \cdot Q_{k,s2} + 1.5 \cdot 0.3 \cdot 1.1 \cdot Q_{k,w2}$$

H Snow load s_3 leading

$$\sum_{j\geq 1} 1.0 \cdot 1.1 G_{k,j} + 1.5 \cdot 1.1 \cdot Q_{k,s3} + 1.5 \cdot 0.3 \cdot 1.1 \cdot Q_{k,w1}$$

I Snow load s_3 leading

$$\sum_{j\geq 1} 1.0 \cdot 1.1 G_{k,j} + 1.5 \cdot 1.1 \cdot Q_{k,s3} + 1.5 \cdot 0.3 \cdot 1.1 \cdot Q_{k,w2}$$

The basic equations behind these load combinations are equations (6.10a) and (6.10b) in EN 1990.

$$\sum_{j\geq 1} \gamma_{G,j} G_{k,j}" + "\gamma_P P" + "\gamma_{Q,1}\psi_{0,1} Q_{k,1}" + "\sum_{i>1} \gamma_{Q,i}\psi_{0,i} Q_{k,i}$$

$$\sum_{j\geq 1} \xi_j \gamma_{G,j} G_{k,j}" + "\gamma_P P" + "\gamma_{Q,1} Q_{k,1}" + "\sum_{i>1} \gamma_{Q,i}\psi_{0,i} Q_{k,i}$$

The Danish NA (table A.1.2(B+C)) determines the partial factors γ as listed in table C.4 and the combination factors Ψ as listed in table C.5 (Danish Standards Foundation, 2013a). The factor $K_{Fi} = 1.1$ corresponds to consequence class 3, which was specified in section 6.1.

Table C.4: Governing Load Combinations with Safety Factors γ

Load Combination	1	2
Reference formula	(6.10a)	(6.10b)
Permanent action, unfavourable: $\gamma_{G;sup} K_{FI}$	$1.2 K_{FI}$	$1.0 K_{FI}$
Permanent action, favourable: $\gamma_{G;inf}$	1.0	0.9
Variable action, leading, unfavourable: $\gamma_{Q,1} K_{FI}$	0	$1.5 K_{FI}$
Variable action, other, unfavourable: $\gamma_{Q,i} K_{FI}$	0	$1.5 \psi_0 K_{FI}$

Table C.5: Combination Factors Ψ according to Danish NA

	ψ_0	ψ_1	ψ_2
Snow load, combination with leading wind load	0.0	0.0	0.0
Snow load, otherwise	0.3	0.2	0.0
Wind load	0.3	0.2	0.0

Load combination A is derived from the second column of table C.4. Load combinations B - I are derived from the thrid column of the same table.

The structural analysis software that is used for evaluating the internal forces does not have a built in functionality to combine load cases. The load combinations and the factors for the load cases remain the same for all geometries, only the contributions of the loads change. Hence, from a perspective of programming, it is deemed as an efficient approach to assign the partial and combination factors to the loads prior to the analysis, so that the internal forces that are obtained from the computation are design values that can be used for strength and stability verifications without further manipulation.

The internal forces are obtained by applying the load combinations to the finite element model. The following figures evaluate the internal forces of the geometric design proposal S9V2 for load combination B.

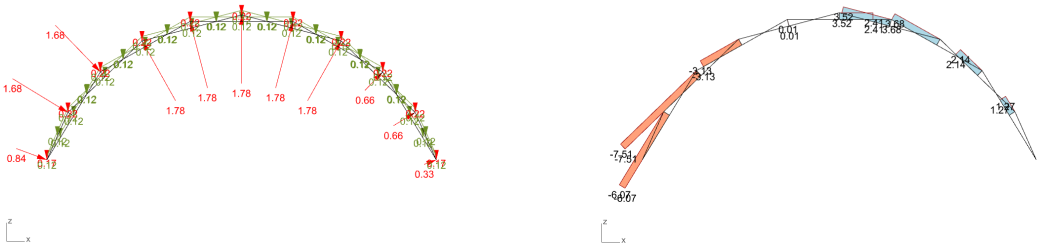

(a) Design Values of Loads for Load Combination B

(b) Normal Forces in the Eccentricity Elements [kN]

Figure C.21: Load Combination B

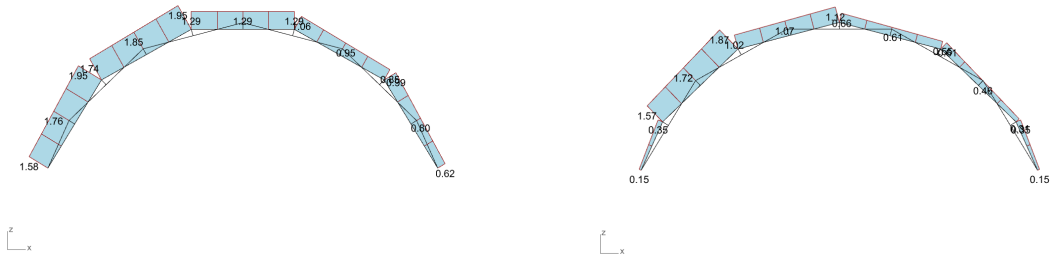

(a) Main Arch

(b) Auxiliary Arch

Figure C.22: Normal forces in the interwoven Arches for Load Combination B [kN]

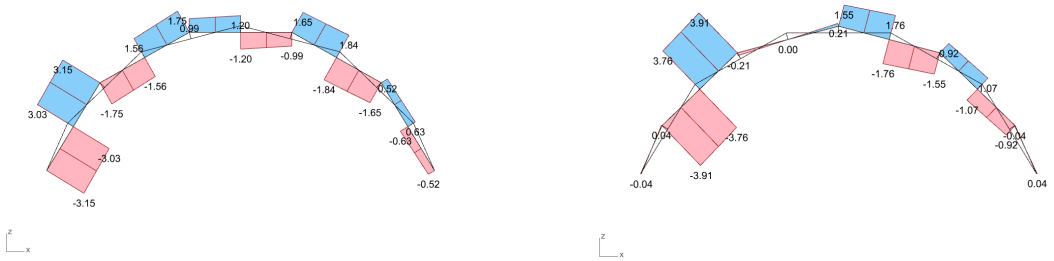

(a) Main Arch

(b) Auxiliary Arch

Figure C.23: Shear Forces in the interwoven Arches for Load Combination B [kN]

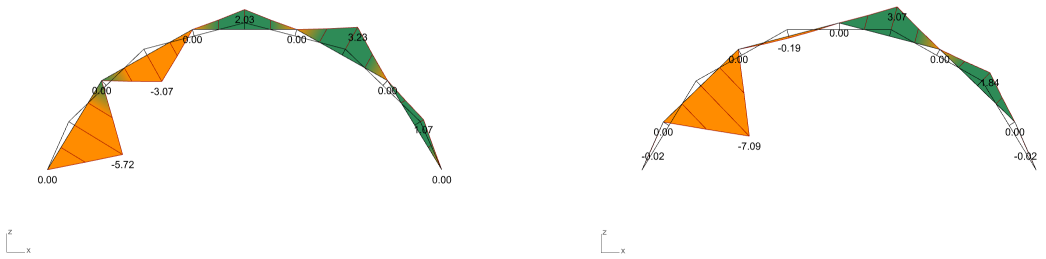

(a) Main Arch **(b)** Auxiliary Arch

Figure C.24: Moments in the interwoven Arches for Load Combination B [kNm]

Material Resistance

The material resistance is computed according to EN 1995 (European Committee for Standardization, 2020d). The design value of the strength parameter X_d depends on the characteristic value of the strength parameter X_k as well as the modification factor k_{mod} and the material factor γ_M.

$$X_d = k_{mod} \frac{X_k}{\gamma_M}$$

The Danish NA specifies a partial material factor of $\gamma_M = 1.35$ for solid timber (Danish Standards Foundation, 2013b). The k_{mod} is chosen in correspondence with the load case that has the shortest duration class in the load combination that the action which the resistance is compared with results from. For load combination A it holds that $k_{mod} = 0.6$. For all other load combinations it holds that $k_{mod} = 1.1$, because the wind load, which the referenced Danish NA specifies as instantaneous action, is present.

The characteristic tension and bending strength are increased by the size factor according to EN1995 3.2, if the cross-sectional width and the cross-sectional height respectively are smaller than 150 mm.

The strength parameters are computed per RT stack for every load combination. This is required in order to assign the k_{mod} factors specific for the load combination and a potential increase of the strength parameter due to the size factor. For illustration, the strength values of S9V2 with load combination B and a strength grade of C18 are determined.

$$f_{v,d} = k_{mod,B} \cdot \frac{f_{v,k}}{\gamma_m} = 1.1 \cdot \frac{3.4 \frac{N}{mm^2}}{1.35} = 2.77 \frac{N}{mm^2}$$
$$f_{c,d} = k_{mod,B} \cdot \frac{f_{c,k}}{\gamma_m} = 1.1 \cdot \frac{18 \frac{N}{mm^2}}{1.35} = 14.67 \frac{N}{mm^2}$$
$$f_{t,d} = k_{mod,B} \cdot \frac{f_{t,k}}{\gamma_m} = 1.1 \cdot \frac{1.01 \cdot 10 \frac{N}{mm^2}}{1.35} = 8.15 \frac{N}{mm^2}$$
$$f_{m,d} = k_{mod,B} \cdot \frac{f_{m,k}}{\gamma_m} = 1.1 \cdot \frac{18 \frac{N}{mm^2}}{1.35} = 14.67 \frac{N}{mm^2}$$

C.4.2. Strength Verifications

Two expressions are required to be satisfied to verify that the stresses, which act in the structural members, do not exceed the strength of the material.

The first expression requires that the shear stress is lower than the shear strength.

$$\tau_d \leq f_{v,d}$$

The shear stress is computed from the shear force V_z and the cross-sectional dimensions. The width b is reduced to an effective width by the cracking factor k_{cr}. The Danish NA specifies $k_{cr} = 1.0$ (Danish Standards Foundation, 2013b).

$$\tau_{d,max,rectangular} = \frac{3 \cdot V_z}{2 \cdot h \cdot b_{ef}}$$
$$b_{ef} = k_{cr} \cdot b$$

For S9V2 the maximum shear force $V_{z,max} = 3.91$ kN is present in one of the longitudinal members that connects to position J3, compare figure C.23. The comparison of the stress and strength leads to a safe unity check.

$$\frac{\tau_{d,max}}{f_{v,d}} = \frac{0.209}{2.77} = 0.08 \leq 1.0$$

The second expression addresses the normal stress that results from bending and axial action. It is distinguished between a tension and a compression force.

$$\frac{\sigma_{t,0,d}}{f_{t,0,d}} + \frac{\sigma_{m,y,d}}{f_{m,y,d}} \leq 1$$
$$\left(\frac{\sigma_{c,0,d}}{f_{c,0,d}}\right)^2 + \frac{\sigma_{m,y,d}}{f_{m,y,d}} \leq 1$$

Four steps are programmed to identify which geometric design proposals are safe regarding the two expressions above. First, the internal forces from the first-order analysis are retrieved at the critical cross-sections for every load combination and for every longitudinal element. An exception are the side members, they are not considered in the strength verifications. This is on the safe side, because shear forces and bending moments are lower than in other members and normal forces are of the same magnitude as in neighboring elements. The transverse beams which are represented by the eccentricity lines are assessed in the context of the joint design in chapter 10. The critical cross-sections, i.e. the cross-sections in which the internal forces reach their maxima, can be identified with help of the investigation of the structural behavior in section 9.3.1. The bending moment has its largest value at $x = \frac{L}{2}$. Since the stress related to the normal force and the bending moment are added up and the change of normal force is insignificant, the normal force is also retrieved at $x = \frac{L}{2}$. The shear force is considered at the position of the support $x = 0$ and at $x = \frac{L}{2}$.

Second, the stress components in the expressions are computed. The formulation of the shear stress was already provided above. The normal stress is computed according to the following formulas.

$$\sigma_{c,0,d} = \frac{N}{A}$$
$$\sigma_{m,y,d} = |\frac{M_y}{\frac{b \cdot h^2}{6}}|$$

Third, the strength verification for combined bending and normal stress is evaluated for every load combination and every member. Fourth, the load combination and element that yield the largest value for an action are identified. Because, the structure is composed of members with identical cross-section, it is sufficient to verify the element with the largest utilitzation. Conversely, if the element with the largest value for a strength verification has a value of smaller than one, then the structure is safe with regards to that action. To identify the desired member, first for each load combination the elements are ordered by their value of utilization. Second, the load combinations are ordered by the element with the highest utilization. To evaluate the safety of a geometry with regards to an expression, only one value is outputted. This approach implies, that for different expressions different load combinations, always the most critical, are considered for the safety verification.

For S9V2 the governing position to verify combined bending and axial force is in the same member as the maximum shear force. The values of the bending moment and the normal force are retrieved at mid span $N_{d,max} = 1.72kN$ and $M_{d,max} = -7.09kNm$, compare figures C.22 and C.24. The comparison of the stress and strength leads to a safe unity check.

$$\frac{\sigma_{t,0,d}}{f_{t,0,d}} + \frac{\sigma_{m,y,d}}{f_{m,y,d}} = \frac{0.06}{8.15} + \frac{7.60}{14.67} = 0.53 \leq 1$$

Stability Verifications

Lateral buckling and lateral torsional buckling are assessed for each structural member. For stability calculations the characteristic elastic modulus $E_{m,0,k}$ is applied.

The expression that needs to be satisfied to ensure that no lateral buckling occurs in a structural member is as follows.

$$\frac{\sigma_{c,0,d}}{k_{c,z} \cdot f_{c,0,d}} + \frac{\sigma_{m,y,d}}{f_{m,y,d}} \leq 1$$

Only buckling around the weak axis is considered. The buckling factor $k_{c,z}$ is determined in dependence of the relative slenderness ratio $\lambda_{rel,z}$ and the factor k_z.

$$k_{c,z} = \frac{1}{k_z + \sqrt{k_z^2 - \lambda_{rel,z}^2}}$$
$$\lambda_{rel,z} = \frac{\lambda_z}{\pi}\sqrt{\frac{f_{c,0,k}}{E_{m,0,k}}}$$
$$k_z = 0.5(1 + \beta_c(\lambda_{rel,z} - 0.3) + \lambda_{rel,z}^2)$$

The factor β_c reflects the straightness limits of the material, for solid timber $\beta_c = 0.2$. The slenderness λ_z is defined as the ratio between the buckling length l_{ef} and the radius of gyration i_z. The buckling length is the product of the member length l and the effective length factor β. The effective length factor is dependent on the boundary conditions of the considered structural member. All longitudinal members of the PRFA are simply supported beams, thus it holds that $\beta = 1.0$ which corresponds to the second Euler case. The radius of gyration is dependent on the cross-section A and the second moment of inertia I_z.

$$\lambda_z = \frac{l_{ef}}{i_z}$$
$$l_{ef} = \beta \cdot l$$
$$i_z = \sqrt{\frac{I_z}{A}}$$

For S9V2 the governing internal forces for the stability verifications are in the same longitudinal element as for the strength verification. However, the governing load combination is load combination G. The critical normal force is $N_{d,stab} = -4.34kN$ and the critical moment is $M_{d,stab} = 3.93kNm$. The buckling factor is determined to be $k_{c,z} = 0.38$ with $k_z = 1.76$ and $\lambda_{rel,z} = 1.51$. This leads to a safe unity check.

$$\frac{\sigma_{c,0,d}}{k_{c,z} \cdot f_{c,0,d}} + \frac{\sigma_{m,y,d}}{f_{m,y,d}} = \frac{|-0.16|}{0.38 \cdot 14.67} + \frac{4.21}{14.67} = 0.32 \leq 1$$

The expression that needs to be satisfied to ensure that no lateral torsional buckling occurs in a structural member is as follows:

$$\left(\frac{\sigma_{m,y,d}}{k_{crit} \cdot f_{m,y,d}}\right)^2 + \frac{\sigma_{c,0,d}}{k_{c,z} \cdot f_{c,0,d}} \leq 1$$

The factor k_{crit} is dependent on the relative slenderness for bending, which is a function of the characteristic bending strength $f_{m,k}$ and the critical bending stress $\sigma_{m,crit}$.

$$k_{crit} = \begin{cases} 1 & \lambda_{rel,m} \leq 0.75 \\ 1.56 - 0.75\lambda_{rel,m} & 0.75 < \lambda_{rel,m} \leq 1.4 \\ \dfrac{1}{\lambda_{rel,m}^2} & 1.4 < \lambda_{rel,m} \end{cases}$$

$$\lambda_{rel,m} = \sqrt{\frac{f_{m,k}}{\sigma_{m,crit}}}$$

The critical bending stress can be determined in a simplified way, for the present case, for solid rectangular cross-sections are considered.

$$\sigma_{m,crit} = \frac{0,78 \cdot b^2}{h \cdot l_{ef}} E_{m,0,k}$$

The effective length l_{ef} is defined as 80% of the member length for the case that a simply supported beam has a concentrated force at midspan and as 90% for a uniformly distributed load respectively. Both types of forces are acting on the members of the PRFA, as the concentrated force is governing and as the corresponding effective length leads to a lower reduction factor, the effective length is set to $l_{ef} = 0.8\,L$ for all members.

For S9V2 the critical factor is determined as $k_{crit} = 1.0$ with $\sigma_{m,crit} = 173\,\frac{\mathrm{N}}{\mathrm{mm}^2}$ and $\lambda_{rel,m} = 0.32$. This leads to a safe unity check.

$$\left(\frac{\sigma_{m,y,d}}{k_{crit} \cdot f_{m,y,d}}\right)^2 + \frac{\sigma_{c,0,d}}{k_{c,z} \cdot f_{c,0,d}} = \left(\frac{4.21}{1.0 \cdot 14.67}\right)^2 + \frac{|-0.16|}{0.38 \cdot 14.67} = 0.11 \leq 1$$

The buckling factor $k_{c,z}$ and the critical factor k_{crit} are computed only once for a geometric design proposal. The reference length of the longitudinal members is considered. The side members are not verified separately, because if the regular longitudinal members are safe, the safety of the side members is ensured as well. The stresses that were used for the strength verifications, namely bending stress and axial stress at midspan, are used as base for the verifications. Only the elements with a compressive axial force are considered for the stability phenomena. The output of the verifications is the result of the two expressions for the member and load combination that generates the largest value. The procedure to determine these values is identical with the one applied for the strength verifications.

Besides assessing the stability for each member, the stability of the arch is assessed globally by computing the buckling factor of the structure. It is expected that the global stability is not an issue due to the transverse beams that act as lateral supports for the arch. Thus the buckling factor is not considered in the safety analysis. Only in the second step, it will be ensured by evaluating the buckling factor that the global stability indeed does not lead to failure of the structure.

C.4.3. Serviceability Limit State

Actions

To determine the values for the deflections that are considered in the SLS, a set of eight load combinations that are different to those in the ULS is generated.

1. Wind load $w1$ leading
$$\sum_{j \geq 1} G_{k,j} + Q_{k,w1}$$
2. Wind load $w2$ leading
$$\sum_{j \geq 1} G_{k,j} + Q_{k,w2}$$
3. Snow load $s1$ leading
$$\sum_{j \geq 1} G_{k,j} + Q_{k,s1} + 0.3Q_{k,w1}$$
4. Snow load $s1$ leading
$$\sum_{j \geq 1} G_{k,j} + Q_{k,s1} + 0.3Q_{k,w2}$$

5. Snow load $s2$ leading
$$\sum_{j\geq 1} G_{k,j} + Q_{k,s2} + 0.3Q_{k,w1}$$
6. Snow load $s2$ leading
$$\sum_{j\geq 1} G_{k,j} + Q_{k,s2} + 0.3Q_{k,w2}$$
7. Snow load $s3$ leading
$$\sum_{j\geq 1} G_{k,j} + Q_{k,s3} + 0.3Q_{k,w1}$$
8. Snow load $s3$ leading
$$\sum_{j\geq 1} G_{k,j} + Q_{k,s3} + 0.3Q_{k,w2}$$

The basic equation behind these load combinations is equation (6.14b) from the Eurocode, which is detailed further in the code's table A1.4 (European Committee for Standardization, 2020a).

$$\sum_{j\geq 1} G_{k,j} \text{ "+"P"+" } Q_{\text{k},1} \text{ "+" } \sum_{i>1} \psi_{0,\text{i}} Q_{\text{k,i}}$$

Limiting criteria

The motivation for limiting the deflection of a building's structure is to ensure that its functionality is not affected and that the comfort of the people is not disturbed visually. The Eurocode does not prescribe a binding numeric limit for deflections, instead it instructs parties involved in the building process to agree on limit criteria that related to the intended functions (European Committee for Standardization, 2020a).

For the shape of the arch, no references for deflection limit criteria were identified. The EN 1995 and the corresponding Danish NA suggest deflection limits for simple beams in relation to their span (Danish Standards Foundation, 2013b; European Committee for Standardization, 2020d). These values are adapted to arches by substituting the reference length to the approximate length of the line between the zero values of the moment functions. This means, for load combinations with a governing wind load or with the snow load s_2 or s_3 governing and with $x_{arc} = \frac{L_{arc}}{4}, \frac{3 \cdot L_{arc}}{4}$ being the point at which the deflection is assessed the diagonal that connects the center of the arch with a support point is the reference length. For the load combinations with self-weight and leading snow load s_1 with $x_{arc} = \frac{L_{arc}}{2}$ being the point at which the deflection is assessed the distance between the supports is governing respectively. The reference lengths and the points at which the deflections are assessed are illustrated in figure C.25. Table C.6 displays the adapted limit criteria for different load cases, both instantaneous w_{inst} and final deflections w_{fin} are considered.

Table C.6: SLS Limit Criteria

	w_{inst}	w_{fin}
limiting values EN 1995	$\frac{L}{300}$ to $\frac{L}{500}$	$\frac{L}{150}$ to $\frac{L}{300}$
self weight (DK NA)		L/400
characteristic snow loads (DK NA)	L/400	
characteristic wind action (DK NA)	L/250	

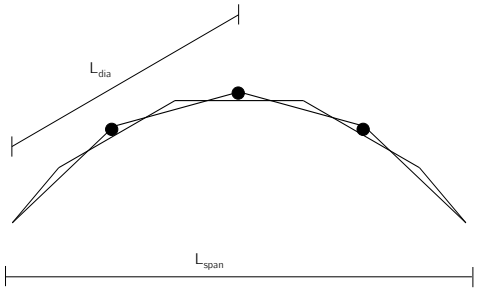

Figure C.25: Reference Lengths for SLS Limit Criteria

Computing the deformation

The first step in computing the deformations is to determine the characteristic instantaneous deflections for every load case separately. The deflections are computed at the three nodes that were selected in the previous section. On the basis of these deflections, the required values are computed. To retrieve the total instantaneous deflection, the characteristic deflections are added according to the load combinations in section C.4.3.1. To compute the total final deflection, the following formula is applied:

$$w_{fin} = w_{fin,G} + w_{fin,Q,1} + w_{fin,Q,i}$$

The order of the variable actions is determined by the load combinations. The final deflections per load case are computed in the following manner:

$$w_{fin,G} = w_{inst,G}(1 + k_{def}) w_{fin,Q,1} = w_{inst,Q,1}(1 + \psi_{2,1} k_{def}) w_{fin,Q,i} = w_{inst,Q,1}(\psi_{0,i} + \psi_{2,i} k_{def})$$

For the computation of the final deflection due to self weight, the formula, to compute $w_{fin,G}$ suffices. For the computation of the instantaneous deflection due to characteristic snow and wind load, the values from the first step are sufficient. The final step is to compare the deflections with the limit criteria.

C.5. Geometric Design Proposal Assessment Plots

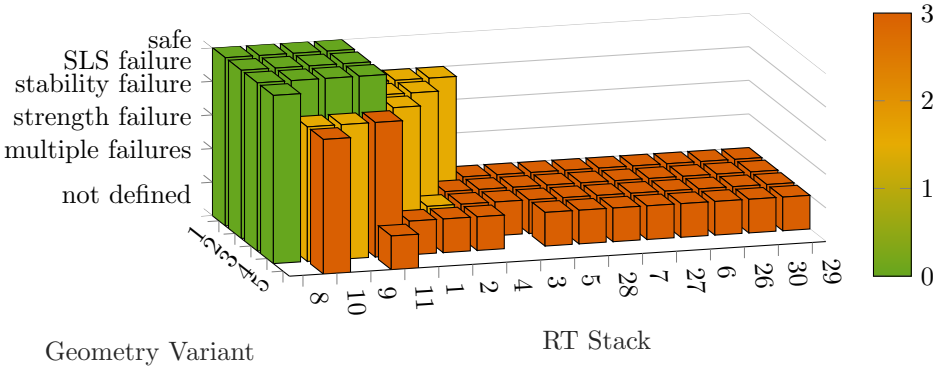

Figure C.26: UC R1a

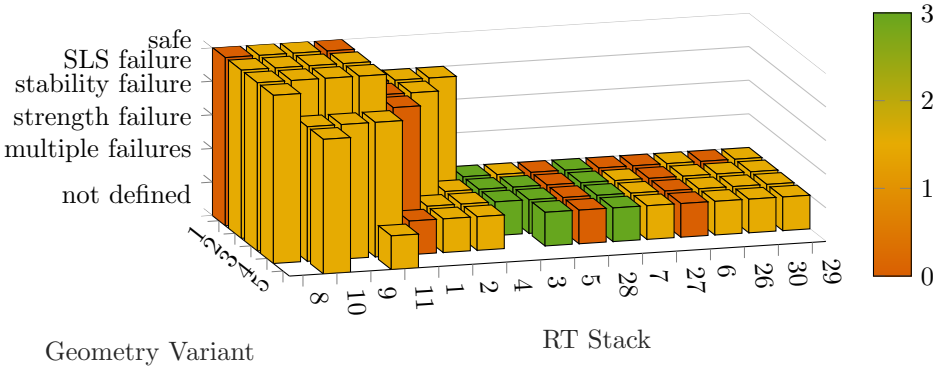

Figure C.27: ec/h Ratio R1a

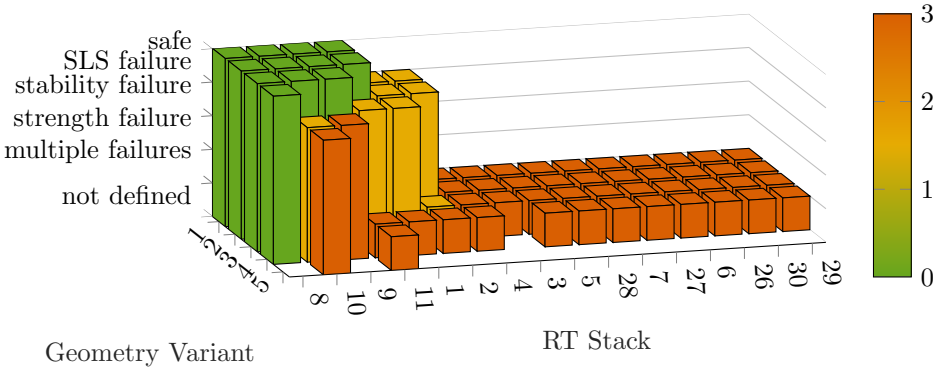

Figure C.28: UC R1b

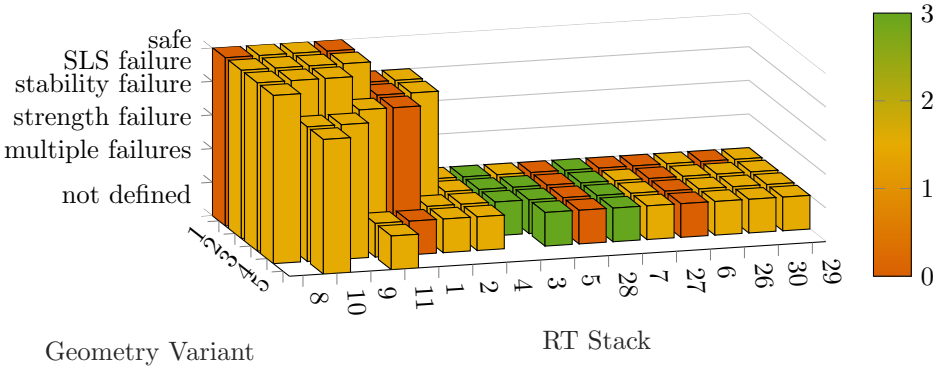

Figure C.29: ec/h Ratio R1b

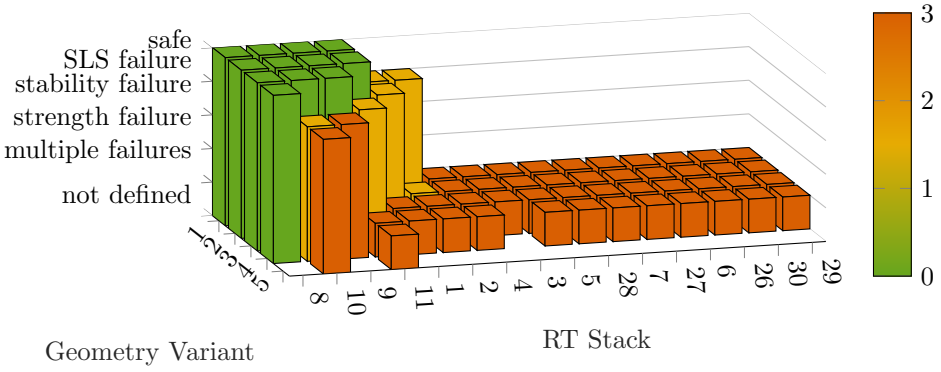

Figure C.30: UC R2

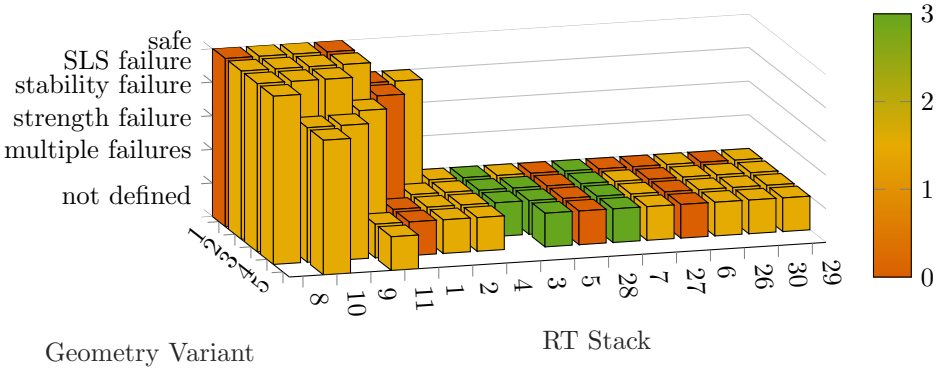

Figure C.31: ec/h Ratio R2

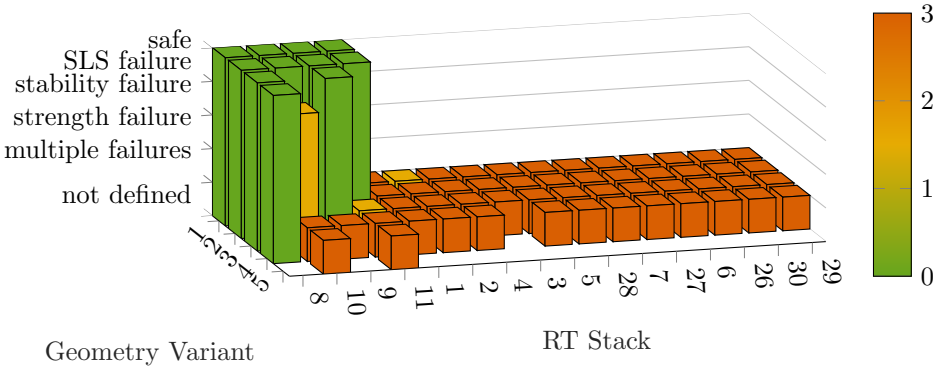

Figure C.32: UC R3b

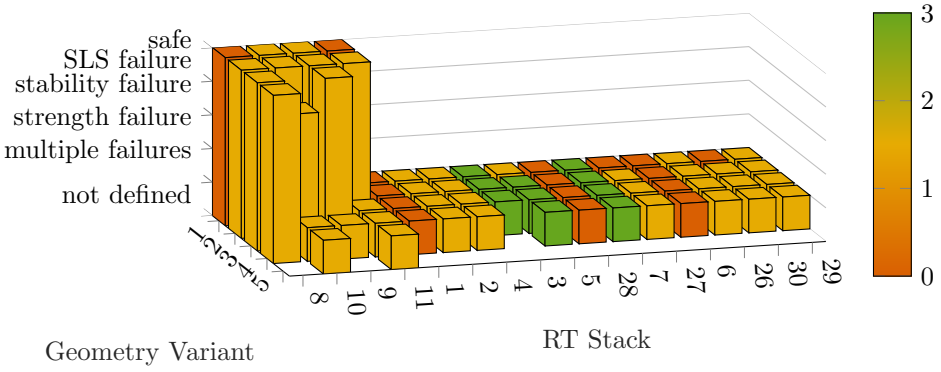

Figure C.33: ec/h Ratio R3b

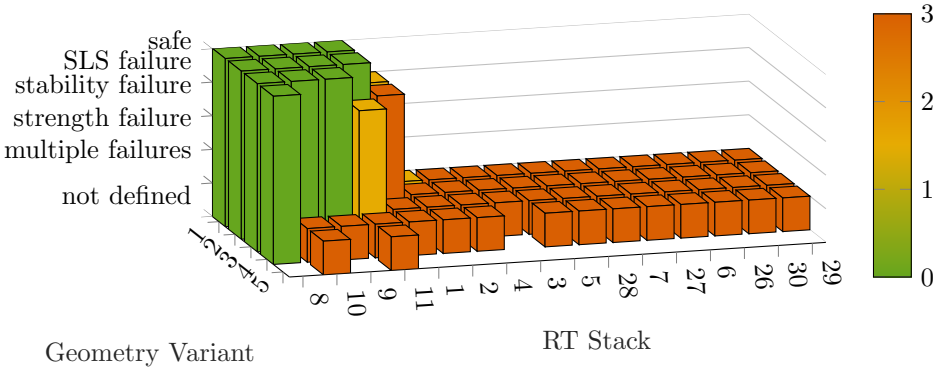

Figure C.34: UC R4

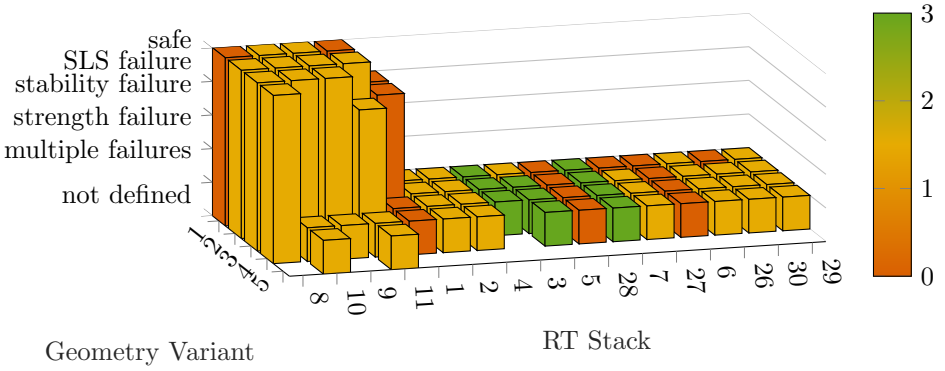

Figure C.35: ec/h Ratio R4

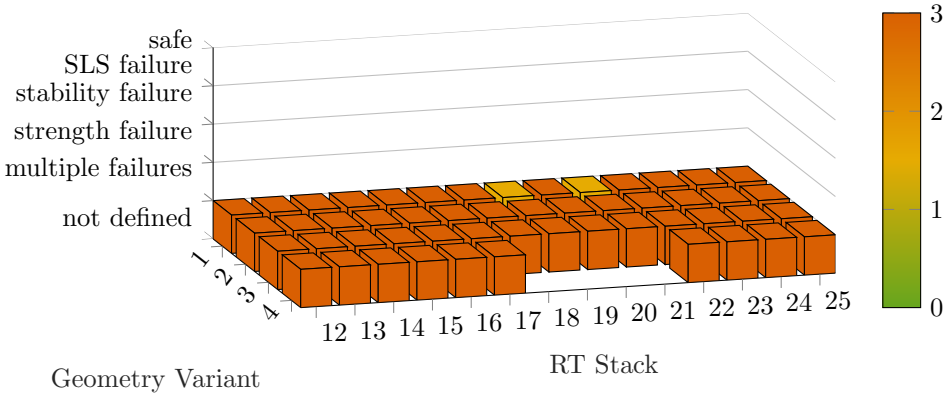

Figure C.36: UC AM

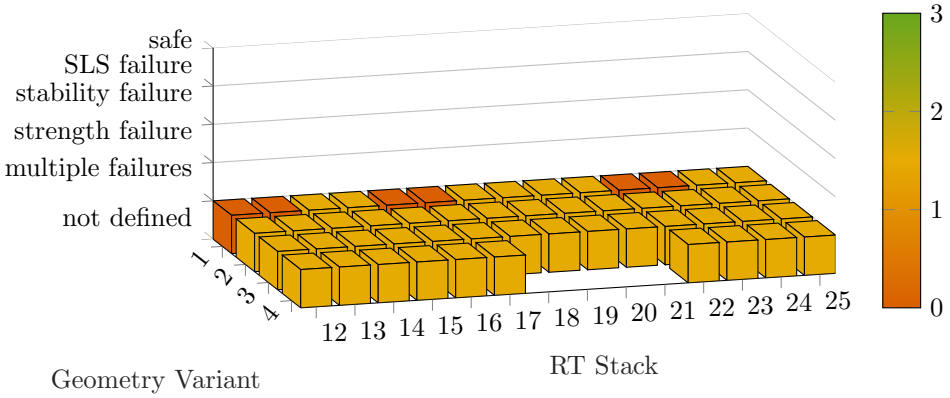

Figure C.37: ec/h Ratio AM

C.6. Detailing of the PRFA Joint

Connection I

01 Description

This connection joins the transverse beam, the timber block and the longitudinal beam at midspan. Compression is transferred via contact. To transfer tension forces screws are inserted.

02 Geometry and Material

Part to be connected	Profile [mm x mm]	Material
Transverse beam (TB)	bxh = 140 x 200	C18
Timber block (BL)	bxh = 140 x 19.7	C18
Longitudinal beam (LB)	bxh = 140 x 200	C18

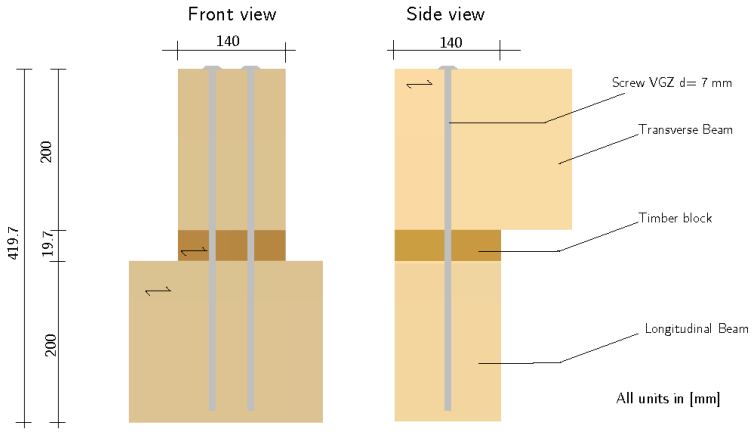

03 System Parameters

All governing internal forces were taken from a load combination that contains a wind load case. According to the Danish Standards Foundation, this implies the following kmod-factor (2013):

$$k_{mod} := 1.1$$

The material factor is (European Committee for Standardization, 2020):

$$\gamma_m := 1.35$$

04 Cross Section Parameters

$f_{c.90.k} := 2.2 \ \frac{N}{mm^2}$

$h_{TB} := 200 \ mm$ $b_{TB} := 140 \ mm$

$A_c := 140 \ mm \cdot 140 \ mm = (1.96 \cdot 10^4) \ mm^2$ $h_{BL} := 19.7 \ mm$ $b_{BL} := 140 \ mm$

$h_{LB} := 200 \ mm$ $b_{LB} := 140 \ mm$

$\rho_k := 320 \ \frac{kg}{m^3}$

05 Screw Parameters

Screw VGZ (Rothoblaas, 2022; ETA Danmark, 2022):

$d := 7 \ mm$ $L_{screw} := 380 \ mm$

$f_{tens.k} := 15.4 \ kN$ $f_{ax.k} := 15 \ \frac{N}{mm^2}$ $f_{head.k} := 10.5 \ \frac{N}{mm^2}$

06 Structural Analysis

The maximum forces in the eccentricity element are extracted from the structural analysis

$N_{c.max.d} := 7.24 \ kN$ $N_{t.max.d} := 4.35 \ kN$

Hence, the maximum stress in the eccentricity element is

$\sigma_{c.90.d} := \frac{N_{c.max.d}}{A_c} = 0.369 \ \frac{N}{mm^2}$

07 Compression perpendicular to the Grain

The verification is conducted according to EN 1995 6.1.5 (European Committee for Standardization, 2020):

A. Contact Surface Transverse Beam - Timber Block

1. The factor taking into account the load configuration, possibility of splitting and degree of compressive deformation is determined to be

$k_{c.90.1} := 1.0$

The reason is that the timber block does not extend the width of the contact surface, thus none of the member arrangements specificied in the corresponding Eurocode section apply. If an increase in strength was required the timber block could be extended in direction of the longitudinal beam below.

2.The resulting compressive strength equals to:

$$f_{c.90.d} := k_{mod} \cdot \frac{f_{c.90.k}}{\gamma_m} = 1.793 \ \frac{N}{mm^2}$$

3. Unity Check:

$$\frac{\sigma_{c.90.d}}{k_{c.90.1} \cdot f_{c.90.d}} = 0.206 \quad < \quad 1 \quad \text{OK.}$$

B. Contact Surface Timber Block - Longitudinal Beam Below

1. For simplicity the value for the strength factor is also taken as 1.0 (this is on the conservative side).

$$k_{c.90.2} := 1.0$$

2. The resulting compressive strength has the same value as computed above.

3. Unity Check:

$$\frac{\sigma_{c.90.d}}{k_{c.90.2} \cdot f_{c.90.d}} = 0.206 \quad < \quad 1 \quad \text{OK.}$$

The unity checks for compression perpendicular to the grain are not critical, even though they were conducted conservatively considering the membrance effects. If the membrane effect was accounted for, an even lower unity check would be obtained.

08 Axially loaded Screws

The verification is conducted according to EN 1995 8.7.2 (European Committee for Standardization, 2020):

1. The following failure modes are to be verified:
   a) Withdrawal Capacity of the threaded Part
   b) Tear off Capacity of the Screwhead
   c) Pull through Strength of the Screwhead
   d) Tension Strength of the Screw
   e) Failure along the Circumference of a Group of Screws

2. Because no steel plate is used for the connection, failure modes b) and e) are not relevant and do not need to be verified.

3. Choice of the screw:
Only a low tension force is present. A small cross section area motivates the choice for a small screw diameter. Small screw diameters have limited screw length. The VGZ from Rothoblass offers a good compromise in diameter and length. The following dimensions are chosen.

$$d = 7 \ mm \qquad L_{screw} = 380 \ mm$$

A washer is used in combination with the screw to increase pull through resistance. A countersunk head is chosen, to accomodate the washer.

4. Minimum spacing requirements

Assumption: Use two screws, because it is required to have more than one for safety. Since a low force is acting, it is expected that no more than two screws are needed.

$a_1 := 5 \cdot d = 35\ mm$
$a_2 := 5 \cdot d = 35\ mm$
$a_{1.CG} := 10 \cdot d = 70\ mm$
$a_{2.CG} := 4 \cdot d = 28\ mm$

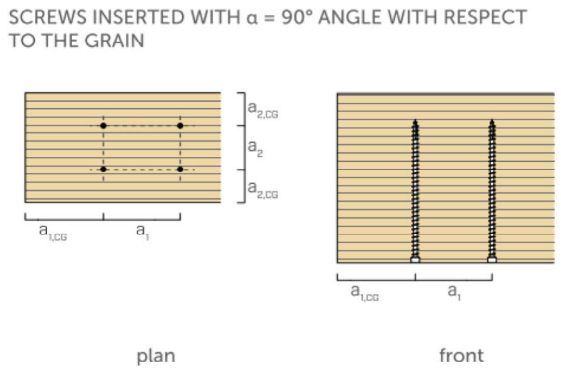

Graphic obtained from Rothoblass (2022)

5. Selected spacing

$a_2 := 50\ mm$
$a_{1.CG} := 70\ mm$
$a_{2.CG} := 40\ mm$

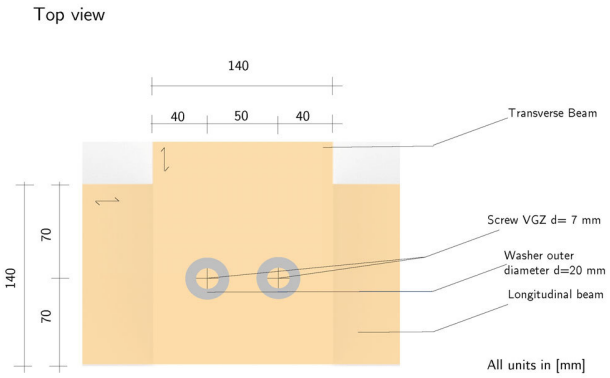

6. Compute Strength of Failure Modes

a) Withdrawal Capacity

Parameters (compare Eurocode for parameter description):

$n := 2 \qquad n_{ef} := n^{0.9} = 1.866$

$l := h_{TB} + h_{BL} + h_{LB} = 419.7\ mm$

$L_{LB.screw} := L_{screw} - \left(h_{TB} + h_{BL}\right) = 0.16\ m \qquad l_{ef} := L_{LB.screw} - d = 0.153\ m$

The effective length is the length of the threaded part in the beam on the point side.

$$\alpha := 90\ ° \qquad f_{ax.\alpha.k} := \frac{f_{ax.k}}{(\sin(\alpha))^2 + 1.5 \cdot (\cos(\alpha))^2} = 15\ \frac{N}{mm^2}$$

$$aux_1 := 1\ mm^{-2} \qquad aux_2 := 1\ mm^2$$

$$F_{ax.\alpha.Rk.1} := n_{ef} \cdot \left(\pi \cdot d \cdot l_{ef} \cdot aux_1\right)^{0.8} \cdot f_{ax.\alpha.k} \cdot aux_2 = 18.589\ kN$$

c) Pull through Strength of the Screw Head
Parameters (compare Eurocode for parameter description):

$$d_h := 20\ mm \qquad \rho_a := 350\ \frac{kg}{m^3}$$

These values above are taken from ETA Danmark (2022).

$$F_{ax.\alpha.Rk.2} := n_{ef} \cdot f_{head.k} \cdot {d_h}^2 \cdot \left(\frac{\rho_k}{\rho_a}\right)^{0.8} = 7.295\ kN$$

d) Tension Strength of the Screw

The strength is computed according to ETA Danmark (pg. 10, 2022).

$$F_{tens.k} := 2 \cdot f_{tens.k} = 30.8\ kN$$

7. Overview of the strength values. The lowest strength value is governing.

$$F_{ax.\alpha.Rk.1} = 18.589\ kN$$

$$F_{ax.\alpha.Rk.2} = 7.295\ kN$$

$$F_{tens.k} = 30.8\ kN$$

8. Design Strength

$$F_{ax.\alpha.Rk} := F_{ax.\alpha.Rk.2}$$

$$F_{ax.\alpha.Rd} := k_{mod} \cdot \frac{F_{ax.\alpha.Rk}}{\gamma_m} = 5.944\ kN$$

9. Unity Check

$$\frac{N_{t.max.d}}{F_{ax.\alpha.Rd}} = 0.732$$

References

Danish Standards Foundation. (2013). DS/EN 1995-1-1 DK NA:2014 National. 1–10.

European Committee for Standardization. (2020). NEN-EN 1995-1-1. 1.

ETA-Danmark. (2022). European Technical Assessment ETA-11/0030. In Https://Medium.Com/. https://medium.com/@arifwicaksanaa/pengertian-use-case-a7e576e1b6bf

Rothoblaas. (2022). VGZ Full threaded screw with cylindrical head. https://www.rothoblaas.com/products/fastening/screws/screws-structures/vgz

Connection II-A

01 Description

Connection II joins the end of a longitudinal beam with a side of the transverse beam. The focus of Connection II-A is on the design of the steel plate that is slotted into the longitudinal beam.

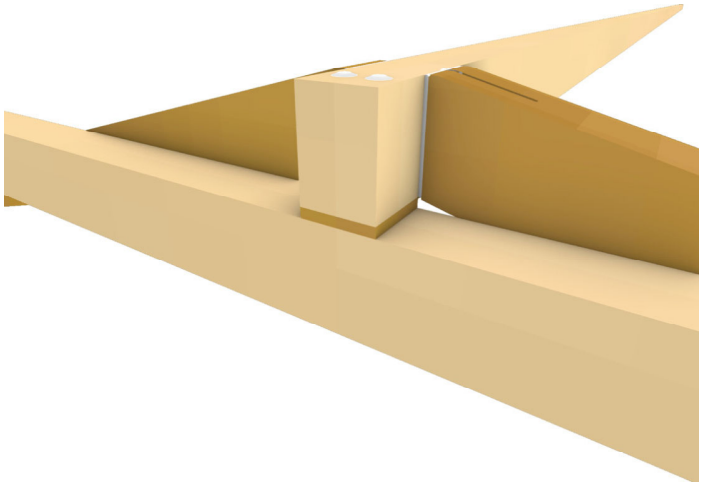

The joint is symmetrical, therefore it suffices to design only one side of the joint. The connection is achieved by a hidden joist hanger. The longitudinal member is slotted at the ends parallel to the grain so that a steel plate can be inserted centrally. Timber and steel are joined through adding dowels and a bolt into predrilled holes. The steelplate is welded to another steel plate which is fastened to the side of the transverse beam by a number of screws. The screws in the transverse beam are considered in Connection II-B.

02 Geometry and Material

Part to be connected	Profile	Material
Longitudinal beam (LB)	bxh = 140 mm x 200 mm	C18
Transverse beam (TB)	bxh =140 mm x 200 mm	C18
Steel plate	t = 7 mm	S235

03 System Parameters

All governing internal forces were taken from a load combination that contains a wind load case. According to the Danish Standards Foundation, this implies the following kmod-factor (2013):

$$k_{mod} := 1.1$$

The material factor is (European Committee for Standardization, 2020):

$$\gamma_m := 1.35$$

04 Cross Section Parameters

$f_{c.90.k} := 2.2 \ \frac{N}{mm^2}$ $f_{c.0.k} := 18 \ \frac{N}{mm^2}$

$h_{TB} := 200 \ mm$ $b_{TB} := 140 \ mm$

$A_c := 200 \ mm \cdot 140 \ mm = (2.8 \cdot 10^4) \ mm^2$ $h_{LB} := 200 \ mm$ $b_{LB} := 140 \ mm$

$t := 7 \ mm$

$\rho_k := 320 \ \frac{kg}{m^3}$

05 Dowel & Bolt Parameters

$d_{dowel} := 7 \ mm$

06 Structural Analysis

The joint is designed according to the maximum internal forces that act in all members for all load combinations. This reduces the work of structural design, for one joint detail can be applied to all joints.

$N_{c.max.d} := 7.85 \ kN$ $\alpha := 14.66 \ °$

$N_{t.max.d} := 2.12 \ kN$

$V_{max.d} := 3.79 \ kN$

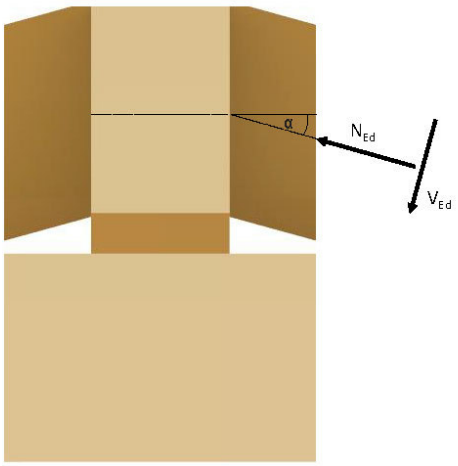

07 Compression under an Angle to the Grain

The verification is conducted according to EN 1995 6.2.2 (European Committee for Standardization, 2020):

1. The factor taking into account the load configuration, possibility of splitting and degree of compressive deformation is determined to be

$$k_{c.90.2} := 1.0$$

This is on the conservative side. Moreover, the steel plate in between the two beams is not taken into account. This is also conservative because the steel plate would distribute the load more uniformly, thus leading to a lower utility.

2.To compute the compressive stress, the compression force on the transverse beam is computed:

$$F_{c.d} := \cos(\alpha) \cdot N_{c.max.d} + \sin(\alpha) \cdot V_{max.d} = 8.554 \ kN$$

3.The compressive stress equals:

$$\sigma_{c.90.d} := \frac{F_{c.d}}{A_c - (h_{LB} \cdot (7 \ mm + 2 \cdot 2 \ mm))} = 0.332 \ \frac{N}{mm^2}$$

4. The compressive strength is computed:

$$f_{c.0.d} := k_{mod} \cdot \frac{f_{c.0.k}}{\gamma_m} = 14.667 \ \frac{N}{mm^2}$$

$$f_{c.90.d} := k_{mod} \cdot \frac{f_{c.90.k}}{\gamma_m} = 1.793 \ \frac{N}{mm^2}$$

$$f_{c.d} := \frac{f_{c.0.d}}{\frac{f_{c.0.d}}{k_{c.90.2} \cdot f_{c.90.d}} \cdot (\sin(\alpha))^2 + (\cos(\alpha))^2} = 10.046 \ \frac{N}{mm^2}$$

4. Unity Check:

$$\frac{\sigma_{c.90.d}}{f_{c.d}} = 0.033 \quad < \quad 1 \quad \text{OK.}$$

The unity check for compression under an angle to the grain is not critical, even though it was conducted conservatively.

08 Steel-to-Timber-Connection

The verification is conducted according to EN 1995 8.2.3 and 8.6 (European Committee for Standardization, 2020):

1. According to the Johanson-model, the following failure modes are to be verified:
   - f) No Plastic Hinge per Shear Plane
   - g) Single Plastic Hinge per Shear Plane
   - h) Two Plastic Hinges per Shear Plane

   For each failure mode the strength is computed. In failure modes g and h plastic hinges develop before failure. This adds ductility to the joint. Thus the connection is designed so that one of these modes is governing.

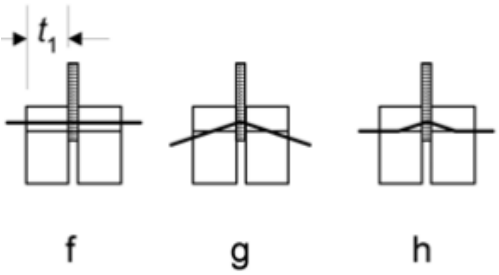

Graphic obtained from European Committee for Standardization (2020)

2. Choose a dowel diameter:
According to the code the size of the dowel must greater than 6 mm and smaller than 30 mm. Due to low forces, a small diameter is selected.

$$d_{dowel} = 7 \ mm$$

Dowels are preferable to bolts because they have less slip. The bolt that is required to hold the connection together is assumed to be of the same diameter. Dowels are prefered over bolts, because bolts have larger slip. Two dowels are used to have a symmetric arrangement

3. Minimum spacing requirements:
Assumption: Use two dowels and one bolt. The connection elements are placed vertically, to reduce the eccentricity of the connection.

i) The angle between grain and resulting force is computed:

$$\alpha := \operatorname{atan}\left(\frac{V_{max.d}}{N_{t.max.d}}\right) = 60.779 \ ° \qquad \alpha_1 := \pi - \alpha = 119.221 \ °$$

ii) The minimum distances for dowels are specified in table 8.5 of the Eurocode (European Committee for Standardization, 2020).

$a_1 := \left(3 + 2 \cdot \left|\cos\left(\alpha_1\right)\right|\right) \cdot d_{dowel} = 27.835\ mm$

$a_2 := 3 \cdot d_{dowel} = 21\ mm$

For edge and end spacings the direction in which the dowel pushes is governing.

Loaded End:

$-\alpha = -60.779\ °$

$a_{3.t} := \max\left(7 \cdot d_{dowel}, 80\ mm\right) = 80\ mm$

Loaded edges (consider both edges as loaded for the direction of the forces can change):

$\alpha = 60.779\ °$

$a_{4.t} := \max\left(\left(2 + 2 \cdot \sin\left(\alpha\right)\right) \cdot d_{dowel}, 3\ d_{dowel}\right) = 26.218\ mm$

iii) Minimum distances for the bolt are specified in table 8.4 of the Eurocode (European Committee for Standardization, 2020).

$a_{2.bolt} := 4 \cdot d_{dowel} = 28\ mm$

$a_{3.t.bolt} := a_{3.t} = 80\ mm$

4. Selected spacing

$a_{2.bolt} := 60\ mm$

$a_{3.t} := 80\ mm$

$a_{4.t} := 40\ mm$

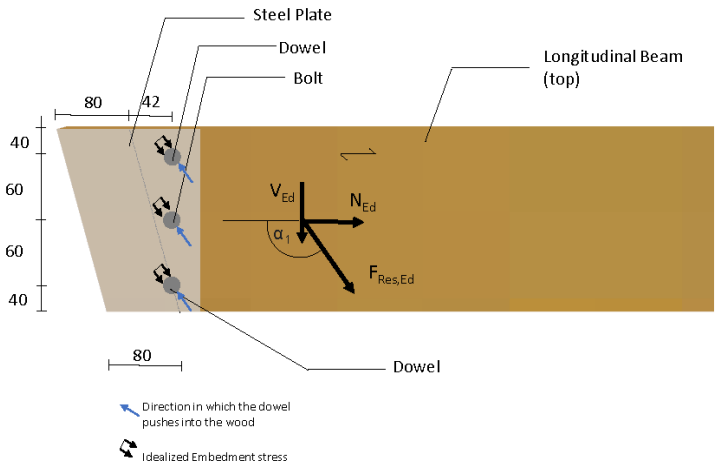

All units in [mm]

5. Resistance of the steel plate as central member of a double shear connection
Assumption: The plate thickness is identical to the dowel diameter.

$d_{plate} := t = 7\ mm$

Assumption: For the thickness of the timber member, it is considered that the steel plate is placed central and 2 mm on each side are left as space to move in the steel plate during construction

$t_1 := \frac{\left(b_{LB} - \left(t + 4\ mm\right)\right)}{2} = 64.5\ mm$

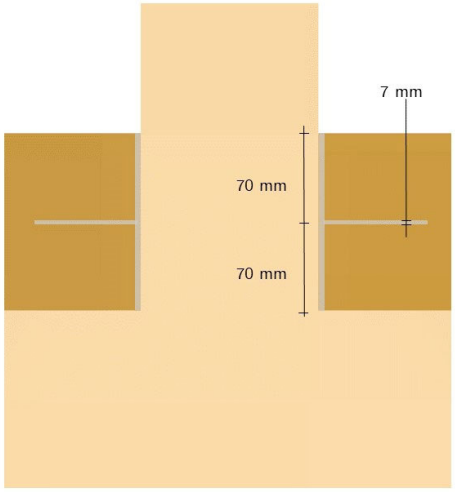

i) The embedment strength is determined according to the European Committee for Standardization, equation 8.32 (2020)

$aux1 := 1\ m^3 \cdot \frac{N}{kg \cdot mm^2}$ $aux2 := 1\ m^3 \cdot \frac{N}{kg \cdot mm^3}$

$f_{h.0.k} := 0.082 \cdot \left(1 \cdot aux1 - 0.01 \cdot d_{dowel} \cdot aux2\right) \cdot \rho_k = 24.403\ \frac{N}{mm^2}$

$\alpha = 60.779\ deg$ $k_{90} := 1.35 + 0.15 = 1.5$

$f_{h.\alpha.k} := \frac{f_{h.0.k}}{k_{90} \cdot \left(\sin\left(\alpha\right)\right)^2 + \left(\cos\left(\alpha\right)\right)^2} = 17.673\ \frac{N}{mm^2}$

$f_{h.1.k} := f_{h.\alpha.k}$

The embedment strength is identical for bolts and dowels.

ii) The resistance of the three characteristic failure modes is determined according to the European Committee for Standardization, section 8.2.3 (2020)

Failure mode f)

$F_{V.Rk.f} := f_{h.1.k} \cdot t_1 \cdot d_{dowel} = 7.979\ kN$

Failure mode g)

Plastic capacity of the dowel, tensile strength for S235:

$$f_{u.k} := 360 \ \frac{N}{mm^2} \qquad aux3 := 1 \ \frac{mm^3}{mm^{2.6}}$$

$$M_{y.Rk} := 0.3 \cdot f_{u.k} \cdot d_{dowel}^{2.6} \cdot aux3 = \left(1.701 \cdot 10^4\right) \ N \cdot mm$$

$$F_{V.Rk.g} := f_{h.1.k} \cdot t_1 \cdot d_{dowel} \cdot \left(\sqrt[2]{2 + 4 \cdot \frac{M_{y.Rk}}{f_{h.1.k} \cdot d_{dowel} \cdot t_1^{\,2}}} - 1 \right) = 3.672 \ kN$$

Failure mode h)

$$F_{V.Rk.h} := 2.3 \cdot \sqrt[2]{M_{y.Rk} \cdot f_{h.1.k} \cdot d_{dowel}} = 3.336 \ kN$$

iii) The governing resistance is the minimum resistance of the three characteristic failure modes. This resistance is multiplied with the number of dowels/bolts and with the number of shear planes per dowel/bolt. The resistance for dowels and bolts is identical. It is a simplification on the safe side that the rope effect is not taken into account for the bolt.

$$F_{V.Rk} := 3 \cdot 2 \cdot min\left(F_{V.Rk.f}, F_{V.Rk.g}, F_{V.Rk.h}\right) = 20.018 \ kN$$

iv) Design Strength

$$F_{V.Rd} := k_{mod} \cdot \frac{F_{V.Rk}}{\gamma_m} = 16.311 \ kN$$

vi) Resulting Force on the Connection

$$F_{res.Ed} := \sqrt[2]{V_{max.d}^{\ 2} + N_{t.max.d}^{\ 2}} = 4.343 \ kN$$

vi) Unity Check

$$\frac{F_{res.Ed}}{F_{V.Rd}} = 0.266 < 1.0 \text{ OK}$$

The unity check identifies that the connection is overly safe. It is not possible to increase efficiency much, because of the minimal dowel diameter and the notion to keep the connection symmetrical.

References

Danish Standards Foundation. (2013). DS/EN 1995-1-1 DK NA:2014 National. 1–10.

European Committee for Standardization. (2020). NEN-EN 1995-1-1. 1.

Connection II-B

01 Description

Connection II joins the end of a longitudinal beam with a side of the transverse beam. The focus of Connection II-B is on the design of the steel plate that is attachted to the transverse beam.

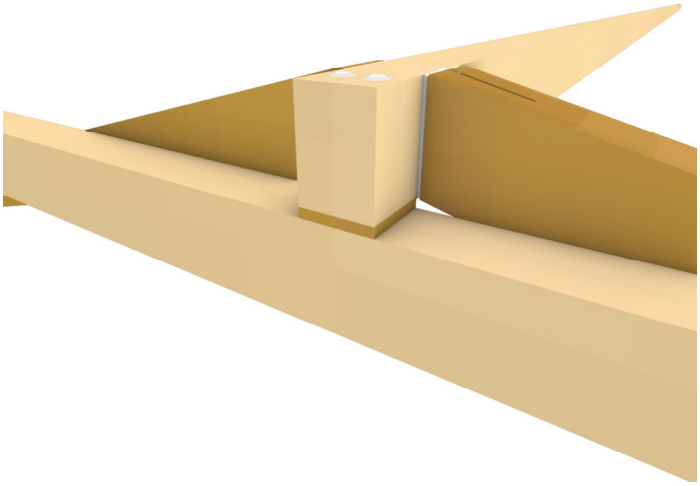

The joint is symmetrical, therefore it suffices to design only one side of the joint. The connection is achieved by a hidden joist hanger. The backbone of the slotted in steel plate is a steel plate joined to the transverse beam with a symmetrical pattern of screws. This connection needs to transfer shear and axial tension.

02 Geometry and Material

Part to be connected	Profile	Material
Transverse beam	bxh = 140 mm x 200 mm	C18
Steel plate	t = 5 mm	S235

03 System Parameters

All governing internal forces were taken from a load combination that contains a wind load case. According to the Danish Standards Foundation, this implies the following kmod-factor (2013):

$$k_{mod} := 1.1$$

The material factor is (European Committee for Standardization, 2020):

$$\gamma_m := 1.35$$

04 Cross Section Parameters

$f_{c.90.k} := 2.2 \ \frac{N}{mm^2}$ $f_{t.perp} := 0.4 \ \frac{N}{mm^2}$ $h_{TB} := 200 \ mm$ $b_{TB} := 140 \ mm$

$A_c := 140 \ mm \cdot 200 \ mm = (2.8 \cdot 10^4) \ mm^2$ $h_{LB} := 200 \ mm$ $b_{LB} := 140 \ mm$

$\rho_k := 320 \ \frac{kg}{m^3}$

05 Screw and Plate Parameters

Screw HBS Softwood with countersunk head (Rothoblaas, 2022)

$d := 5 \ mm$ $L_{screw} := 120 \ mm$ $L_{threaded} := 60 \ mm$ $d_h := 10 \ mm$

$f_{tens.k} := 8 \ kN$ $f_{ax.k} := 12 \ \frac{N}{mm^2}$ $f_{head.k} := 13 \ \frac{N}{mm^2}$

Plate Thickness: Assume the plate thickness to be equal to the thickness of the screw diameter, as recommended by the producer.

$t := d = 0.005 \ m$

06 Structural Analysis

The joint is designed according to the maximum internal forces that act in all members for all load combinations. This reduces the work of structural design, for one joint detail can be applied to all joints.

$N_{c.max.Ed} := 7.85 \ kN$ $\alpha := 14.66 \ °$

$N_{t.max.Ed} := 2.12 \ kN$

$V_{max.Ed} := 3.79 \ kN$

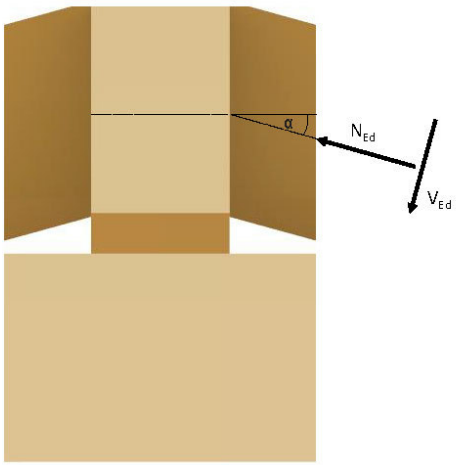

i) Transfer the forces into the orientation of the transverse beam:

$$N_{t.Ed} := V_{max.Ed} \cdot \sin(\alpha) + N_{t.max.Ed} \cdot \cos(\alpha) = 3.01\ \boldsymbol{kN}$$

$$V_{Ed} := V_{max.Ed} \cdot \cos(\alpha) + N_{t.max.Ed} \cdot \sin(\alpha) = 4.203\ \boldsymbol{kN}$$

$$N_{c.d} := \cos(\alpha) \cdot N_{c.max.Ed} + \sin(\alpha) \cdot V_{max.Ed} = 8.554\ \boldsymbol{kN}$$

ii) Compute the additional tension force due to moment that occurs because of the eccentricity in the connection. A leverarm of 100 mm is assumed.

$$ecc := (80\ \boldsymbol{mm} + \tan(\alpha) \cdot (200\ \boldsymbol{mm} - 100\ \boldsymbol{mm})) \cdot \cos(\alpha) = 0.103\ \boldsymbol{m}$$

$$M_{add} := V_{Ed} \cdot ecc = 0.432\ \boldsymbol{kN \cdot m} \qquad h_{lever} := 100\ \boldsymbol{mm}$$

$$N_{t.add} := \frac{M_{add}}{h_{lever}} = 4.317\ \boldsymbol{kN}$$

07 Compression perpendicular to the Grain

The verification is conducted according to EN 1995 6.1.5 (European Committee for Standardization, 2020):
1. The factor taking into account the load configuration, possibility of splitting and degree of compressive deformation is determined to be

$$k_{c.90.1} := 1.0$$

This is on the conservative side. Moreover, the steel plate in between the two beams is not taken into account. This is also conservative because the steel plate would distribute the load activating more beam area, thus leading to a lower utility.

2.The compressive stress equals:

$$\sigma_{c.90.d} := \frac{N_{c.d}}{A_c} = 0.305\ \frac{\boldsymbol{N}}{\boldsymbol{mm}^2}$$

3. The compressive strength is computed:

$$f_{c.90.d} := k_{mod} \cdot \frac{f_{c.90.k}}{\gamma_m} = 1.793\ \frac{\boldsymbol{N}}{\boldsymbol{mm}^2}$$

4. Unity Check:

$$\frac{\sigma_{c.90.d}}{k_{c.90.1} \cdot f_{c.90.d}} = 0.17 \qquad < 1 \qquad \text{OK}$$

08 Axially loaded screws

The verification is conducted according to EN 1995 8.7.2 (European Committee for Standardization, 2020):

1. Screws are used to transfer the tension force through the transverse and between the longitudinal beams, the following failure modes are to be verified:
   a) Withdrawal Capacity of threaded Part
   b) Tear off Capacity Screwhead
   c) Pull through Strength of the Screwhead
   d) Tension Strength of the Screw
   e) Failure along the Circumference of a Group of Screws
   f) Failure of transferring the Tension Force through the Timber via rolling Shear

2. Because a steel plate is used for the connection, failure mode c) is not relevant. Failure mode e) does not need to be verified because the force component parallel to the grain is not accounted for. Block shear and plug shear are not relevant for this connection, because the force component is not parallel to the grain and the beam extends for a relatively large distance of 160 mm in grain direction. This is assumed to prevent block and plug shear.

3. Choice for a screw:
The HBS Softwood fulfills the requirements for the screw head, length and diameter. That is to be joined with a steel plate, to have a length just shorter than the width of the transverse beam and to have a small diameter to reduce minimum spacing requirements.

4. Minimum spacing requirements
   Assumption: The transverse beam is prepared with pre-driled holes.

   i) First the minimum spacing for axially loaded screws is considered according to the Eurocode (European Committee for Standardization, 2020).

   Minimum spacing: $4\ d = 20\ mm$

   Minimum edge distance: $4\ d = 20\ mm$

   i) Second, the minimum spacing for laterally loaded screws that are loaded perpendicular to the grain are considered according to the Eurocode. As the diameter is smaller than 6 mm. The screws can be considered as nails, this reduces spacings by 30% (European Committee for Standardization, 2020). Consider that both edges can be loaded, for the direction of the shear force can change.

$a_1 := 0.7 \cdot 4 \cdot d = 0.014\ m$ $a_2 := 0.7 \cdot 4 \cdot d = 0.014\ m$

$a_{3.t} := 7 \cdot d = 0.035\ m$ $a_{3.c} := 7 \cdot d = 0.035\ m$

$a_{4.c} := 3 \cdot d = 0.015\ m$ $a_{4.t} := 7 \cdot d = 0.035\ m$

6. Selected spacing

The screw pattern is symmetric to avoid eccentricity in the force transfer. Considering that screws are entered from the left and from the right of the transerse beam, a staggered formation is selected. End distances are not relevant because the beam continues beyond the steelplate to both sides in the direction of the grain. Hence, an end distance of 20 mm from the edge of the steel plate is assumed.

$a_1 := 40\ mm$

$a_2 := 20\ mm$

$a_{4.t} := 40\ mm$

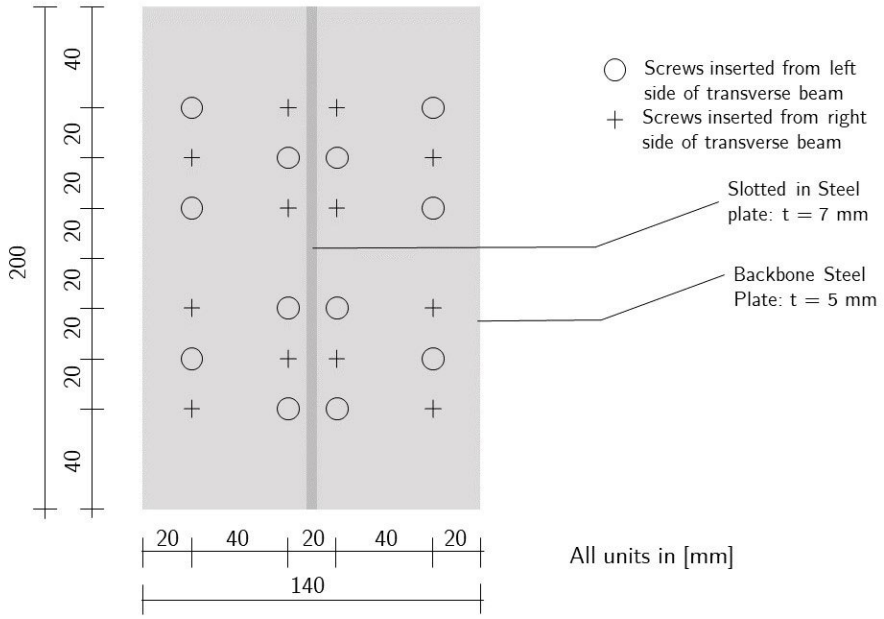

7. Compute the Strength of the Failure Modes

a) Withdrawal Capacity of the threaded Part

Parameters (compare Eurocode for parameter description):

$n := 12$

$n_{ef} := n^{0.9} = 9.36$

$l_{ef} := L_{threaded} - d = 0.055\ m$

$\alpha_{grain} := 90\ °$

$$f_{ax.\alpha.k} := \frac{f_{ax.k}}{\left(\sin\left(\alpha_{grain}\right)\right)^2 + 1.5 \cdot \left(\cos\left(\alpha_{grain}\right)\right)^2} = 12\ \frac{N}{mm^2}$$

$aux_1 := 1\ mm^{-2}$ $\qquad$ $aux_2 := 1\ mm^2$

$$F_{ax.\alpha.Rk.1} := n_{ef} \cdot \left(\pi \cdot d \cdot l_{ef} \cdot aux_1\right)^{0.8} \cdot f_{ax.\alpha.k} \cdot aux_2 = 25.097\ kN$$

b) Tear Off Capacity of Screw Head

The code requires that the tear off capacity of the screw head must be greater than the tensile strength of the screw. The producer states for this type of screw that "generally the steel tensile strength is binding with respect to head separation or pull-through" (Rothoblaas, 2022). Thus the tear off capacity is not computed separately, instead if the tensile strength is complied with, then it is assumed that the head will also not be separated.

d) Tension strength screw

$$F_{tens.k} := 12 \cdot f_{tens.k} = 96 \ kN$$

f) Transfer of tension in timber through shear

For the tension force to be transferred with this connection, the tension must travel through the timber, because the screws from the opposing sides are not directly connected to each other. It is assumed that the tension force in the screws is transferred via rolling shear (both stress components are perpendicular to the grain) in the timber section.

It is assumed that in between the screws from the opposing sides, horizontal shear planes develop with the height being the length of the screw part that overlaps and the width being the distance between the outer screws. This is considered conservative, as due to the membrance effect is is likely that a larger area functions as shear plane and the interaction between screws in vertical shear planes is neglected.

The tension force is divided over the shear planes. The tension force due to the moment is only applied to the top two shear planes which will then be governing.

i) The acting shear stress in the top shear planes is computed as follows:

$$\tau_{d.tens} := \frac{\left(3 \cdot \left(\frac{N_{t.Ed}}{5} + \frac{N_{t.add}}{2}\right)\right)}{2 \cdot \left(L_{screw} - 20 \ mm\right) \cdot 100 \ mm} = 0.414 \ \frac{N}{mm^2}$$

The code specifies that the the shear strength for rolling shear is approximately equal to twice the tension strength perpendicular to grain

ii) The resistance against rolling shear is computed as follows:

$$f_{v.d.rolling} := 2 \cdot k_{mod} \cdot \frac{f_{t.perp}}{\gamma_m} = 0.652 \ \frac{N}{mm^2}$$

7. Overview of the strength values. The lowest strength value is governing.

$F_{ax.\alpha.Rk.1} = 25.097\ \boldsymbol{kN}$

$F_{tens.k} = 96\ \boldsymbol{kN}$

$F_{ax.\alpha.Rk} := F_{ax.\alpha.Rk.1}$

8. Design Strength

$$F_{ax.\alpha.Rd} := k_{mod} \cdot \frac{F_{ax.\alpha.Rk}}{\gamma_m} = 20.45\ \boldsymbol{kN}$$

9. Unity Checks

$$\frac{N_{t.Ed} + N_{t.add}}{F_{ax.\alpha.Rd}} = 0.358$$

$$\frac{\tau_{d.tens}}{f_{v.d.rolling}} = 0.635$$

09 Laterally loaded screws

The verification is conducted according to EN 1995 8.3 and 8.7 (European Committee for Standardization, 2020)

1. The screws that are used to transfer tension, are used to transfer the shear force acting on the steel plate into the transverse beam as well. The connection is classified as single shear connection with a thick plate. According to the Johanson-model, the following failure modes are to be verified:

c) No Plastic Hinge
d) Single Plastic Hinge
e) Two Plastic Hinges

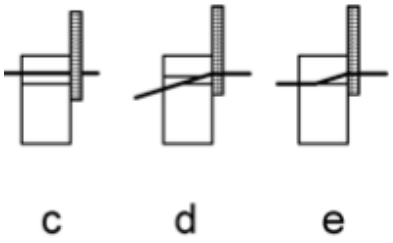

Graphic obtained from European Committee for Standardization (2020)

2. Choice for a screw, minimum and selected spacings have already been adressed when designing the axially loaded screws, hence the embedment strength can directly be computed. According to the Eurocode screws with diameter of less than or equal to 6 mm, can be considered as nails. It is assumed that holes are pre-drilled.

$$aux1 := 1\ m^3\ \frac{N}{kg \cdot mm^2} \qquad aux2 := 1\ m^3\ \frac{N}{kg \cdot mm^3}$$

$$f_{h.k} := 0.082 \cdot (1 \cdot aux1 - 0.01 \cdot d \cdot aux2) \cdot \rho_k = 24.928\ \frac{N}{mm^2}$$

3. The resistance of the three characteristic failure modes is determined

i) Failure mode e)

$$t_1 := L_{screw} = 0.12\ m$$

$$F_{V.Rk.e} := f_{h.k} \cdot d \cdot t_1 = (1.496 \cdot 10^4)\ N$$

ii) Failure mode d)

The characteristic fastener yield moment of the carbon steel screw with d=5mm is given by the producer as (ETA-Danmark, 2022)

$$M_{y.Rk} := 5.4\ N \cdot m$$

Johanson and the additional strength due to the rope effect are computed separately to ensure that a maximum of 100% of the Johanson part is counted from the rope effect part, as specified in 8.2.2 (2). The characteristic withdrawal capcity of the screw is computed with equation (8.38) while disregarding the effective number of screws.

$$F_{ax.Rk} := \frac{F_{ax.\alpha.Rk.1}}{n_{ef}} = (2.681 \cdot 10^3)\ N$$

$$F_{V.Rk.rope} := \frac{F_{ax.Rk}}{4} = 670.359\ N$$

$$F_{V.Rk.d.Johanson} := 2.3 \cdot \sqrt[2]{M_{y.Rk} \cdot f_{h.k} \cdot d} = (1.887 \cdot 10^3)\ N$$

The full part of the rope effect can be accounted for

$$F_{V.Rk.d} := F_{V.Rk.d.Johanson} + F_{V.Rk.rope} = (2.557 \cdot 10^3)\ N$$

iii) Failure mode c)

$$F_{V.Rk.c.Johanson} := f_{h.k} \cdot t_1 \cdot d \cdot \left(\sqrt{2 + 4 \cdot \frac{M_{y.Rk}}{f_{h.k} \cdot d \cdot {t_1}^2}} - 1 \right) = 6.259 \ \boldsymbol{kN}$$

The full part of the rope effect can be accounted for

$$F_{V.Rk.c} := F_{V.Rk.c.Johanson} + F_{V.Rk.rope} = \left(6.929 \cdot 10^3\right) \ \boldsymbol{N}$$

7. The lowest strength value is governing.

$$F_{V.Rk} := 12 \cdot min\left(F_{V.Rk.c}, F_{V.Rk.d}, F_{V.Rk.e}\right) = 30.687 \ \boldsymbol{kN}$$

8. Design Strength

$$F_{V.Rd} := k_{mod} \cdot \frac{F_{V.Rk}}{\gamma_m} = 25.005 \ \boldsymbol{kN}$$

9. Unity Checks

$$\frac{V_{Ed}}{F_{V.Rd}} = 0.168 \ < 1.0 \text{ OK}$$

Unity check for combined Tension and Shear

$$\left(\frac{N_{t.Ed} + N_{t.add}}{F_{ax.\alpha.Rd}}\right)^2 + \left(\frac{V_{Ed}}{F_{V.Rd}}\right)^2 = 0.157 \quad < 1.0 \text{ OK}$$

References

Danish Standards Foundation. (2013). DS/EN 1995-1-1 DK NA:2014 National. 1–10.

European Committee for Standardization. (2020). NEN-EN 1995-1-1. 1.

ETA-Danmark. (2022). European Technical Assessment ETA-11/0030. In Https://Medium.Com/. https://medium.com/@arifwicaksanaa/pengertian-use-case-a7e576e1b6bf

Rothoblaas. (2022). HBS SOFTWOOD. https://www.rothoblaas.com/products/fastening/screws/screws-carpentry/hbs-softwood